THE LONG SHOT EXPERIMENT. VOLUME II. COMPREHENSIVE ANALYSIS

D. G. Lambert, et al

Teledyne Industries, Incorporated
Alexandria, Virginia

25 June 1969

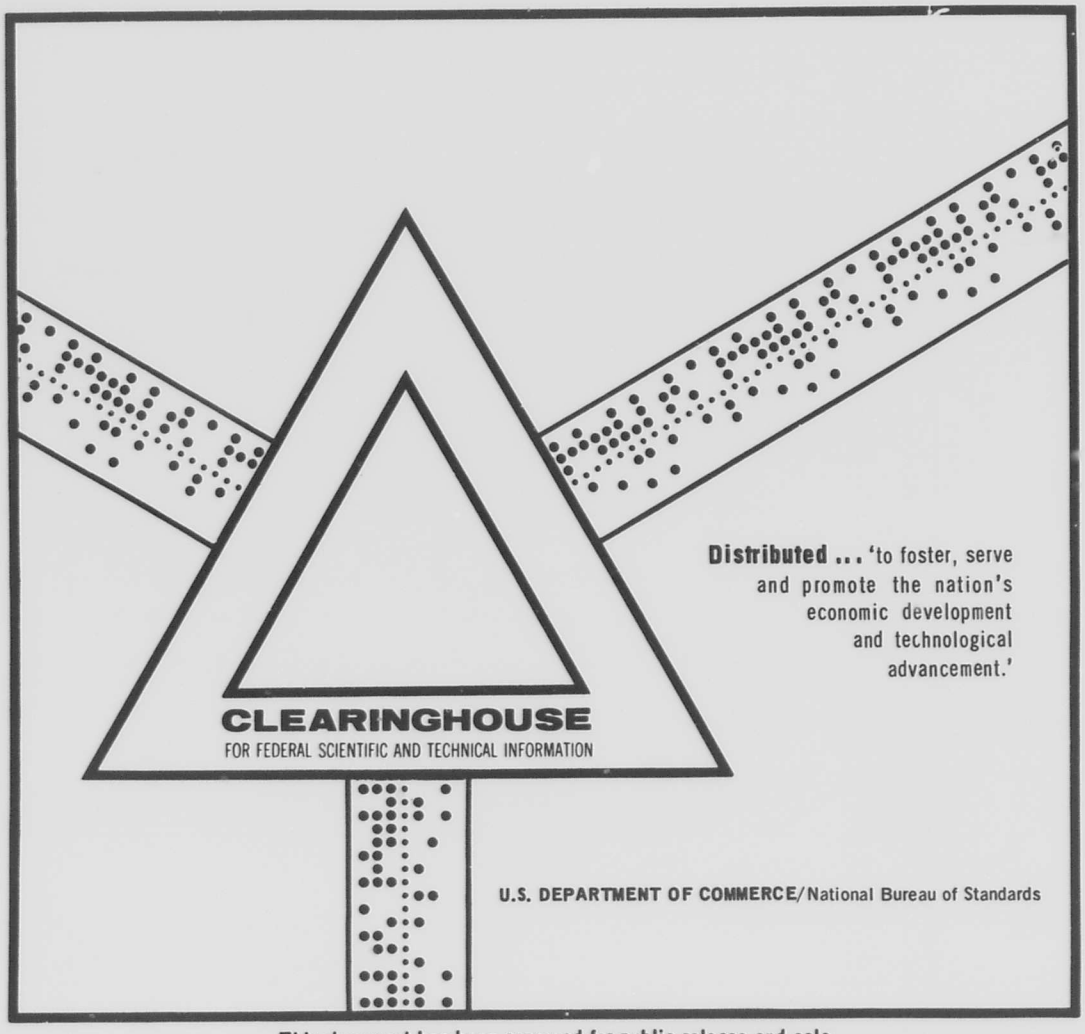

THE LONG SHOT EXPERIMENT

VOLUME II

COMPREHENSIVE ANALYSIS

PREPARED FOR

AIR FORCE TECHNICAL APPLICATIONS CENTER
WASHINGTON, D.C.

BY

D. G. LAMBERT
D. H. VON SEGGERN
S. S. ALEXANDER
G. A. GALAT

SEISMIC DATA LABORATORY

UNDER

PROJECT VELA UNIFORM

SPONSORED BY

ADVANCED RESEARCH PROJECTS AGENCY
NUCLEAR MONITORING RESEARCH OFFICE
ARPA ORDER NO. 624

THE LONG SHOT EXPERIMENT

VOLUME II

COMPREHENSIVE ANALYSIS

SEISMIC DATA LABORATORY REPORT NO. 234

AFTAC Project No.:	VELA T/9706
Project Title:	Seismic Data Laboratory
ARPA Order No.:	624
ARPA Program Code No.:	9F10
Name of Contractor:	TELEDYNE INDUSTRIES, INC.
Contract No.:	F33657-69-C-0913
Date of Contract:	2 March 1969
Amount of Contract:	$ 950,000 (Letter Contract)
Contract Expiration Date:	1 March 1970
Project Manager:	Royal A. Hartenberger (703) 836-7647

P. O. Box 334, Alexandria, Virginia

This research was supported by the Advanced Research Projects Agency, Nuclear Monitoring Research Office, under Project VELA-UNIFORM and accomplished under technical direction of the Air Force Technical Applications Center under Contract F33657-69-C-0913.

TABLE OF CONTENTS

TABLE OF CONTENTS (Cont'd.)

LIST OF TABLES

LIST OF FIGURES

LIST OF FIGURES (CONT'D.)

LIST OF FIGURES (CONT'D.)

LIST OF FIGURES (CONT'D.)

LIST OF FIGURES (CONT'D.)

LIST OF FIGURES (CONT'D.)

LIST OF FIGURES (CONT'D.)

LIST OF FIGURES (CONT'D.)

INTRODUCTION

One of the very important research and development efforts of the United States Government in recent years has been concerned with the detection, location, and identification of underground nuclear explosions. Such a capability is important to the security of the United States both in terms of accurately documenting the nuclear weapons testing programs of foreign powers and in monitoring any test ban treaty which would prohibit the detonation of underground nuclear devices. The responsibility for this effort is vested in the Advanced Research Projects Agency of the United States Government which has sponsored a vigorous technical program (project VELA-Uniform) directed toward developing the desired detection and identification capability.

One of the major experiments in this program was Project LONG SHOT in which an underground nuclear explosion was detonated on Amchitka Island in the Aleutians. The overall purpose of LONG SHOT was to test and improve our ability to locate and identify seismic events from observations at large distances. This was an important experiment because most of our previous experience had been with explosions at the Nevada Test Site recorded primarily at regional distances (< 3000 km) within the United States and Canada. As a result we needed a quantitative test of our ability to locate and identify distant events occurring in a geological and tectonic setting different from that at the Nevada Test Site.

Some of the reasons for selecting the Aleutian Island Arc as the test area for LONG SHOT were:

(1) it provided a favorable distribution of recording stations in both azimuth and distance, especially the superior-quality U.S. stations.

(2) It is a tectonically active region that provides earthquakes for direct comparison with LONG SHOT.

(3) It resembles the Kuril arc and Kamchatka where more than 60% of all earthquakes in the Soviet Union occur.

(4) It is in a continental margin area where many of the earthquakes occur under the ocean. Calibration furnished by LONG SHOT would assist in developing reliable means of determining whether or not an event occurred on land. (The events occurring on land are of most interest since completely contained underwater explosions can be detected in the open oceans and identified as explosions from the characteristic hydroacoustic signals they produce.)

(5) It is in an area with different geological structure than NTS so that location and identification procedures previously developed could be rigorously tested.

(6) The area is remote and yet accessable so that the necessary geophysical and geological surveys of the area surrounding the test site and the detonation itself could be carried out without disrupting any local domestic activities.

The LONG SHOT explosion took place on Amchitka Island in the Aleutians on 29 October 1965. The event was sufficiently large (80 kilotons equivalent TNT with a P-wave magnitude of 5.85) to be recorded clearly at a large number of receiving stations around the world. The excellent data provided by this experiment have been analyzed intensively and numerous publications relevant to various aspects of the problem of distinguishing explosions from earthquakes have resulted. However, to date there has not been an integrated study which brings together the salient information gained from LONG SHOT.

The purpose of the present study is to document in a

single comprehensive report the important results relating to the location and identification of underground nuclear explosions obtained from the LONG SHOT experiment. This synthesis has involved not only the collection of basic observations from LONG SHOT and critical review of previous work based on LONG SHOT data, but also considerable additional data analysis to aid in the overall interpretation of LONG SHOT results.

The report is contained in two volumes. Volume I presents the basic observational data obtained for all the available stations which recorded the LONG SHOT event. To illustrate the quality of seismic recordings from LONG SHOT obtained throughout the world, reproductions of a large number of seismograms are included. In addition, Volume I contains a complete bibliography of publications which deal with LONG SHOT.

Volume II presents a comprehensive analysis of the LONG SHOT explosion including both near-source and far-field observations. It is written and illustrated such that frequent reference to Volume I is not required. Included are discussions of the physical setting of LONG SHOT, near-source behavior, and location and magnitude estimates. We have also applied the principal identification criteria to LONG SHOT in an effort to assess the effectiveness of each diagnostic for this source region. In addition we compare LONG SHOT directly with equivalent magnitude earthquakes from the same source region to elucidate their differences and similarities.

It is hoped that this comprehensive report will serve as a point of departure for future work both on LONG SHOT and the Aleutian Arc source region and that it will aid in evaluating any future experiments in other localities.

PHYSICAL SETTING OF THE LONG SHOT EVENT

Regional Geology and Tectonics

Many of the results of the LONG SHOT experiment are best interpreted within the framework of the total geological setting around Amchitka Island. The island lies toward the western end of the Aleutian Arc (Figure 1). This volcanic arc is one of the earth's major structural features extending nearly 3200 kilometers from Kamchatka Peninsula through the Commander Islands, Aleutian Islands, and the Alaska Peninsula to Cook Inlet. A transition from oceanic to continental crustal structure occurs between the Aleutian Islands and the Alaska Peninsula. For detailed descriptions of the lithology and the physiography of the arc see Murray (1945), Menard and Dietz (1951), Gibson and Nichols (1953), Gates and Gibson (1956), Ewing et al (1965), and Nichols and Perry (1966).

Evidence that the Aleutian Arc is one of the most active seismic regions of the earth is documented by Gutenberg and Richter (1954) and the Preliminary Determination of Epicenter (PDE) cards of the United States Coast and Geodetic Survey (USC&GS). Shallow earthquakes are frequent. Some intermediate-depth earthquakes have been recorded from this region, but no deep events. The pattern of epicenter locations with depth as determined by Murdock (1967) from data collected in the VELA-Uniform 1964 Aleutian Island Experiment are consistent with a model of the lithosphere dipping beneath the island arc due to sea-floor spreading in a manner that has been detailed for the Tonga-Kermadec Arc and other arcs by Isacks et al (1968). Stauder (1968) has shown that the shallow shocks in the Rat Islands can be separated into two distinct spatial and focal-mechanism groups. One group consists of foci at or

slightly south of the island chain. These foci have mechanisms which can be interpreted as the result of underthrusting of the oceanic side of the lithosphere along a gently dipping plane (15°-20°) under the island arc. The other group lies about 100 kilometers south of the island arc and beneath the Aleutian trench. These foci have mechanisms showing horizontal tension in the upper mantle normal to the trend of the arc. This fact is consistent with the forces that would be acting on the top of the lithosphere bending at this point to dip under the arc. Thus, the seismicity of this region seems to be intimately related to global tectonic activity and characteristic of zones where the lithosphere is being underthrust.

Further evidence for the sea-floor spreading hypothesis in the Aleutian arc is given by Hayes and Heirtzler (1968) who summarize and interpret magnetic observations for that region. They show that magnetic lineations south of the arc are parallel to it.

Local Structure Near Amchitka Island

The first full-scale seismic refraction studies in the Aleutians were conducted by Scripps Institute of Oceanography in 1956-57 and again in 1961. Shor (1962 and 1964) reported on the results of these refraction surveys and proposed a crustal model across the Aleutian Arc. The VELA-Uniform program supported a series of refraction surveys in the Aleutians near Amchitka Island in the years 1963-1968; results and proposed models are presented by Schneider (1964), Murdock (1967), and Guidroz et al (1968).

Raw data from the 1964 Aleutian Island Experiment are given by the Geotechnical Corporation (Technical Report 65-130).

Murdock (1967) used these data together with the data of Shor and Schneider to construct a composite profile through Adak Island, 300 kilometers east of Amchitka Island, normal to the arc. The extent of coverage of the three investigations is shown in Figure 2 and the composite profile is shown in Figure 3. The Moho depth of 14 km in the Bering Sea and the 22 km depth about 20 km north of Adak Island were obtained by Shor. Reduced travel times from the 1964 Aleutian Island Experiment led Murdock to infer a velocity of 8.4 km/sec and a depth in agreement with Shor's just north of Adak. Murdock suggests a synclinal Moho structure beneath the island reaching a 40 km depth (Figure 3). For the area immediately south of the island, he found that the Moho refractions terminate abruptly. This led to the proposed structural discontinuity seen in Figure 3. Murdock again found refractions (M_2) with the 8.4 km/sec velocity about 75 km south of the island. Data there revealed a Moho depth of 40 km, rapidly decreasing southward under the Aleutian trench to a depth of about 20 km at 150-200 km south of Adak.

The most recent crustal profile has been constructed through Amchitka Island itself by Guidroz et al and is shown in Figure 4. The depths to the Moho at the northern end of the profile (15 km), near the northern shore of Amchitka (40 km), and at the southern end of the profile (12 km) are in good agreement with Murdock's composite profile through Adak Island (Figure 3). The upper mantle velocities of 8.0-8.1 km/sec, however, do not agree with Murdock's velocities. Due to shot-receiver geometry, there is a hiatus in the profile under Amchitka Island where, going southward, the Moho appears to rise 15 km in a horizontal distance of 100 km. The structure thus defined cannot exactly accommodate Murdock's proposed structural features

for the section beneath Adak Island. However, each profile is probably a reasonable picture for the structure across the arc at their respective locations. Not only are Adak and Amchitka Islands laterally separated along the arc, but also they do not occupy the same position on a line normal to the arc (see Figure 1). Although the two profiles, taken together, do give a consistent picture of the gross structure across the Aleutian Arc, details are as yet unresolved and, owing to the apparent complexity of the region, Moho velocities and dips cannot be heavily relied on. Further, Figure 4 shows that the crustal structure immediately below Amchitka Island is still conjectural.

The evidence presented above from seismic profiling suggests that a thrust fault dipping northward exists under the Aleutian Arc. This interpretation is consistent with the model of the lithosphere dipping beneath the arc as inferred from earthquake locations and focal mechanism studies and from the magnetic data discussed earlier. A very generalized cross-section of the possible crust and upper mantle structure on a north-south profile through Amchitka Island is presented in Figure 5. A structure such as pictured in Figure 5 should have discernible effects on travel times and amplitudes. As will be shown later in this report, travel times from the LONG SHOT site to teleseismic stations do give credence to a structure of this sort.

Geologic Details of the LONG SHOT Site

Geological, hydrological, and geophysical data regarding Amchitka Island are presented in a joint report by the U. S. Army Engineer District and the U. S. Geological Survey (1965). Figure 6, taken from that report, shows the surface geology

of Amchitka Island. At the LONG SHOT site, faults and lineations strike about 50°-60° NE, with faulting and jointing being nearly vertical. This is subparallel to the bedding which dips at about 15° towards the SE. The direction of faulting and jointing on the island is reflected by submarine topography to the south of Amchitka (Gibson and Nichols, 1953).

In order to determine the structure at the LONG SHOT site, seismic surveys were conducted and exploratory core holes were drilled. The surface weathered layer was found to be no more than 13 meters thick in the vicinity of the shot. Underneath, the first competent beds had a velocity of 2.74 km/sec or greater. Three core holes revealed the stratigraphy at the LONG SHOT site (Figure 7). The majority of the section is brecchia with interbedded tuff, siltstone, and graywacke. An andesite sill between the depths of 670 and 762 meters was the detonation point of LONG SHOT. From sonic logs in the core holes, velocities of the brecchia were found to range from 2.74 to 3.66 km/sec. Velocity of the andesite sill was found to be 4.27 km/sec. The average uphole velocity for LONG SHOT is 3.38 km/sec. Table 1 summarizes velocity, density, and porosity with depth at the shot hole.

This site on Amchitka Island is different lithologically from any previous site of a United States nuclear explosion. Tests in Nevada have been detonated chiefly in tuff and alluvium. A few events have been placed in hard rock (granite, rhyolite, salt, basalt) in the U.S. testing program and the VELA-Uniform series of special shots, but LONG SHOT was the first to be detonated in andesite.

NEAR SOURCE BEHAVIOR

Certain aspects of the near-source behavior are relevant to far-field observations. Of primary importance is the question of magnitude-versus-yield which involves the near-field nonlinear displacements and how these affect the far-field magnitude measurements.

The term "magnitude" as used here refers to a measure of body-wave amplitude (or energy) corrected for propagation and distance effects. Magnitude is determined in exactly the same manner for both earthquakes and explosions. An explicit definition is given under RECORDED AMPLITUDES AND MAGNITUDE DETERMINATIONS.

The term "yield" refers to explosive size. For LONG SHOT the yield was reported as 80 kilotons (U.S.A.E.C., 1967) where one kiloton $\approx 4 \times 10^{19}$ ergs.

The magnitude/yield relationship is in effect a measure of the ratio of propagated seismic energy to total explosive energy. Empirical curves of magnitude-versus-yield as determined for NTS explosions are shown in Figure 8 taken from SIPRI, 1968. This figure clearly indicates variations of ratios as functions of rock types and water content.

As stated in the previous section, LONG SHOT was the first nuclear explosion in andesite. Consequently no magnitude/yield curves are available for andesite; however, it is reasonable to expect that the magnitude/yield curve for andesite will closely parallel that for granite, another hard, crystalline igneous rock. The magnitude difference obtained by relating the LONG SHOT value to the curve for granite provides a measure of the far-field amplitudes of LONG SHOT compared with a comparable yield event in granite. The LONG SHOT

amplitudes are about three times greater.

Particle velocity measurements were made in a well (EH-5) about six meters from the shot hole. Six accelerometers and velocity meters were located at depths ranging from 0 to 335 meters as reported by Day and Murrell (1967). The fact that peak radial velocity levels occur prior to spalling (Day and Murrell, 1967) is apparent from the accelerometer and velocity records (Figures 9 through 14). Figure 15 shows the peak radial velocity versus slant range for various shot media (Sauer et al, 1964). The observed velocity points have the same slope as the granite curve and are approximately two times greater in amplitude. The amplitude recorded by the surface meter demonstrates the effect of a free surface on that amplitude (approximately doubling it). That the amount of water in the shot media is of importance is apparent from the partially saturated and fully saturated valley tuff magnitude/yield curves (Figure 8). The radial velocity factor of two above the granite may be due to the presence of water in the andesite sill and the tuffs and breccias near the sill. The porosities of these strata are indicated in Table 1; however, no information concerning the degree of water saturation is available.

Nonlinearity caused by spalling and close-in nonhomogeneous geological conditions can be seen from lateral variations in surface vertical velocity and displacement measurements (Figures 16 and 17). It is apparent that the southeast profile shows higher particle velocity and displacement values than either the west or northeast profile. The aspect of azimuthal variation in amplitude relative to far-field radiation patterns will be discussed later in the report. However, it is significant that spalling occurs between 36 and 80 milliseconds after the initial shock and with considerable intensity,

because the additional seismic energy introduced by spalling could account for all or part of the observed differential in scaling levels (magnitudes) between close-in and far-field measurements.

Summarizing then, for LONG SHOT set off in andesite, close-in scaling results in amplitudes two times greater than for granite; this may be partially attributed to the water content in the andesite sill and tuffs and breccias near the sill. The far-field scaling (magnitude/yield) gives a factor of three greater than for granite. Further, the additional seismic energy due to spalling could account for all or part of the differences between far-field and near-field scaling.

We have assumed in the above discussion that the LONG SHOT yield was equivalent to 80 kilotons, and if the yield was greater than 80 kilotons, then the energy transmission characteristics in scaling of the LONG SHOT medium would become more closely related to granites at NTS.

ESTIMATES OF LOCATION FROM FAR-FIELD OBSERVATIONS

Location Using Standard P-Wave Travel Times

One of the primary purposes of the LONG SHOT experiment was to test teleseismic location capability in an area of apparent upper mantle inhomogeneity. The shot was large enough to be recorded world-wide, with P-waves recorded out to epicentral distances of 100°. In computing the LONG SHOT epicenter, the P-wave arrival times from 329 stations between 20° and 100° were selected which were less than 7.0 seconds off the predicted time of the 1940 Jeffreys-Bullen (JB) Seismological Tables. (This 7.0 second criterion discarded only two stations: Sterling Forest, New York, and Raman, Turkey). Travel times for stations at less than 20° were not used because their deleterious effects upon epicenter locations has long been known (Herrin and Taggart, 1962). The majority of arrival time observations were made on the North American continent, and the preponderance of values from this narrow azimuthal aperture must be kept in mind since results will be accordingly weighted heavily by North American observations.

Any large error in the computed epicenter of LONG SHOT would cast doubts on all other computed epicenters in the Aleutian Island region, and in fact on locations of many events throughout the world. The recent publication of the new P travel times (H68) by the committee headed by Eugene Herrin (Bulletin of the Seismological Society of America, August, 1968) has presented the opportunity of comparing the JB travel times with these most recent revisions. The plot of the raw JB residuals, corrected for ellipicity but not elevation, versus distance shown in Figure 18 reveals

that, in general, travel times from LONG SHOT relative to JB predicted times were very fast. The majority of negative residuals are greater than three seconds. Travel times based on nuclear explosions from various other areas (Carder et al, 1966) cannot account for the large negative residuals from LONG SHOT. The most probable indication is that the LONG SHOT event is located in an area of anomalously high upper mantle velocity. A similar plot of raw H68 residuals versus distance is shown in Figure 19. Here it is again evident that LONG SHOT residuals are mostly negative when compared to this most recent revision of the JB travel times. Obviously depth and origin time of the event will be wrong on the computed epicenter using either the JB or H68 tables.

Using the 329 stations described above, the program SHIFT (Chiburis, 1968) was used to locate the epicenter first without restraining the depth. The results are listed in Table 2, where it is seen that both JB and H68 travel times give equally poor locations. Had nothing been announced about this event, a hypo-centered location 60-80 km deeper than actual and about 20 km more north than actual with an origin time 5-10 seconds later than actual would have been obtained and the event would have been immediately classified as an earthquake (disregarding the lack of depth phases). The lesser standard deviation of the final travel-time residuals (relative to the computed epicenter) for the H68 location shows that the new tables are somewhat better but no more accurate than the JB tables for this source region.

In addition to the origin time-depth error, a more serious error is the shifting of the epicenter about 20 km northward. Immediately after LONG SHOT, a similar location result using fewer stations led observors to question whether the location of Amchitka Island might be in error; however,

a review of available geodetic and astronomical observations showed that the probable error in the LONG SHOT site with respect to the North American Datum of 1927 at Meades Ranch, Kansas, is approximately 1 kilometer (Helterbran and Jordan, 1966). Bias in the LONG SHOT travel times is evident and real. Azimuthal bias in observed P travel times will be discussed in detail in the next section. Although the term "source bias" will be used in this discussion since it has been previously used to describe systematic mislocations of epicenter, this term may be misleading because the bias is not necessarily associated with the physical properties of the earth in the immediate area of the LONG SHOT source.

Source Bias

In order to properly study the azimuthal source bias, SHIFT was rerun with the depth constrained to zero and confidence ellipses were computed for latitude-longitude. Figure 20 shows the results and Table 3 lists them for JB and H68 travel time tables. Figure 20 reveals again that the computed epicenter is shifted northward about 20 km from the actual site. This location is in the Bering Sea off Amchitka Island by more than 10 km (see Figure 6). The 99.9% confidence ellipse in both cases fails to cover the epicenter. Therefore it is evident that travel times to the north from LONG SHOT are generally faster than to the south for the same epicentral distances.

Cleary (1967a) and Herrin and Taggart (1968b) have discussed this azimuthal variation in the LONG SHOT travel times. To illustrate this variation, plots of the JB and H68 travel-time residuals calculated from the true LONG SHOT

location are plotted versus azimuth from LONG SHOT in Figure 21 and 22 respectively for the 329 stations used in the location program. Cleary reasoned that a single-cycle sine curve fit to these residuals would, when subtracted from the residuals, give a more accurate location and would be physically consistent with a structure dipping beneath the arc. Both he and Herrin and Taggart produced location errors of less than five kilometers when they used the arrival times corrected for this azimuthal bias from groups of about 100 stations. Using all of the available 329 arrival times, the least-squares fit of a sine curve to the JB residuals versus azimuth is given by:

$$JB_i = -2.9 + 1.4 \sin (W_i + 269°)$$

where

JB_i = travel-time residual with respect to JB at station i,

W_i = azimuth from LONG SHOT of recording station i.

The amplitude and phase of the sine curve estimated by Cleary using 83 stations is 1.5 seconds and 250° respectively. Again using all of the 329 arrival times, the sine-curve fit to the H68 residuals is:

$$H68_i = -0.4 + 1.2 \sin (W_i + 283°)$$

where

$H68_i$ = travel-time residual with respect to H68 at station i.

The Herrin and Taggart estimates using 106 stations are 1.3 seconds amplitude and a 273° phase.

The standard deviations of the residuals are reduced when related to the sine curve. For the JB residuals, the standard deviation of the residuals with respect to the sine curve is 1.12 seconds and with respect to their mean value is 1.49 seconds. For the H68 residuals, the values are 1.10 seconds and 1.27 seconds respectively. It is not implied that a single-cycle sine curve is the best fit to the residuals vs azimuth. Any number of periodic curves or even polynomials could have been fitted to these plots. However, the sine curve is one that can be easily related to the effects of an upper mantle structure such as shown in Figure 5.

After subtracting a value given by the above functions from each of the 329 station arrival times, the epicenter was relocated. The results are shown in Figure 23 and listed in Table 3. The H68 travel times give a better location, but it is not significantly better. Again the H68 residuals for the final location have a smaller standard deviation than the JB residuals, but the difference is nearly insignificant. In both cases, the 75% confidence ellipse covers the epicenter.

Using different sets of stations, Cleary and Herrin and Taggart obtained final locations of LONG SHOT with about this accuracy, which, of course, results from empirical corrections derived from independent knowledge of the true location of LONG SHOT. Without this knowledge, the use of the teleseismic travel-time data can only result in epicentral errors of about 20 km as shown in Figure 20.

If explanation of source bias is to be limited to the

source area, the postulated structure must not only account for the azimuthal variation in travel times but must be physically realizable and in accord with basic geophysical knowledge of the source area. A structure which will give travel times on the order of two to three seconds faster to the north than to the south is required. Such a difference cannot be attributed to some anomalous crustal structure near the source as Cleary (1967a) has shown. Rather he proposes a model beneath Amchitka Island which has a slab of anisotropic olivine dipping northward at an angle defined by earthquake zones in the Aleutian Arc. Such a model is consistent with current interpretation of sea floor spreading near continental margins. The alignment of high-velocity axes of olivine crystals downward along this zone for a few hundred kilometers could conceivably account for the observed azimuthal bias in travel times. If the depth of the anomalous zone is limited to 200 km, however, which is deeper than any recorded earthquakes in the Aleutians, then there must be a difference of about 6% in velocity between the anomalous dipping structure and the surrounding mantle (see Figure 5) on the basis of an upper mantle velocity of 8.0 km/sec down to 300 km depth in order to account for just two seconds travel-time difference between rays to stations north of the arc and rays to stations south of the arc. If it is postulated that the anomalous zone extends to 500 km in the Aleutians, as it does for the Tonga-Kermadec Arc, then only a 3% higher velocity in the dipping anomalous zone would be required. Since Oliver and Isacks (1967) ascribe only a 1-2 percent higher velocity to the corresponding anomalous zone in the Tonga-Kermadec Arc and since there is no geophysical evidence for continuation of the anomalous zone in the Aleutians to deeper than 300 km, we conclude that no more than about one-third of the observed bias of

travel-times from LONG SHOT (Figures 21 and 22) can be accounted for by an anomalous dipping structure under the Aleutian Arc. There must then be another explanation of the apparently large source bias indicated by these curves. This is investigated in an analysis of LONG SHOT residuals with respect to distance and region in the next section.

Travel-Time Residuals Versus Distance and Region

LONG SHOT afforded the first opportunity to study travel-time residuals at teleseismic distances from a large source in the North Pacific having a known location and origin time. Contour maps of P (including Pn) and PKP residuals with respect to JB travel times for a surface focus are shown on polar projections from Amchitka Island and its antipode in Figures 24 and 25. These are the residuals plotted in Figure 18 and are corrected for ellipticity, but not elevation, as stated earlier. For convenience JB-T instead of T-JB units have been shown to eliminate the need to use negative signs. Contours of residuals have been drawn where data were sufficiently dense, and dashed lines represent areas of very sparse or no data. The actual residual values at the recording sites were deleted for ease in reduction of the maps. Figures 24 and 25 are intended to show a very rough picture of the global pattern of travel-time residuals and are not suited for detailed interpretation.

Of particular interest is the North American continent because of the high density of stations and the well-known crustal structure. Using all the travel-time observations available in North America, Figures 26 and 27 show the contours of the JB and H68 travel-time residuals respectively. Although the H68 travel times constituted a major revision of the JB

tables, the residuals on both maps show the same spatial patterns. The relative lows in the St. Lawrence Valley and the midwestern and southern United States and the relative highs on the west coast and in Alaska appear on both. The important point to be seen from these figures is that, assuming the H68 travel times to be a very accurate representation of the earth as a whole, there appear regional differences of travel time at teleseismic distances of as much as five seconds for the LONG SHOT event. This regional residual pattern across the United States and Canada has also been documented for other events; e.g., the Salmon explosion (Archambeau et al, 1966) and for groups of events (Hales et al, 1968; Cleary and Hales, 1966; and Carder et al, 1966). King's (1959) tectonic map, Figure 28, can be used to relate these residual patterns to tectonic provinces.

These regional anomalies constitute an important factor in the azimuthal bias of travel-time residuals recorded by LONG SHOT as shown in Figures 21 and 22. In these plots, the least-squares fit of the sine curve is controlled by the great number of stations in North America between the azimuths of 40° and 85°. The large number of Hawaiian stations and Australian stations concentrated in two narrow apertures at about 140° and 205° respectively, also heavily weight the fit. Finally, there is a large group of stations in France and Germany at 350°-360° azimuths which control this portion of the sine-curve fit. The effect is that the sine-curve fit and its relation to source bias may actually cloak what is really a problem in regional variations of travel-time.

If these stations which control the fit of the sine curve exhibit the same azimuthal bias for all events which they record, then the case for a source bias related to an anomalous structure under the Aleutians is diminished, Herrin

and Taggart (1968a) have listed station corrections to be added to the predicted H68 travel times to account for regional variations in travel time and to improve epicenter locations. They list 145 stations common to the 329 used in the LONG SHOT location for which they have computed a station correction. Because of the close proximity of many stations recording LONG SHOT to stations listed by them, the number of stations with corrections has been extended to 236 of the 329 stations. Figure 29 shows these 236 station corrections plotted versus azimuth to be compared with Figure 22. The station corrections, as given by Herrin and Taggart, are azimuthally dependent themselves, and the values plotted are those which satisfy the azimuthally-dependent function [A + B sin (W+C)] with W equal to the back azimuth to LONG SHOT from the particular station.

A sine curve was fitted by least squares to the station corrections as shown in Figure 29 and is given by:

$$T_i = 0.25 + 0.25 \sin (W_i + 288°)$$

where

T_i = station correction applicable to LONG SHOT at station i

W_i = azimuth of station i from LONG SHOT

The phase of the sine curve (288°) is nearly identical to that of Figure 22 and shows that station corrections derived from many events are compatible with observed H68 residuals from LONG SHOT. The epicenter was relocated using the original 329 stations with station corrections now applied to 236 of them in addition to the source correction for H68 residuals. Figure 30 shows the results of this

location and Table 3 lists the results for H68 travel times. The station corrections have over-compensated for the bias and have caused the computed epicenter to be moved south of LONG SHOT. This supports the premise that the regional anomalies associated with the recording sites contribute some what to the observed bias from LONG SHOT. It is evident, however, that present station corrections applied to the observed travel times could not significantly improve the original computed location of LONG SHOT which is in error by more than 20 km.

Consider, for example, what would result if instead of the large number of Australian and Hawaiian stations which weight the southern azimuths from LONG SHOT with positive residuals, a large number of stations were concentrated near Guam (GUA) in the Marianna Islands with its -2.0 seconds H68 residual, near the Cook Islands (RAR) with its -2.1 seconds residual, in New Zealand where Chateau (CNZ) shows a -2.0 second residual, and near Mount John (MJZ) which shows a -1.8 second residual. Similarly, North American and European locations might be chosen which would, when their residuals were plotted, nearly eliminate the bias shown in Figure 22. In other words, another suitably deployed network of 329 stations might show no bias in the LONG SHOT travel times or even a bias oppositely directed to that observed in Figures 21 and 22.

Therefore, the sine-curve correction applied to the 329 stations which results in the very good locations shown in Figure 23 cannot be arbitrarily applied to obtain good locations using any small subset of these 329 stations. The sine curve provides only an operational method to obtain an improved location for LONG SHOT, since it cannot be wholly due to an anomalous upper mantle under Amchitka

Island. Earlier we estimated that only about one-third of the sine-curve amplitudes in Figures 21 and 22 can be attributed to the structure immediately beneath the source. The remaining part is due to regional anomalies and an accumulated residual along the entire travel path to these particular 329 stations.

Thus, the region has not been calibrated in the sense that the simple sine-curve correction of amplitude and phase given in Figures 21 and 22 can be applied to an arbitrary set of stations to give an accurate location of events in the Aleutian Arc. However, a precise and easy method of calibrating the area is available in the method of relative travel-time anomalies as discussed by Chiburis (1968), wherein, knowing the relative travel-time differences between stations as determined from LONG SHOT arrivals, a small network of stations was used to relocate earthquakes in the region of LONG SHOT. From a study of many events relocated in this manner, better knowledge of the tectonics of this arc can be gained in the future.

We conclude, therefore, that the "source bias" of LONG SHOT is largely a result of the geographical distribution of the 329 recording stations and their associated variations in travel-time residuals. Only about one-third of the bias can be introduced by the anomalous dipping structure under the arc as discussed above.

Additional Considerations on Source Bias

The PcP arrival was detected at 148 of the 329 stations used in the LONG SHOT locations. Although the arrival times are often indistinct, an analysis of these travel times should be made to verify the regional anomalies exhibited

by the direct P-waves. To test further the source bias, the PcP residuals with respect to distance for JB standard and H68 standard are plotted in Figures 31 and 32. The very large scatter attests to the difficulty in picking their arrival times. As for P residuals, these were then plotted versus azimuth from LONG SHOT in Figures 33 and 34. A sine curve was again fitted for both the JB and H68 cases. Only those residuals which were considered fairly certain on the basis of record quality and amplitude of PcP were used in the least-squares fit; this then involved only 85 of the original 148 residuals. The results can be expressed as:

$$JB_i = -3.4 + 1.6 \sin (W_i + 283°)$$

$$H68_i = -0.7 + 1.9 \sin (W_i + 283°)$$

The almost exact duplication of phase angles and consistency of amplitudes for these sine-curves and the one fitted to the P residuals in Figures 21 and 22 is an interesting and important result. Again, it must be pointed out that the fit of the sine curves is mainly controlled by the preponderance of North American stations.

The same arguments concerning regional effects on P travel times and their contributing to "source bias" will apply to the PcP times. In spite of a much narrower cone of take-off angles at the source for PcP rays, the travel paths of PcP rays show as much bias with azimuth as the travel paths of P rays from LONG SHOT. Any effect of source bias due to near source structure such as postulated in Figure 5 should be reduced by the narrowed cone of take-off angles of PcP rays to teleseismic stations. Again, we conclude that the apparent "source bias" is accumulated along the entire travel paths through the mantle and not just beneath the Aleutian Arc.

One other argument weighs against the bias being due to the structure beneath the arc. Douglas (1967) presented a method of correcting the LONG SHOT bias without using the knowledge of the true epicenter location. Termed "joint epicenter determination", this method requires several other events of known depth within the same region. Using thirty good stations, he located LONG SHOT independently in the conventional manner with an error of 23 km to the north. However, locating LONG SHOT and six earthquake simultaneously, he found only a 1 km error in the computed epicenter of LONG SHOT. The fact that the earthquakes used extended over a wide range of the Aleutian Arc (approximately 300 km) and are considerably south of the Arc further indicates that the "source bias" exhibited by LONG SHOT is not due to the postulated anomalous structure beneath Amchitka Island but is characteristic of the travel times to teleseismic distances from a large region surrounding Amchitka Island.

RECORDED AMPLITUDES AND MAGNITUDE DETERMINATIONS

Preliminary Remarks

If radiation patterns can be discounted, as suggested by the observed data at distances less than 30°, the LONG SHOT explosion gives a clear picture of the regional effects on amplitudes and magnitudes at teleseismic distances, especially in North America where a large number of P-wave amplitudes were measured. LONG SHOT body-wave amplitudes and magnitudes plotted as a function of epicentral distances show considerable scatter in Figures 35 and 36 respectively. A similar scattering in amplitudes and magnitudes recorded from NTS shots is documented in numerous Long Range Seismic shot reports by the Seismic Data Laboratory. The long-period Rayleigh-wave amplitudes and magnitudes in Figures 37 and 38 show less scatter. The purpose of this section is to point out regional effects on amplitude (A/T) and magnitude values for LONG SHOT, to investigate the possibility of distance-dependence for body-wave magnitudes as computed by the standard formula, and to investigate the relation between long-period Rayleigh-wave and short-period body-wave magnitude estimates. We also compare the body-wave amplitude pattern of LONG SHOT and that of an assumed explosion on Novaya Zemlya. Other comparisons with NTS shots are also included.

In this section, body-wave magnitudes are computed by this standard "unified body-wave magnitude" formula:

$$m_b = \log_{10} (A/T) + B$$

where

A = maximum zero-to-peak ground motion (millimicrons) of the P phase within the first three or four cycles of motion,
T = period of maximum ground motion (seconds),
B = distance correction factor.

Unless otherwise mentioned, the distance correction factors (B) are those taken from Gutenberg and Richter (1956).

Long-period Rayleigh-wave magnitudes are computed by the formula:

$$M_s = \log_{10} (A/T) + 1.66 \log_{10} \Delta - 0.18$$

where

A = maximum peak-to-peak ground motion (millimicrons) of the Rayleigh wave in the period range 16-24 seconds,
T = period of maximum ground motion (seconds),
Δ = epicentral distance (degrees).

Regional Effects on Body-Wave Amplitudes

Spherical spreading and attenuation of seismic energy from LONG SHOT is illustrated on polar projections from Amchitka and its antipode with contours of equal A/T values for Pn, P and PKP waves in Figures 39 and 40. The actual A/T values, taken from Volume I, are not reproduced to allow suitable reduction of the maps. The contours are in A/T units of millimicrons per second measured from zero to peak. Dotted contour lines represent areas of few or

or no recordings. As for the polar projection maps of travel-time residuals, these contoured maps of amplitude are not intended for detailed analysis but only to illustrate the pattern of amplitudes recorded world-wide from LONG SHOT. From the epicenter out to about 30°, LONG SHOT exhibits a circular radiation pattern. Between 30° and 90° distance, the contours outline several areas of high and low amplitudes. Beyond 100° distance, the core interrupts transmission and amplitudes of recorded waves decrease greatly.

Detailed interpretation in North America was possible because of the station concentration and intimate knowledge of the geological structure of this continent. A North American conic projection showing contours and the actual A/T values for LONG SHOT is shown in Figure 41. The contours were drawn with reference only to the actual values in order not to bias the contouring to coincide with tectonic provinces. None the less, North American physiographic provinces can be positively related to these contours. These provinces have already been given in Figure 28. LONG SHOT data shown on a similar conic projection in Figure 41 outlines the Canadian Shield with its high amplitudes. The low amplitudes in western Canada and the U.S. throughout the Coastal Ranges and Cordilleran System are prominent. The Interior Lowlands have high values which extend across the Colorado Plateau. A province of great sediment accumulation and high amplitudes is the Gulf Coastal Plain. The old mountain systems, Wichita and Appalachian, exhibit low amplitude values.

An event at high latitudes (Novaya Zemlya, 27 October 1966 with a 6.3 magnitude) allows a comparison to be made over North America of LONG SHOT amplitudes and those recorded from the large, distant assumed explosive source.

Analogous to Figure 41 for LONG SHOT, Figure 42 illustrates the pattern of recorded amplitudes from the Novaya Zemlya event, which, although fewer values are available, shows basically the same pattern over Canada and the U.S. and supports the validity of notable regional effects on amplitude.

Regional patterns of amplitudes over North America and their relation to tectonic provinces and other measurements such as Pn velocity and gravity have been studied by Jordan et al (1965) and Sutton et al (1967) for explosions and earthquakes, by Cleary (1967b) for earthquakes, and by Currie (1967) for LONG SHOT specifically. These investigators detail more precisely the regional amplitude variations and offer some explanations in terms of upper mantle and crustal structure. Pasechnik (1962) has shown that regional amplitude variations in the USSR are just as prominent as in North America.

P amplitudes at any particular station depend on: 1) radiation patterns of the source, 2) regional effects of upper mantle absorption, 3) local crustal structure at the station itself, and 4) distance from the epicenter. The first effect can be discounted by assuming LONG SHOT was a symmetric explosive source, an assumption which appears valid, as will be discussed more fully under IDENTIFICATION CRITERIA APPLIED TO LONG SHOT. The second is discussed by Sutton et al (1967) and has a very great effect on amplitude. The third, as analyzed by Van Nostrand (1964), could cause large variations in amplitude between stations at the same distance; he shows that, under ideal conditions, signal amplitudes could vary by a factor of four due to crustal structure underlying the stations. The last effect, distance from the epicenter, can be eliminated by changing the

amplitudes to magnitudes with an appropriate distance-correction curve; after this correction the true regional effects on amplitude can be seen more clearly. With this discussion as background we will now proceed into a study of body-wave magnitudes computed for LONG SHOT by the Gutenberg-Richter formula given above.

Body-Wave Magnitude Determination for LONG SHOT

The distance correction factors of Gutenberg and Richter (1956) for body-wave magnitude calculations should render the magnitudes independent of distance. Figure 36, however, shows that LONG SHOT magnitudes still appear to be distance dependent. In the distance range 56°-76°, the magnitudes are mostly above the overall average and in the range 76°-96°, mostly below the overall average. To illustrate this point more clearly, a histogram of average magnitude values for each 5° interval of distance was prepared using all available magnitudes (Figure 43). Seven magnitudes calculated for stations at less than 12° were disregarded entirely because their very high values indicate that the standard distance correction factors are not applicable here. Evernden (1967) has discussed the problems in calculating magnitudes at regional distances. Also, the distance range 10°-30° was divided into only two 10° intervals due to the sparsity of stations. Compared to the overall average of 5.85, the range 20°-45° yields low magnitudes, the range 55°-75° yields high magnitudes, and the range 75°-100° yields low magnitudes again.

Next, to discriminate against effects of doubtful readings, all the questionable magnitudes were discarded (about 100 of the original 274 magnitudes). The remaining stations

still show essentially the same variations about the average magnitude (Figure 44).

The location of stations in the various distance intervals is important, for each 5° interval of distance does not represent a sampling of many varying tectonic provinces. The 20°-45° distance range includes mostly stations along the Cordillera of North America where amplitudes are lower than average for LONG SHOT. Hawaiian stations (35°-40°) cause a slight rise in the low average for the 20°-45° distance range because of their higher than average magnitudes. The 55°-75° distance range gives high values. This range includes stations in the Canadian shield; the stable interior of the U.S.; the Appalachian, Gulf, and Atlantic coastal regions of the U.S.; and the Baltic shield of Europe. Cleary (1967b) has shown that the U.S. stations in this 55°-75° distance range record higher than average amplitudes for natural events also. The range of 80°-85° distance is heavily biased by stations in Germany and France which reported very low amplitudes.

These regional variations in magnitude can be seen in Figure 45, a polar projection from Amchitka Island showing contours of equal magnitude for LONG SHOT. A contour map of North American magnitudes is shown in Figure 46; the magnitude contours clarify the features seen on the amplitude contour map (Figure 41) since the distance effect on amplitudes has been removed.

Most of the variation in magnitude on a regional basis in Figure 46 can be attributed to true regional upper mantle and crustal effects. However, there is indication, according to the histograms in Figures 43 and 44, that the Gutenberg-Richter correction factors may be in error, at least for LONG SHOT. Carpenter et al (1967) and Cleary (1967b) have respectively undertaken statistical studies of explosions

and earthquakes recorded by standardized stations in order to improve the amplitude versus distance relation of Gutenberg and Richter. Figure 47 reveals that Cleary's amplitude-versus-distance curve shows the appropriate deviations from Gutenberg and Richter's in the ranges of distance where LONG SHOT magnitudes are too great or too small. Thus, when magnitude values for LONG SHOT are recalculated using distance correction factors (B) taken from Cleary's curve, the histogram of magnitude in 5° intervals shows smaller deviations from the overall average magnitude as shown in Figure 48. The correction is however, not sufficient to account for the observed variation, and regional effects on magnitude still persist.

These regional effects on magnitude present a problem analogous to the regional effects on travel time. That is, they preclude a precise determination of the event magnitude just as the regional variations in travel time are mostly responsible for the poor location of LONG SHOT. Using the 274 magnitudes, an average value for LONG SHOT is 5.85. With a standard deviation of the individual values of $\pm$ 0.44 from the average, the 95% confidence interval for the average is $\pm$ .05, assuming a normal distribution for the given magnitudes. This is a small number, and to conclude that the LONG SHOT magnitude has been determined to this accuracy, even with 274 observations, is wrong. First of all, it cannot be assumed that the 274 magnitudes are a reasonable sample of the real population of possible magnitudes over the earth. The point is that a different set of 274 values from a network of stations deployed elsewhere around the world could give an average magnitude much different than 5.85. The standard deviation of $\pm$ 0.44 itself means that, statistically, about 33 percent of the stations reported magnitudes deviating more than 0.44 from the mean magnitude. Certain subsets of the

274 stations also give average magnitudes different than 5.85. For instance, the 41-station subset of LRSM stations and VELA observatories in North America gives an average magnitude of 5.97. Regional variations in magnitude, then, are serious enough to lead to estimates of average magnitude which vary significantly. A calibration of the Aleutian area has been achieved, however, in the sense that the magnitude of a similar event in this region can be estimated relative to the LONG SHOT magnitude by employing the same stations used in estimating the LONG SHOT magnitude -- all 274 or some smaller subset common to both events.

One further aspect of the magnitude values obtained for LONG SHOT is worth considering. This is a comparison of the scatter of LONG SHOT magnitudes with that for other explosions and with earthquakes. Figure 49 shows a histogram of magnitude residuals from the 274 teleseismic stations having magnitude values for LONG SHOT. For comparison, magnitude residuals for typical explosions at NTS (Carpenter, 1965) and average magnitude residuals for 17 earthquakes with epicenters in the Aleutian Arc (Currie, 1967) are shown also. It should be noted that Cleary's and Carpenter's results are from North American stations only while the LONG SHOT histogram represents world-wide coverage. Other than the skewness to the right, LONG SHOT shows no significant change in scatter compared to the group of explosions or earthquakes. A recent large explosion at NTS, BOXCAR, produced recordings on the WWSSS network of the USC&GS, and 31 magnitude values were listed on the PDE card for that event. The standard deviation of these values was $\pm$ 0.39, a figure less than obtained for LONG SHOT. Also, 91 magnitude values were taken from the USC&GS for the Novaya Zemlya explosion discussed earlier. The standard deviation of these values is $\pm$ 0.37. Compared to

other large-yield explosions, LONG SHOT then shows a larger scatter in its reported teleseismic magnitudes, but this may be attributed in part to the great number of non-standard stations reporting and the often large concentration of stations in areas of very high (e.g., Hawaii) or very low (e.g., France and Germany) recorded amplitudes.

It is evident then that large regional variations in magnitude will result in large standard deviations for magnitude estimates. The effects are such that magnitude estimates for explosions may have standard deviations as great as earthquakes whose radiation patterns are expected to produce significant deviations in observed magnitudes. This suggests that very precise body-wave magnitude estimates are only obtainable in a relative sense.

Surface Wave Magnitudes

Rayleigh waves from LONG SHOT were observed at 55 stations on records available to SDL. Most of these observations were recorded at the Long Range Seismic Measurements (LRSM) stations. Signal-to-noise ratios were generally very small, and most amplitudes (A/T) and magnitudes are uncertain. Except for the long-period waves observed at Matsushiro, Japan (MAT) and Quetta, Pakistan (QUE), all the observations were in a narrow aperture from LONG SHOT towards North America. This, coupled with the few recordings of long-period data, prevented any detailed analysis of regional effects on long-period amplitudes and of observing a possible radiation pattern.

An earthquake of magnitude 4 is reported to have occurred near the west end of Unalaska Island about 3 minutes after LONG SHOT (Lieberman et al, 1966). Surface waves from this

event would have nearly identical travel times to most North America stations. However, towards MAT and QUE at azimuths of 259° and 305° respectively from LONG SHOT, the surface waves should be well separated in the 16-24 second period range where amplitudes are largest. Careful viewing of these two records showed that, even though Rayleigh waves from LONG SHOT were barely discernible, the waves from the reported earthquake were not evident. On this basis, it is assumed that LONG SHOT surface-wave amplitudes at North American stations are relatively unaffected by this later event.

The Rayleigh-wave (M_s) magnitudes for LONG SHOT versus distance are shown in Figure 38. Just as for the body-wave magnitudes, there is considerable scatter. These surface-wave magnitudes also show regional variations as seen in Figure 50 where contours of equal magnitude have been drawn. This map correlates in gross detail with the body-wave magnitudes in Figure 46. The high magnitudes on the Canadian shield and the low magnitudes in the western Cordillera are present on both. However, variations in surface-wave magnitudes are due to the entire travel path and should not match too closely with regional physiographic provinces.

The average Rayleigh-wave magnitude from the 55 observations for LONG SHOT is 4.06 with a standard deviation of $\pm$ 0.22. The small standard deviation of 0.22 for surface-wave magnitude compared to the body-wave standard deviation of 0.44 shows the former to be a more consistent estimator of event size, at least in this case.

There is then, for LONG SHOT, a difference of 1.79 units between m_b and Ms. Such a large difference between body and surface-wave magnitudes is distinctly atypical for shallow earthquakes but typical for explosions. Brune et al (1963)

and Press et al (1963) have shown this large difference to be normal for NTS shots. This point will be discussed further in the next section of the report.

Lastly, Love waves were not positively identified visually at any station for LONG SHOT. Alexander and Rabenstine (1967) employed a matched filter approach to detecting surface waves from LONG SHOT. Using the waveforms of a reference earthquake in the Aleutian Islands, they filtered the recordings of LONG SHOT around the predicted time of arrival for Rayleigh and Love waves at eight LRSM stations. Love waves were questionably detected at only two stations, JP-AT and WN-SD. The Love wave amplitudes were determined to be about 10 times less than Rayleigh amplitudes at the same stations. Thus, no surface-wave estimate of LONG SHOT could be made using the LQ phase.

IDENTIFICATION CRITERIA APPLIED TO LONG SHOT

Introduction

One of the primary objectives of the VELA program has been to develop seismological criteria for distinguishing between underground nuclear explosions and earthquakes. Prior to LONG SHOT considerable effort had been devoted to establishing diagnostic criteria making use of NTS explosions primarily and earthquakes from both the Western United States and elsewhere. LONG SHOT afforded an excellent opportunity to apply these identification criteria to ascertain their general applicability and limitations for a new source region. As we shall see the principal difficulties for an event the size of LONG SHOT appear to be in obtaining accurate location and depth of focus from teleseismic measurements alone. All the other criteria place LONG SHOT in the general explosion population. However, LONG SHOT was a relatively large explosion (80 kilotons; P-wave magnitude 5.85) and we cannot infer that a smaller explosion in the same area would be as distinct as LONG SHOT.

As mentioned above, since we know the location, origin time, and size of the LONG SHOT explosion it is important to show the degree to which LONG SHOT revealed itself seismologically as an explosion in this new, tectonically active test area. Therefore, in this section we discuss the following identification criteria as applied to LONG SHOT: (1) location and depth of focus, (2) first motion, (3) energy ratios between various arrivals, (4) P-wave spectra, (5) complexity, (6) Rayleigh wave spectra, and (7) radiation patterns.

Location and Depth of Focus

Since both location and depth of focus for an explosion are physically limited by present drilling technology, these parameters can be an important aid in determining whether an event is an earthquake. The location must be on land or in shallow water where drilling and detonations are feasible. This limited technology precludes drilling under deep water and sufficiently far into the sea floor to contain a large nuclear explosion. However, LONG SHOT demonstrates that great caution must be used in dismissing events as earthquakes on the basis of epicenter location, because the unconstrained location of LONG SHOT was 10-20 kilometers north into the Bering Sea (See under ESTIMATES OF LOCATION FROM FAR-FIELD OBSERVATIONS for details).

Similarly the depth of focus for explosions is restricted to relatively shallow depths (less than 5 km) so that the significantly deeper events are earthquakes. Seismologically, the presence of depth phases (pP, pS, etc.) provides a measure of depth. However, some earthquakes at all depths have no observable depth phases, and all explosions, of course, are too shallow to produce records with distinct surface reflections. Thus the primary measure of depth for these events is the result of hypocenter location using first arrivals. Hypocentral depth determinations often are subject to large errors; in fact, for many areas, hypocentral depths determined from first arrivals must be deep into the mantle before the event can be removed from the class of possible explosions. The magnitude of error in depth determination from first arrivals was shown using the SHIFT program as discussed under ESTIMATES OF LOCATION FROM FAR-FIELD OBSERVATIONS. With the depth unrestrained, depth estimates for LONG SHOT of 60 to 80 kilometers were obtained. This places LONG SHOT well into the

general earthquake population. However, no depth phases could be observed, so the depth of focus results must be considered inconclusive. Here again LONG SHOT demonstrates the pratical limitations in using depth of focus as a reliable diagnostic aid for events in new source areas.

First Motion

A compressional spherical wavefront is the prominent feature of an explosion and the character of this wavefront should not change due to propagation through layered media. At any particular station however the direction of first motion may be obscured by either low signal amplitude and/or high background noise.

For earthquakes, tectonic sources show separation of compressional and rarefactional first motion into alternate quadrants described by two orthogonal great circles drawn on the focal sphere. Stauder (1968) shows the fault plane solutions for fifteen events in the Aleutian Island region using not only P but the polarization of S motion as well. The patterns of compressional and rarefactional first motions, where they are clearly defined, are indicative of an earthquake source. However, the first-motion criterion cannot identify explosions, but only earthquakes, since the absence of rarefactions may only indicate that all the recording stations were located within the two compressional quadrants of a tectonic source or that first-motion signal-to-noise ratios were too small for reliability. For LONG SHOT, no distinct rarefactions were observed for any of the stations analyzed at the SDL. A large number of records spanning a wide range of distance and azimuth reproduced in Volume I confirms this. Therefore, LONG SHOT behaved as expected for an explosion.

M_s Versus m_b

The formula which relates Rayleigh-wave magnitude (M_s) to P-wave magnitude, is an empirical relation which, for earthquakes, is given by $M_s = 1.59\ m_b - 3.97$, Gutenberg (1956). It has been shown that nuclear explosions generate smaller surface waves than shallow earthquakes of magnitude 5 and larger (Brune et al, 1963 and Press et al, 1963).

For LONG SHOT, the Rayleigh-wave magnitude of 4.06 compared to the body-wave magnitude of 5.85 indicates that surface waves for LONG SHOT are about 19 times smaller than for an earthquake of the same unified body-wave magnitude. Lieberman et al (1966) obtained a factor of 50 using the relation between Gutenberg's surface wave magnitude and unified body-wave magnitude. They also showed that 29 earthquakes (unified body-wave magnitudes of 4.5-7.0) in the Aleutian region generated surface waves equal to values predicted by Gutenberg (1956) from their unified body-wave magnitudes. On this basis, then, LONG SHOT was distinctly different from earthquakes in the same region. In addition, a comparison of LONG SHOT with values for various events from the same and other source regions listed in Table 4 and plotted in Figure 51, shows that LONG SHOT falls into the explosion population. Thus, LONG SHOT was distinct from earthquakes from the same as well as different regions but typical of explosions.

Energy Ratios Among Various Arrivals

Theoretically, it is well known that excitation of shear energy would not be expected from a purely compressional source in an isotropic homogeneous medium. The fact that some shear energy is observed for most explosions in the form of

Love waves and S waves is one of the complications which makes it difficult to distinguish seismologically nuclear explosions from earthquakes. Generally however, the shear energy associated with explosions is less than that for equivalent P-wave magnitude earthquakes. Press and Archambeau (1962) indicate that the release of tectonic strain for the Nevada Test Site explosions could account for all shear energy observed. Previous studies (Toksöz et al, 1965; Toksöz and Clermont, 1967) have indicated that observations of Love waves for the nuclear explosions Shoal and Bilby in Nevada can be explained in terms of a compressional source accompanied by tectonic strain release. It should also be noted that the shear energy observed for these events may alternatively be due to energy conversions from compressional to shear energy near the source occasioned by the complicated jointing, faulting, and structural variations known to exist there.

For LONG SHOT, short-period and long-period horizontal-component seismograms from over 150 stations were available to the SDL. From visual analysis of the short-period records, it appears that shear phases were recorded by only three stations (ScP at stations Hailey, Idaho, and Yreka, California, and S at station Shillong, India). The ScP phase may in fact be PcS and therefore not attributable to shear energy released at the source. P-phase signal-to-noise ratios at these three stations exceeded 250. The one observation of a direct shear phase for LONG SHOT (at Shillong, India, $\Delta = 69°$) give a SH/P ratio of 0.076.

On the long-period seismograms, shear phases, including Love waves, are not identifiable by visual means. Although signal-to-noise ratios are small for Rayleigh waves from LONG SHOT, the ratio LQ/LR <0.2 from the matched filter surface wave analysis (Alexander and Rabenstine, 1967).

The fact that the SH/P and LQ/LR ratios are very small or for the most part not measurable, coupled with the compressional first motions discussed above strongly suggests that the source mechanism of LONG SHOT was nearly an ideally compressive one as expected for an explosion.

One earthquake of the same P-wave magnitude located near the LONG SHOT site gave energy ratios substantially larger than those for LONG SHOT (see under COMPARISON OF LONG SHOT WITH EQUIVALENT MAGNITUDE EARTHQUAKES IN THE ALEUTIAN REGION). If this earthquake is representative of earthquakes in this region, as other evidence suggests, then we must conclude that LONG SHOT is very atypical for this region.

P-Wave Spectra

Kelly (1968) shows that the ratio of integrated P amplitude spectra between 0.4 and 0.8 cps to the integrated amplitude spectra between 1.5 and 1.9 cps at LASA separates shallow earthquakes from explosions. That is, for 48 shallow earthquakes from the Soviet Union, China and Eastern Europe, including Greece and Turkey, relatively more long-period P-wave energy is excited by earthquakes than by 19 explosions chiefly from one site in the USSR.

This P spectral ratio for LONG SHOT is 0.67 and m_b is 6.27 computed from the record at the center instrument (LAO) of LASA. This point plotted on Figure 52 falls well into the explosion population.

Complexity

Theoretically, an explosion can be considered a point source causing a sharp arrival of P-wave energy at a recording

station. Complicated earthquake source mechanism plus depth phases causes more prolonged arrival of P energy. Carpenter (1965) illustrates the difference between explosions and earthquakes recorded at British arrays by an integration through time of the arriving seismic energy.

Kelly (1968) shows that complexity (inverse ratio of the energy received in the first five seconds of the P phase to the subsequent 30 seconds) determined at LASA for 48 shallow earthquakes and 19 explosions from the Soviet Union, China and Eastern Europe, including Greece and Turkey, tend to separate into two populations, earthquakes and explosions (Figure 53). The complexity factor for LONG SHOT (Fc = 2.14 at the center (LAO) of LASA) is also plotted in Figure 53. This point falls well into the explosion population as designated by Kelly.

Rayleigh Wave Spectra

Keylis-Borok (1960) predicted theoretically that differences should occur in surface-wave spectra between earthquakes and explosions. Pasechnik et al (1960) reported empirical differences in these spectra. As a gross measure of differences in spectra, Turnbull et al (1968) determined ARZ (area enclosed by the Rayleigh wave) and ERZ (total energy in the Rayleigh wave) for LONG SHOT and compared these two quantities with 6 explosions and 12 earthquakes from various seismic regions. (The definitions of ARZ and ERZ are explained more fully under COMPARISON OF LONG SHOT WITH EQUIVALENT MAGNITUDE EARTHQUAKES IN THE ALEUTIAN REGION).

Rayleigh wave spectra for LONG SHOT are shown in Figures 86 through 94 and Appendix III. These will be examined in more detail in the next section.

Table 4 lists the events and pertinent epicenter data. Figures 54 and 55 show ARZ and ERZ respectively. The LONG SHOT quantities fall into the explosion population for both measurements.

Radiation Patterns

Important differences in body and surface wave radiation patterns between earthquakes and explosions should exist. The elastodynamic source theory due to Archambeau (1964) indicates that explosions (assumed to be purely symmetrical sources in a homogeneous, non-jointed half space) should have symmetrical radiation patterns and that earthquakes (assumed to be asymmetrical sources) should have asymmetrical radiation patterns. Other studes (Toksöz et al, 1965; Toksöz and Clermont 1967) have shown that observations of non-circular radiation patterns for the nuclear explosions, Hardhat, Haymaker, Shoal and Bilby can be explained in terms of a compressional source accompanied by the release of tectonic strain. (Other equally valid explanations exist, however.)

The information contained under RECORDED AMPLITUDES AND MAGNITUDE DETERMINATIONS shows quite dramatically that amplitudes for short-period body waves are greatly influenced by path and site response. To describe quantitatively the radiation pattern of LONG SHOT, the program RADPAT (Jarosch, 1968) was used. This program determines the dip, slip, and strike of a standard double couple source model for the best least squares fit to body-wave magnitudes. Since RADPAT contains only the body-wave double-couple representation for a source mechanism, no meaningful solution would be expected for a purely compressional source; but for the combination source mechanism (compressional + tectonic strain release) a

meaningful solution would be expected assuming that the variance in magnitudes due to radiation pattern is greater than the variance caused by site response (perhaps a poor assumption).

RADPAT was used on LONG SHOT P-magnitude data with this in mind. A solution (strike = 55°, dip = 50°, and slip = 100°) was obtained from 40 stations having reliable magnitudes in all quadrants from LONG SHOT. It is interesting to note that the strike angle of 55° corresponds approximately to the direction of fracturing near the LONG SHOT epicenter (see Figure 6). However the above solution is considered less than good. The criterion for stating this is that the variance (0.17) of the 40 input magnitude values with respect to their mean was less than the standard deviation (0.21) of the input magnitudes with respect to the predicted magnitudes resulting from the source parameters computed by RADPAT. Thus, the radiation pattern for the double couple failed to fit the observed magnitudes better than a circle of radius equal to the mean of the observed magnitudes. We conclude that the far-field radiation pattern was symmetric and most characteristic of an explosion. Stauder (1968) shows radiation-pattern solutions for earthquakes in the Aleutian region which are distinctly different for both P and S waves. Also see Jarosch (1968).

With regard to the non-linear near-source effects recorded from a cone of upward traveling rays (see under NEAR SOURCE BEHAVIOR) versus the small cone of downward ray paths for body waves received at teleseismic distances from LONG SHOT, no quantitative correlation between near-field and far-field P-wave radiation patterns appears feasible.

Following this result for the short-period P phase, no attempt was made to compute a source mechanism solution for LONG SHOT using the long-period Rayleigh wave magnitudes which are confined to a narrow azimuthal sector except for

stations Matsushiro, Japan, (MAT) and Quetta, Pakistan, (QUE). The interaction of body waves with the free surface or plane layering is responsible for the excitation of Rayleigh waves. No similarities are observed between the near-source non-linear effects (under NEAR SOURCE BEHAVIOR) and the Rayleigh wave magnitudes (Figures 15, 16, and 56). However, it is apparent that a slightly non-circular Rayleigh-wave pattern exists in Figure 56. The larger magnitude values in the north sector correspond to the group of stations across the Canadian shield and into northeastern United States. The smaller magnitude values correspond to a profile, passing through the Rocky Mountains and into southwestern United States. This is very probably a path effect and not a true source effect.

Thus, from body-wave information, a circular (symmetric) radiation pattern would seemingly be the most valid answer. However, from the discussion under RECORDED AMPLITUDES AND MAGNITUDE DETERMINATIONS, it would be possible to select other subsets of stations and obtain a statistically meaningful apparent radiation pattern, which may or may not be due solely to path and regional effects on the P amplitudes.

Insufficient azimuthal data on Rayleigh-wave amplitudes and the uncertain effects of travel path preclude the determination of a radiation pattern for the surface wave.

Summary

The accompanying table summarizes the results of applying the various discriminates discussed above to LONG SHOT. It is clear that, except for inconclusive evidence on location and source depth, the results for LONG SHOT place it well into the explosion population as based on our current experience in comparing earthquakes and explosions from

Identification Criterion	Characteristic of An Explosion?	Comments
Location and depth of focus	?	The results from the locate program indicate a location some 20 km north of the actual epicenter with 60 to 80 km depth. However, no depth phases were observed.
First motion	yes (?)	There were no definite rarefactions observed at SDL; however, first motion criterion can not identify explosions, only earthquakes which give rarefactions at some stations.
Surface wave::body wave magnitude (M_s::m_b)	yes	Compared with observations for shallow quakes from many seismic regions including the Aleutian arc and a number of explosions, LONG SHOT clearly falls in the explosion population.
Energy ratios between various arrivals	yes	No shear phases, LP or SP, were observed except for SP where SNR were greater than 250 or LP matched filter techniques were applied.
P-wave spectra	yes	The spectral ratio criterion was satisfied at LASA. Further comparisons were not possible due to lack of "standard" curves for other sites.
Complexity	yes	The criterion was satisfied at LASA. Further comparisons were not possible due to lack of published "standard" curves.
Rayleigh wave	yes	ARZ and ERZ are essentially spectral measures of M_s. Further study of individual Rayleigh wave spectra is necessary to define the relation between Rayleigh wave spectra and m_b for Aleutian events.
Radiation patterns	yes(?)	Radiation patterns of LONG SHOT are affected by path and site effects, but still appear quite symmetrical. Earthquakes in the same area show distinct radiation patterns.

LP = Long period
SP = Short period
SNR = Signal-to-noise ratio

various parts of the earth. In fact, in several respects (e.g., M_s versus m_b, and energy ratios) LONG SHOT was more "explosion-like" than events of comparable size at NTS. Based on limited evidence for earthquakes from the LONG SHOT source region it appears that LONG SHOT is also distinctly different from the earthquake population in the same area. However, we need results from a larger sample of earthquakes to establish conclusively that none are as atypical as LONG SHOT.

Therefore, LONG SHOT produced no major surprises in terms of the identification criteria developed previously. It did, however, demonstrate that we still have difficulty in accurately locating events and determining their focal depths.

COMPARISON OF LONG SHOT WITH EQUIVALENT MAGNITUDE EARTHQUAKES IN THE ALEUTIAN REGION

Scope of this Comparison

The objective of this section is to determine more quantitively the differences between LONG SHOT and typical earthquakes in the Aleutian Islands within the general framework of criteria discussed in the previous section.

The procedure is to use data for events close to the LONG SHOT location so that the effects of path and receiving site can be minimized with the use of common recording stations. We consider primarily two events, 6 November 1965, and 22 November 1965, which had a surface-wave magnitude and a body-wave magnitude, respectively, equivalent to those for LONG SHOT. It is important to note that there is observational evidence suggesting that these events are typical of many large shallow earthquakes from that region (Stauder, 1968; Liebermann et al, 1966; Turnbull et al, 1968; and Jarosch, 1968). Pertinent epicenter data for these two events are listed in Table 5.

In addition to comparing the events for such standard criteria as first motion, M_s versus m_b, etc., we also include in this section comparisons of interference of the pP-P type, and spectral shape and spectral ratios for various body and surface wave arrivals.

First Motion

As stated under IDENTIFICATION CRITERIA APPLIED TO LONG SHOT, there appear to be no distinct rarefactional first motions on LONG SHOT records. For the 22 November 1965 earthquake in the Rat Islands, only 2 of 88 observed first motions

are listed as dilatational by Jarosch (1968). Stauder (1968) shows only compressional first motion since the stations used are in one quadrant only. For this criterion, then, the explosion and earthquake of the same m_b do not appear to differ significantly and the earthquake appears to be in the general explosion population.

Amplitude Ratios

The near absence of shear arrivals for LONG SHOT was discussed under IDENTIFICATION CRITERIA APPLIED TO LONG SHOT, and this serves as a good diagnostic aid. For comparison, seismograms from 22 LRSM and 55 WWSSS stations recording the 22 November 1965 earthquake were visually analyzed. A direct shear phase was observed at 32 stations on the short-period components and at 61 stations on the long-period components. Also, long-period P phases were observed at most stations while none were observed for LONG SHOT. The average amplitude ratios of S_v/P and S_h/P are 0.15 and 0.26 respectively for short-period recordings and 0.38 and 0.44 for long-period recordings of this earthquake. The single observed S phase for LONG SHOT (at Shillong, India, $\Delta = 69°$) gave a S_h/P amplitude ratio of .076 which is about 3.5 times less than that for the earthquake. It is very significant that there were no observable long-period P or S phases recorded for LONG SHOT with which to compare the earthquake ratios.

In addition, for the 22 November 1965 earthquake, Love waves were readily identifiable at 60 of the 73 stations analyzed, and the average LQ/LR ratio is 0.62. Under IDENTIFICATION CRITERIA APPLIED TO LONG SHOT, it was noted that the LQ/LR ratio was less than 0.2 for LONG SHOT; this is an upper bound because of the uncertainty of the Love wave

identifications for LONG SHOT.

Thus, LONG SHOT excitated very little shear energy and that which was observed gave shear-to-compressional ratios three to four times less than the amplitude ratios of the 22 November 1965 earthquake in the Rat Islands of equivalent body-wave magnitude.

Short-Period Amplitude Spectral Ratios

The presence of long-period P for the 22 November 1965 earthquake and the absence of this phase for LONG SHOT proves that a different or at least a broader range of frequencies is generated by the earthquake. Since there are only two short-period phases, P and PcP, consistently recorded for LONG SHOT, a spectral comparison with the earthquake is then limited to amplitude spectra for these phases.

Thirteen P and ten PcP amplitude (A/T) spectra for stations common to LONG SHOT and the 22 November 1965 earthquake are shown in Figures 57 through 68. An additional twenty-nine P and twenty PcP amplitude spectra for LONG SHOT are shown in Appendix I. These figures also show the corresponding signal analyzed. From visual inspection of amplitude spectra of the 13 P and 10 PcP phases at common stations (Figures 57 through 68), it is clear that peak amplitudes occur at lower frequencies for the 22 November 1965 earthquake than for LONG SHOT. Inspection of all P and PcP spectra for LONG SHOT indicates the presence of nulls in the amplitude spectra in the range 1.7 to 2.1 cps. The significance of these nulls will be discussed later in this section.

All short-period seismograms were digitized at 20 points per second (pps) except from stations YKA, EKA, GBA and WRA which were sampled at 10 pps. Prior to digitization, all

records were band-passed filtered between 0.017 and 10.0 cps, with a 48 db/octave cutoff.

Amplitude spectra are estimated using the SDL subroutine GRTZSPEC, a program which computes sine-cosine Fourier transforms. Care is taken in the selection of signal end points, and both ends are tapered with a cosine function to prevent truncation errors.

Amplitude spectra are computed for a signal and a noise sample of equal length; then the noise spectrum is subtracted. Further, corrections for static magnification and system response are applied, and the spectra are plotted for a frequency band of 0.2 to 6.0 cps in terms of A/T (mμ/sec). Signal sample lengths range from 2.5 to 4.5 seconds (real time) after the first detectable motion of the P or PcP phase.

Kelly (1968) discusses an approach for event discrimination which uses the ratio of integrated amplitude spectra from 0.4 to 0.8 cps to the integrated amplitude spectra from 1.5 to 1.9 cps. Using the thirteen stations common to both LONG SHOT and the 22 November 1965 event, P spectral amplitude ratios were calculated in a manner similar to Kelly's as follows:

$$R = \sum_{f_1}^{f_2} A(f_i) / \sum_{f_3}^{f_4} A(f_i)$$

$A(f_i)$ = value of amplitude spectrum at each 0.1 cps interval

f_1 = 0.5 cps

f_2 = 1.0 cps

f_3 = 1.1 cps

f_4 = 2.0 cps.

The choice of frequency bands employed is arbitrary. Ratios calculated are listed in Table 6 and plotted as a function of distance in Figure 69. For LONG SHOT, disregarding PG-BC, the amplitude spectral ratios obtained are less than 2 whereas those from the reference earthquake range from 2 to 10. The large spectral ratio at PG-BC for LONG SHOT is attributed to an anomalously low-signal-to-noise ratio. This systematic difference in short period P-wave spectral ratios clearly shows more energy present in the lower frequencies for the 22 November 1965 earthquake relative to LONG SHOT.

Depth of Focus

The visual analysis of the LRSM records across North America for the 22 November 1965 event revealed a depth phase pP which was consistent from station to station and which resulted in a depth calculation of approximately 20 km. Thus this event could be tentatively classified as an earthquake on the basis of focal depth alone.

LONG SHOT recordings, on the other hand, showed no consistent phases other than P, PcP, and PP within the first few minutes of signal. This lack of a pP phase would tentatively classify it as a possible explosion. However, as discussed under ESTIMATES OF LOCATION FROM FAR-FIELD OBSERVATIONS and IDENTIFICATION CRITERIA APPLIED TO LONG SHOT, the unconstrained depth estimated from first arrivals for LONG SHOT gave a depth of 60-80 km. Since some relatively deep earthquakes do not have clearly observable depth phases, the absence of pP at the times expected for 60-80 km source depth is not sufficient to prove that this depth estimate is erroneous. All we can really say at this point is that the evidence on depth of focus is inconclusive. This result for

LONG SHOT illustrates the difficulty in obtaining reliable depth estimates in a new source region even when the event is large and well-recorded.

A technique for finding small pP time delay and relating it to depth for an explosions has recently been presented by Cohen (1969). On the basis of this work the presence of nulls in the LONG SHOT P and PcP amplitude spectra may be due to the interference of pP with P, and of pPcP with PcP. However, nulls may also result from interference of crustal reverberations at the recording stations. Phase interference of P-pP type may be represented by the formula:

$$Z(t) = y(t) + \beta y(t + \tau)$$

where

τ = delay time associated with the surface reflection,
$y(t)$ = initial source time function,
β = the surface reflection coefficient (≤ 1.0).

The power spectra of Z(t) is then:

$$P(\omega) = \left| \int_{-\infty}^{\infty} z(t)\, e^{-i\omega t}\, d\omega \right|^2$$

which becomes

$$P(\omega) = |Y(\omega)|^2 [1 + \beta^2 + 2\beta \cos\omega\tau].$$

Therefore, troughs in the spectra will occur $1/\tau$ cps apart. Further, for a free-surface reflection ($\beta = -1.0$), the first null occurs at the frequency of $1/\tau$ cps.

The relation between the first null frequency (f_n) and the depth of an explosion is given by:

$$1/f_n = \tau = 2d\left[\frac{1}{\bar{V}\cos\theta} - \frac{\tan\theta}{V_{Pn}}\right]$$

where

θ = take-off angle,
$\bar{V}$ = average P velocity from source to surface-air interface,
V_{Pn} = Moho velocity,
d = vertical distance to source from surface.

For teleseismic distances this can be adequately represented by:

$$\tau = 2d/\bar{V}.$$

Summation of normalized spectra from many stations should retain the coherent nulls due to depth phases and remove random nulls and those caused by site reverberations, since a slight variation in site structure significantly alters the interference pattern. Figure 70 compares the sum of the spectra at the thirteen stations common to LONG SHOT and the 22 November 1965 earthquake. This figure also shows the summed spectra for all the LRSM stations recording LONG SHOT. To obtain the sum, the basic A/T spectra described above were first reduced to amplitude spectra, squared, and then normalized so that the shape of the spectrum at each station would be given equal weight. These normalized spectra were summed and divided by the number of stations to obtain the average power spectrum for each event.

The smoothness of the LONG SHOT spectrum relative to the earthquake spectrum is apparent in Figure 70. This may be

due to factors of both source depth and source mechanism. The differences between the spectra of LONG SHOT and the earthquake below 1.7 cps are evident. These differences were revealed generally by the spectral ratios discussed in this chapter.

In regard to Cohen's method of depth estimation, the deep troughs in the LONG SHOT spectra in Figure 70 at about 1.8, 3.9, and 5.2 cps are important. No significance should be attached to the first apparent trough at 0.5 cps since the sample length (always less than five seconds) used in determining the basic A/T spectra cannot provide good spectral estimates below 0.5 cps. The trough at about 1.85 cps is taken as the first null in the LONG SHOT spectra. This given $\tau = 0.54$ for the above formulas. Using an average compressional-wave velocity from source to surface at the LONG SHOT site of 3.38 km/sec (under PHYSICAL SETTING OF THE LONG SHOT EVENT), the estimate of source depth is about 914 meters, or 30 percent greater than the actual depth of 702 meters. The two other dominant troughs in the LONG SHOT average spectra at about 3.9 and 5.2 cps occur nearly at increments of $1/\tau$ cps above 1.8 cps and support the choice of 1.8 cps as the first null frequency.

It is evident in Figure 70 that the 22 November 1965 average spectrum does not show similar troughs indicating interference of pP and P; indeed it should not because the pP arrival is beyond the time window (about the first five seconds of signal) used to compute these spectra. Thus, this additional information would suggest a very shallow depth (<1 km) for LONG SHOT, and a pP-P interval greater than 5 seconds (hence depth greater than 10 km) for the earthquake.

Complexity Factors

Carpenter (1965) illustrated the difference between explosions and earthquakes recorded at British arrays by integration through time of the arriving seismic energy. The P-wave coda for earthquakes is usually observed to be larger than that for explosions due to the more complex nature of the source and additional depth phases. This has led to the definition of a complexity factor (F_c) at the SDL where events recorded at LASA are routinely analyzed to test this diagnostic aid.

The method involves squaring the digitized signal amplitudes and integrating the result with a three-second integration window moved by increments of one-twentieth of a second to produce each point on the integrated trace. The square root of this trace is then taken as the final trace. The portion of the record used is from 30 seconds before the P arrival to 35 seconds after. A noise correction is subtracted from the signal on the final trace using a 30-second noise sample just prior to the P arrival. The last step is to calculate F_c by ratioing the noise-corrected area of the final trace as defined above from 5 to 35 seconds after the signal to the noise-corrected area of the final trace for the first 5 seconds of signal.

Complexity factors for fourteen stations calculated in this manner for LONG SHOT and the 22 November 1965 earthquake are tabulated in Table 7. The corresponding plots of the signal traces, SPZ, the squared signal trace $(SPZ)^2$, the squared signal trace integrated, $\overline{(SPZ)^2}$, and the square root of the squared signal trace integrated, $[\overline{(SPZ)^2}]^{\frac{1}{2}}$, are shown in Figure 71 to 84 for the two events. Complexity factors for additional stations (LRSM, VELA, AWRE, and the LASA center seismometer) recording LONG SHOT on tape are given in

Appendix II. Table 7 shows that only two stations (WN-SD and BE-FL) of the fourteen used for comparison had a factor higher for LONG SHOT than for the earthquake. Strong noise bursts at WN-SD may explain it's being atypical, but there is no apparent reason for the result at BE-FL. Over all, the complexity factor appears to be a good discriminant between LONG SHOT and the earthquake as there is a factor of nearly two between the average values of F_c. However, we need complexity factors for many more earthquakes to assure that this earthquake is typical of the Aleutian source region as assumed.

The complexity factor reflects the time distribution, as defined above, of P energy arriving at a station, and therefore complexity should be distance dependent. A plot of F_c versus distance for both LONG SHOT and the 22 November 1965 earthquake is shown in Figure 85. This plot shows an overall decrease in the value of F_c with distance and also shows the separation of LONG SHOT complexities from those for the earthquake. This figure points out that average complexities should be interpreted carefully, for an average from near stations would be much different than an average from distant stations. Complexity is meaningful in studying several events only when these events are at approximately the same distance from the stations.

Figure 85 shows considerable scatter in the values of F_c with distance. This may be due to at least three factors: (1) number of direct arrivals within the 35 second signal interval over which F_c is computed, (2) azimuthal variation in the geologic structure surrounding the source, and (3) differences in crustal structures at the receiving stations. The second cannot be a significant factor here because all stations except NP-NT and the AWRE arrays are in the sector of 45°-85° azimuth from LONG SHOT and the earthquake and

because stations at nearly the same azimuth (e.g., WS-AT and JP-AT) show large differences in the value of F_c. The third cannot be discussed in detail here but does deserve thorough study because of its potentially strong effect upon the complexity factor.

The factor of multiple arrivals can, however, be discussed. Shear arrivals occur within 35 seconds after the first compressional arrival only at short epicentral distances. The arrival time of the phase pP is depth dependent and may have significant influence on the value of F_c if it is a strong surface reflection from an earthquake. The arrival time of the phase PP is more than 35 seconds after P for $\Delta > 25°$. However, there remain in the 35-second interval after the first P arrival other direct mantle arrivals which are associated with cusps in the travel time curve. Julian and Anderson (1968) present travel-time curves derived from the earth models of various investigators, and these show that the greatest distance at which to expect more than one direct arrival through the mantle to a recording station is about 40°.

Beyond the distance of 40° the seismograms of explosions should contain only P and its reverberations within the crustal structure at the source and at the station within 35 seconds after the first motion. For LONG SHOT, Figure 85 vaguely suggests that this occurs. The data are actually too sparse and crustal structure at the station is probably too overriding a factor to permit a detailed comparison to be made between the values of F_c for LONG SHOT and branches of travel-time curves for $\Delta < 40°$.

M_s Versus m_b and Energy Relationships

The method of plotting surface-wave magnitude versus

body-wave magnitude is straightforward and provides an excellent criterion for distinguishing between explosions and shallow earthquakes as seen in Figure 51. In particular, LONG SHOT is well separated from the 22 November 1965 earthquake which has very nearly the same m_b as LONG SHOT. The 6 November 1965 earthquake also conforms to the expected pattern for an earthquake. Data on the other sixteen events plotted are given in Table 4. Included in Figure 51 are many Aleutian Island earthquakes used by Liebermann et al (1966) and this shows that LONG SHOT can be clearly distinguised from these events.

Because the M_s measurement corresponds to only a small portion of the surface wave at about twenty-seconds period where maximum trace amplitudes occur, certain investigators have sought to improve the surface-wave measurement by including the whole wave train. Originally, Brune et al (1963) used the (AR) included in the envelope of surface waves recorded by a standard seismograph with a given magnification to distinquish between earthquakes and explosions. They show that earthquakes have larger values of AR than explosions having comparable body-wave magnitudes.

Turnbull et al (1968), in developing an automated process for calculating this value for Rayleigh waves, redefined AR as

$$ARZ = \int_{T_1}^{T_2} |f(t)|dt$$

where f(t) is the time series and T_2-T_1 refers to a time interval for an appropriate group velocity window. Since this quantity has no real physical meaning, they then defined a quantity ERZ as being proportional to the total energy in the Rayleigh wave:

$$ERZ = \int_{T_1}^{T_2} f^2(t)\, dt$$

For this analysis, all long-period seismograms were digitized at 4 pps and band-passed filtered between 0.002 and 0.5 cps, with a 24 db/octave cutoff. The digitized time series is then band-passed filtered between 0.02 and 0.10 cps, detrended, tapered, and corrected for static magnification. The ARZ for a signal and a noise sample is computed using Simpson's rule of integration. The ARZ for the noise is ther subtracted from the signal ARZ. For the ERZ, the amplitude spectrum is calculated for a signal and a noise sample by Fourier transformation, corrected for system response, and squared. The noise energy spectra is then subtracted from the signal energy spectra and the result is integrated between 0.02 and 0.067 cps to obtain the value of ERZ. The ARZ and ERZ values for a given event show considerable scatter when plotted as a function of distance. Turnbull et al show that the scatter is significantly reduced when these values are normalized according to the difference between the station magnitudes and the average surface-wave magnitude of the given event. A least-squares curve is then fit to the individual values, and a value read from this curve at 1000 km distance is assigned as the ARZ and ERZ for the given event.

Figure 54 showed ARZ versus m_b for the events listed in Table 4. The 22 November 1965 earthquake gives an ARZ 15.7 times greater than that for LONG SHOT. The plot of ERZ versus m_b, Figure 55, indicates that the ratio of total Rayleigh-wave energy of the 22 November 1965 earthquake to LONG SHOT is 175. Using the matched filter method Alexander and Rabenstine (1967) obtained similar relative excitation of Rayleigh waves for this same pair of events.

It is clear that the 22 November 1965 earthquake does

contain more Rayleigh-wave energy than LONG SHOT. Moreover, the M_s vs m_b data from the Aleutians discussed earlier shows that Rayleigh excitation for this earthquake is typical of that region. Further, for the additional events listed and plotted, earthquakes and explosions having comparable body-wave magnitude belong to distinctly different populations even though many differing source regions are represented. Therefore, our previous confidence in this diagnostic criterion was strengthened by the LONG SHOT results.

Rayleigh-Wave Spectra

For comparative purposes, Rayleigh-wave spectra for stations common to LONG SHOT and the 22 November 1965 (m_b = LONG SHOT) earthquake are presented in Figures 86 to 88. Comparison of LONG SHOT with the 6 November 1965 (M_s = LONG SHOT) earthquake is made in Figures 89 to 94. Long-period spectra for the remaining LRSM and VELA stations which recorded surface waves from LONG SHOT are included in Appendix III.

In order to detect possible differences in long-period spectral content between LONG SHOT and the two earthquakes, the spectra for common sets of stations were summed for each event (sixteen for the 6 November event and eight for the 22 November event) in the same manner as the short-period spectra as described in this chapter under Depth of Focus. The process of summing smears out the spectrum because of frequency dependent attenuation with distance. The peak frequencies in the sum are thus less distinct. However, as long as the same set of receivers is averaged, the composite is still meaningful for comparison of events.

The results for the 6 November 1965 earthquake and LONG

SHOT are shown in Figure 95. Here it is evident that LONG SHOT generated a smoother and somewhat flatter spectrum but does not differ significantly in the frequencies at which peak energy is observed. The results for the other event on 22 November 1965 and LONG SHOT are shown in Figure 96. In this case LONG SHOT again shows a somewhat flatter spectrum; however, there is about a 0.015 cps difference in the frequency interval at which peak energy is observed. The LONG SHOT summed spectrum peaks at about 0.058 cps and the earthquake at about 0.043 cps. In the case of the 22 November 1965, the absolute level of the power spectra has been scaled down to the level of the LONG SHOT power spectrum in order to compare the shapes of the spectra, not their absolute level. The large peaks and troughs in the summed LONG SHOT spectrum beyond 0.075 cps probably indicate that noise is dominant on most recordings above this frequency. Visual analysis of records confirms this.

Using events in the same source region, we have shown that the Rayleigh-wave spectra from LONG SHOT are recognizably different from those of an earthquake of equivalent body-wave magnitude, 22 November 1965. On the other hand, LONG SHOT Rayleigh-wave spectra do not significantly differ from those of an earthquake having an equivalent surface-wave magnitude, 6 November 1965. Since these shallow earthquakes appear to be typical of this source region, this suggests that spectral shape as well as excitation level of Rayleigh waves vs m_b may be useful in identifying explosions seismologically. Much additional data are needed, however, to assess the utility of this approach for small events.

Radiation Patterns

As discussed under IDENTIFICATION CRITERIA APPLIED TO

LONG SHOT, the radiation patterns for Hardhat, Haymaker, Shoal, and Bilby can be explained in terms of a compressional source accompanied by the release of tectonic strain. (Other equally valid explanations exist, however.) This strain release is represented by a double-couple source model. A double-couple solution is also shown for the 1962 Fallon, Nevada, earthquake in Toksöz et al, 1965. All solutions for the above events are based upon some "amplitude equalization" method (Toksöz et al, 1964). "Amplitude equalization" simply means correcting the ground displacement for propagation effects. The source mechanism solutions for the explosions, Bilby and Shoal, and the Fallon earthquake are derived from the ratios of Love-wave amplitudes to Rayleigh-wave amplitudes.

For the 22 November 1965 earthquake, a double couple source mechanism solution (strike = 90°, dip = 50°, slip = 70°) was obtained using body-wave magnitudes in the program RADPAT, as compared to LONG SHOT where a circular pattern was the best fit (under IDENTIFICATION CRITERIA APPLIED TO LONG SHOT). With these parameters, theoretical radiation patterns for Love-to-Rayleigh-wave ratios, Love-wave amplitudes, and Rayleigh-wave amplitudes are computed. To obtain Love-to-Rayleigh-wave amplitude ratios comparable to the observed ratios, the depth had to be decreased from the reported 40 km (USC&GS) to 20 km. Observed and theoretical ratios are plotted in Figure 97. Both theoretical Love and Rayleigh amplitudes are normalized to show magnitude patterns relative to the observed magnitude (Figure 98 and 99).

Since three nodal points and one lobe are well defined, it is evident that observed ratios of Love-to-Rayleigh-wave amplitudes show a more definitive pattern than either of the patterns taken individually. However, the scatter of data points is considerable. Turnbull et al (1968) show that

applying a correction for station site response to the ERZ (total energy in the Rayleigh wave) does not significantly reduce the scatter of ERZ as a function of distance for this crust. Other factors, such as improper orientation of horizontal instruments and different transmission functions for the two phases observed at the same station, must therefore be of importance.

The Love-Rayleigh-wave amplitude result lends strength to the source mechanism determination obtained from body wave measurements and the RADPAT program. However, the scatter of data is considerable and no claim of uniqueness can be made.

Three other facts of importance in this event comparison are: (1) differences in individual station spectra of the two events are a measure of relative excitation at the source since the propagation paths are almost identical; (2) for LONG SHOT no "amplitude equalization" is possible without either knowledge of the crust and mantle structure or additional phase information such that the path and site effects can be accurately taken into account; and (3) for an explosion in a nonstressed homogeneous medium, a circular Rayleigh-wave radiation pattern would be expected, and for the fault-plane solution obtained by Jarosch (1968) for the 22 November 1965 earthquake the theoretical Rayleigh-wave pattern is also nearly circular.

Comparing observed Rayleigh-wave magnitude points between LONG SHOT and the 22 November 1965 earthquake, similarities in their azimuthal variations are apparent (Figures 56 and 99). Since LONG SHOT is known to be an explosion such variations are probably path effects which produce an apparent radiation pattern.

Overall however, for LONG SHOT both body and Rayleigh

wave data give approximately circular radiation patterns which are indicative of an ideally compressive source. The body wave amplitude (not first motion) data for the 22 November 1965 earthquake supports an assymmetrical radiation pattern (Jarosch, 1968), while the Rayleigh wave data supports a nearly circular radiation pattern. However, the variance observed in the teleseismic data reinforces our view that radiation patterns at best can be only diagnostic aids, since this earthquake which we consider typical of the Amchitka source area gives results so similar to LONG SHOT for both first motion and Rayleigh waves.

Summary

The accompanying table summarizes the results of applying the various discriminants discussed above to LONG SHOT and the 22 November 1965 earthquake. It shows to what extent the events do or do not separate. We conclude generally that LONG SHOT is anomalous as compared to the 22 November 1965 earthquake for which there is independent observational evidence suggesting that this earthquake is typical of many large shallow earthquakes from the Aleutian region. However, there were several similarities between LONG SHOT and the earthquakes investigated which deserve further analysis using a much larger sample of earthquakes. Such areas for further research, for example, is suggested by the comparison of the 6 November 1965 earthquake Rayleigh-wave spectra with LONG SHOT Rayleigh-wave spectra, where m_b (earthquake) < m_b (LONG SHOT) and M_s (earthquake) = M_s (LONG SHOT). The Rayleigh wave spectra for this pair show little or no apparent differences in level or shape. Similarities between the 22 November 1965 earthquake and LONG SHOT (equal m_b events) which need further study include the Rayleigh-wave radiation pattern and first motion. Clearly we need to examine a much larger sample of earthquakes from the Aleutians

Summary of the preceding sections tabulated for LONG SHOT and the 22 November 1965 earthquake.

Identification Criterion	Do the Events Separate?	Comments
First Motion	No	Only two stations of many showed dilatation for the 22 Nov. 1965 earthquake, Jarosch (1968).
Amplitude Ratios (SH/P and LQ/LR)	Yes	The amplitude ratios for the earthquake were at least 3 to 4 times larger than the ratios for LONG SHOT.
Short-Period Spectral Ratios	Yes	Spectral ratios for the earthquake range from 2 to 10 whereas for LONG SHOT all but one ratio was less than 2 (atypical of earthquakes).
Depth of Focus	?	Identification of pP for the earthquake was made in the time domain for LONG SHOT it was determined in the frequency domain. Unconstrained depth from first arrival data was 60-80 km well into earthquake population.
Complexity Factors (F_c)	Yes	There was nearly a factor of 2 between F_c for the two events.
M_s::m_b and Energy Relationships	Yes	The earthquake has 175 times more Rayleigh wave energy than LONG SHOT for the same m_b. Several different measures of this relationship gave very similar results.
Rayleigh-Wave Spectra	Yes	The 22 Nov. 1965 earthquake has more total Rayleigh energy and relatively more low frequency energy than LONG SHOT. The 6 Nov. 1965 earthquake with M_s ≈ to M_s of LONG SHOT however, had a Rayleigh wave spectrum similar to LONG SHOT in both shape and level.
Radiation Patterns	No(?)	The observed and theoretical Rayleigh wave patterns are nearly circular for both events. P-wave first motions were compressive for both events, but the earthquake showed some evidence of a radiation pattern in P-wave amplitude.

to establish conclusively that none is atypical overall as LONG SHOT.

Thus, even though LONG SHOT produced no major surprises in terms of the identification criteria developed previously, the comparisons made in this study demonstrate the need for applying the identification criteria collectively rather than relying on only one or two.

SUMMARY AND CONCLUSIONS

1. The geological environment around Amchitka is that of an island arc. Seismic profiling, magnetic lineations, earthquake epicenters, and focal mechanisms are all compatible with the hypothesis of a structure dipping northward underneath Amchitka Island in a manner predicted by sea-floor spreading. The depth of the zone is limited to about 300 kilometers since there is no recorded seismic activity below this depth. Detailed structural interpretation beneath the island chain itself is unresolved.

2. LONG SHOT was detonated in a lithologically different medium than any previous U.S. shot. It was set in an andesite sill overlain by high-velocity beds consisting mostly of volcanic breccia. On the basis of the announced yield of 80 kilotons and both near-field and far-field amplitude observations, we conclude that andesite is a medium which couples seismic energy somewhat more efficiently than granite.

3. Using 329 stations at teleseismic ($\Delta > 16°$) distances, surprisingly large errors were obtained in the location and source depth of LONG SHOT with both the JB and H68 travel times when the depth was unrestrained. With depth-restrained to the surface, a twenty-kilometer error to the north was obtained with both curves, there being no significant improvement with the new H68 times for this region. This large error is attributed to travel-time bias in the earth and to the anomalous upper-mantle structure under Amchitka. Since no more than about one-third of the bias can be realistically assigned to the anomalous structure near the source, the remaining two-thirds of the observed travel-time differences must be accumulated along the entire paths to the 329 stations. The azimuthal variation of LONG SHOT travel-time residuals with respect to

JB or H68 travel-time curves could be fitted by a single-cycle sine curve. This dependence may be physically associated with a dipping structure under the Aleutian arc but alternatively it can be due to regional travel-time variations. Most of the bias in the LONG SHOT location therefore is the result of the geographic positions of these 329 stations. Further evidence for large regional variations in travel time include: a) regional dependence of station corrections which Herrin and Taggart used to locate LONG SHOT accurately, and b) PcP residuals from LONG SHOT, which showed regional patterns nearly identical with those obtained from direct P residuals.

4. Recorded body-wave amplitudes from LONG SHOT showed significant regional variation and contoured values outlined numerous physiographic provinces. The teleseismic unified body-wave magnitude estimate for LONG SHOT was 5.85. The standard deviation of the individual magnitudes, $\pm$ 0.44, reveals the large scatter in LONG SHOT P-wave amplitude from station to station. Regional variations in amplitude prevent an accurate estimate of magnitude and cause individual explosion magnitudes to be as scattered as the earthquake magnitudes which frequently include the effects of a radiation pattern. In the case of LONG SHOT, it was found that Cleary's distance correction factors produced less scatter in the individual magnitudes than the standard Gutenberg-Richter factors.

The surface-wave amplitudes recorded from LONG SHOT showed less scatter than the body wave amplitudes. The surface wave (LR) magnitude estimate was 4.06 with a standard deviation of $\pm$ 0.22. Regional effects on surface-wave amplitudes are not as easily assessed as on body-wave amplitudes because surface-wave amplitudes are affected by varying crustal structure along the entire travel path.

5. LONG SHOT produced no major surprises in terms of the

identification criteria developed previously. Except for location bias and conflicting evidence on focal depth, the other diagnostic criteria placed LONG SHOT in the explosion population. It is important to note that from limited evidence for earthquakes in the LONG SHOT source region, LONG SHOT appears distinctly different from Aleutian earthquakes of comparable P-wave magnitude. However, certain individual criteria (e.g. first motion and surface wave radiation patterns) show essentially no distinction between the two. This illustrates the necessity for using as many diagnostics as possible in attempting to identify teleseismic events. Clearly we need results from a much larger sample of earthquakes to establish conclusively that no other earthquake in this region is as atypical overall as LONG SHOT.

It should also be emphasized that LONG SHOT was a rather large event and consequently all the diagnostic criteria could be applied. For smaller events where some of the diagnostics cannot be applied (e.g. first motion and depth of focus) identification would be much more difficult.

6. By means of the "standard" diagnostic criteria and additional spectral comparisons, it was relatively easy to show that LONG SHOT was different from earthquakes of comparable P-wave and Rayleigh-wave magnitudes from the same source region (see summary under COMPARISON OF LONG SHOT WITH EQUIVALENT MAGNITUDE EARTHQUAKES IN THE ALEUTIAN REGION). The earthquakes selected for comparison were within 100 kilometers of LONG SHOT site, and on the basis of previous studies they appear to be typical of earthquakes in that region. By comparing LONG SHOT with these nearby events the differences observed could be directly attributed to differences in the sources themselves, since the travel paths and receiving stations were common to LONG SHOT and both earthquakes. Although we cannot generalize

without examining many more events from this region, it appears that the major differences observed result from the much stronger generation of shear energy at all frequencies by the earthquake and from the fact that considerably more low-frequency energy is associated with earthquakes of comparable P-wave magnitude.

Thus, the LONG SHOT experiment showed that for the Aleutian Arc the diagnostic criteria previously developed, using primarily NTS events recorded at regional distances, also work well for the identification of teleseismic events once the event is reliably located. However, LONG SHOT demonstrated that we still have great difficulty in reliably locating events in new source regions and determining whether they are shallow or deep. While the different geologic setting of LONG SHOT apparently was important in influencing the location and depth estimates from travel times, it did not significantly change the effectiveness of any of the other identification criteria. The opportunity afforded by LONG SHOT to compare a large explosion with a nearby comparable-magnitude earthquake was important because significant spectral differences and differences in relative excitation of various phases were observed.

However, further research with many more events is needed to determine whether these differences can be used as diagnostics for identifying teleseismic events from this region.

In conclusion, it must be re-emphasized that, although LONG SHOT fell well into the general explosion class of seismic events, small explosions and earthquakes in this source area may well be very difficult to separate.

REFERENCES

Alexander, S.S., and D.B. Rabenstine, "Detection of surface waves from small events at teleseismic distances", Earth Sciences Division, Teledyne Industries, Inc., Seismic Data Laboratory Report No. 175, 1967.

Archambeau, C.B., "Elastodynamic source theory", Ph.D. Thesis, California Institute of Technology, Pasadena, California, 1964.

Archambeau, C.B., E.A. Flinn, and D.G. Lambert, "Detection, analysis, and interpretation of teleseismic signals: 1. Compressional phases from the Salmon event", J. Geophys. Res., 71, 3483-3501, 1966.

Brune, James, Alvaro Espinosa, and Jack Oliver, "Relative excitation of surface waves by earthquakes and underground explosions in the California-Nevada region", J. Geophys. Res., 68, 3501-3513, 1963.

Carder, D.S., D.W. Gordon, and J.N. Jordan, "Analysis of surface-foci travel times", Bull. Seis. Soc. Am., 56, 815-840, 1966.

Carpenter, E.W., "Explosion seismology", Science, 147, 363-373, 1965.

Carpenter, E.W., P.D. Marshall, and A. Douglas, "The amplitude-distance curve for short-period teleseismic P-waves", Geophys. J.R. Astr. Soc., 13, 61-70, 1967.

Chiburis, E.F., "Precision location of underground nuclear explosions using teleseismic networks and predetermined travel-time anomalies", Earth Sciences Division, Teledyne Industries, Inc., Seismic Data Laboratory Report No. 214, 1968.

Cleary, John, "Azimuthal variation of the LONG SHOT source term", Earth and Planetary Science Letters, 3, 29-37, 1967a.

Cleary, John, "Analysis of the amplitudes of short-period P waves recorded by Long Range Seismic Measurements stations in the distance range 30° to 102°", J. Geophys. Res., 72, 4705-4712, 1967b.

Cleary, John and Anton L. Hales, "An analysis of the travel times of P waves to North American stations, in the distance range 32° to 100°", Bull. Seis. Soc. Am., 56, 467-489, 1966.

Cohen, T.J., "Determination of source dpeth by spectral, pseudo-autocovariance, and cepstral analysis", Geotech Division, Teledyne, Inc., Seismic Data Laboratory Report No. 229, 1969.

Currie, Ralph Gordon, "A comparison of LONG SHOT and earthquakes", Arctic Institute of North America, Research Paper No. 40, 1967.

Day, J.D., and D.W. Murrell, "Ground and water shock measurement, Project LONG SHOT", United States Army Engineer Waterways Experiment Station, Vicksburg, 1967.

Douglas, A., "Joint epicenter determination", Nature, 215, 47-48, 1967.

Evernden, J.F., "Magnitude determination at regional and near-regional distances in the U.S.", Bull. Seis. Soc. Am., 57, 591-639, 1967.

Ewing, Maurice, William J. Ludwig, and John Ewing, "Oceanic structural history of the Bering Sea", J. Geophys. Res., 70, 4593-4600, 1965.

Gates, O., and W. Gibson, "Interpretation of the configuration of the Aleutian Ridge", Bull. Geol. Soc. Am., 67, 127-146, 1956.

Geotech Division, Teledyne Industries, Inc., "Seismological bulletin - the Aleutian Island Experiment, 1964", Technical Report No. 65-130, 1965.

Gibson, W., and H. Nichols, "Configuration of the Aleutian Ridge Rat Islands - Semisopochnoi I to west of Buldir I", Bull. Geol. Soc. Am., 64, 1173-1188, 1953.

Green, Paul E., "Seismic discrimination", Semiannual Technical Summary Report to the Advanced Research Projects Agency, Lincoln Laboratory, MIT, 1968.

Guidroz, Ralph R., A. Frank Linville, Terence W. Harley, Ronald D. Bauer, Joseph G. McDermott, R. Fred Howard, Gary D. McNeely, and A. Ronald Medina, "Preliminary analysis report-Aleutian Islands Experiment - ocean-bottom experiments", Texas Instruments, Inc., prepared for ARPA Project VELA-Uniform under ARPA Order No. 624, 1968.

Gutenberg, B., and C.F. Richter, Seismicity of the Earth and Associated Phenomena, Hafner Publ. Co., 1954.

Gutenberg, B., and C.F. Richter, "Magnitude and energy of earthquakes", Ann. Geofis., 9, 1-15, 1956.

Hales, A.L., J.R. Cleary, H.A. Doyle, R. Greene, and J. Roberts, "P-wave station anomalies and the structure of the upper mantle", J. Geophys. Res., 73, 3885-3896, 1968.

Hayes, Dennis E., and James R. Heirtzler, "Magnetic anomalies and their relation to the Aleutian Island Arc", J. Geophys. Res., 73, 4637-4646, 1968.

Helterbran, Wayne, and James N. Jordan, "Teleseismic data from Long Shot", Abstract, Symposium on the Long Shot Nuclear Event, Transactions Am. Geophys. Union, 47, 164, 1966.

Herrin, Eugene, and James Taggart, "Regional variations in Pn velocity and their effect on the location of epicenters", Bull. Seis. Soc. Am., 52, 1037-1046, 1962.

Herrin, Eugene, and James Taggart,"Regional variations in P travel times", Bull. Seis. Soc. Am., 58, 1325-1338, 1968a.

Herrin, Eugene, and James Taggart, "Source bias in epicenter determinations", Bull. Seis. Soc. Am., 58, 1791-1796, 1968b.

Herrin, Eugene, William Tucker, James Taggart, David W. Gordon, and John L. Lobdell, "Estimation of surface-focus P travel times", Bull. Seis. Soc. Am., 58, 1273-1292, 1968.

Isacks, Bryan, Jack Oliver, and Lynn R. Sykes, "Seismology and the new global tectonics", J. Geophys. Res., 73, 5855-5899, 1968.

Jarosch, H., "Body-wave magnitude and source mechanism", Earth Sciences Division, Teledyne, Inc., Seismic Data Laboratory Report No. 225, 1968.

Jensen, Oliver, R.M. Ellis, and R.D. Russell, "Analysis of Canadian Long Shot data", Earth and Planetary Science Letters, 1, 211-221, 1966.

Jordan, James, Rudolf Black, and Charles C. Bates, "Patterns of maximum amplitudes of Pn and P waves over regional and continental areas", Bull. Seis. Soc. Am., 55, 693-720, 1965.

Julian, Bruce R., and Don L. Anderson, "Travel times, apparent velocities, and amplitudes of body waves", Bull. Seis. Soc. Am., 58, 339-366, 1968.

Kelly, E.G., "A study of two short-period discriminants", Lincoln Laboratory, Massachusetts Institute of Technology, Technical Note 1968-8, 1968.

Keylis-Borok, V.I., "The difference in the spectrum of surface waves in earthquakes and underground explosions", Seismic Effects of Underground Explosions, Academy of Sciences, U.S.S.R., 108 pp., 1960.

King, Phillip B., The Evolution of North America, Princeton Univ. Press, 1959.

Liebermann, Robert C., Chi-Yu King, James N. Brune, and Paul W. Pomeroy, "Excitation of surface waves by the underground nuclear explosion Long Shot", J. Geophys. Res., 71, 4333-4339, 1966.

Menard, H.W., and R.S. Dietz, "Submarine geology of the Gulf of Alaska", Bull. Geol. Soc. Am., 62, 1263-1285, 1951.

Murdock, James N., "Configuration of the crust-mantle system in the central Aleutians: an hypothesis", ESSA Technical Memorandum IERTM-EML3, 1967.

Murray, H.W., "Profiles of the Aleutian trench", Bull. Geol. Soc. Am., 56, 757-782, 1945.

Nichols, Haven, and Richard B. Perry, "Bathemetry of the Aleutian Arc", ESSA Monograph 3, 1966.

Oliver, Jack, and Bryan Isacks, "Deep earthquake zones, anomalous structures in the upper mantle, and the lithosphere", J. Geophys. Res., 72, 4259-4275, 1967.

Pasechnik, I.P., "The dependence of earthquake magnitude on the seismogeological features in the district of the observations", Bulletin of the Academy of Sciences, U.S.S.R., Geophysics Series (English translation), No. 11, 937-943, 1962.

Pasechnik, I.P., D.D. Kogan, D.D. Sultanov, and V.I. Tsibulskiy, "The results of seismic observations made during underground nuclear and TNT blasts", Seismic Effects of Underground Explosions, Academy of Sciences, U.S.S.R., 108 pp., 1960.

Powers, H.A., R.R. Coats, and W.H. Nelson, "Geology and submarine physiography of Amchitka Island, Alaska", United States Geological Survey Bulletin 1028-P, 521-553, 1960.

Press, Frank, and Charles Archambeau, "Release of tectonic strain by underground nuclear explosions", J. Geophys. Res., 67, 337-343, 1962.

Press, Frank, Gilbert Delwart, and Ralph Gilman, "A study of diagnostic techniques for identifying earthquakes", J. Geophys. Res., 68, 2909-2928, 1963.

Sauer, F.M., G.B. Clark, and D.C. Anderson, Nuclear Geoplosics, Part Four: Empirical Analysis of Ground Motion and Cratering, Stanford Research Institute 1964.

Schneider, William A., "Ocean-bottom seismometer data collection and analysis", Texas Instruments, Inc., prepared for Air Force Cambridge Research Laboratories, OAR, under contract AF19(604)-8368, 1964.

Shor, George G., Jr., "Seismic refraction studies off the coast of Alaska, 1956-1957", Bull. Seis. Soc. Am., 52, 37-57, 1962.

Shor, George G., Jr., "Structure of the Bering Sea and the Aleutian Ridge", Marine Geology, 1, 213-219, 1964.

SIPRI (International Institute for Peace and Conflict Research), Seismic Methods for Monitoring Underground Explosions - An Assessment of the Status and Outlook, Stockholm, Sweden, 130 pp., 1968.

Stauder, William, "Mechanism of the Rat Island earthquake sequence of February 4, 1965, with relation to island arcs and sea-floor spreading", J. Geophys. Res., 73, 3847-3858, 1968.

Sutton, G.H., W. Mitronovas, and P.W. Pomeroy, "Short-period seismic energy radiation patterns from underground nuclear explosions and small-magnitude earthquakes", Bull. Seis. Soc. Am., 57, 249-268, 1967.

Toksöz, M. Nafi, Kevin Clermont, "Radiation of seismic waves from the Bilby explosion", Earth Sciences Division, Teledyne Industries, Inc., Seismic Data Laboratory Report No. 183, 1967.

Toksöz, M. Nafi, A. Ben-Menahem, and D.G. Harkrider, "Determination of source parameters by amplitude equalization of seismic surface waves: 1. Underground nuclear explosions", J. Geophys. Res., 69, 4355-4366, 1964.

Toksöz, M. Nafi, David G. Harkrider, and Ari Ben-Menahem, "Determination of source parameters by amplitude equalization of seismic surface waves: 2. Release of tectonic strain by underground nuclear explosions and mechanisms of earthquakes", J. Geophys. Res., 70, 907-922, 1965.

Turnbull, L.S., D.G. Lambert, and C.A. Newton, "Rayleigh wave discrimination techniques between underground explosions and earthquakes", Earth Sciences Division, Teledyne Industries, Inc., Seismic Data Laboratory Report No. 211, 1968.

United States Atomic Energy Commission, Nevada Operations Office, Consolidated Data on Selected Effects from Underground Nuclear Detonations, Flintlock Series, Volume I: Emplacement Information, 1967.

United States Army Engineer District, Alaska, and United States Geological Survey, Project LONG SHOT, Amchitka Island, Alaska, Geologic and Hydrologic Investigations (Phase I), 1965.

Van Nostrand, Robert, "Reverberation effects on signal amplitude", Earth Sciences Division, Teledyne Industries, Inc., Seismic Data Laboratory Report No. 110, 1964.

TABLE 1

Physical Parameters of the LONG SHOT Site

Depth Interval meters below surface)	Bulk Specific Gravity (gm/cc)	Velocity (km/sec)	Porosity (percent)
21.3 - 77.7	----	3.04	29
77.7 - 90.5	2.41	3.38	23
90.5 - 103.6	----	2.77	34
103.6 - 152.4	2.43	3.26	25
152.4 - 232.5	2.39	3.04	29
232.5 - 300.2	2.43	3.44	23
300.2 - 331.0	----	3.13	27
331.0 - 364.2	----	3.59	20
364.2 - 379.1	----	3.44	27
379.1 - 423.0	2.33	3.56	21
423.0 - 463.3	2.36	3.23	25
463.3 - 526.3	2.33	3.50	22
526.3 - 608.0	----	3.56	21
608.0 - 656.8	2.37	3.68	20
656.8 - 685.8	2.32	3.56	21
685.8 - 694.9	2.18	3.38	23
694.9 - 770.8	2.55	4.35	13
770.8 - 792.4	2.20	3.35	24

TABLE 2

Computed Epicenter of LONG SHOT with Depth
Unrestrained - 329 Stations

Mode	Origin Time	Depth km	Coordinates	Lateral Displacement	Standard Deviation of Residuals
Actual	21:00:00.1	0.7	51.438N,179.183E		
H68	21:00:09.5	78	51.622N,179.213E	20.6 km, N6°E	0.948
JB	21:00:05.3	58	51.631N,179.231E	21.7 km, N9°E	1.058

TABLE 3

Computed Epicenter of LONG SHOT with Depth
Restrained to Surface - 329 Stations

		Percentage Confidence Ellipse 75	90	95	99	99.9	Epicenter Shifted	Standard Deviation of Residuals
Observed Arrival Times	H68 Area (sq. km)	25.2	42.1	55.4	85.0	129.7	20.1 km N14°W	1.057
	Cover epicenter?	No	No	No	No	No		
	JB Area (sq. km)	24.3	40.6	52.7	81.8	124.9	21.3 km N 4°W	1.117
	Cover epicenter?	No	No	No	No	No		
With Source Correction	H68 Area (sq. km)	21.6	36.0	46.8	72.5	111.1	0.7 km N34°W	1.055
	Cover epicenter?	Yes	Yes	Yes	Yes	Yes		
	JB Area (sq. km)	24.5	40.9	53.1	82.3	125.6	2.2 km N57°W	1.117
	Cover epicenter?	Yes	Yes	Yes	Yes	Yes		
With Source and Station Corrections	H68 Area (sq. km)	19.4	32.5	42.2	65.3	100.0	3.4 km S22°E	1.001
	Cover epicenter?	No	Yes	Yes	Yes	Yes		

TABLE 4

Description of Events for Which M_s Versus m_b Is Plotted

No.	Date	Area/Event	Latitude	Longitude	Origin Time (Z)	Depth (km)	Body-Wave Magnitude	Rayleigh-Wave Magnitude
1	13 Sep 1963	Bilby - N.T.S.	37°03.633'N	116°01.30'W	17:00:00.1	0.76	5.80	3.92
2	26 Oct 1963	Shoal-Sand Springs Range, Nevada	39°12.017'N	118°22.817'W	17:00:00.1	0.37	4.80	2.48
3	29 Oct 1965	Long Shot-Amchitka Island	51°26.294'N	179°10.950'E	21.00:00.1	0.70	5.85	4.06
4	21 Nov 1965	Test-Kazakh	49°48'N	78°06'E	04:57:57.9	----	*5.8	3.97
5	13 Feb 1966	Test-Kazakh	49°48'N	78°06'E	04:57:57.9	----	*6.3	4.51
6	20 Dec 1966	Greely - N.T.S.	37°18.117'N	116°24.500'W	15:30:00.1	1.23	6.29	5.18
7	20 Jan 1967	Bourbon - N.T.S.	37°05.984'N	116°00.233'W	17:40:04.4	0.56	5.10	3.24
8	20 Jul 1962	Fallon, Nevada Eq.	39°38.833'N	118°12.667'W	09:02:08.3	20	4.40	2.85
9	29 Jan 1965	Kamchatka Eq.	54°48'N	161°42'W	09:35:25.7	33	*5.8	4.86
10	08 Feb 1965	Komandorsky Eq.	55°06'N	165°42'W	15:46:49.9	40	*5.6	5.82
11	14 Feb 1965	Komandorsky Eq.	55°06'N	165°36'W	17:01:13.9	20	*5.0	3.99
12	20 Apr 1965	Kamchatka Eq.	54°48'N	161°24'W	06:50:17.6	33	*5.3	4.85
13	20 Apr 1965	Seguam Eq.	52°24'N	172°00'E	06:43:08.8	35	*5.5	4.77
14	06 Nov 1965	Rat Island Eq.	51°24'N	176°42'E	22:30:20.5	40	*5.0	4.33
15	22 Nov 1965	Andreanoff Eq.	51°18'N	179°48'W	20:25:30.4	40	5.86	5.56
16	18 Nov 1966	Greenland Sea Eq.	73°24'N	06°48'E	18:07:54.0	33	*4.6	3.81
17	18 Nov 1966	Greenland Sea Eq.	73°24'N	06°48'E	18:48:43.9	33	*4.9	4.84
18	02 Mar 1967	California-Nevada Border Eq.	36°18'N	117°42'W	14:12:49.1	14	*4.4	2.66
19	13 Apr 1967	Guerrero, Mexico Eq.	18°30'N	100°12'W	19:59:51.9	86	*5.7	4.58

* USC&GS Magnitudes--all other magnitudes computed at SDL.

TABLE 5

Parameters for the Events Used in the Comparative Analysis

Date	Origin Time	Coordinates	From LONG SHOT Dist.*	Azi*	Depth	Magnitude m_b	Magnitude Ms
06 Nov 1965	22:30:20.5	51.4N, 176.7E	172km	270°	40km≠	5.0≠	4.29*
22 Nov 1965	20:25:30.4	51.3N, 179.8W	72km	101°	20km*	5.9≠	5.40*

*Computed by the SDL
≠Computed by the USC&GS

TABLE 6

Short Period P-Wave Spectral Ratios for LONG SHOT and the 22 November 1965 Earthquake

Station	LONG SHOT	22 November 1965 Earthquake
PG-BC	11.52	6.01
JP-AT	1.31	4.54
HV-MA	1.30	5.08
MN-NV	0.48	5.10
KN-UT	2.99	5.98
RG-SD	0.27	2.87
RK-ON	0.52	1.71
WN-SD	0.86	10.17
CR-NB	0.36	1.92
KC-MO	0.42	2.61
EN-MO	0.55	3.64
HN-ME	1.31	4.07
BE-FL	1.84	7.69

TABLE 7

Complexity Factors for LONG SHOT and the 22 November 1965 Earthquake

Station	22 November 1965 EQ		LONG SHOT	
	Distance (km)	Fc	Distance (km)	Fc
NP-NT	3763	5.43	3783	3.01
PG-BC	3787	8.73	3842	7.93
JP-AT	4106	5.92	4161	4.16
HV-MA	4854	3.53	4910	1.70
MN-NV	4929	9.09	4991	1.96
KN-UT	5393	7.31	5455	2.63
RG-SD	5451	4.61	5507	2.28
RK-ON	5673	3.51	5724	1.22
WN-SD	5796	1.74	5852	1.81
CR-NB	6193	3.75	6249	1.66
KC-MO	6429	3.01	6485	1.21
EN-MO	6877	3.21	6933	1.98
HN-ME	7401	2.45	7442	1.21
BE-FL	8067	1.08	8123	1.10
Average	----	4.53	----	2.51

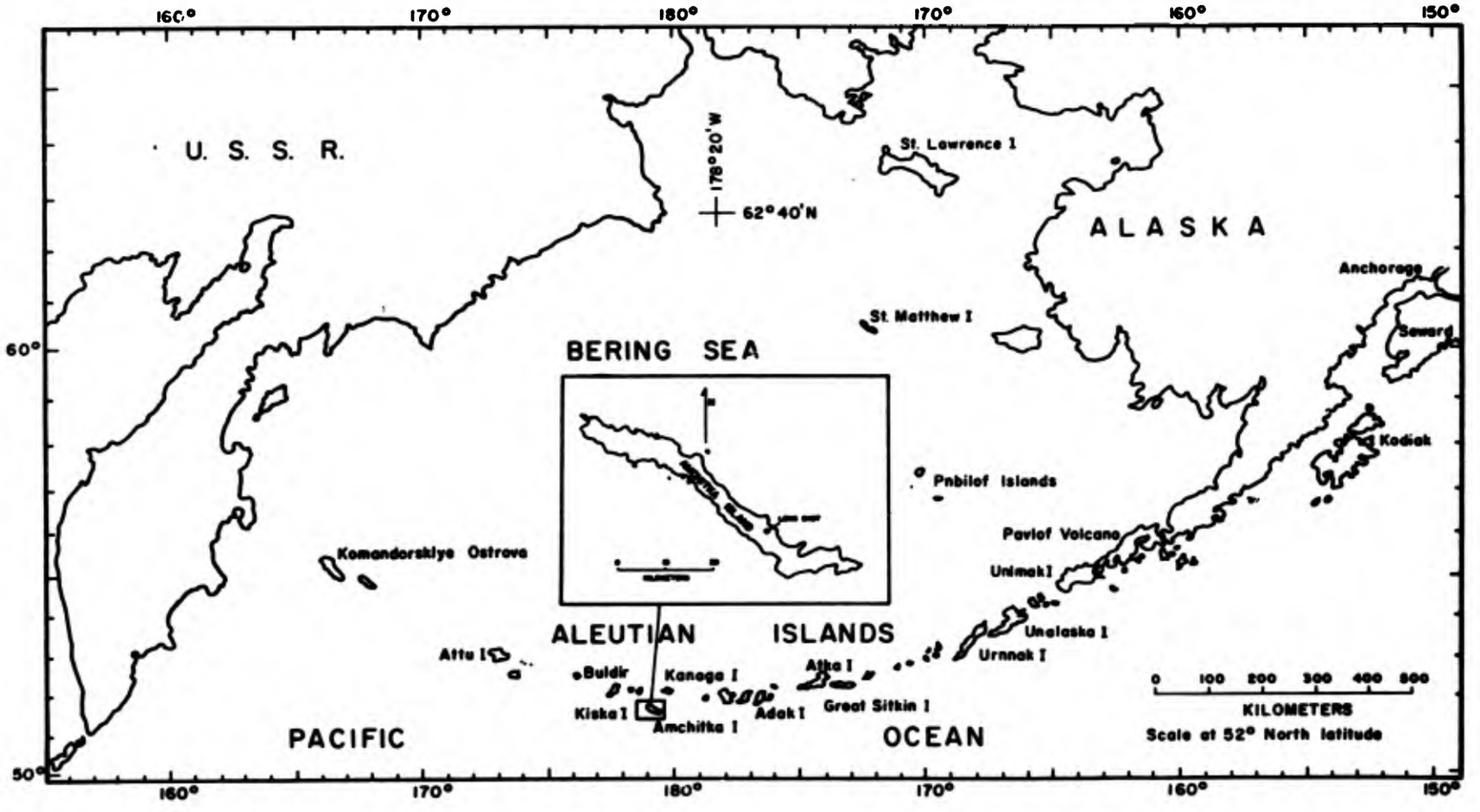

THE ALEUTIAN ARC

Figure 1. The Aleutian Arc

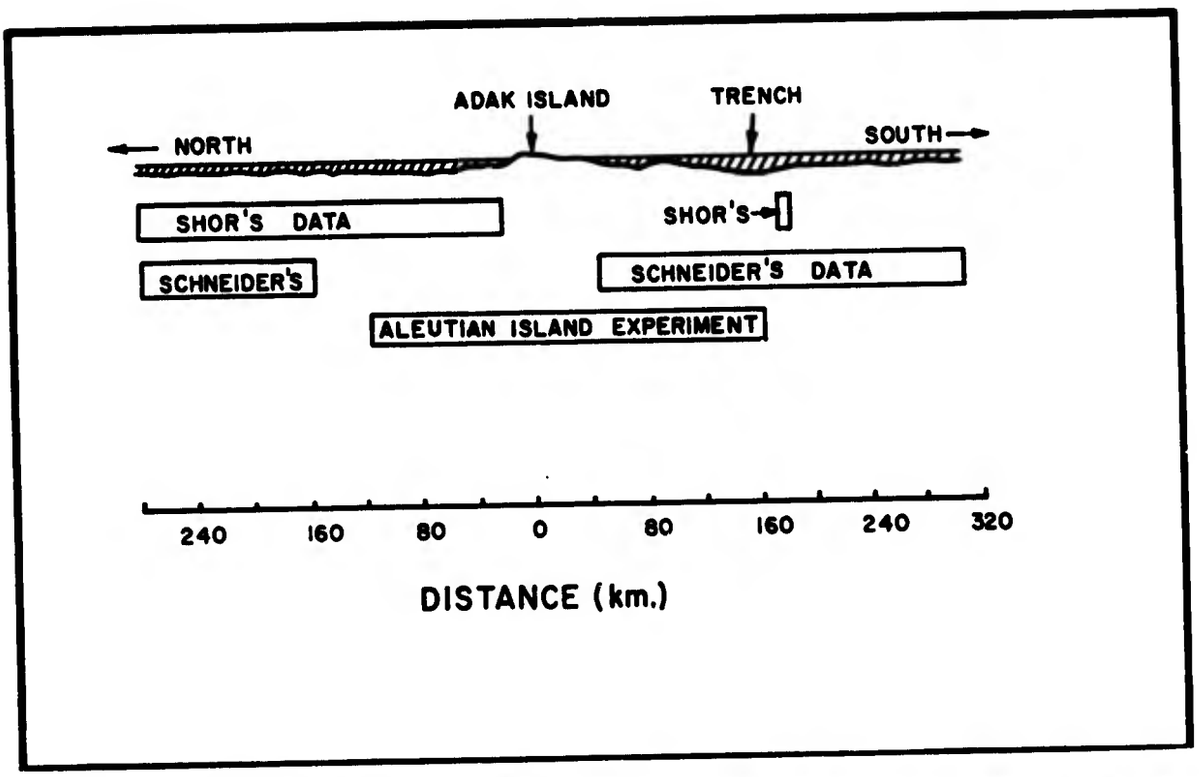

Figure 2. Extent of coverage of various seismic investigations on the Aleutian Arc through Adak Island (after Murdock, 1967).

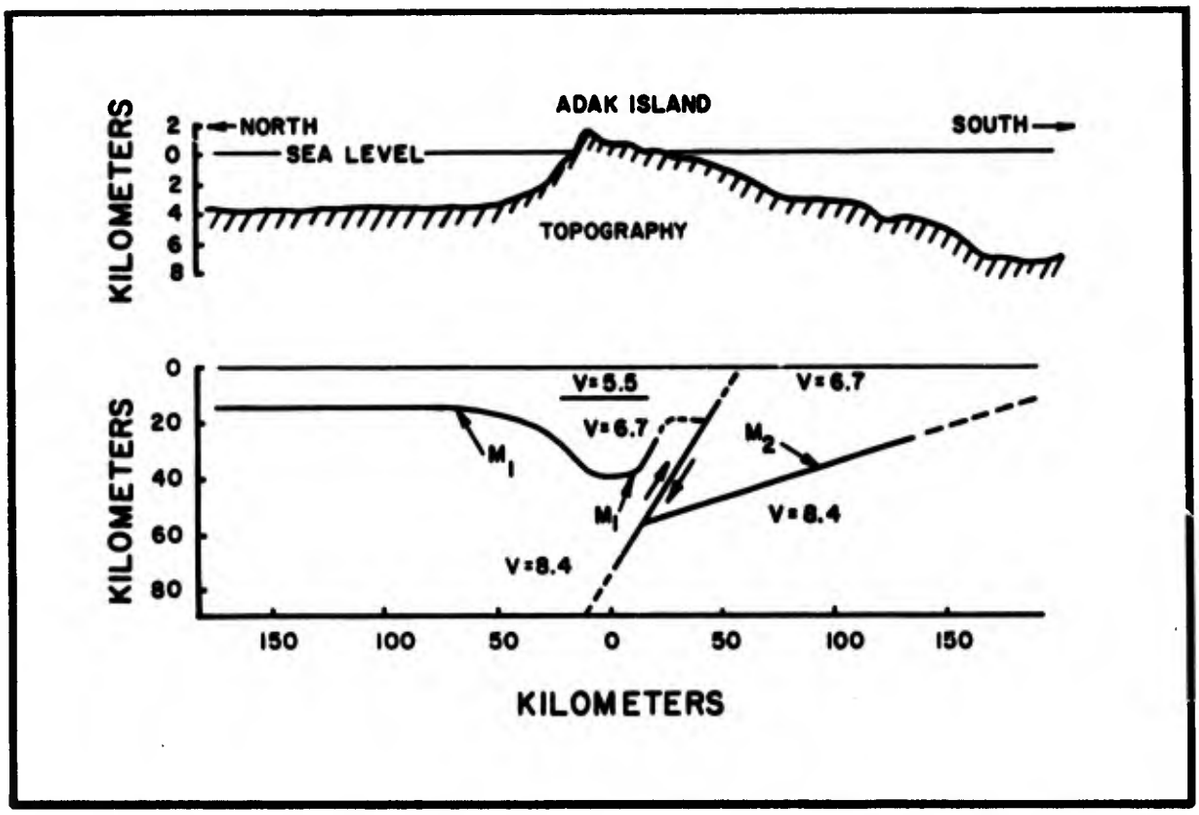

Figure 3. Composite structural profile through Adak Island (after Murdock, 1967).

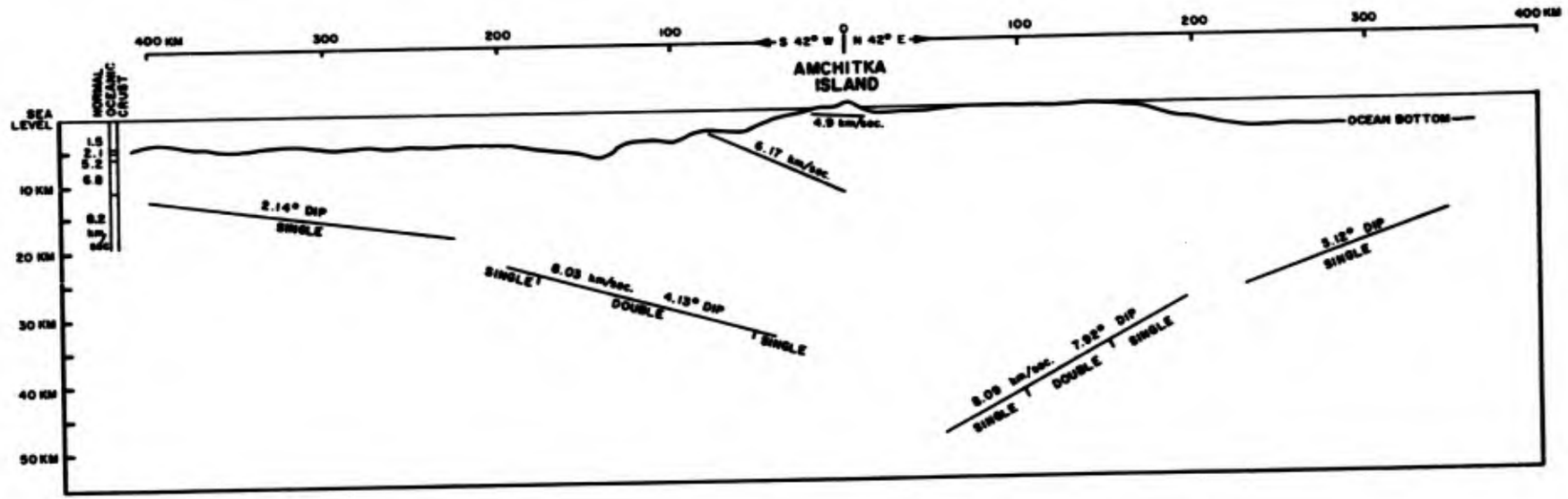

Figure 4. Crustal profile through Amchitka Island (after Guidroz et al, 1968).

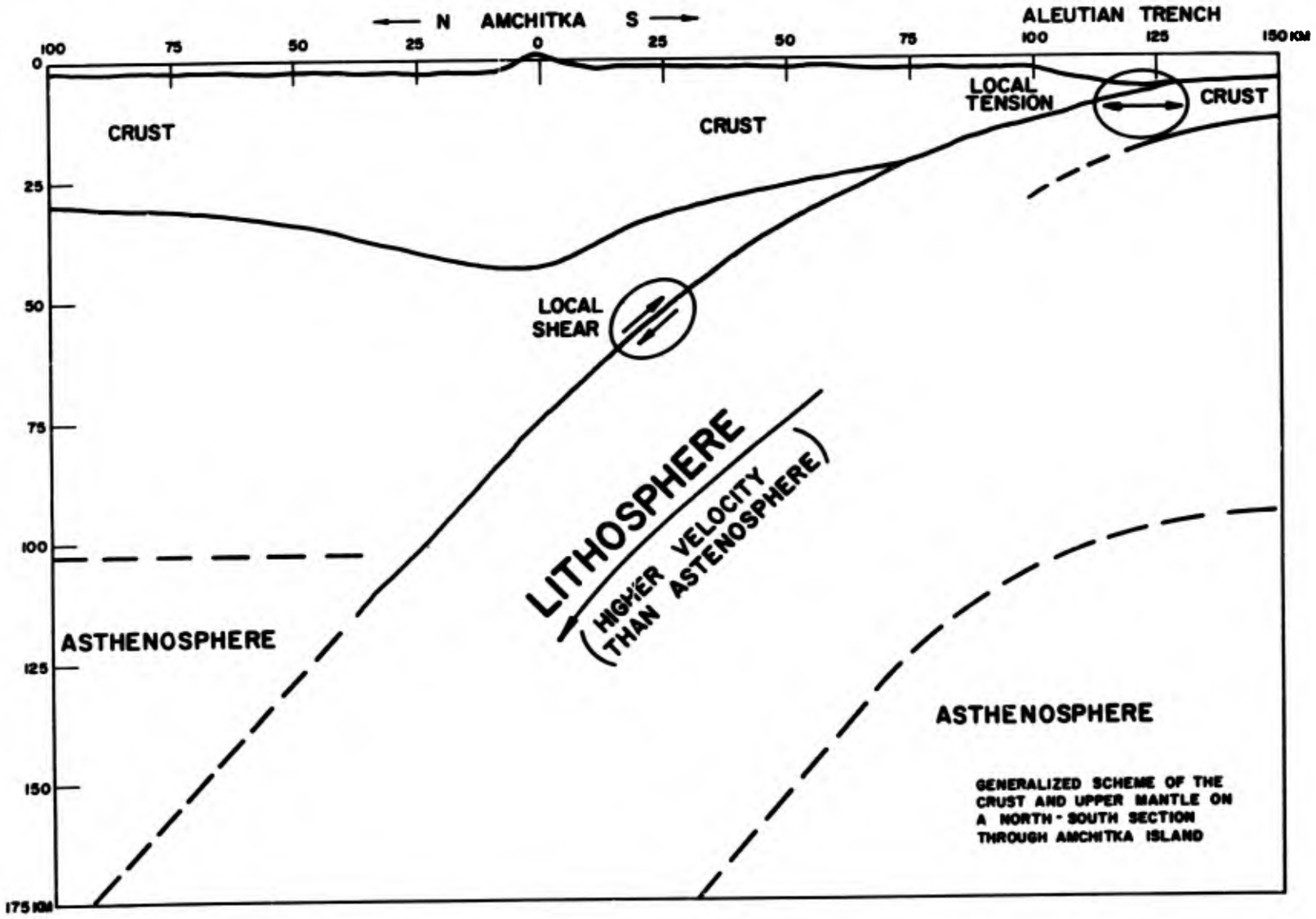

Figure 5. Generalized scheme of the possible crust and upper mantle structure on a north-south profile through Amchitka Island.

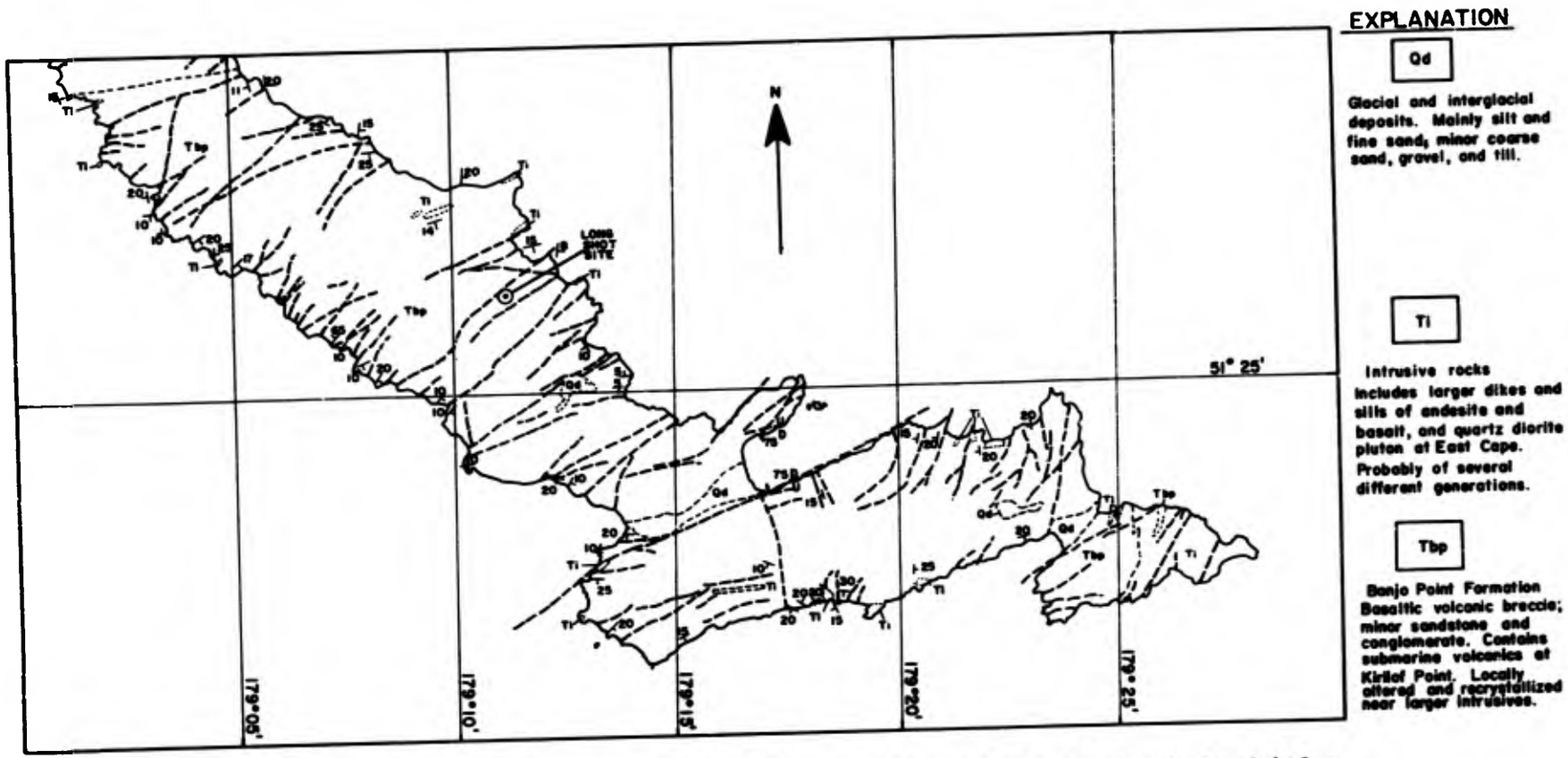

Figure 6. Surface geology of the southeastern part of Amchitka Island (modified from U.S.G.S. Bulletin 1028-P, Plate 69, Geology by L.M. Gard).

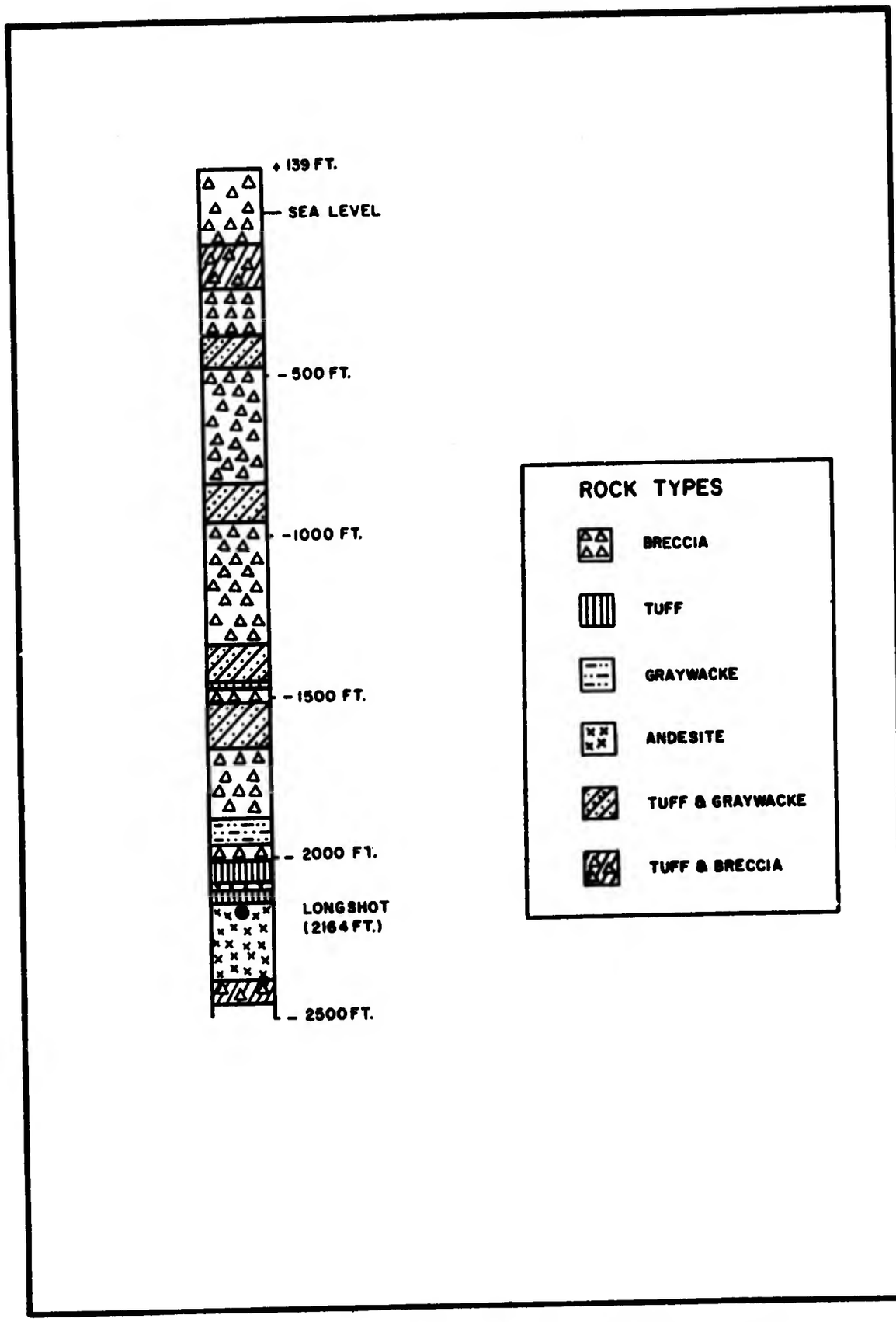

Figure 7. Stratigraphy at the LONG SHOT site.

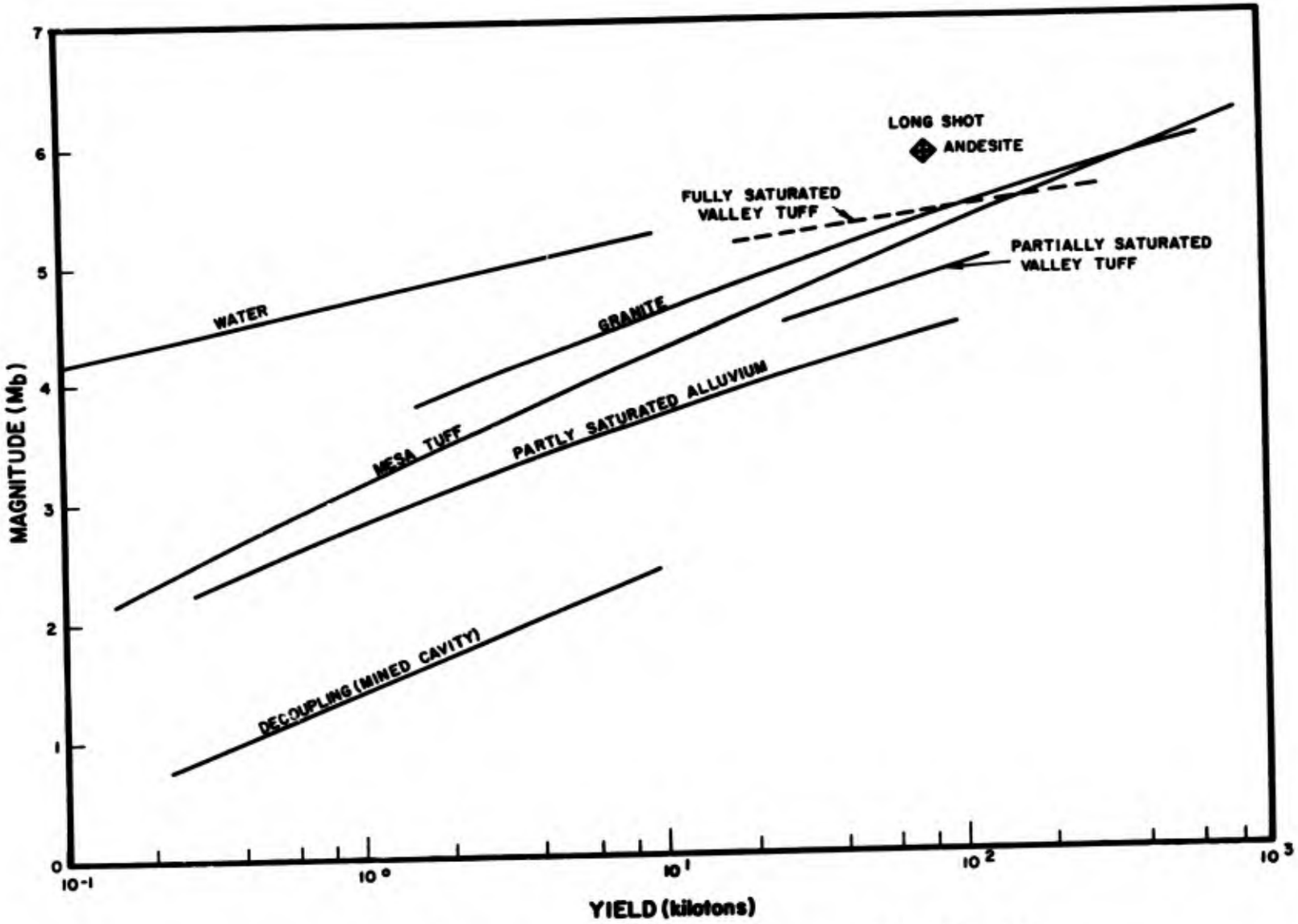

Figure 8. Body-wave magnitude versus yield for various mediums (SIPRI, 1968).

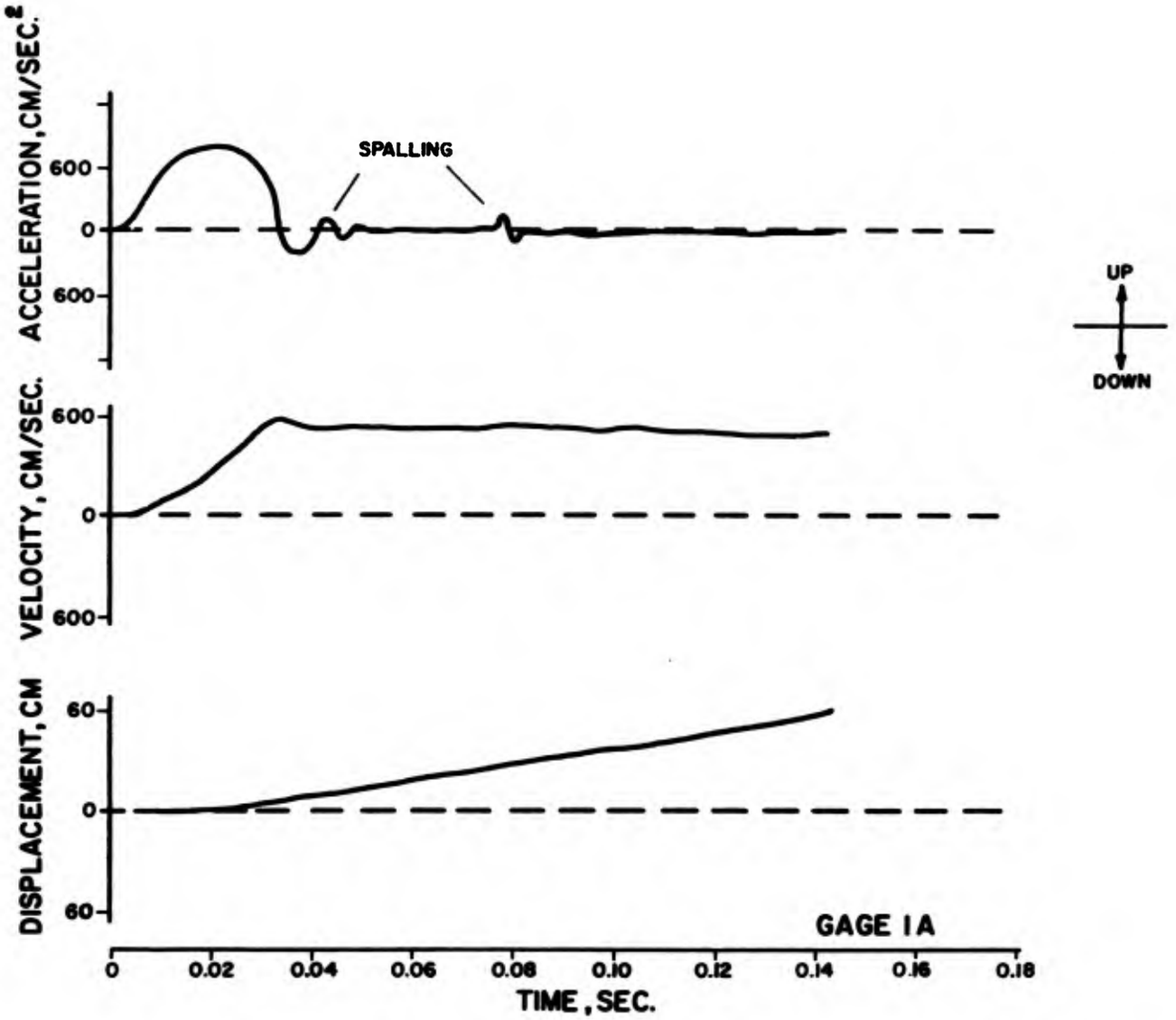

Figure 9. Motion histories in EH-5. Horizontal range 6.1 meters, gage depth 0 meters, and slant range 702.0 meters.

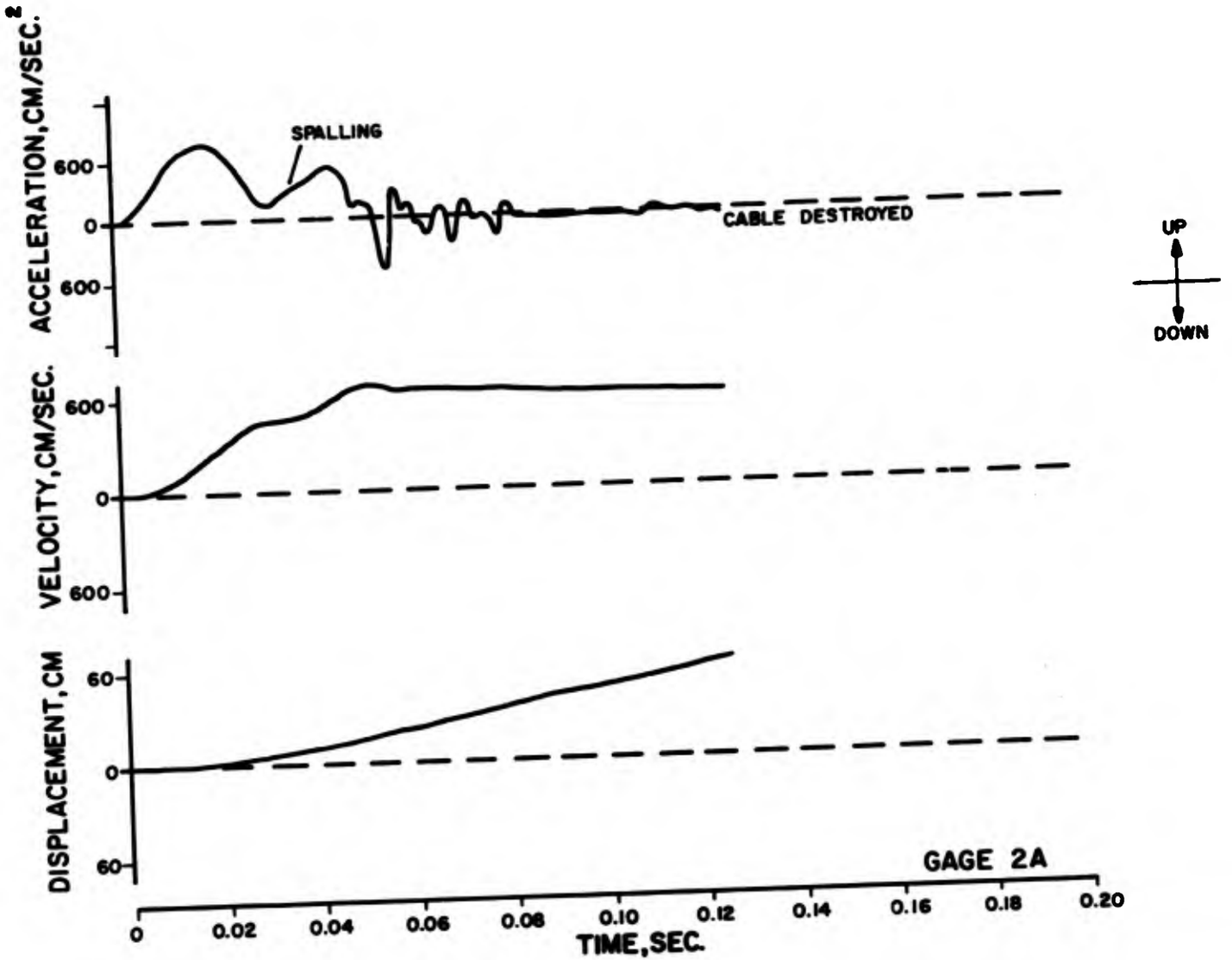

Figure 10. Motion histories in EH-5. Horizontal range 6.1 meters, gage depth 30.5 meters, and slant range 670.6 meters.

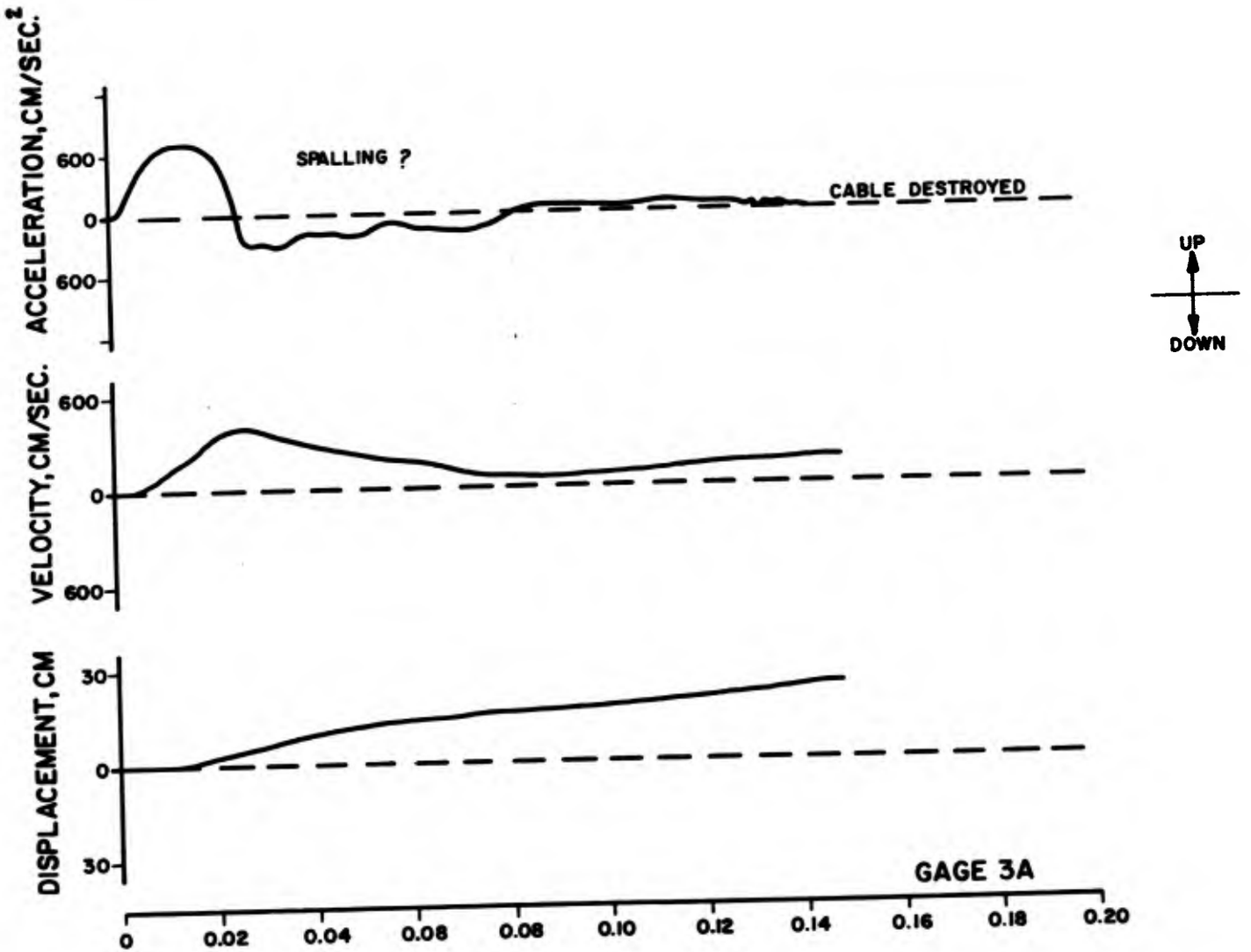

Figure 11. Motion histories in EH-5. Horizontal range 6.1 meters, gage depth 152.4 meters, and slant range 548.6 meters.

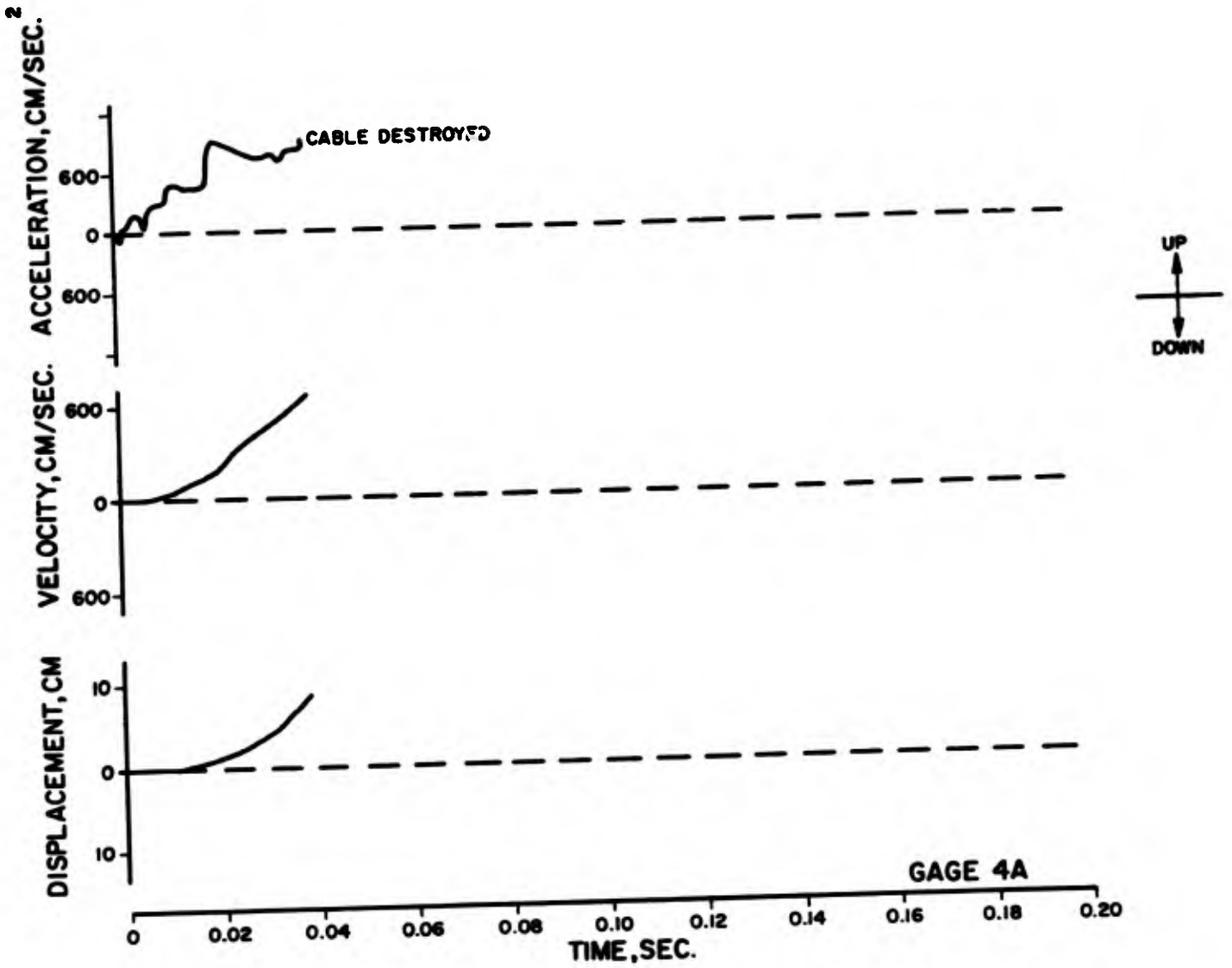

Figure 12. Motion histories in EH-5. Horizontal range 6.1 meters, gage depth 213.4 meters, and short range 487.7 meters.

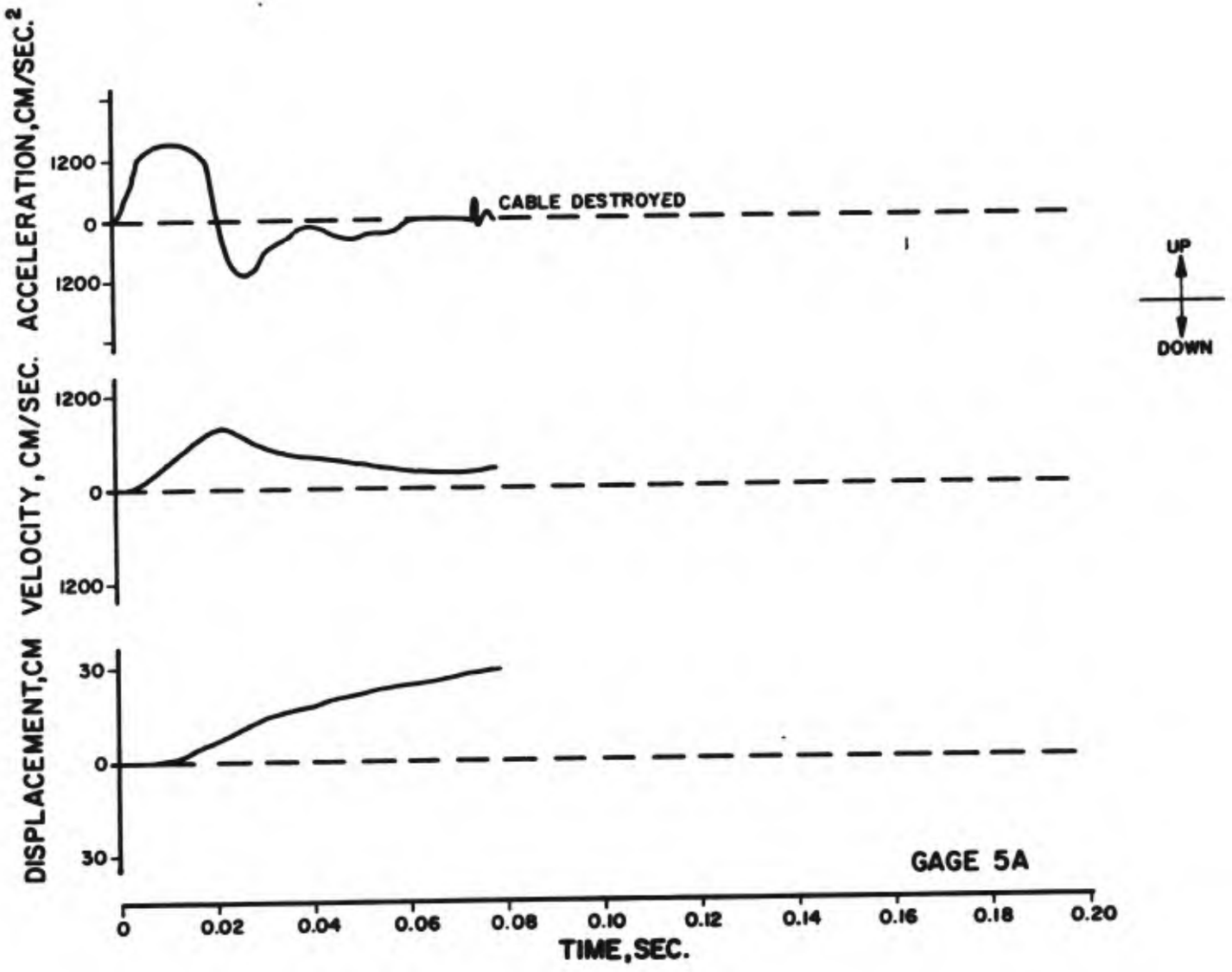

Figure 13. Motion histories in EH-5. Horizontal range 6.1 meters, gage depth 273.3 meters, and slant range 426.7 meters.

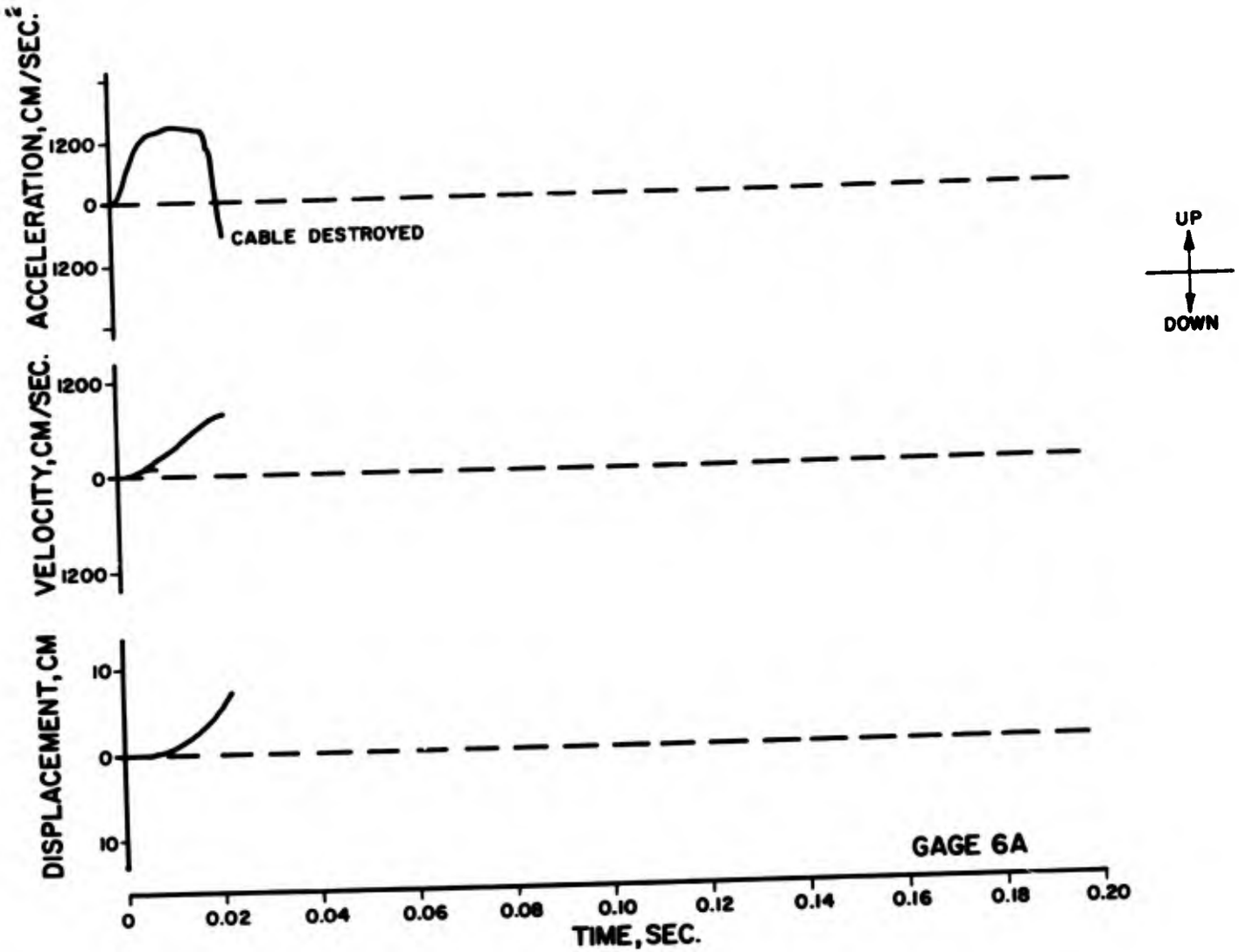

Figure 14. Motion histories in EH-5. Horizontal range 6.1 meters, gage depth 335.3 meters, and slant range 365.8 meters.

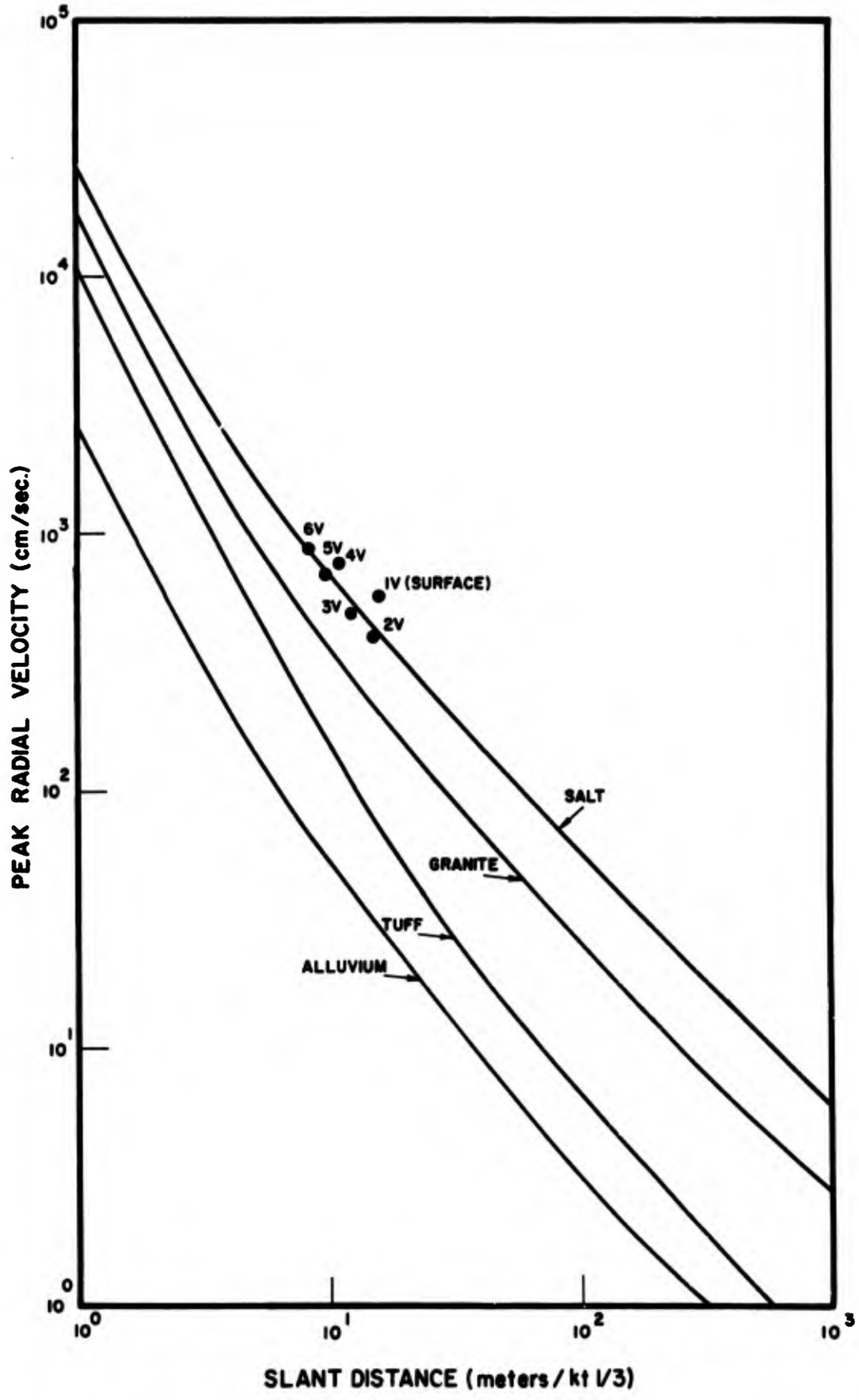

Figure 15. Peak radial velocity versus slant range for various shot media and observed velocities for LONG SHOT in EH-5.

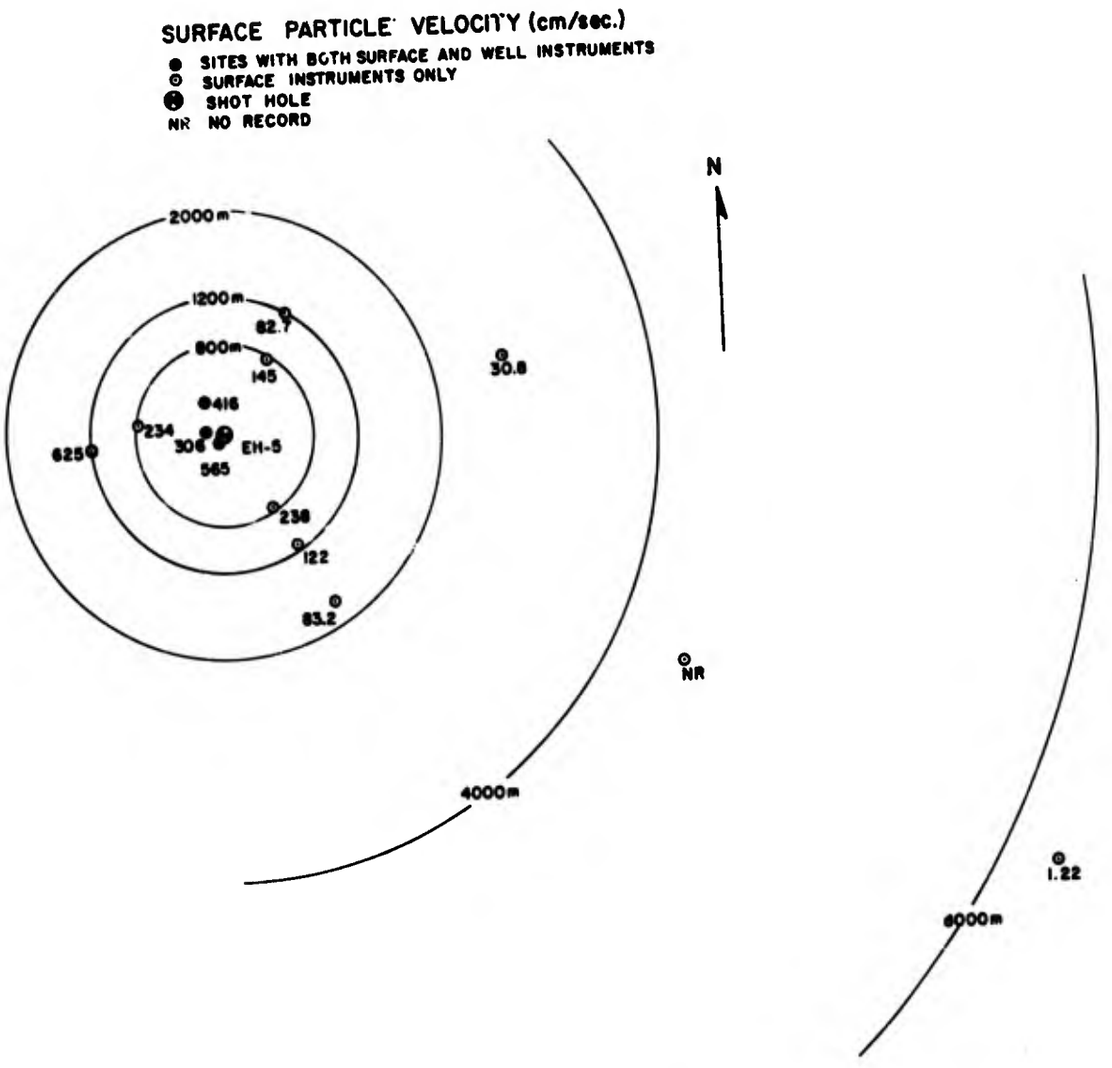

Figure 16. Surface particle velocities measured at the LONG SHOT site.

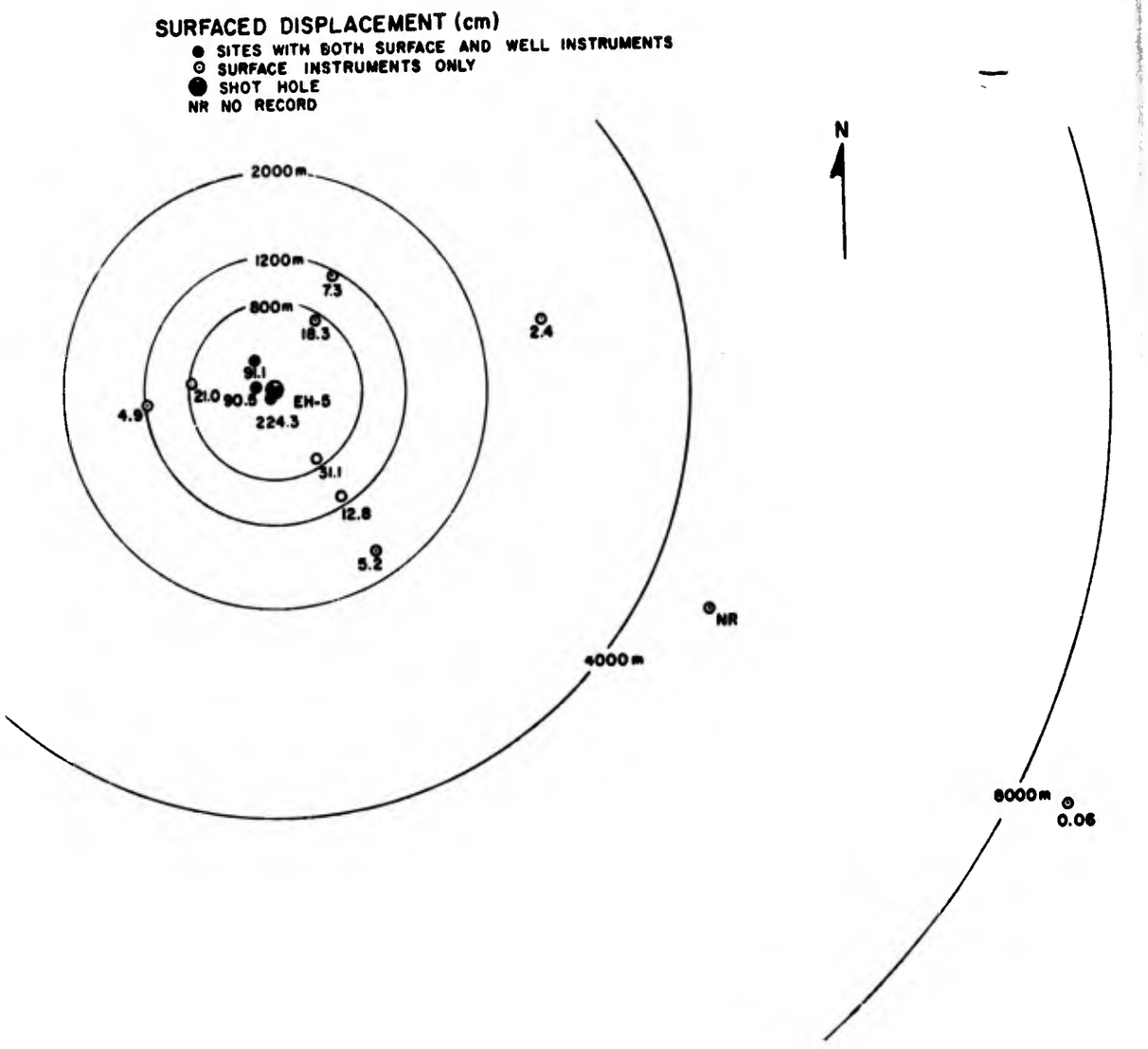

Figure 17. Surface particle displacements measured at the LONG SHOT site.

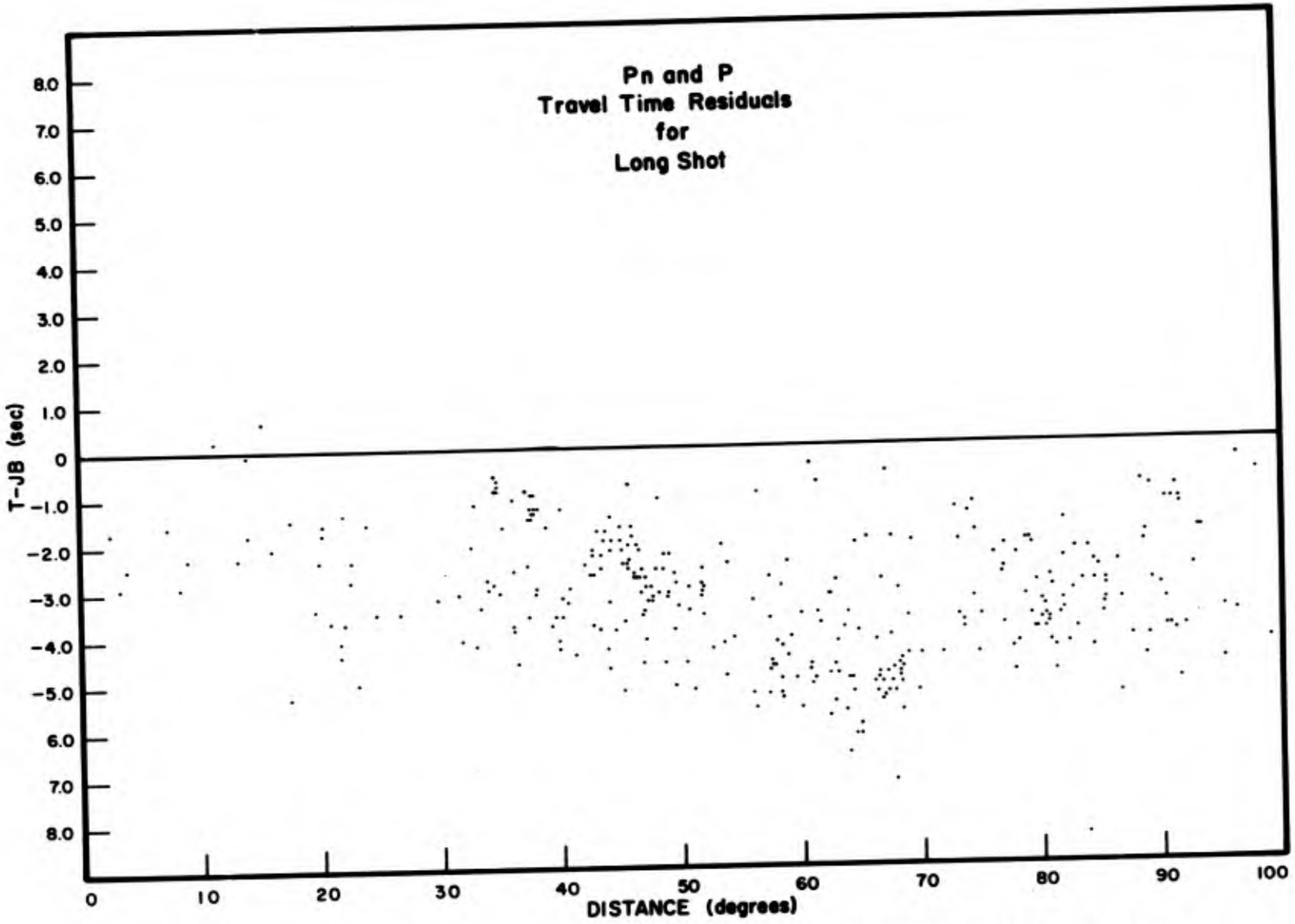

Figure 18. Pn and P travel-time residuals versus distance for LONG SHOT with respect to JB surface-focus travel times.

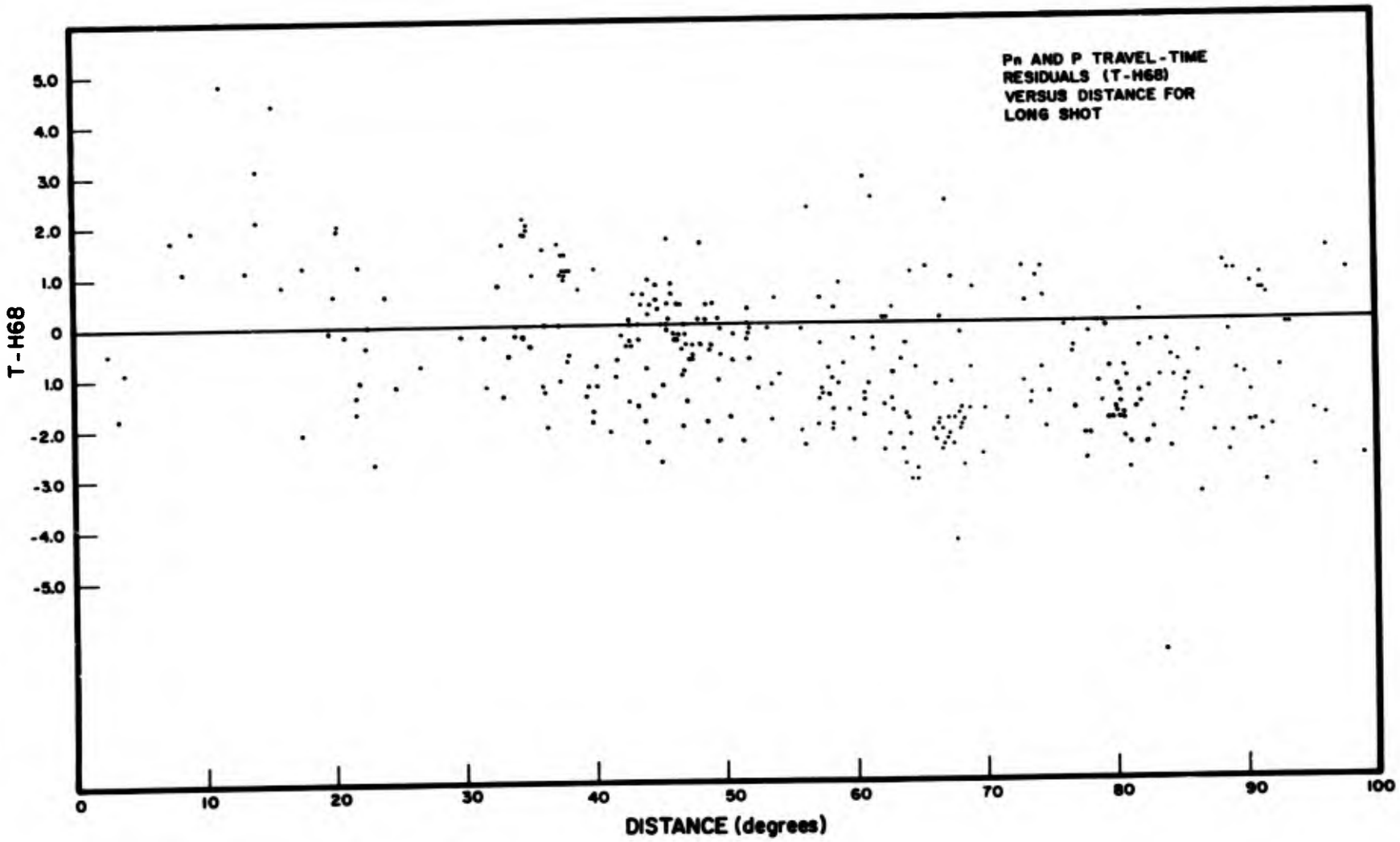

Figure 19. Pn and P travel-time residuals versus distance for LONG SHOT with respect to H68 surface-focus travel time.

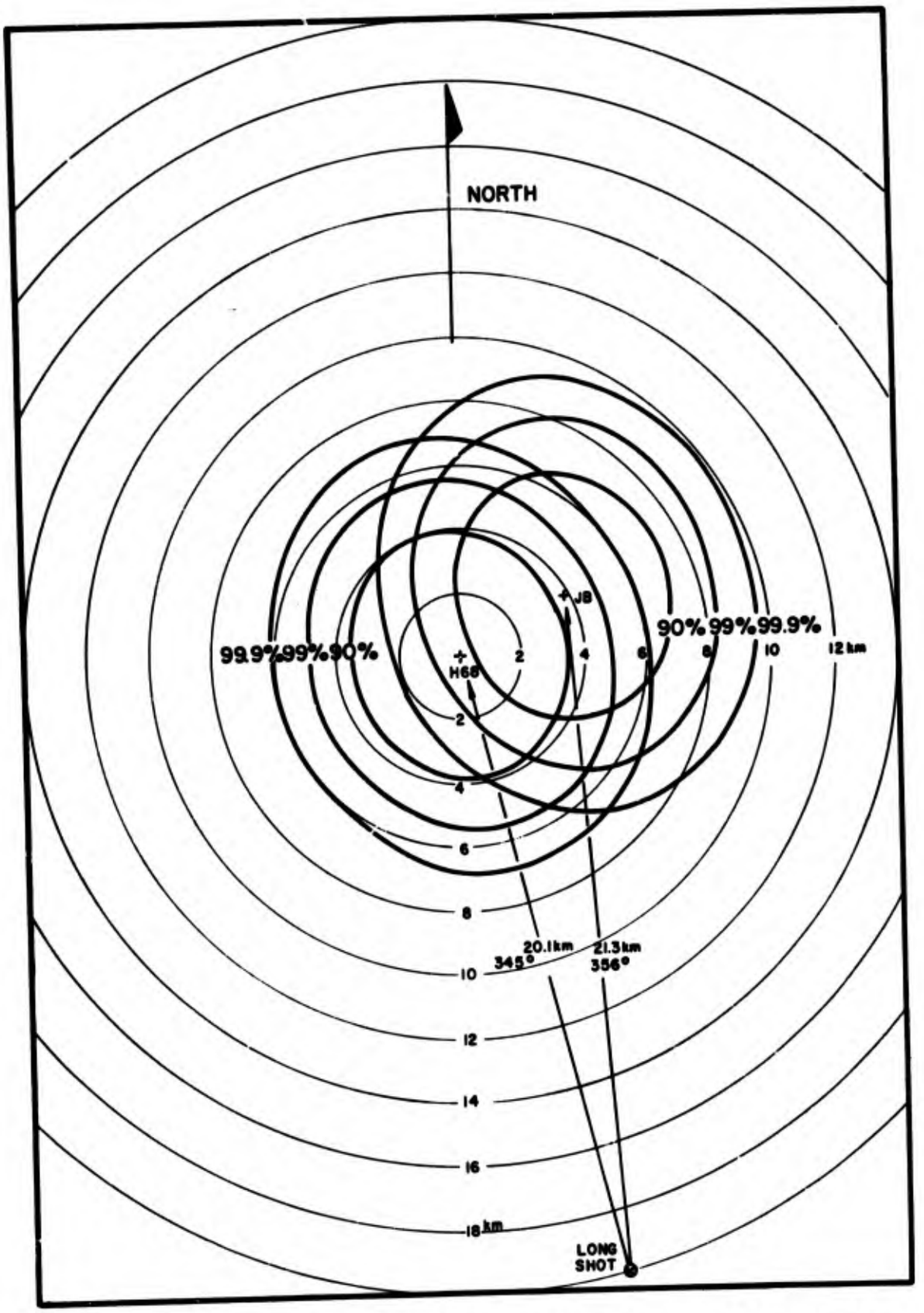

Figure 20. Computed epicenters and confidence ellipses for LONG SHOT with JB and H68 tables-depth restrained to surface.

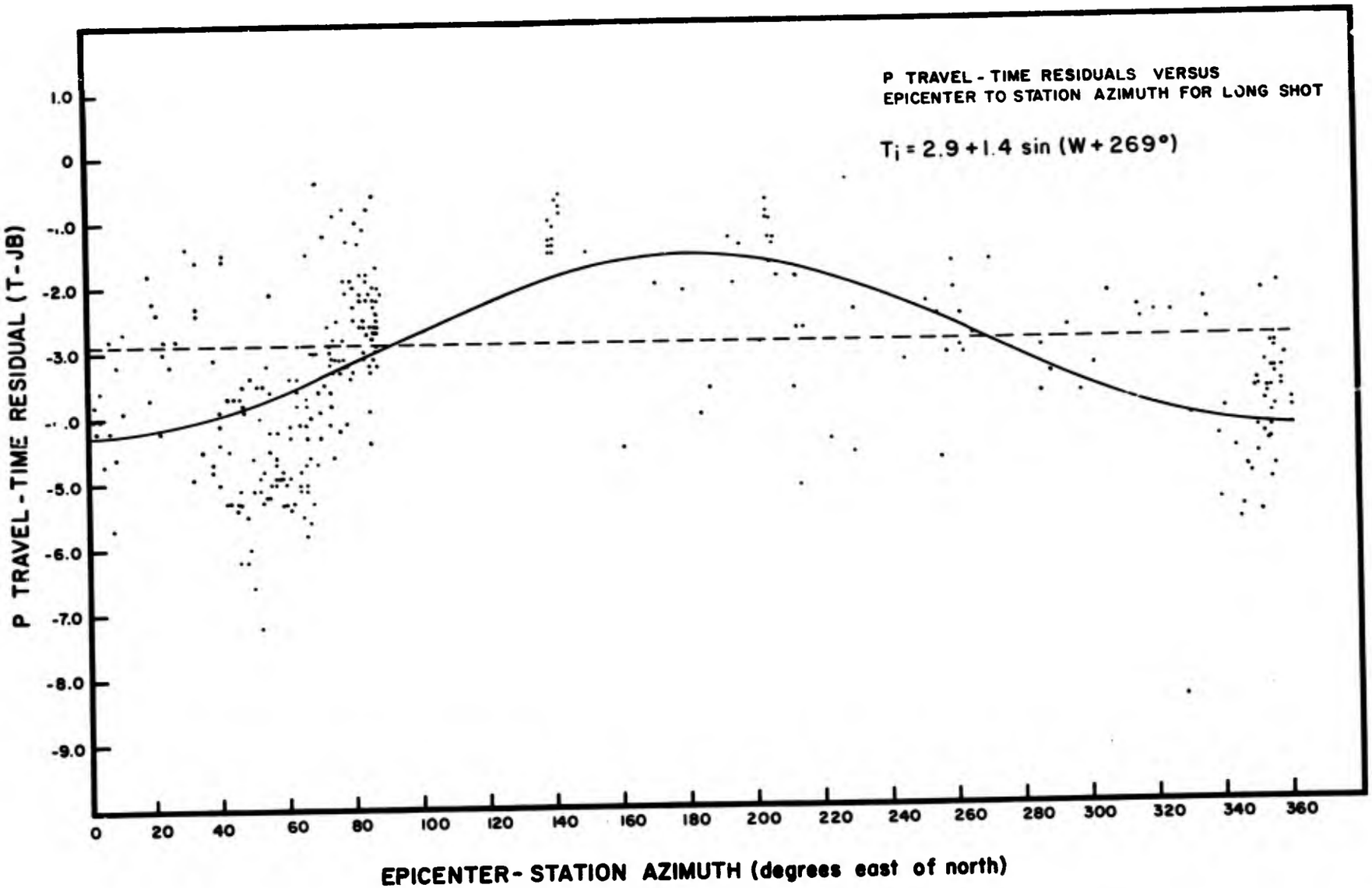

Figure 21. JB travel-time residuals versus azimuth for LONG SHOT P phase.

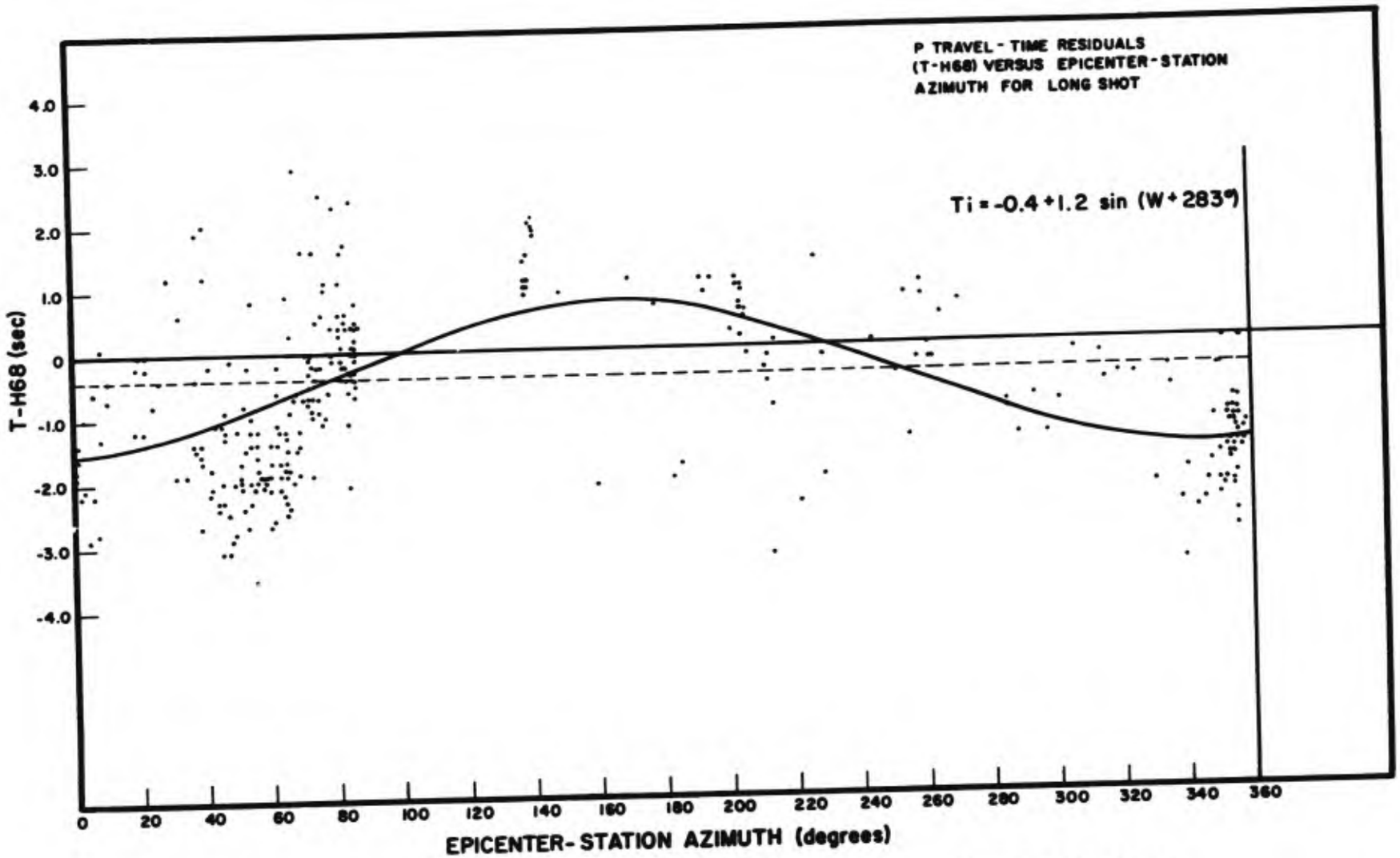

Figure 22. H68 travel-time residuals versus azimuth for LONG SHOT P phase.

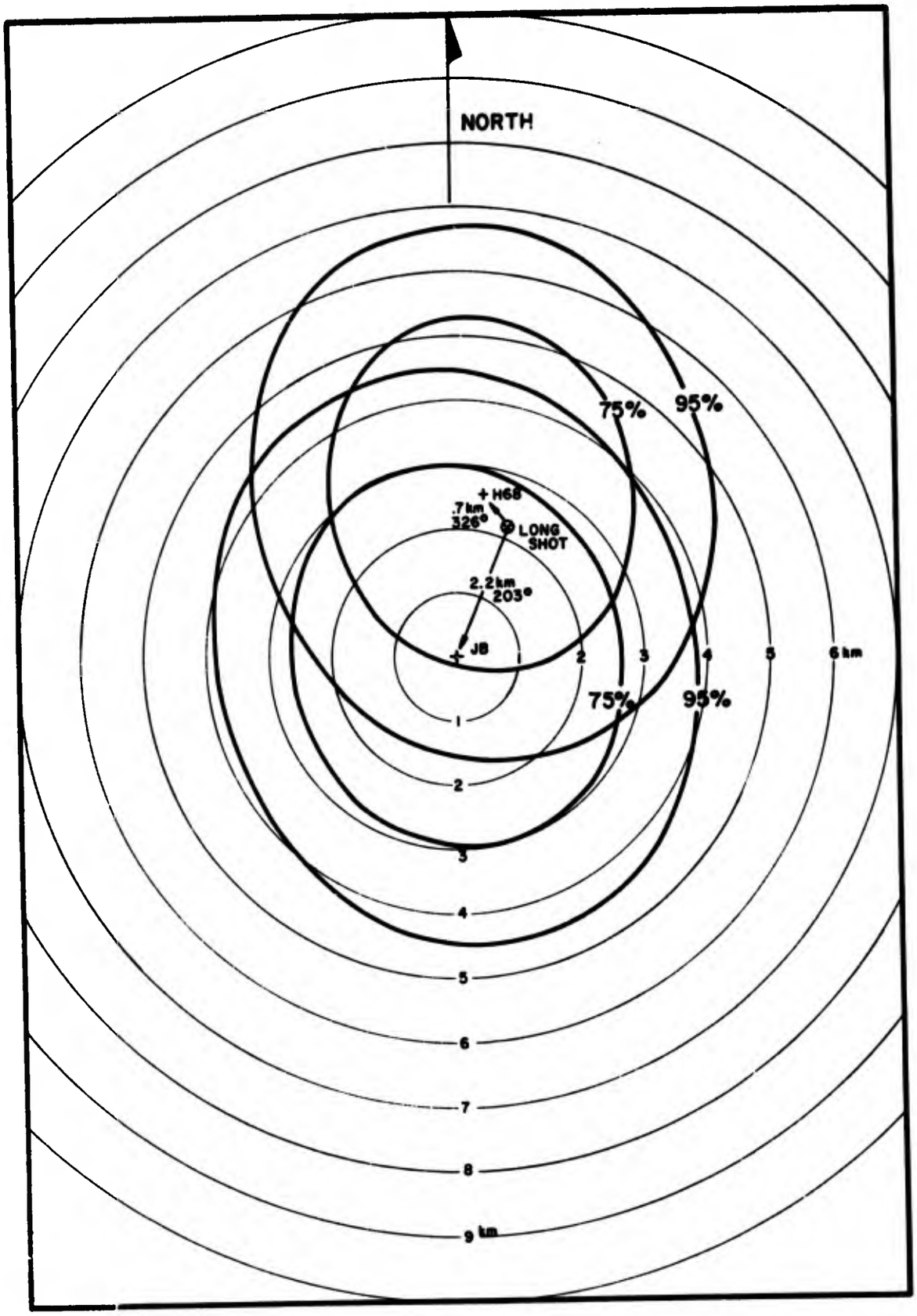

Figure 23. Computed epicenters and confidence ellipses for LONG SHOT with JB and H68 tables after sine-curve azimuthal correction is applied-depth restrained to surface.

Figure 24. Contours of negative JB travel-time residuals for LONG SHOT - equidistant azimuthal oblique polar projection from Amchitka Island.

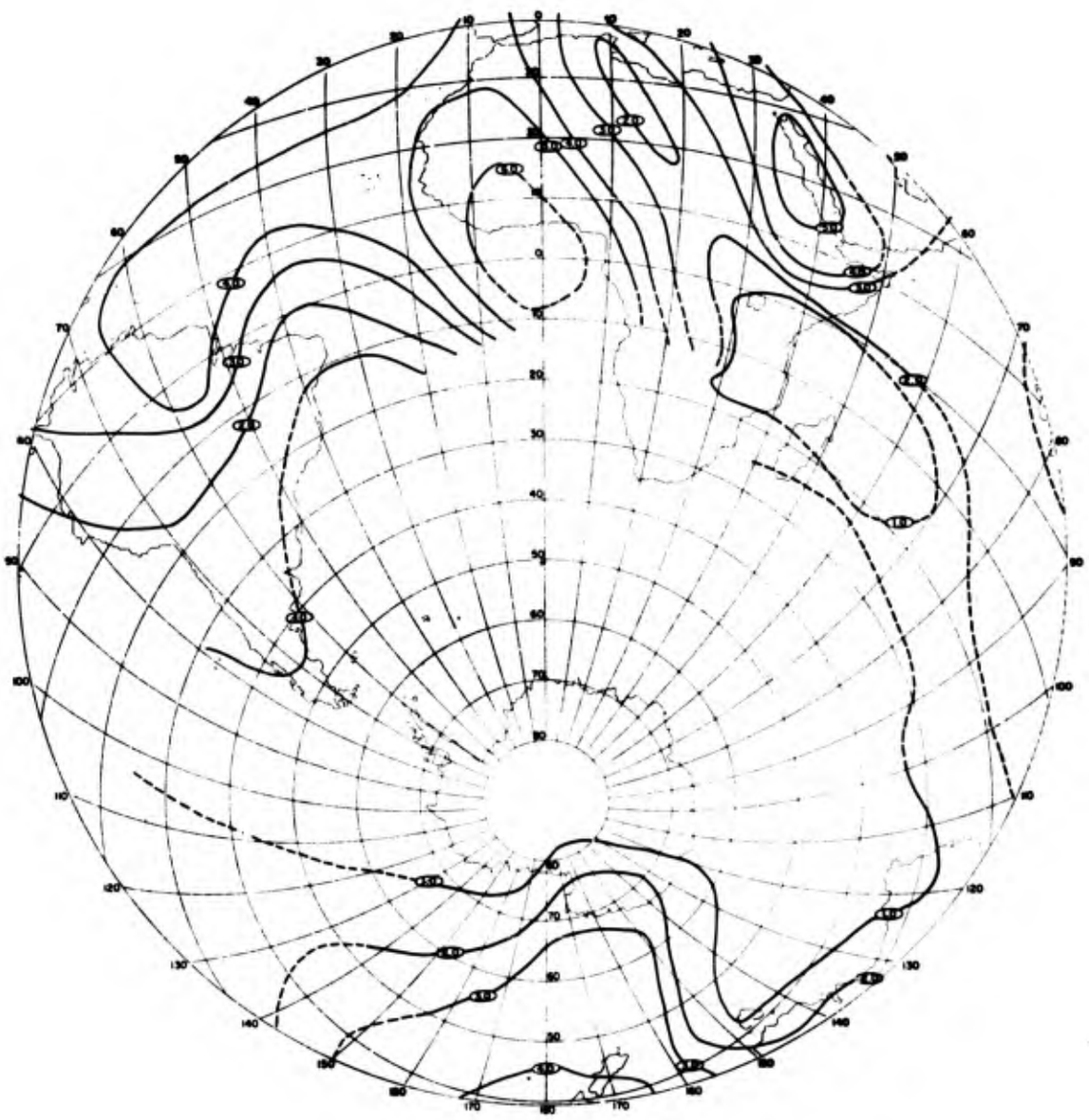

Figure 25. Contours of negative JB travel-time residuals for LONG SHOT - equidistant azimuthal oblique polar projection from the antipode of Amchitka Island.

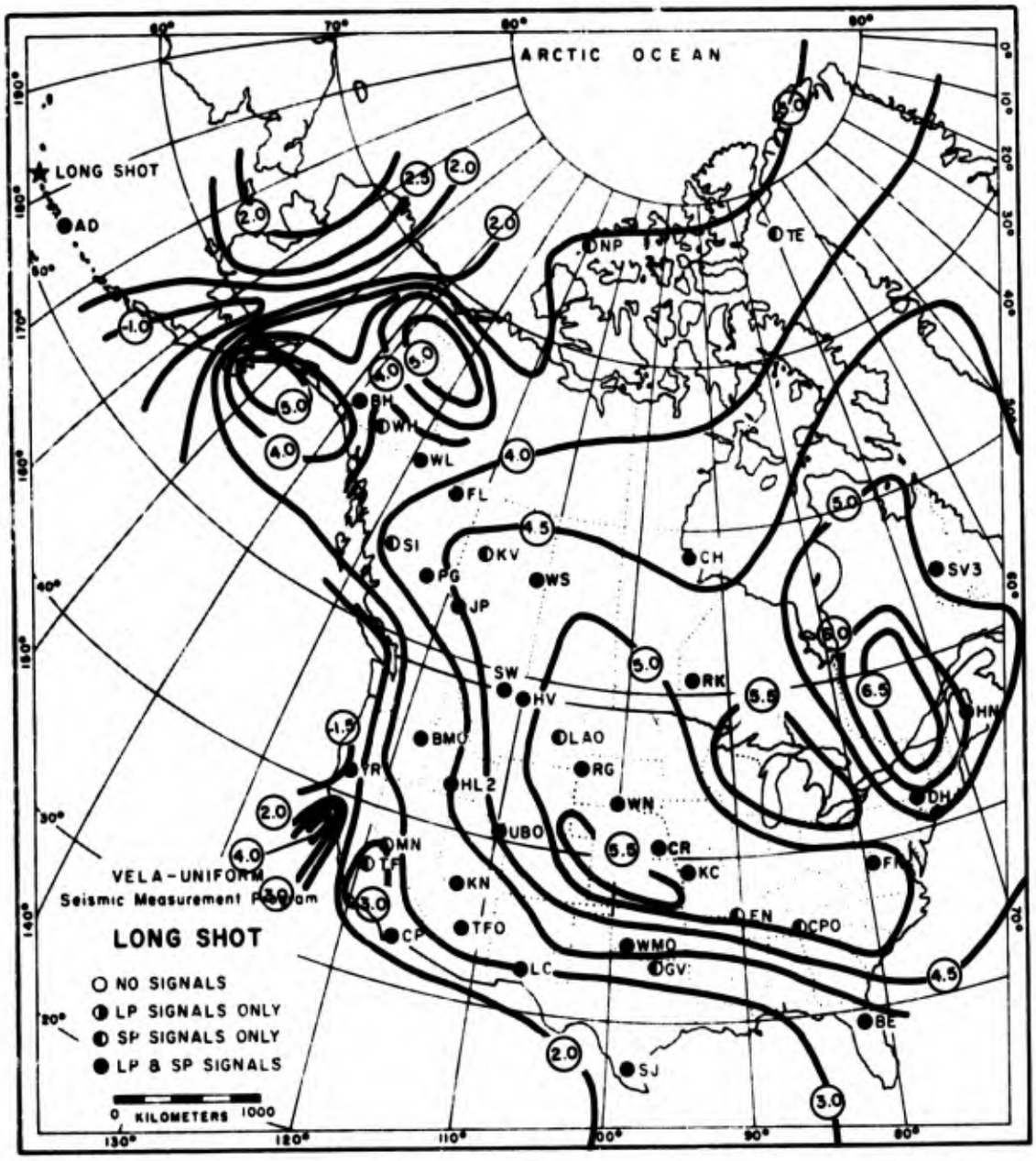

Figure 26. Contours of negative JB travel-time residuals for LONG SHOT P phase on conic projection of North America.

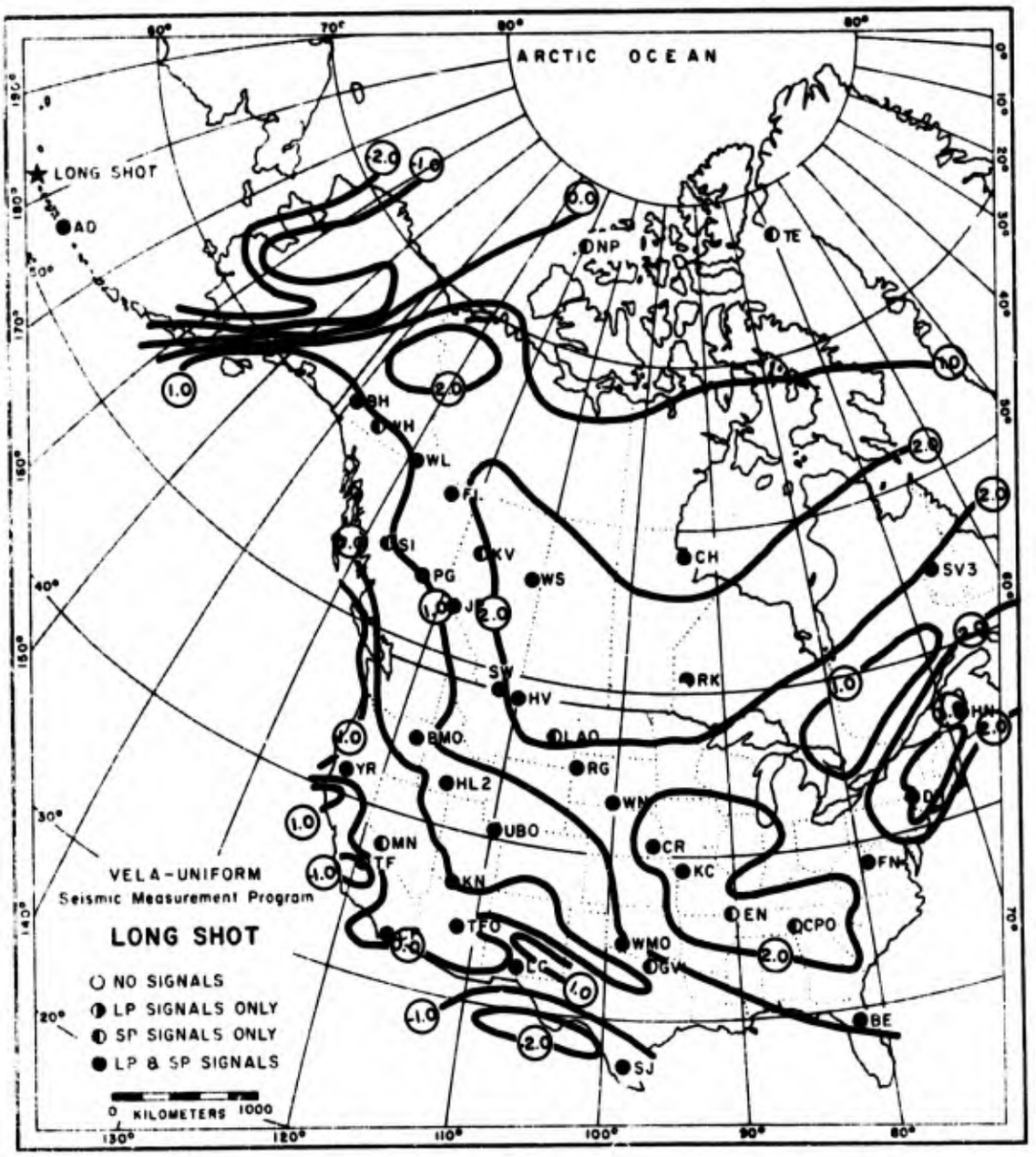

Figure 27. Contours of negative H68 travel-time residuals for LONG SHOT P phase on conic projection of North America.

Figure 28. Tectonic map of North America (King, 1959).

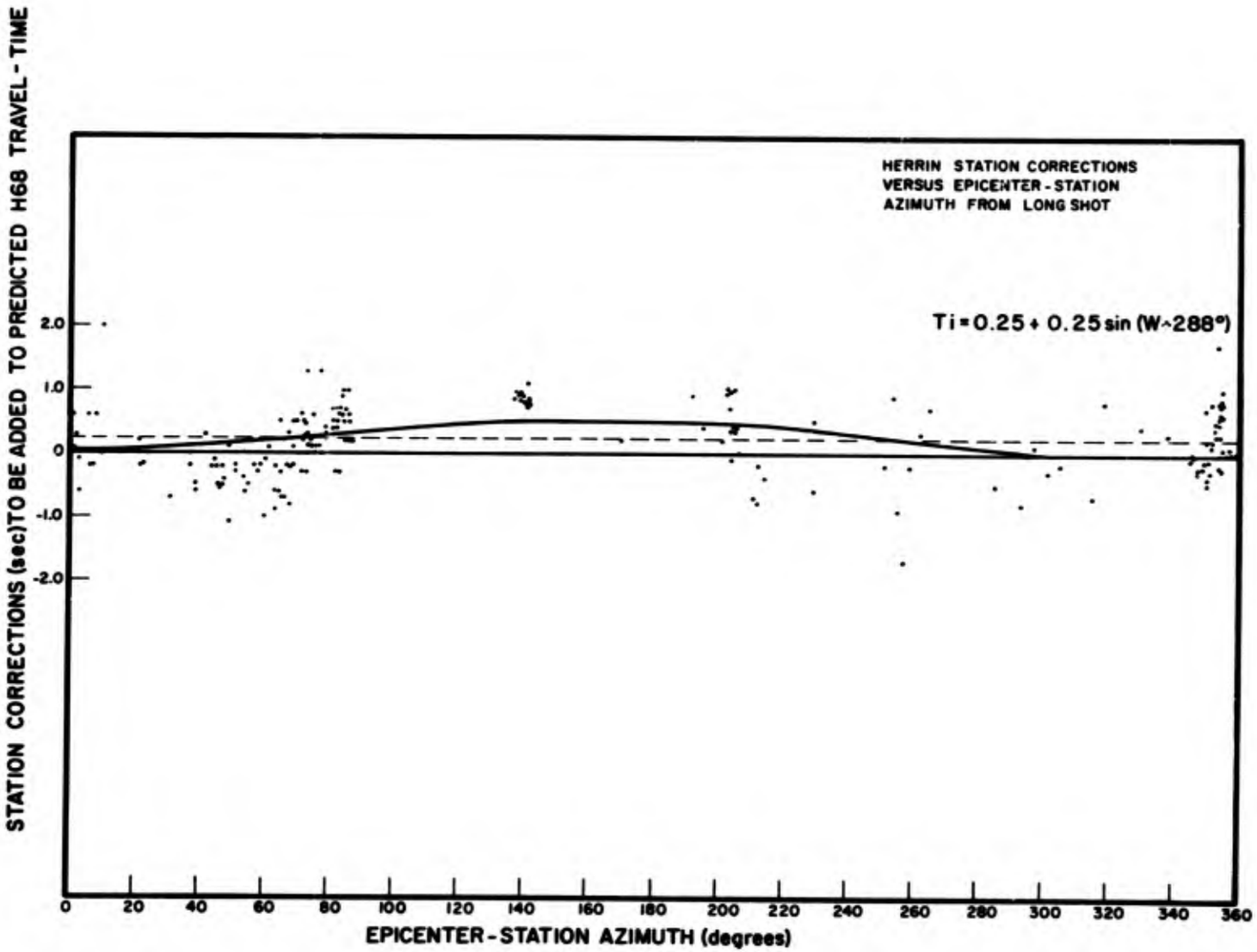

Figure 29. Herrin and Taggart stations corrections versus azimuth for LONG SHOT.

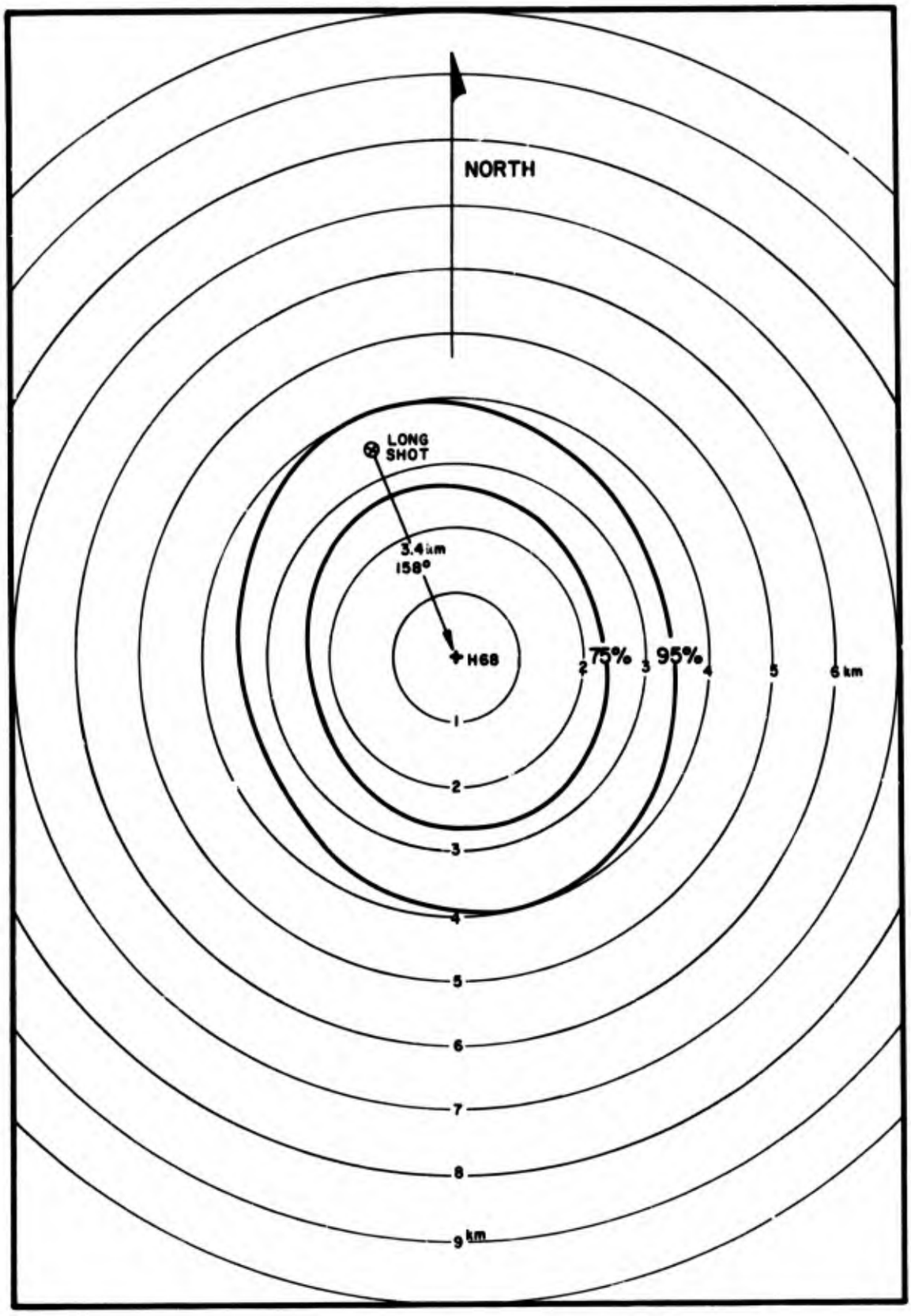

Figure 30. Computed epicenter and confidence ellipses for LONG SHOT with H68 tables after sine-curve azimuthal correction and station corrections are applied-depth restrained to surface.

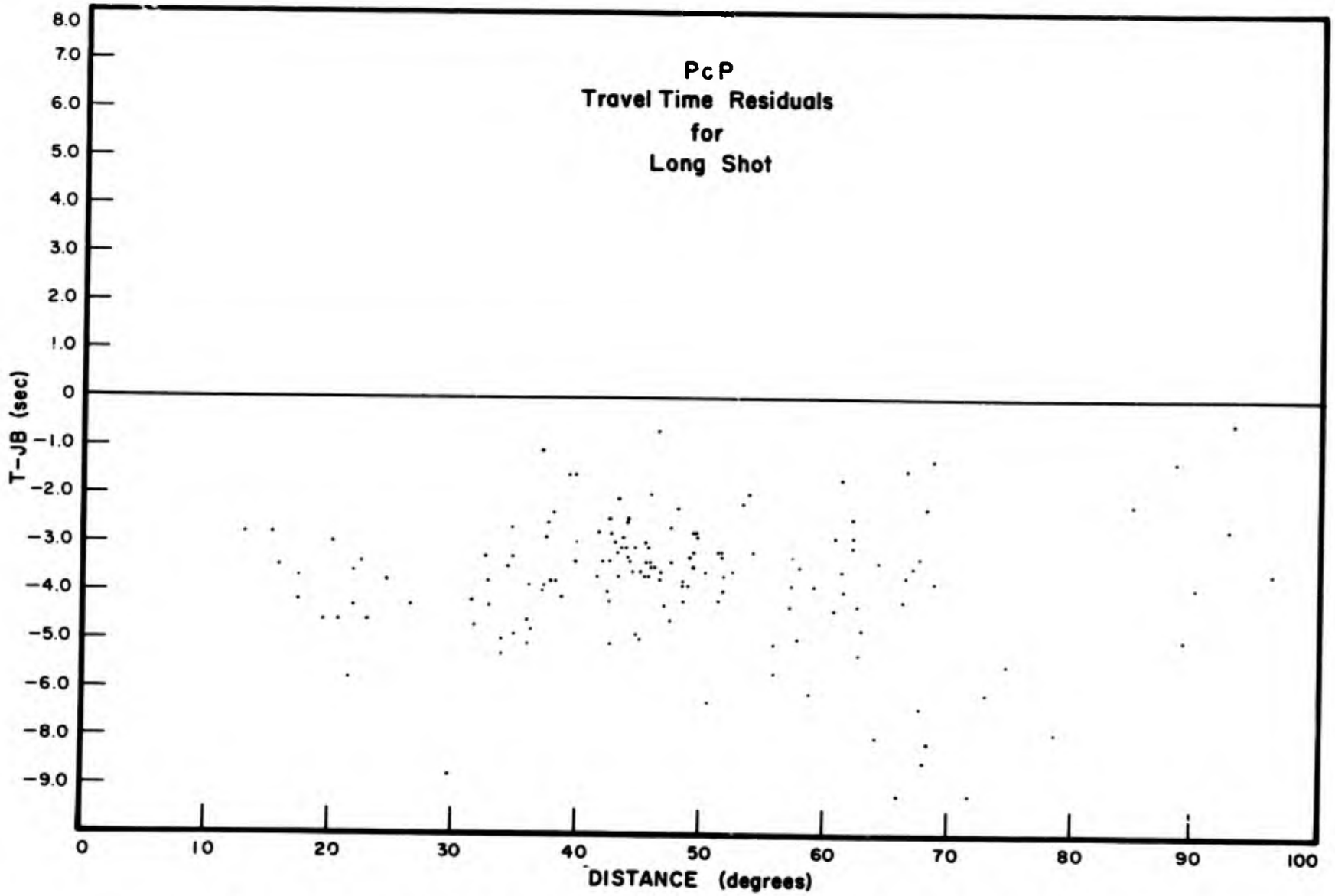

Figure 31. JB travel-time residuals versus distance for LONG SHOT PcP phase.

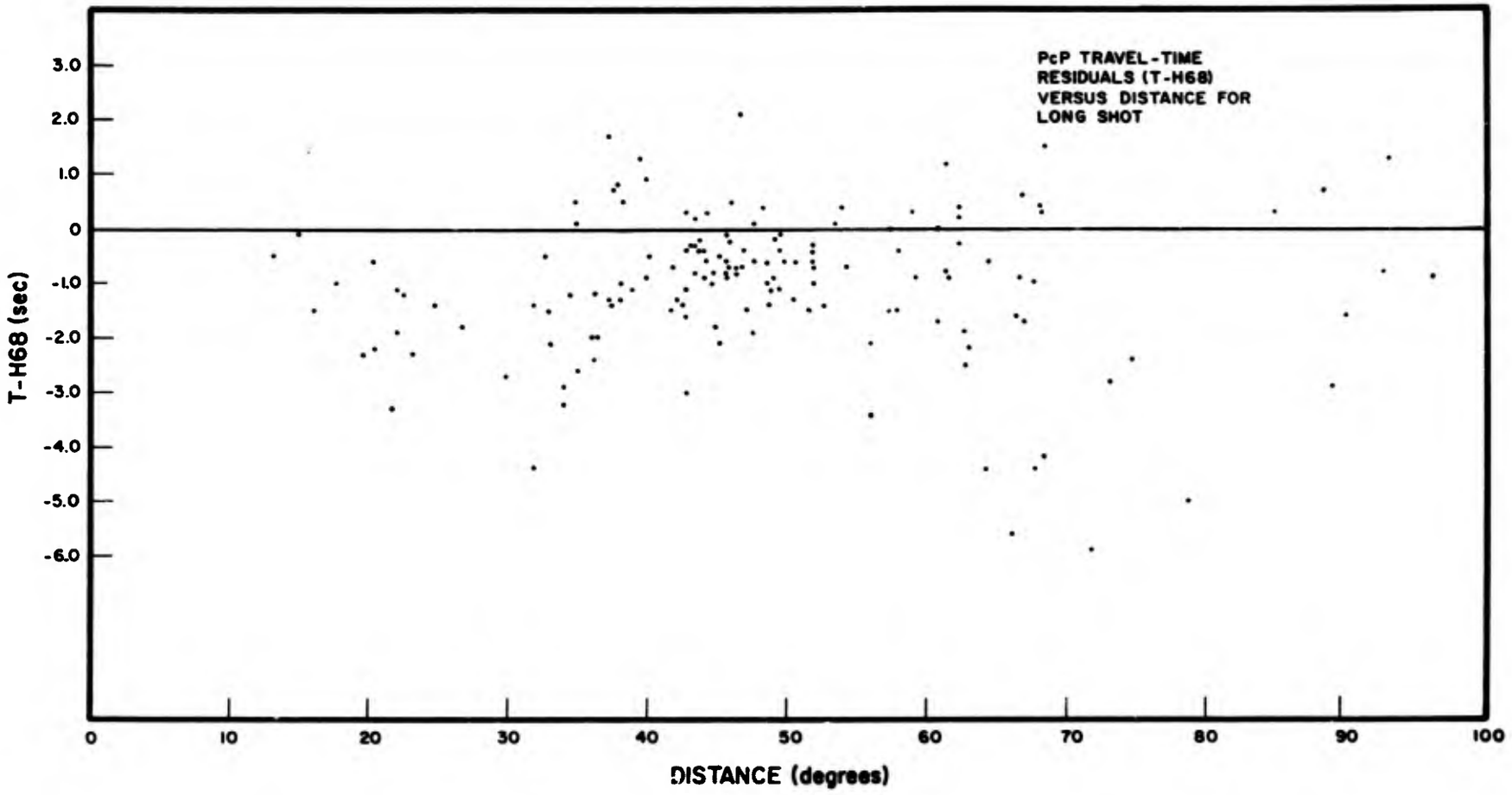

Figure 32. H68 travel-time residuals versus distance for LONG SHOT PcP phase.

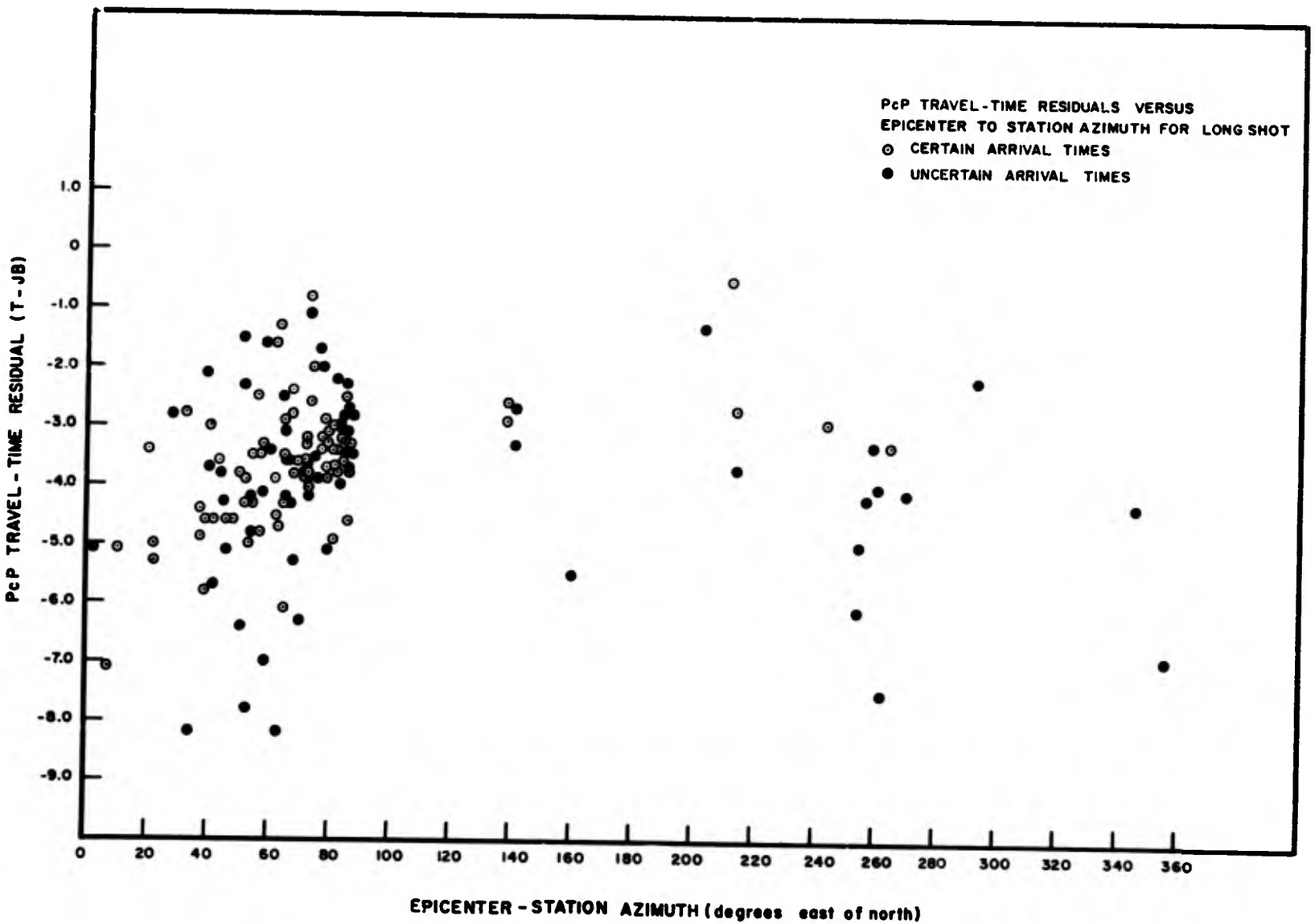

Figure 33. JB travel-time residuals versus azimuth for LONG SHOT PcP phase.

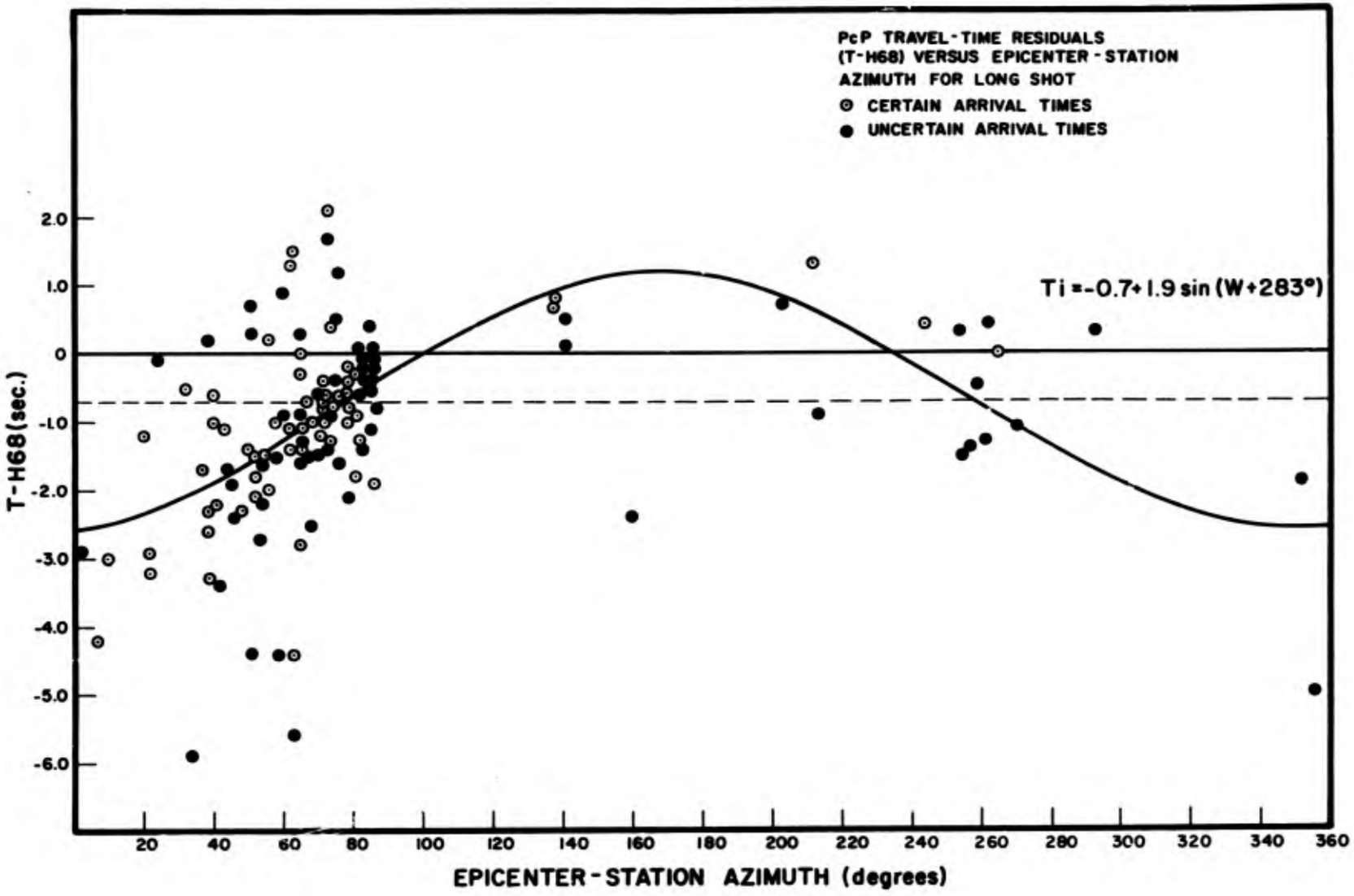

Figure 34. H68 travel-time residuals versus azimuth for LONG SHOT PcP phase.

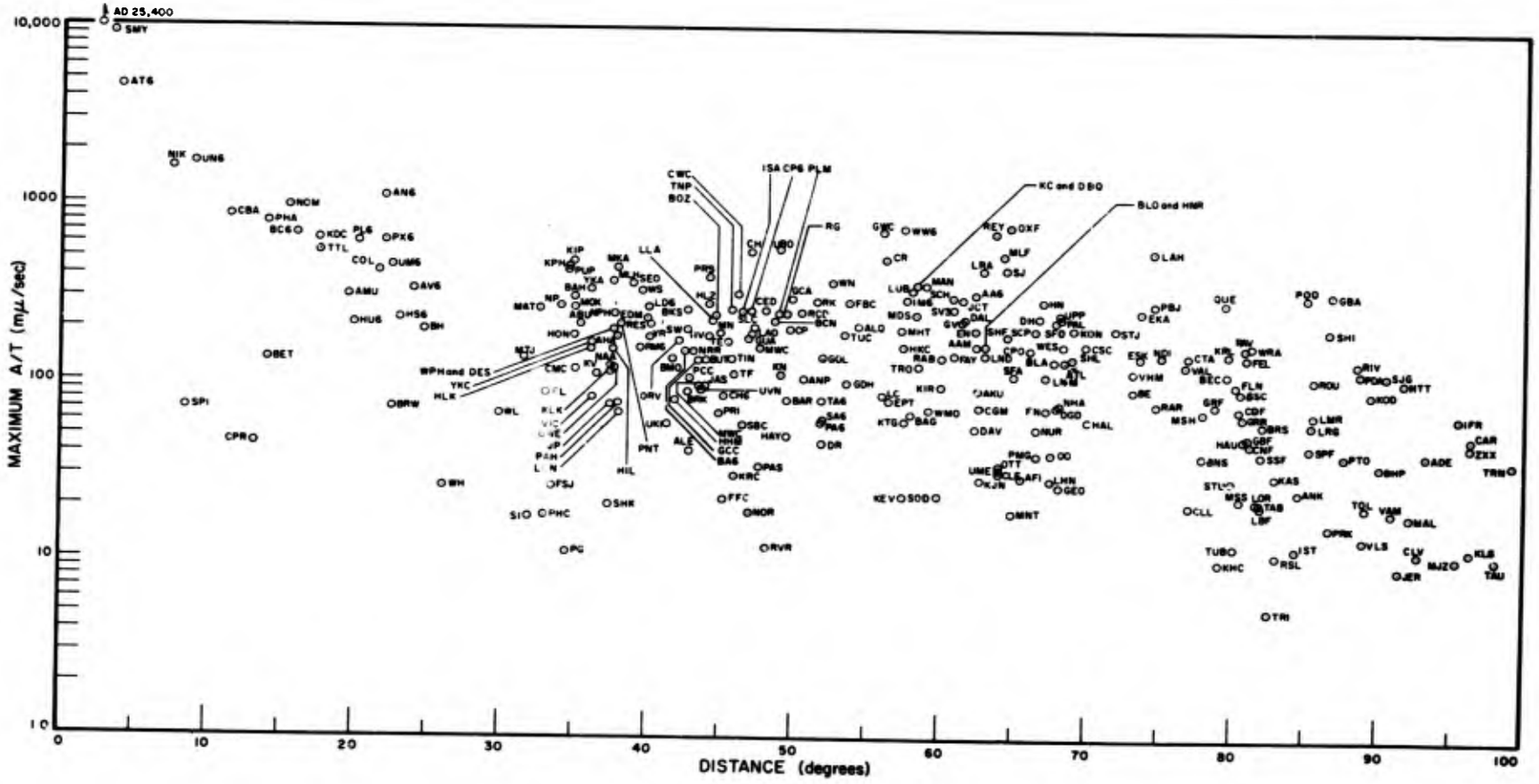

Figure 35. Zero-to-peak maximum amplitudes (A/T) of Pn and P versus distance for LONG SHOT.

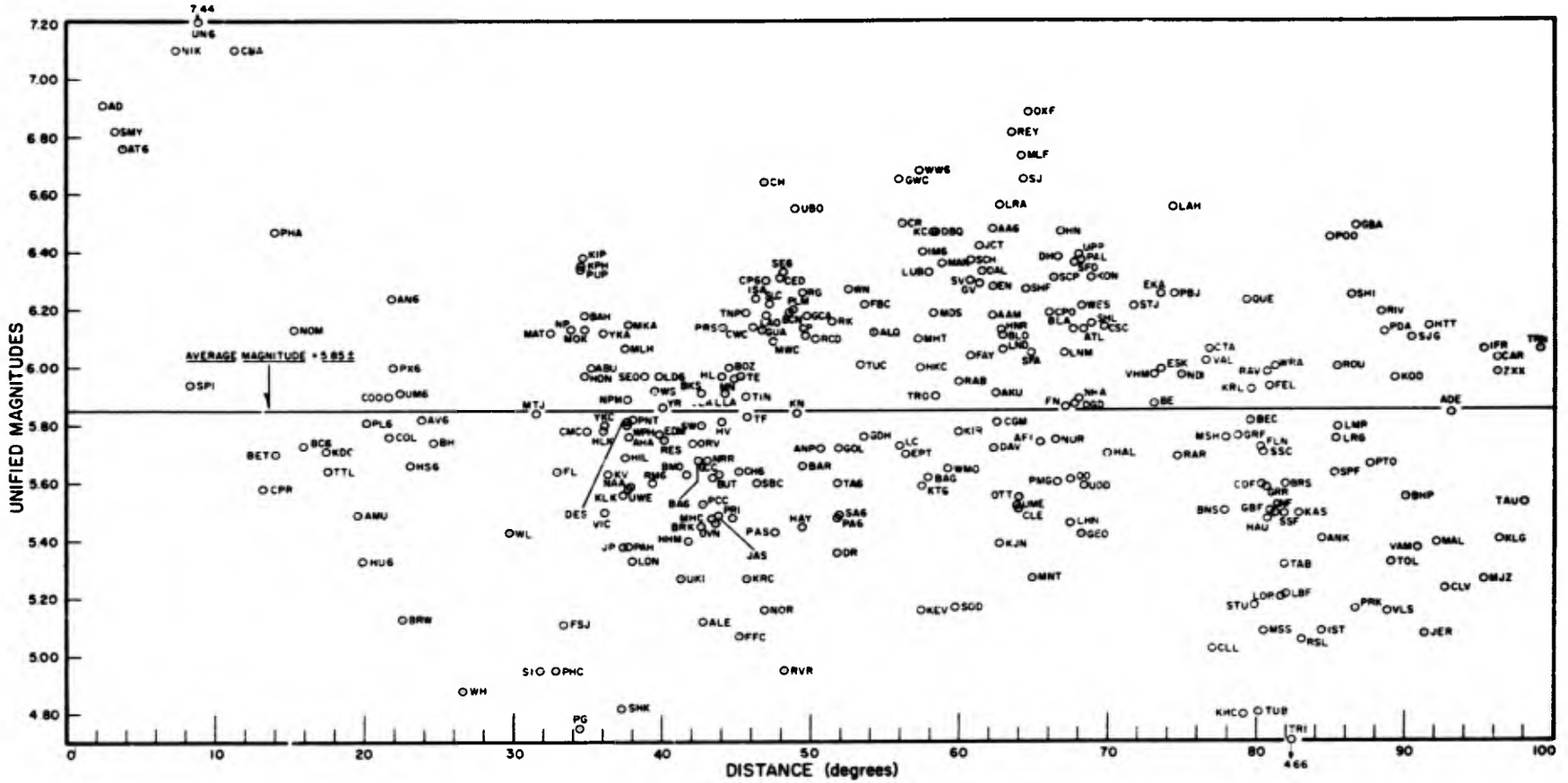

Figure 36. Unified body-wave magnitudes versus distance LONG SHOT.

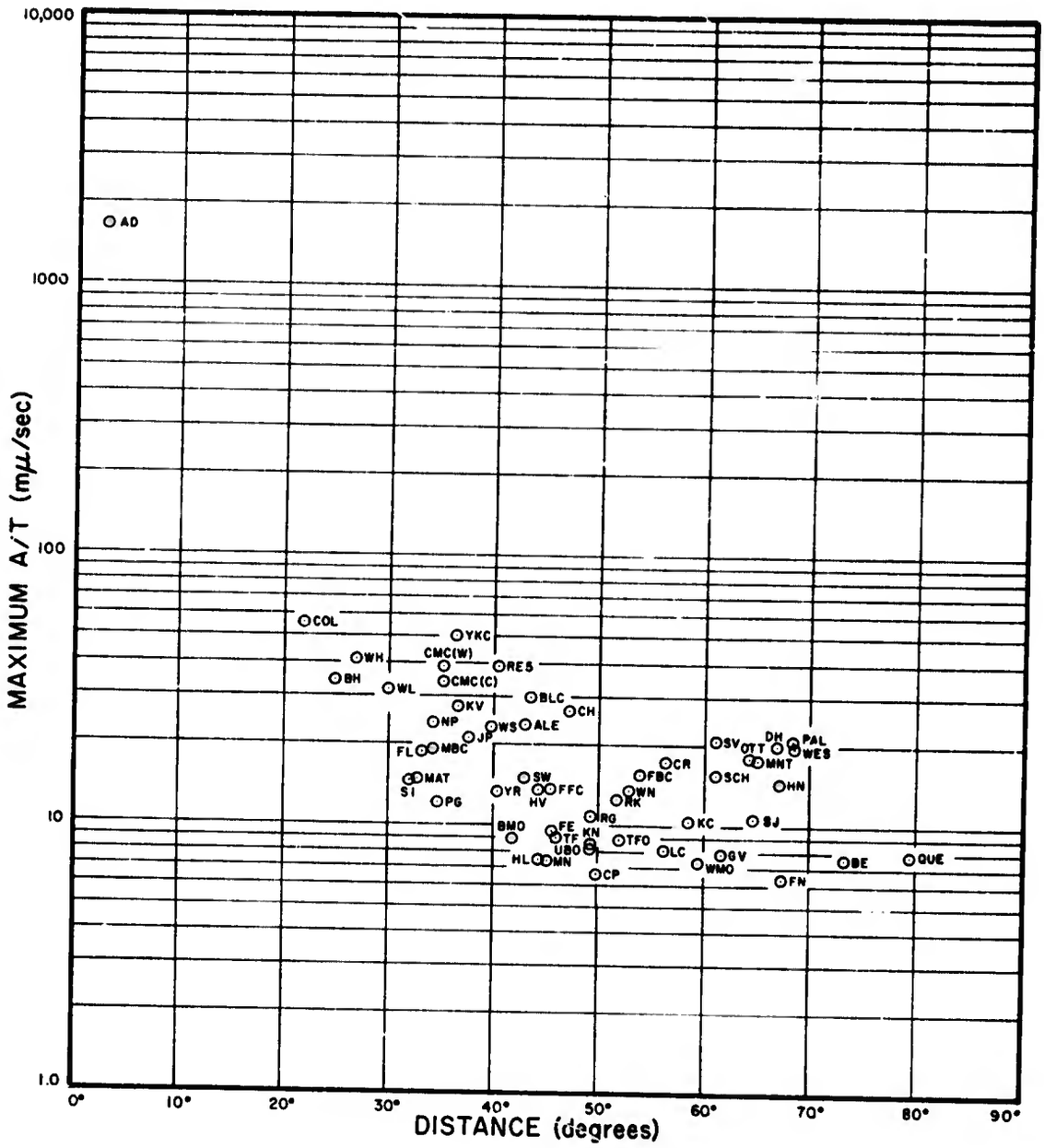

Figure 37. Zero-to-peak maximum amplitudes (A/T) of LR versus distance for LONG SHOT.

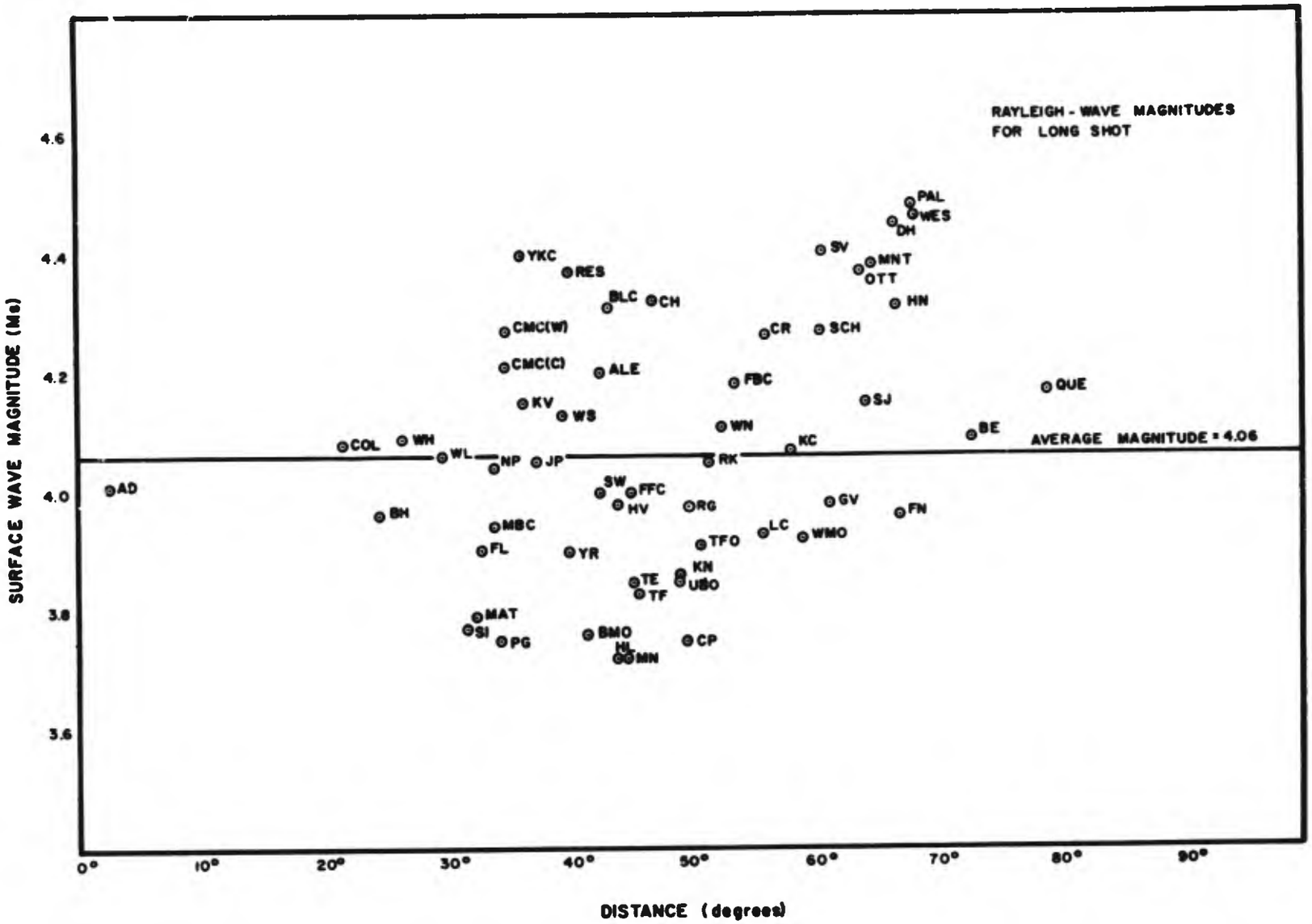

Figure 38. Surface-wave (LR) magnitudes versus distance . LONG SHOT.

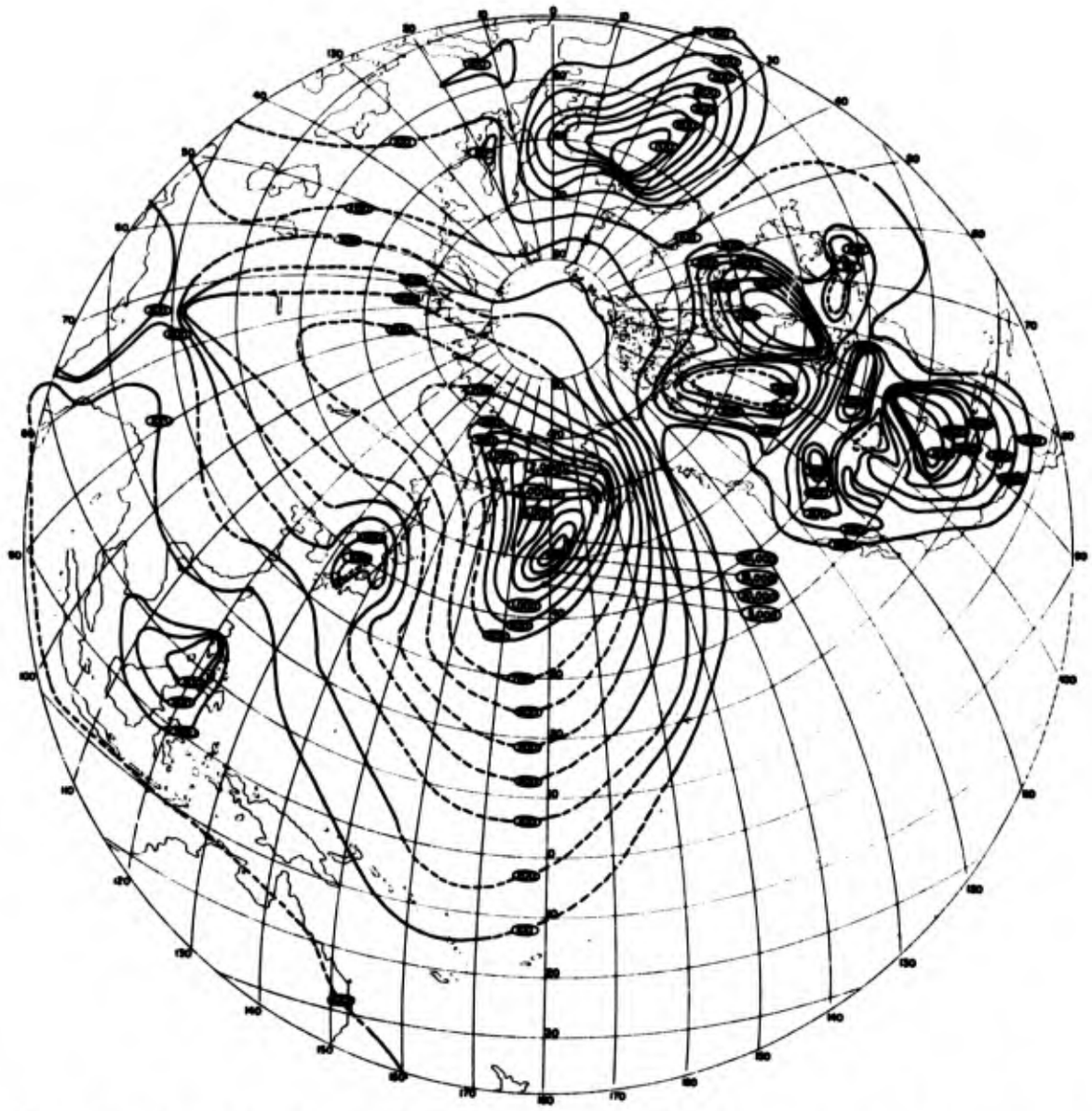

Figure 39. Zero-to-peak Pn and P amplitude contours for LONG SHOT - azimuthal equidistant oblique polar projection with focus on Amchitka Island.

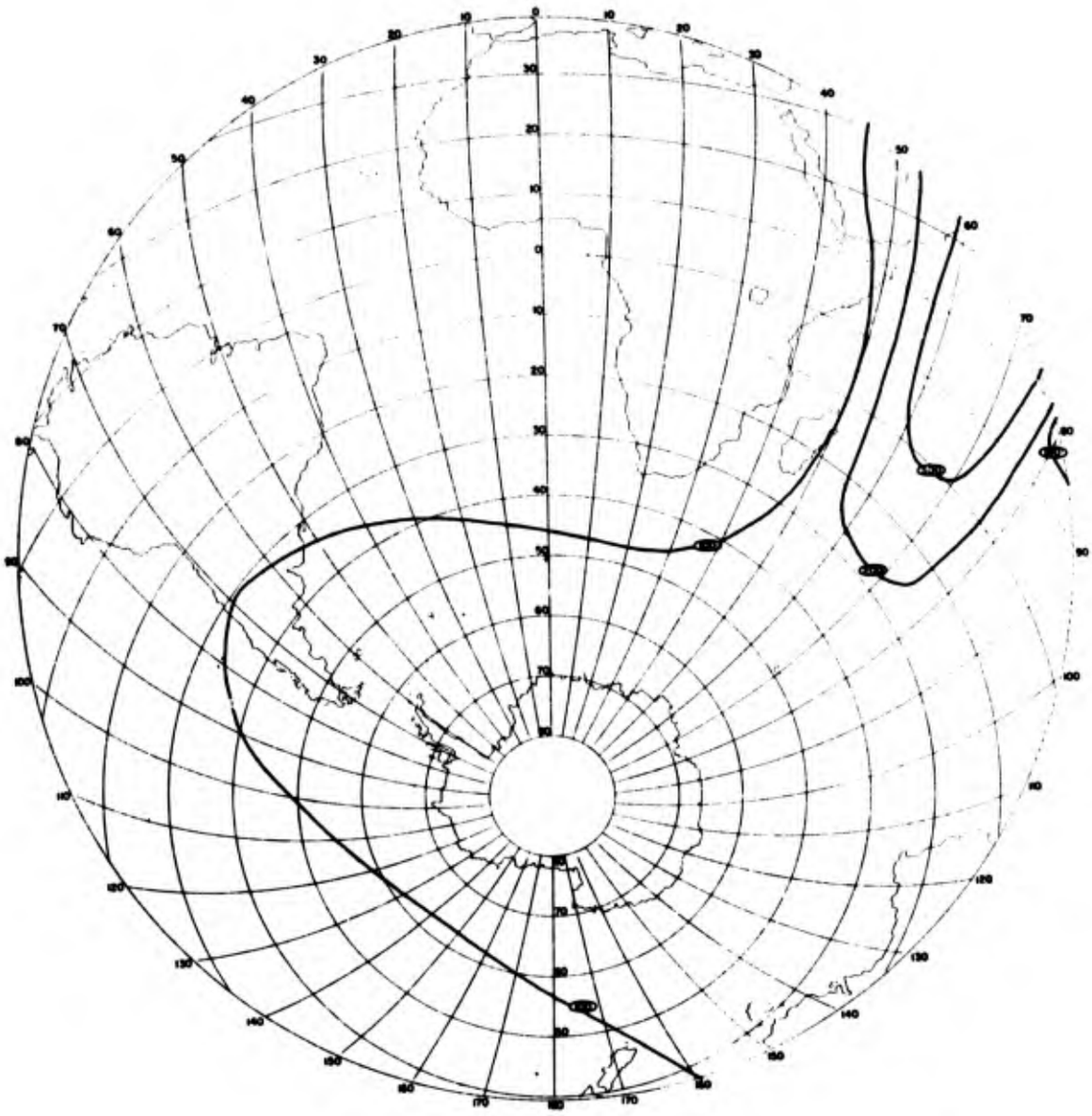

Figure 40. Zero-to-peak P and PKP amplitude contours for LONG SHOT - azimuthal equidistant oblique polar projection with focus on antipode of Amchitka Island.

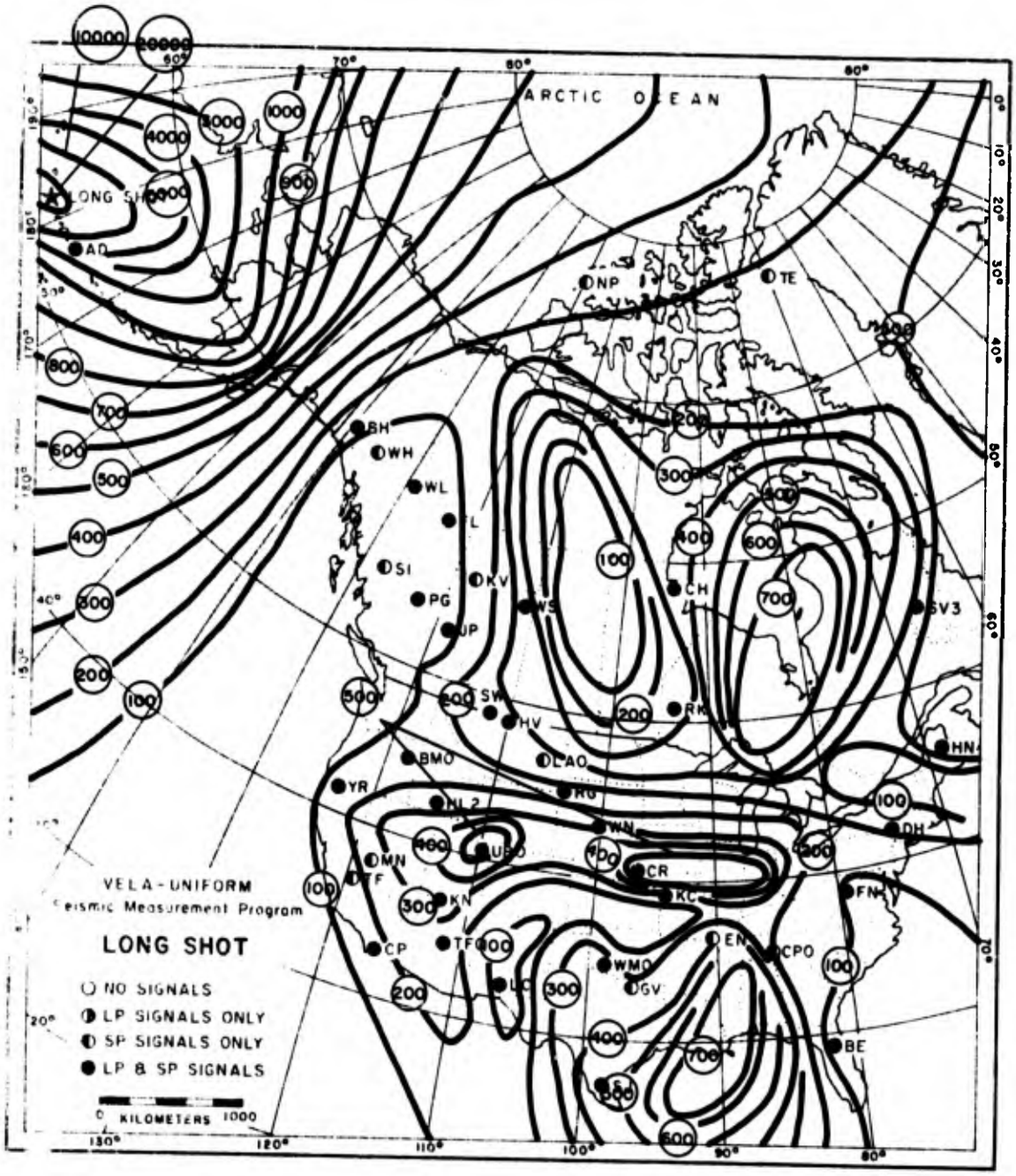

Figure 41. Zero-to-peak Pn and P amplitude contours for LONG SHOT on conic projection of North America.

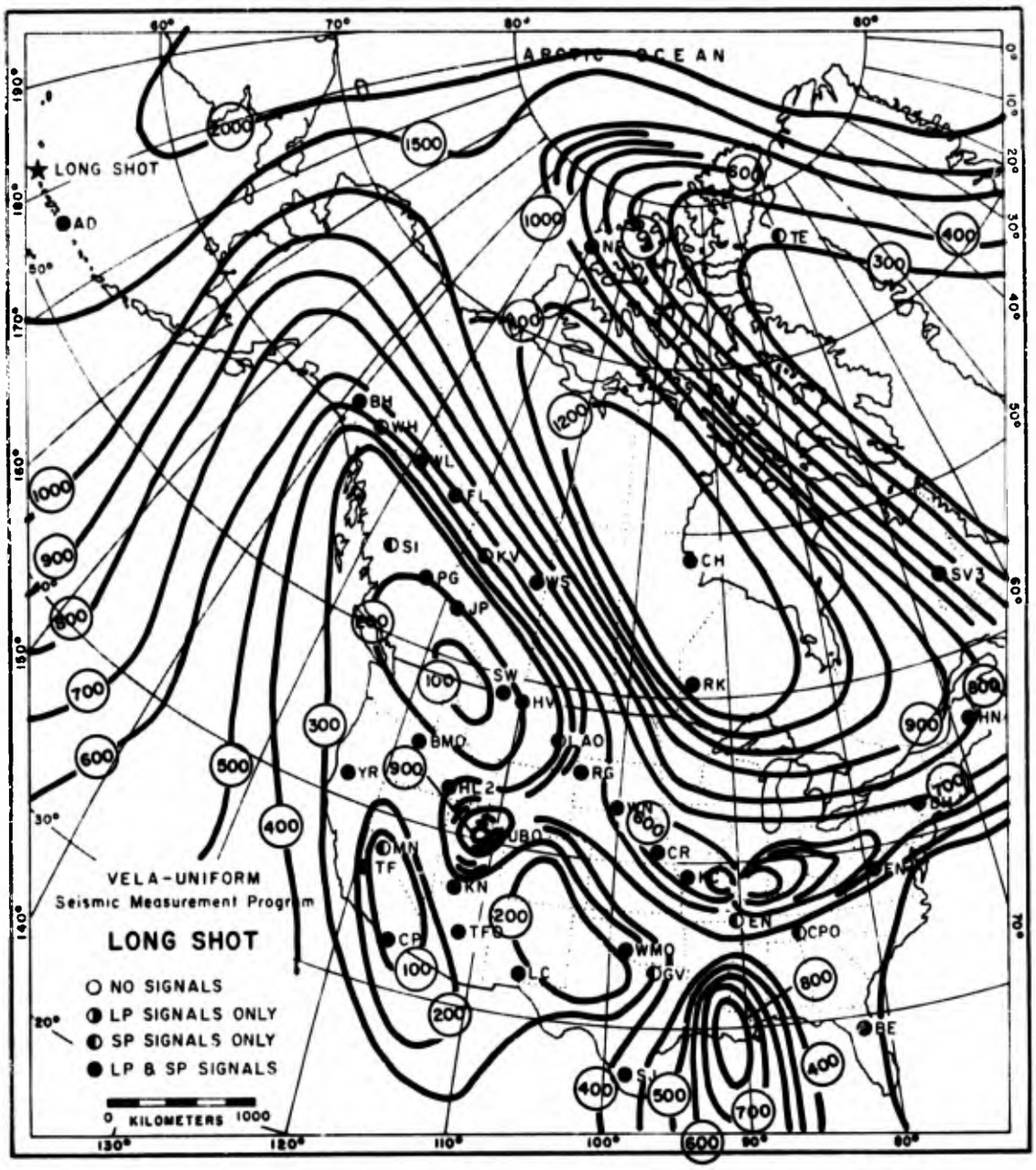

Figure 42. Zero-to-peak Pn and P amplitude contours for Novaya Zemlya event on conic projection of North America.

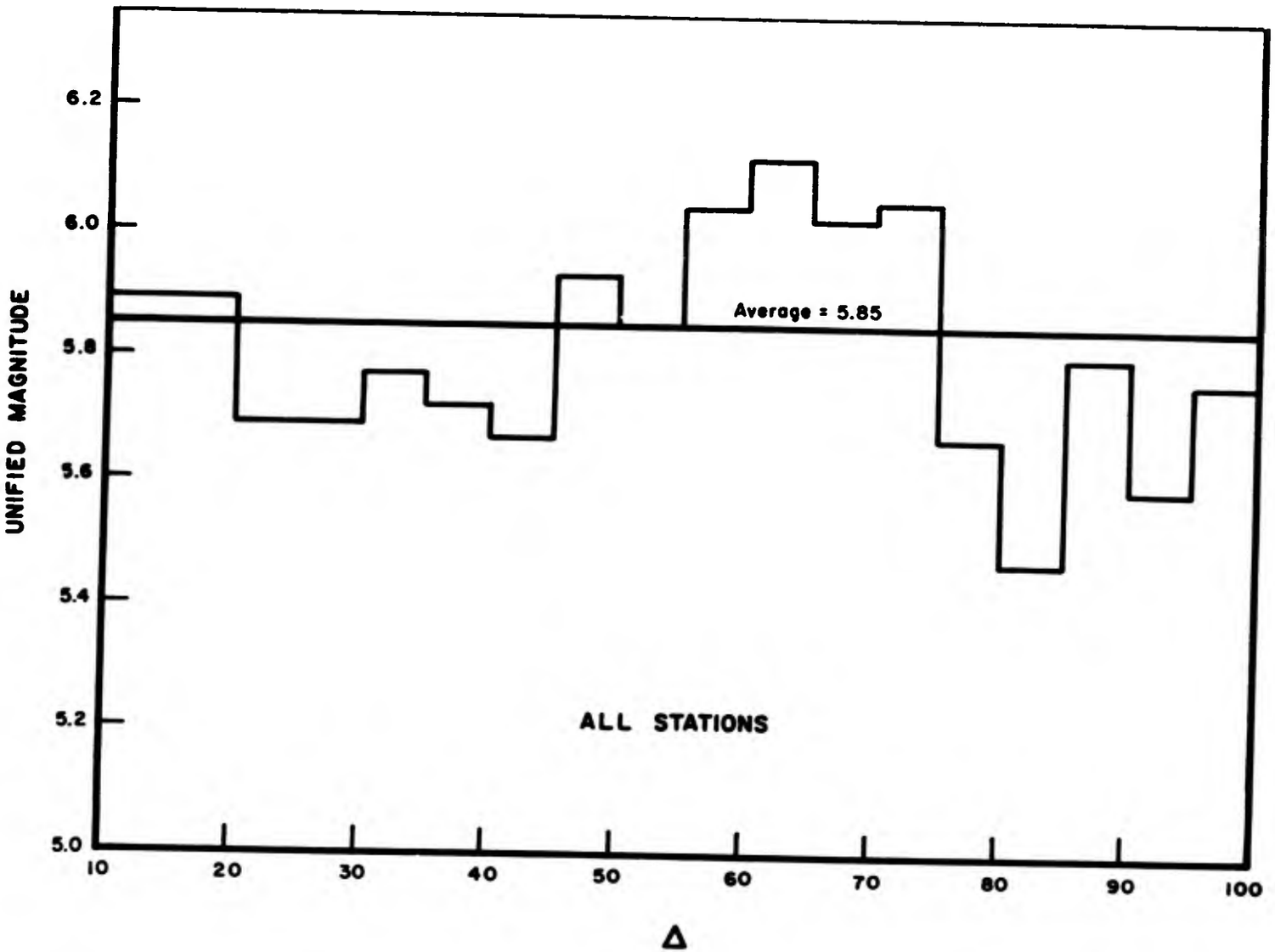

Figure 43. Histogram of average magnitude in each 5° interval of epicentral distance for LONG SHOT.

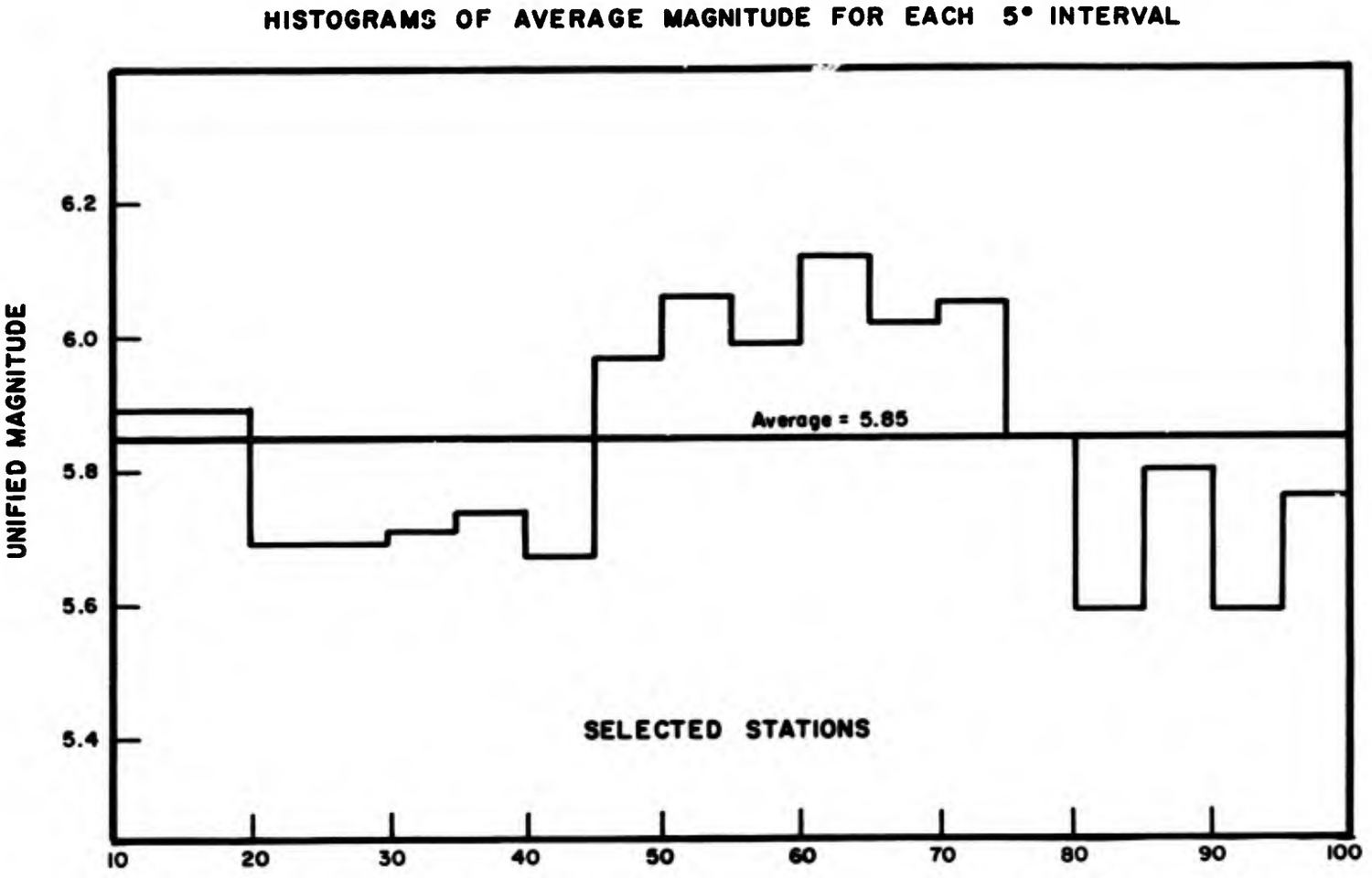

Figure 44. Histogram of average magnitude in each 5° interval of epicentral distance for LONG SHOT with doubtful station magnitude removed.

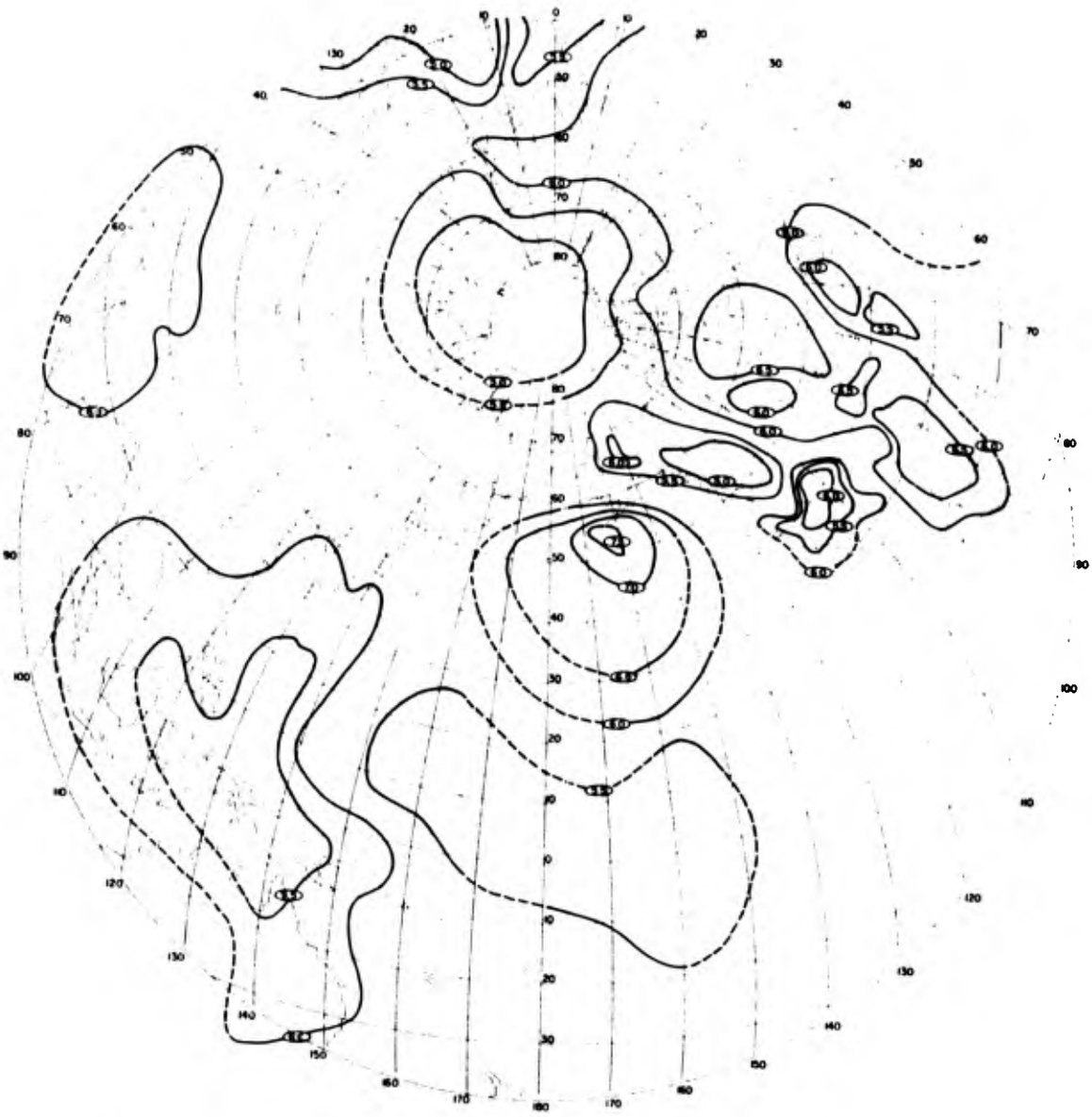

Figure 45. Unified body-wave magnitude cortours for LONG SHOT - azimuthal equidistant oblique polar projection with focus on Amchitka Island.

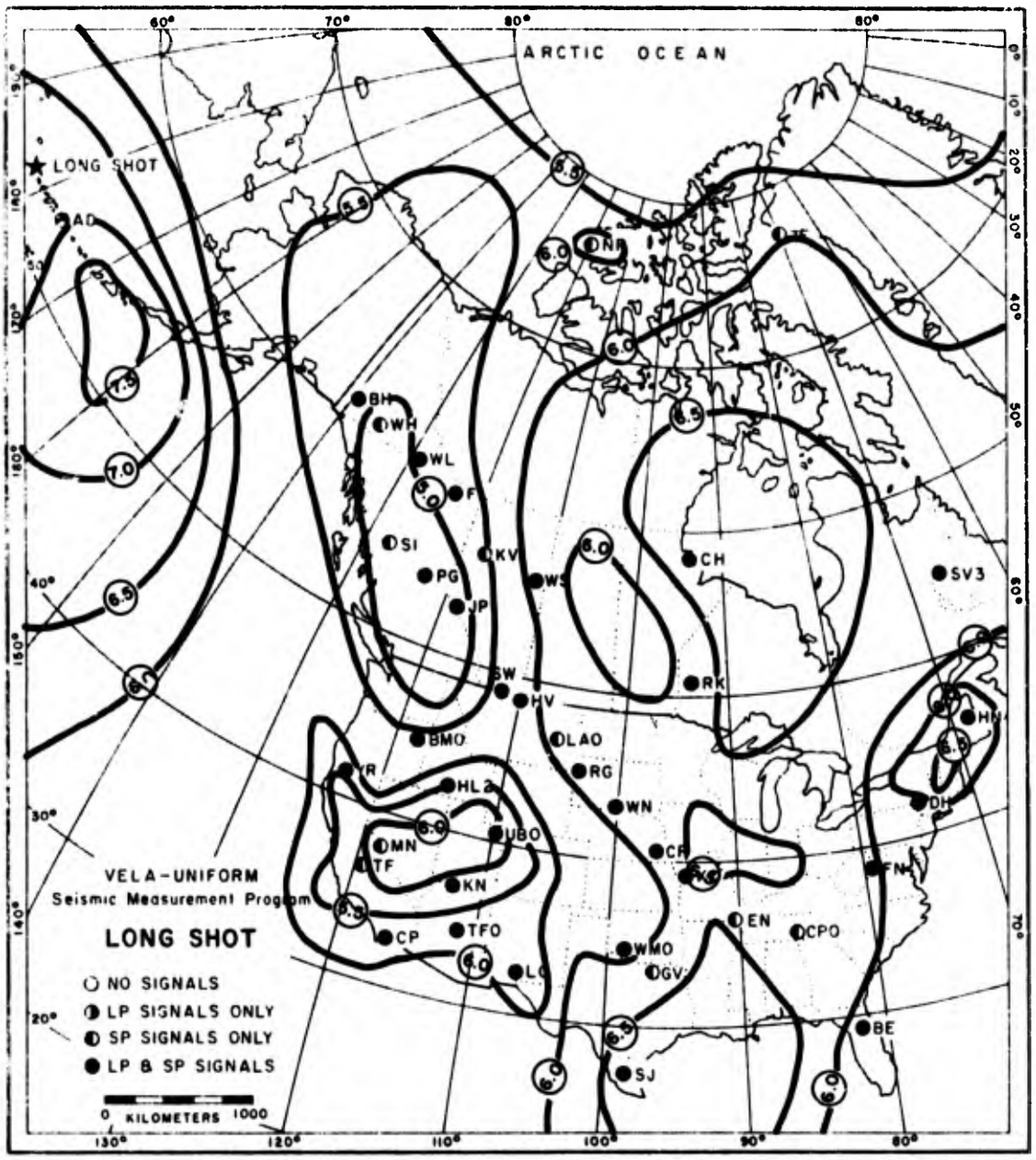

Figure 46. Unified body-wave magnitude contours for LONG SHOT on conic projection of North America.

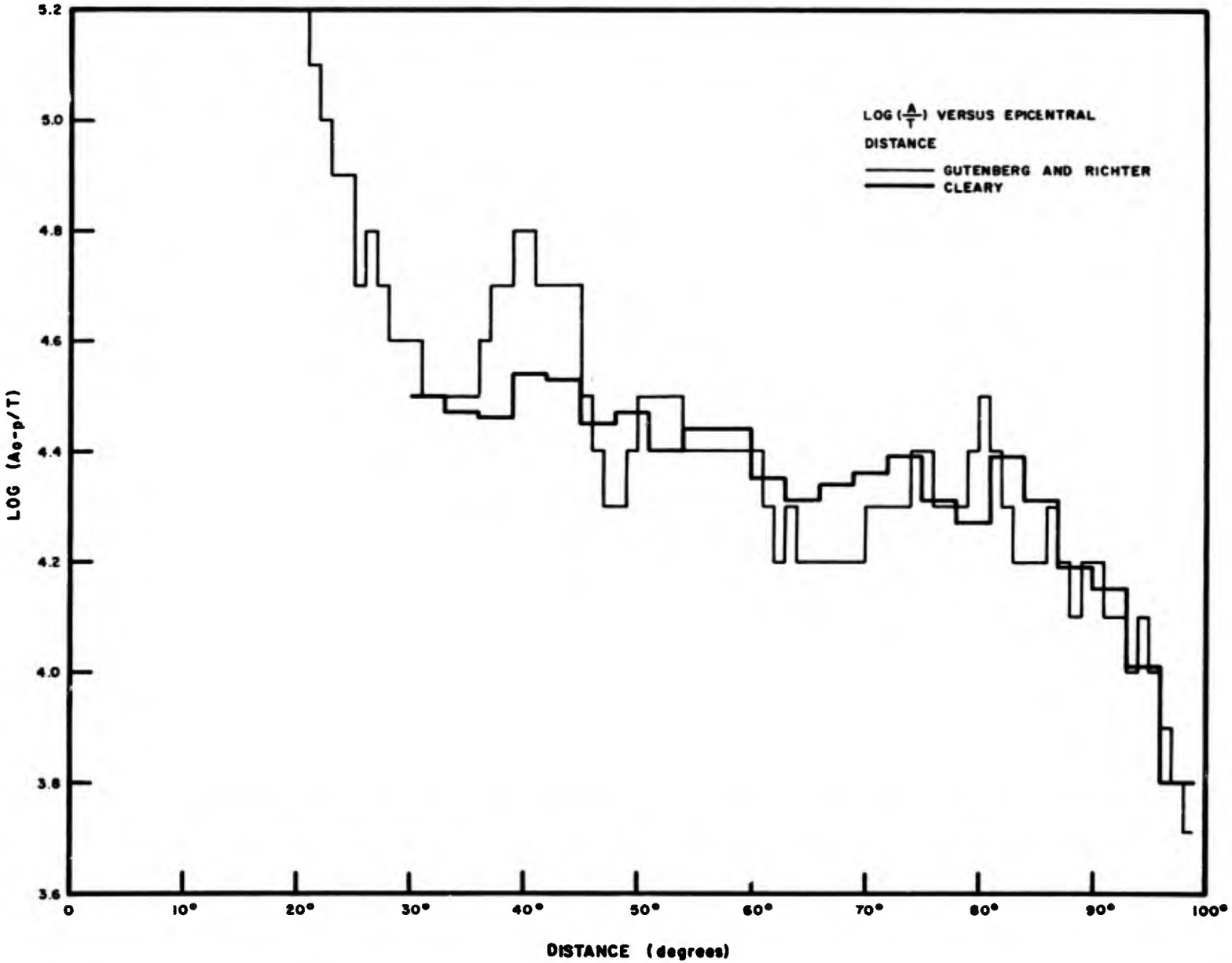

Figure 47. Comparison of the Cleary (1967b) and the Gutenberg-Richter (1956) amplitude-versus-distance curves for a surface source of magnitude 8.2.

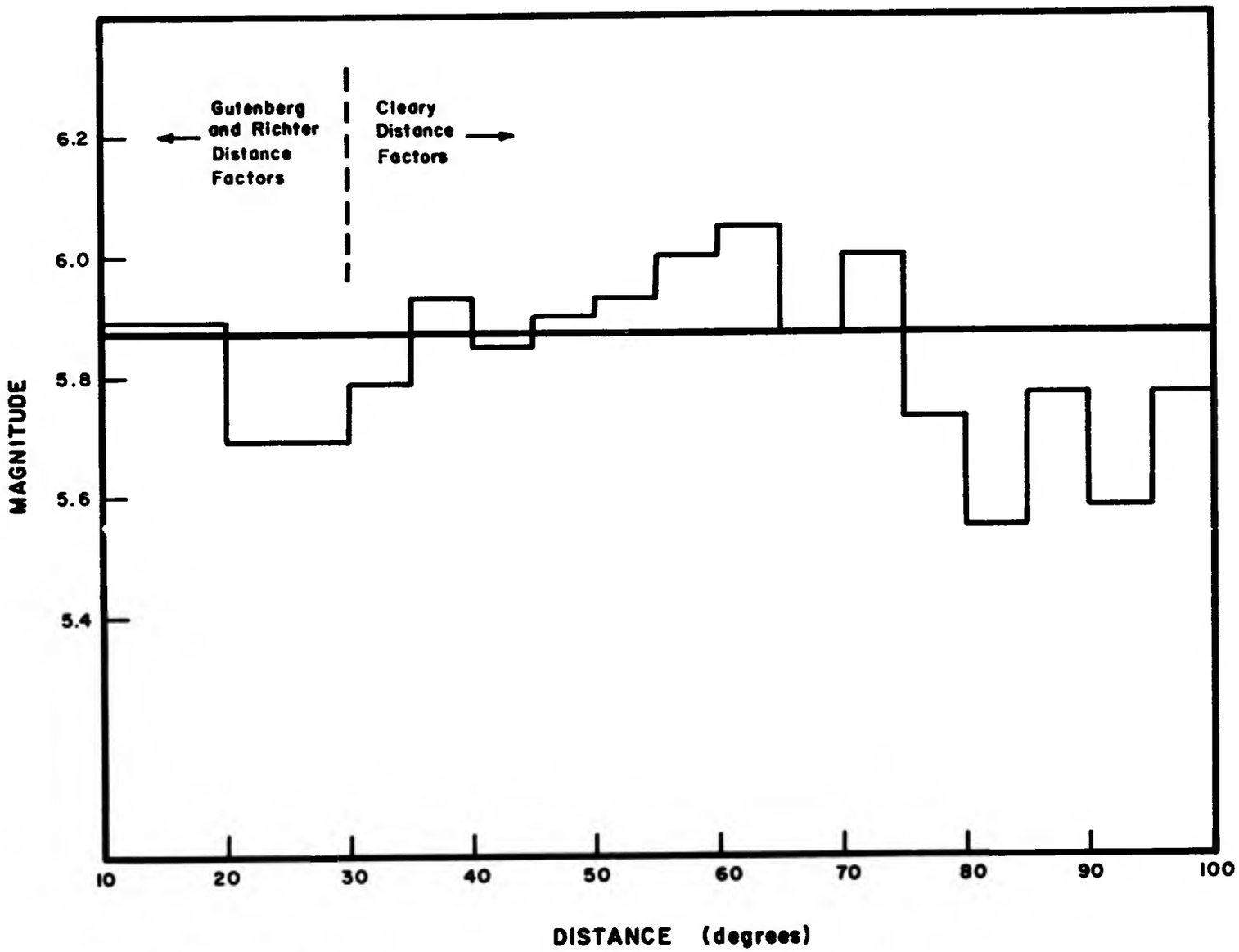

Figure 48. Histogram of average magnitude in each 5° interval of epicentral distance for LONG SHOT using the Cleary (1967b) distance-correction factors.

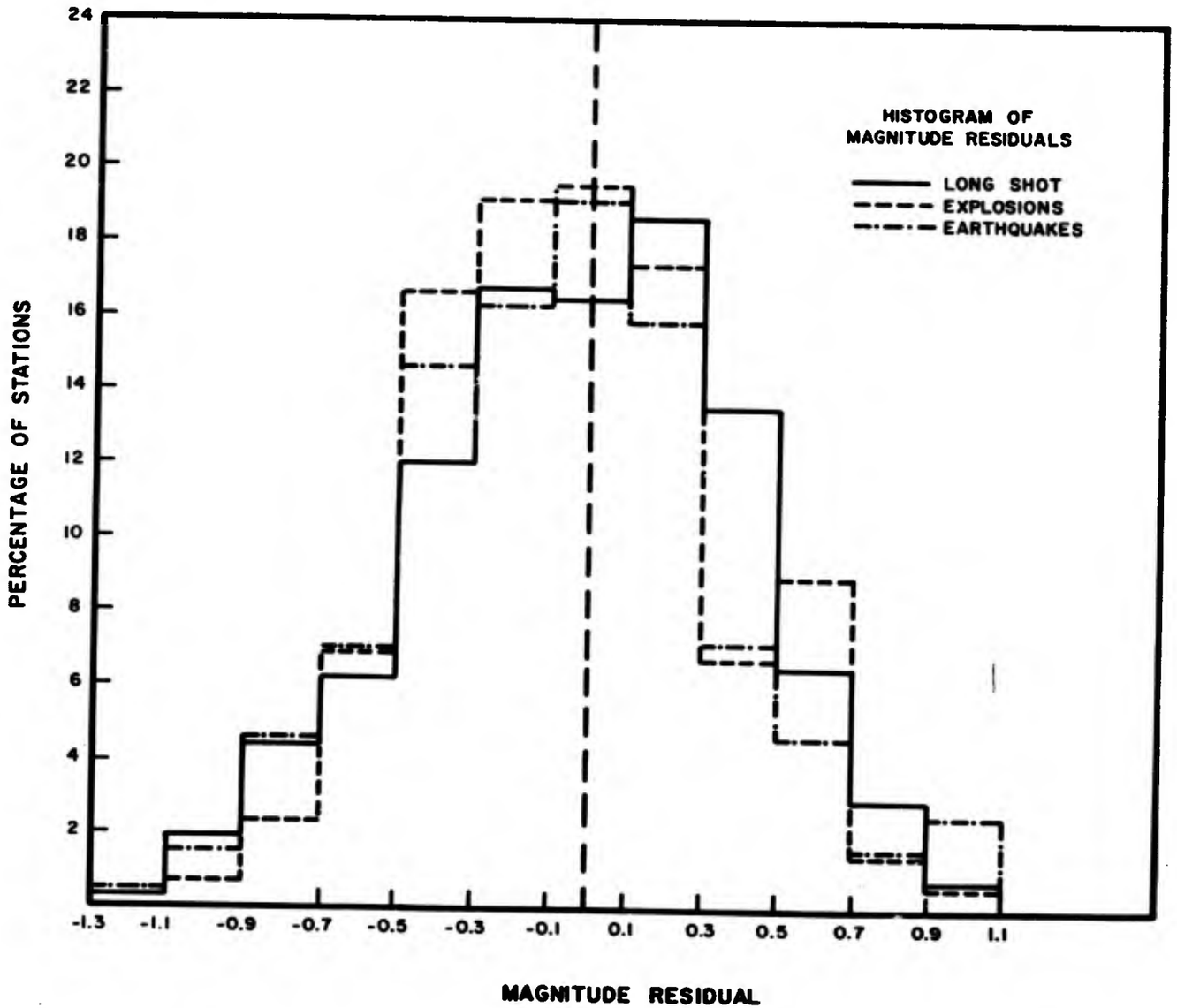

Figure 49. Histogram of magnitude residuals for LONG SHOT, other explosions, and earthquakes.

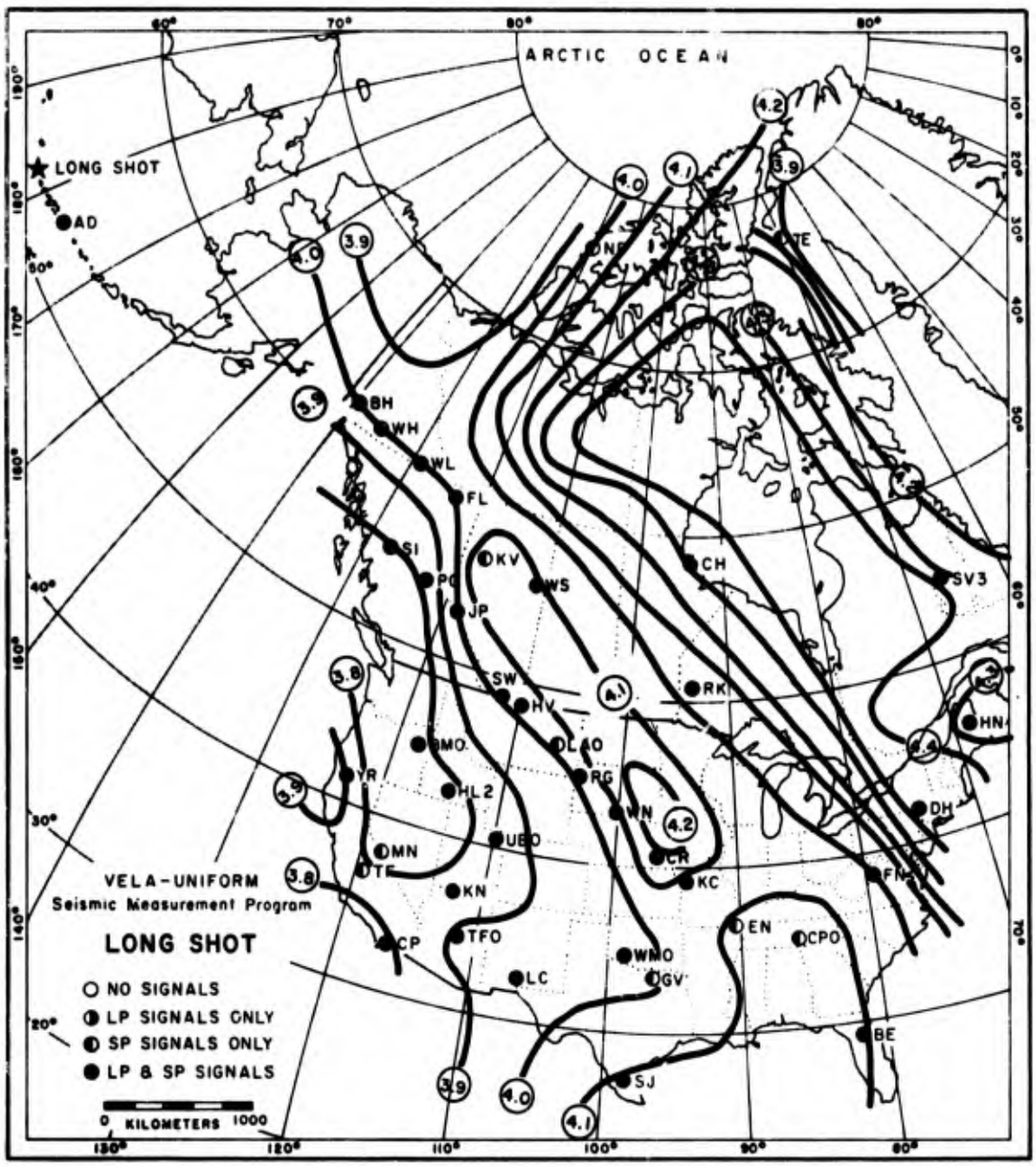

Figure 50. Surface-wave (LR) magnitude contours for LONG SHOT on conic projection of North America.

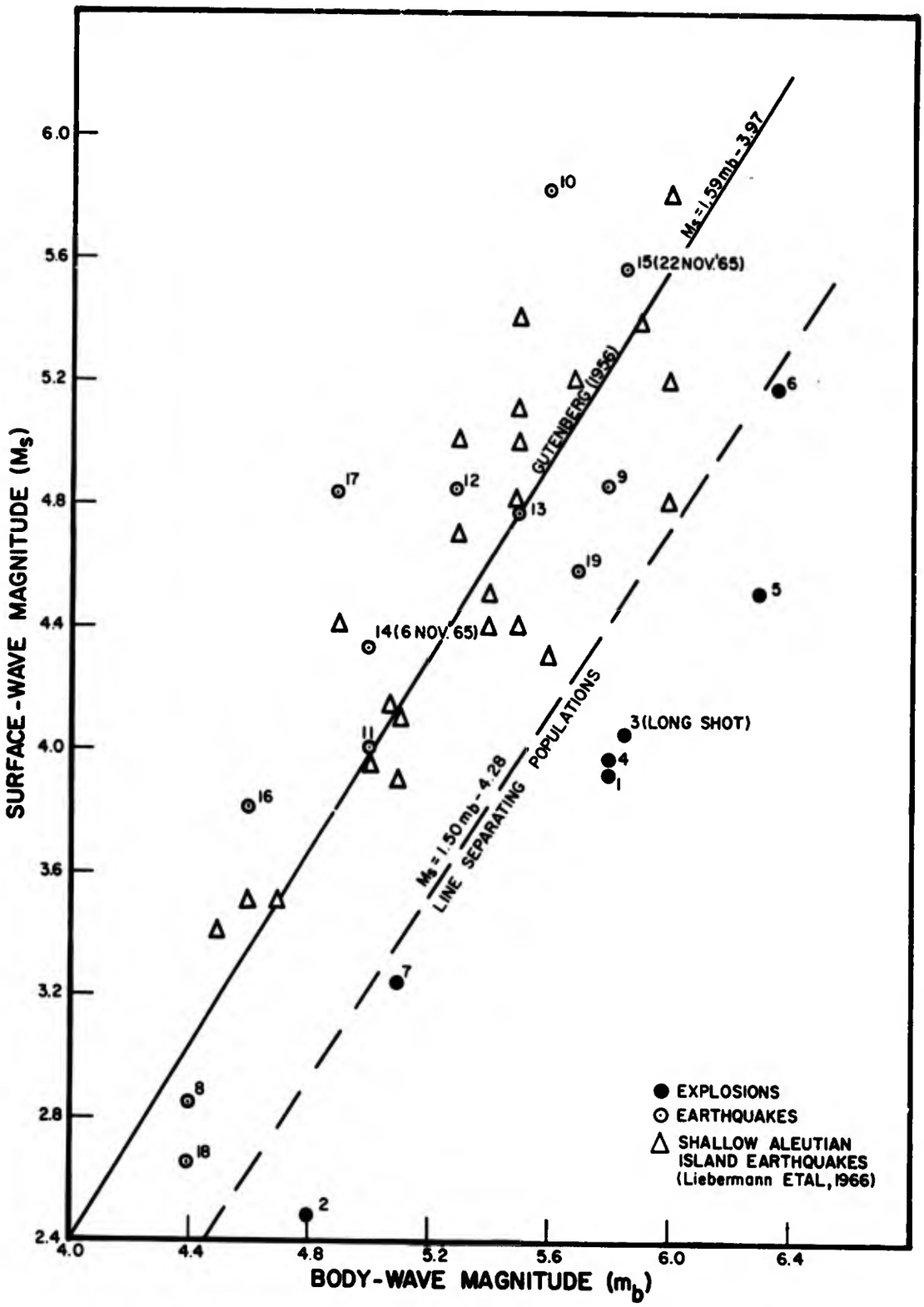

Figure 51. Surface-wave magnitude (M_S) versus unified body-wave magnitude (m_b) for explosions and earthquakes.

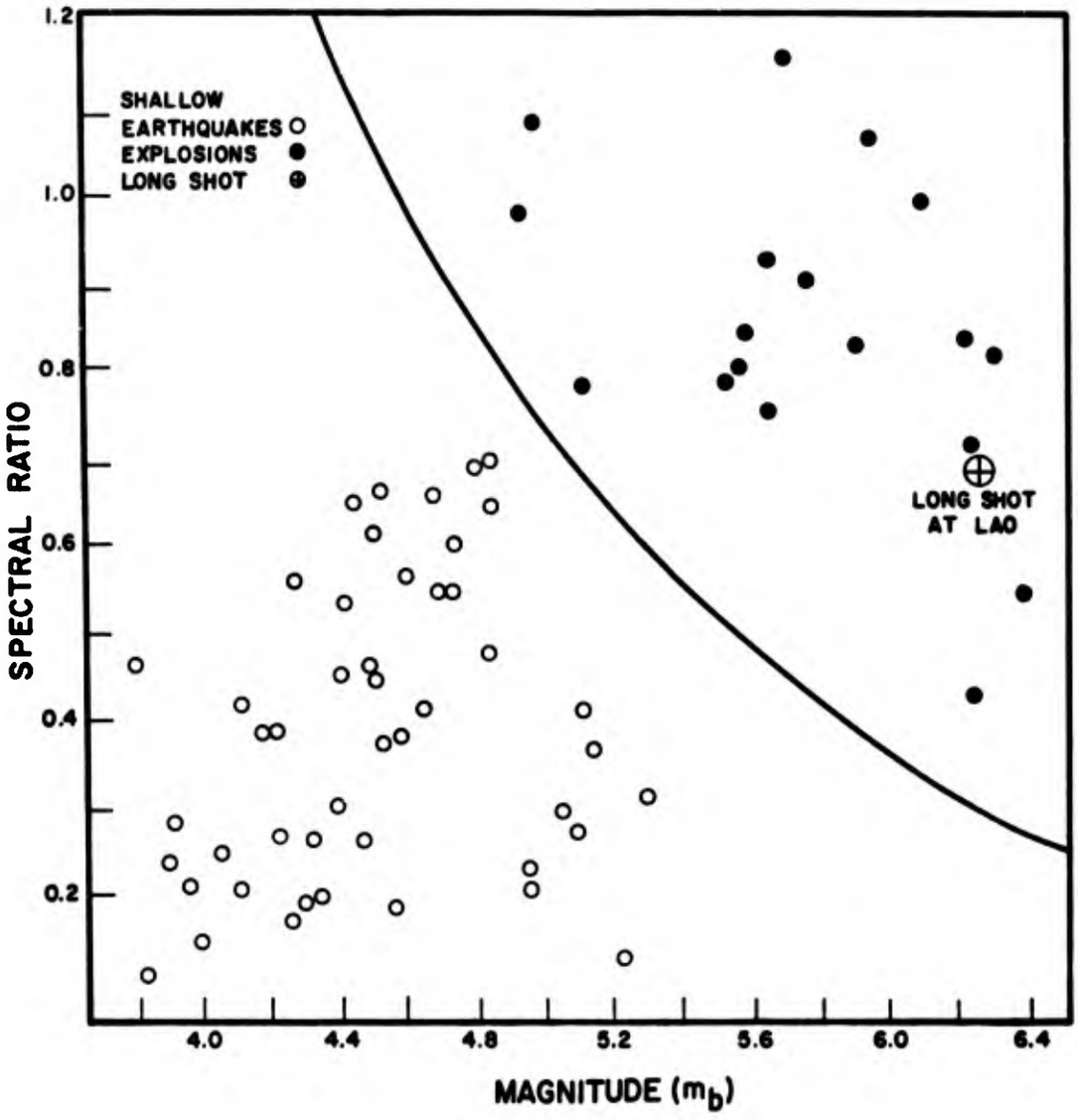

Figure 52. Spectral ratio versus magnitude (m_b) at LASA.

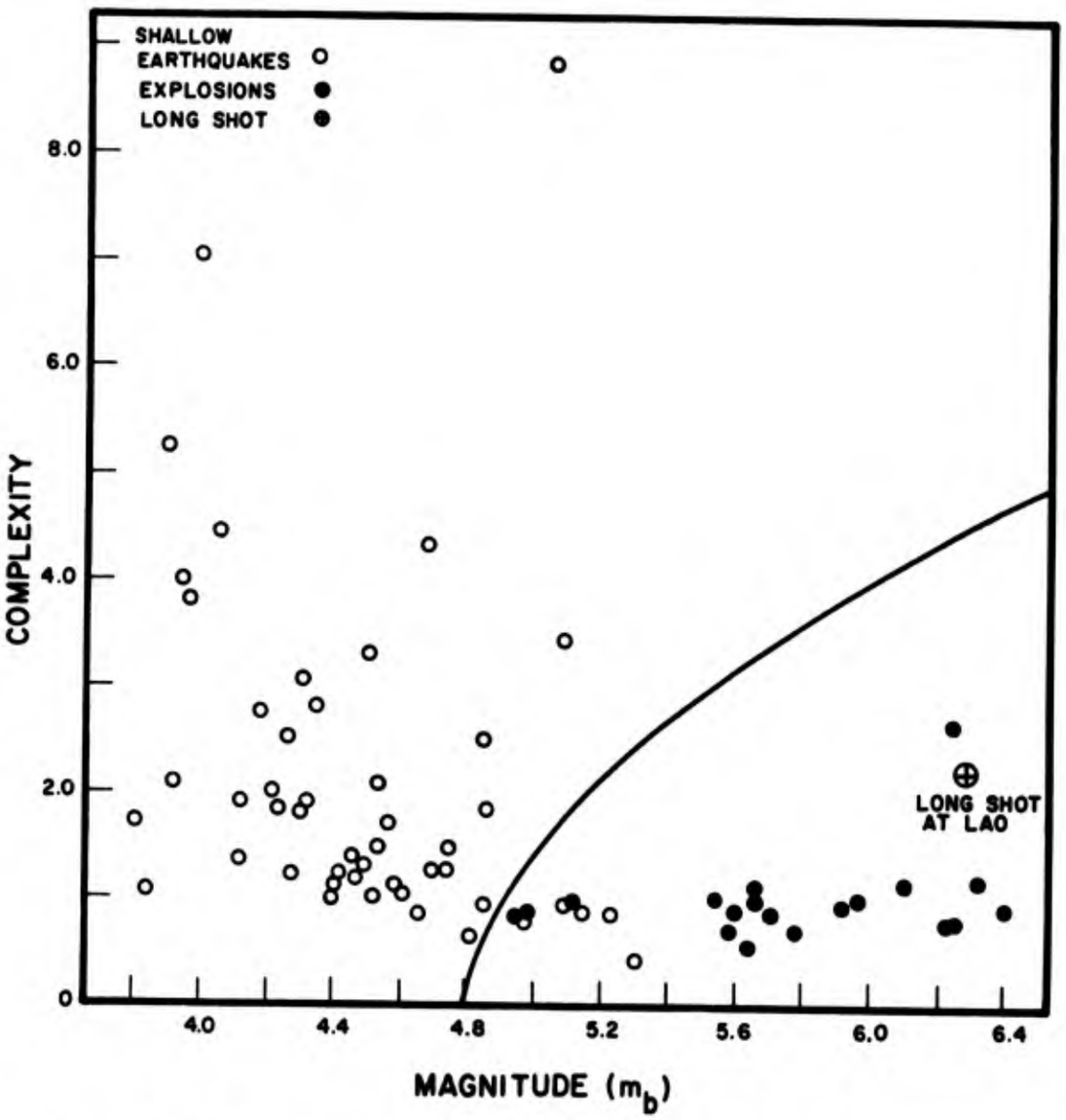

Figure 53. Complexity versus magnitude (m_b) at LASA.

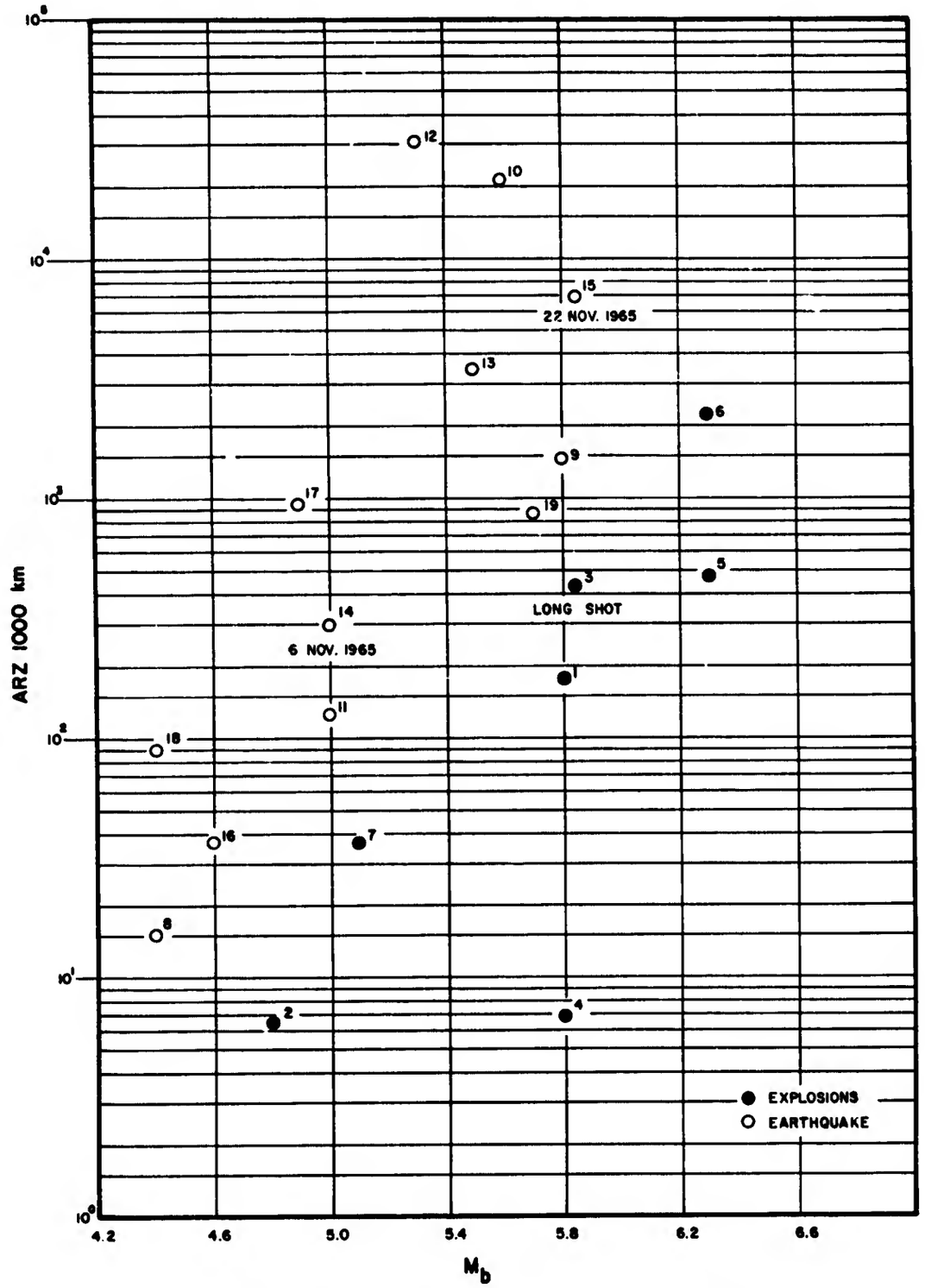

Figure 54. Area of envelope of Rayleigh-wave signals (ARZ) versus magnitude (m_b) for LONG SHOT and various other events.

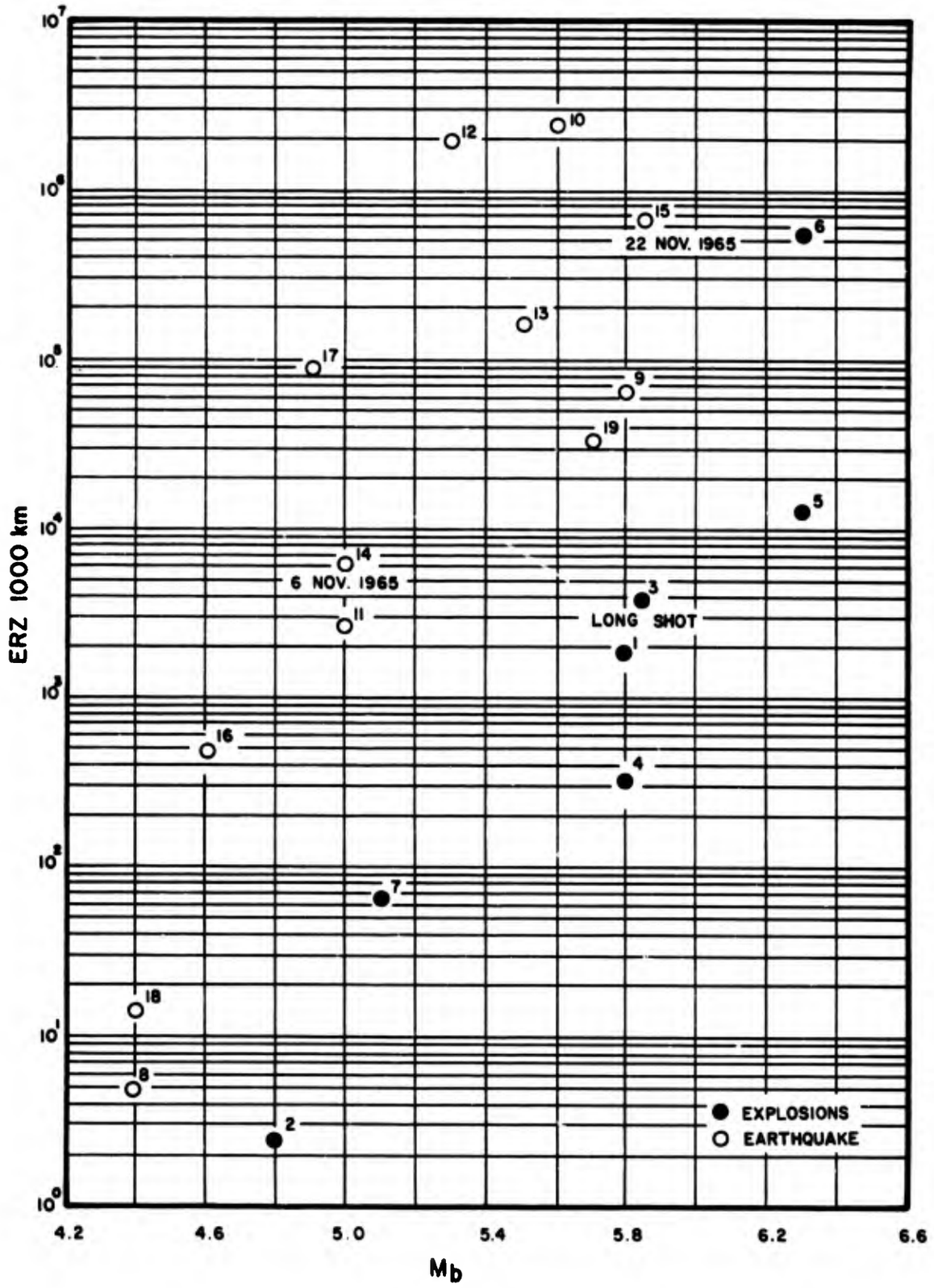

Figure 55. Integrated power density spectra (ERZ) of Rayleigh-wave signals versus magnitude (m_b) for LONG SHOT and various other events.

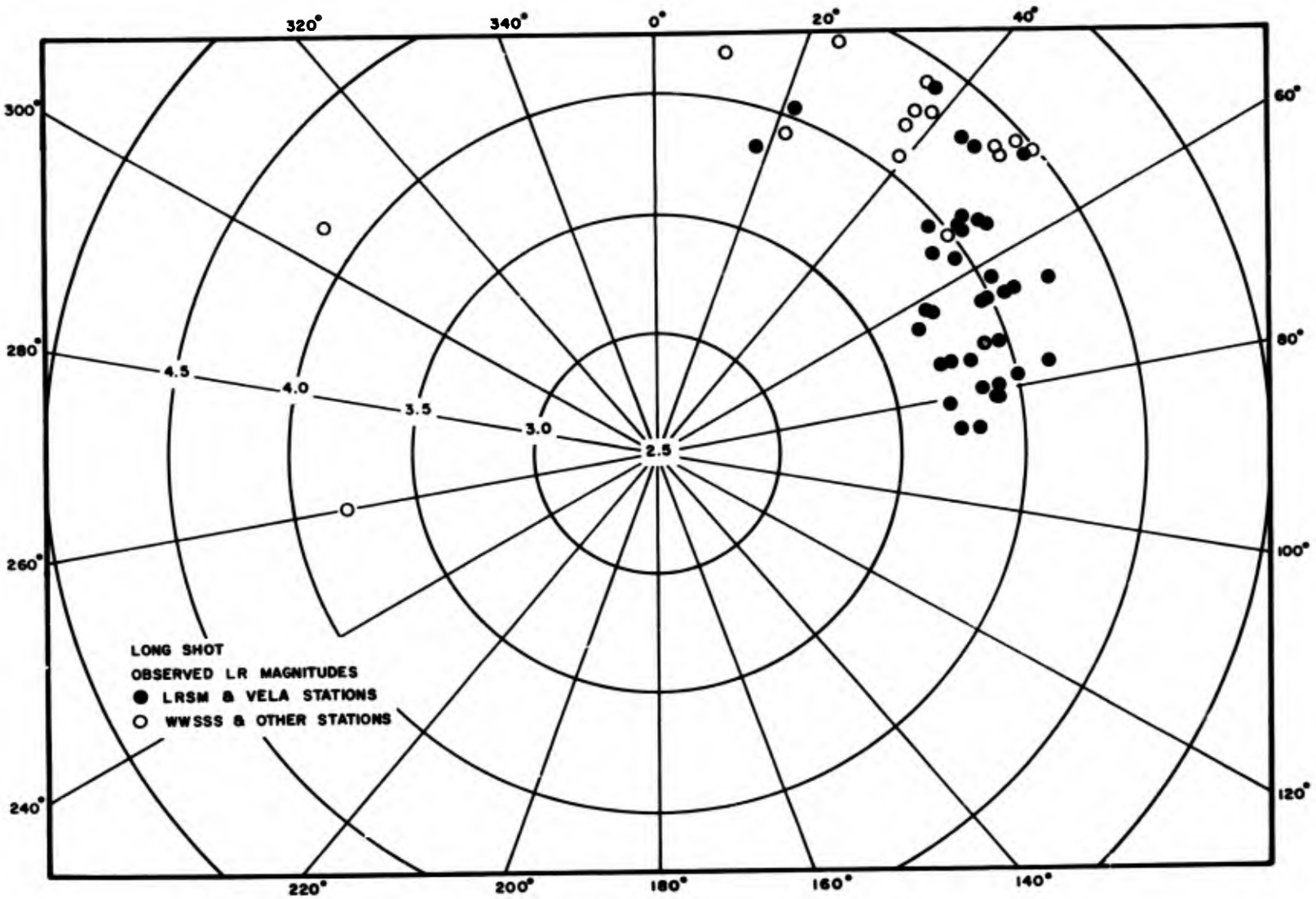

Figure 56. Polar plot of LONG SHOT Rayleigh-wave magnitudes (M_S).

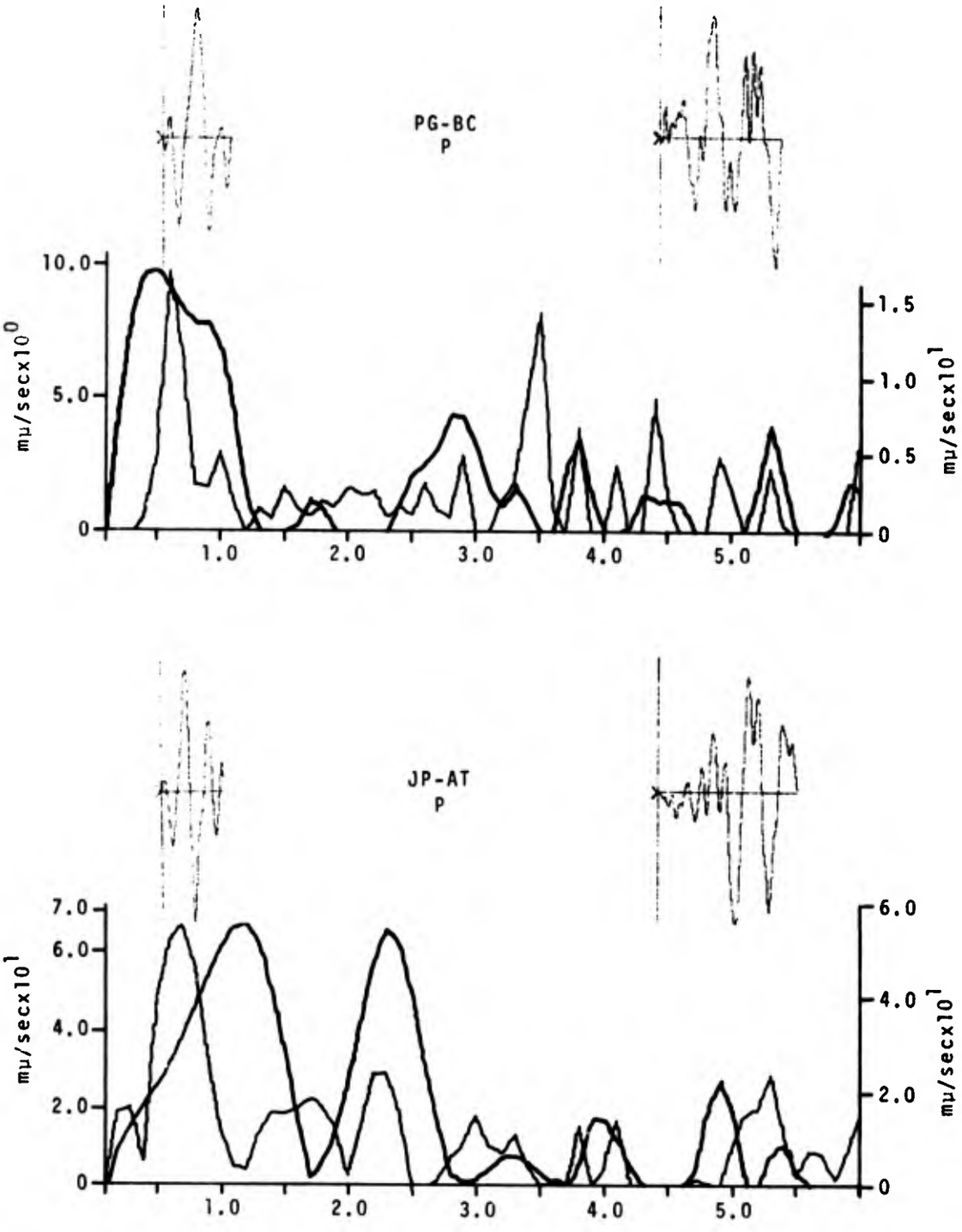

Figure 57. Comparative P time series and amplitude spectra for LONG SHOT and 22 November 1965 earthquake at PG-BC and JP-AT.

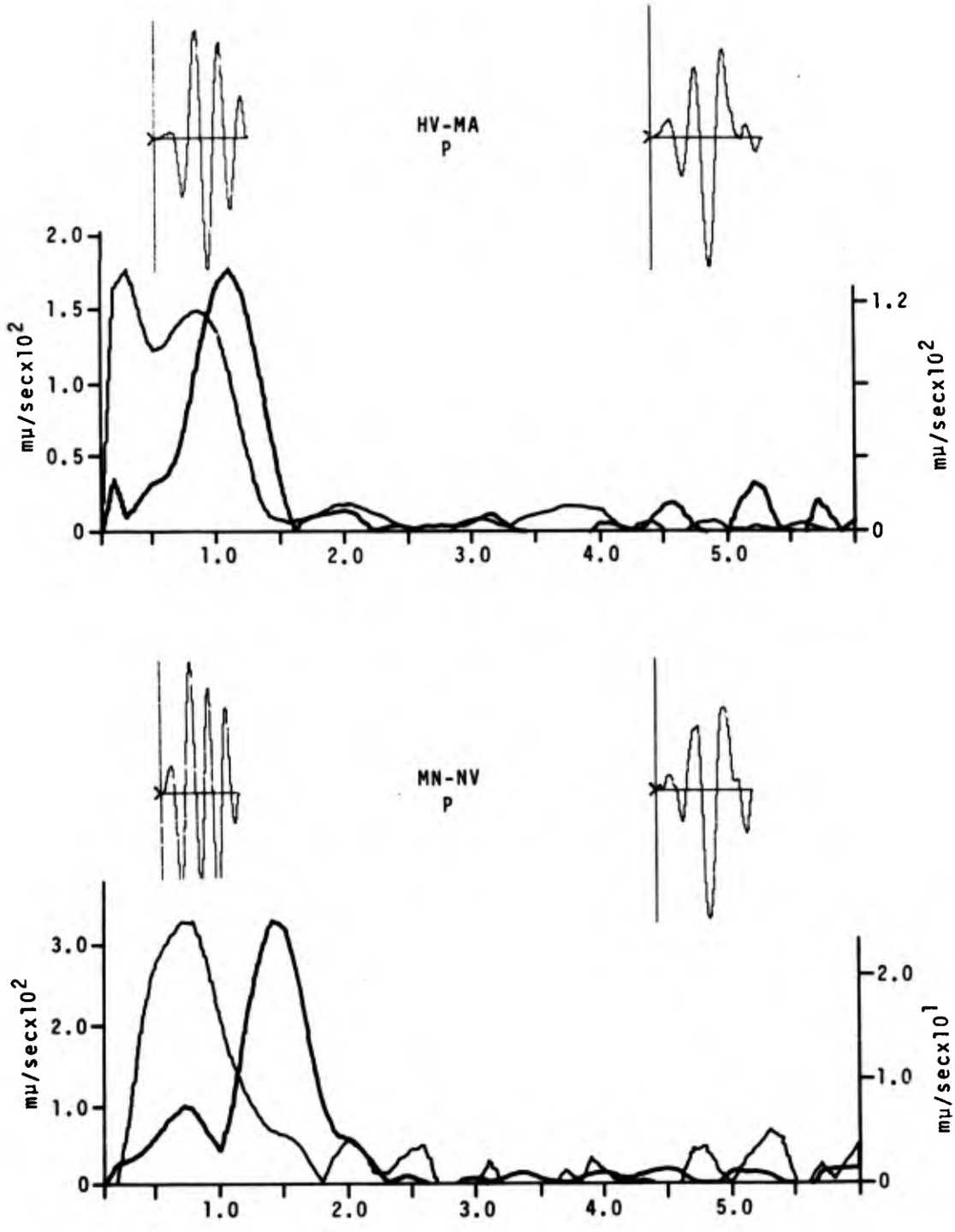

Figure 58. Comparative P time series and amplitude spectra for LONG SHOT and 22 November 1965 earthquake at HV-MA and MN-NV.

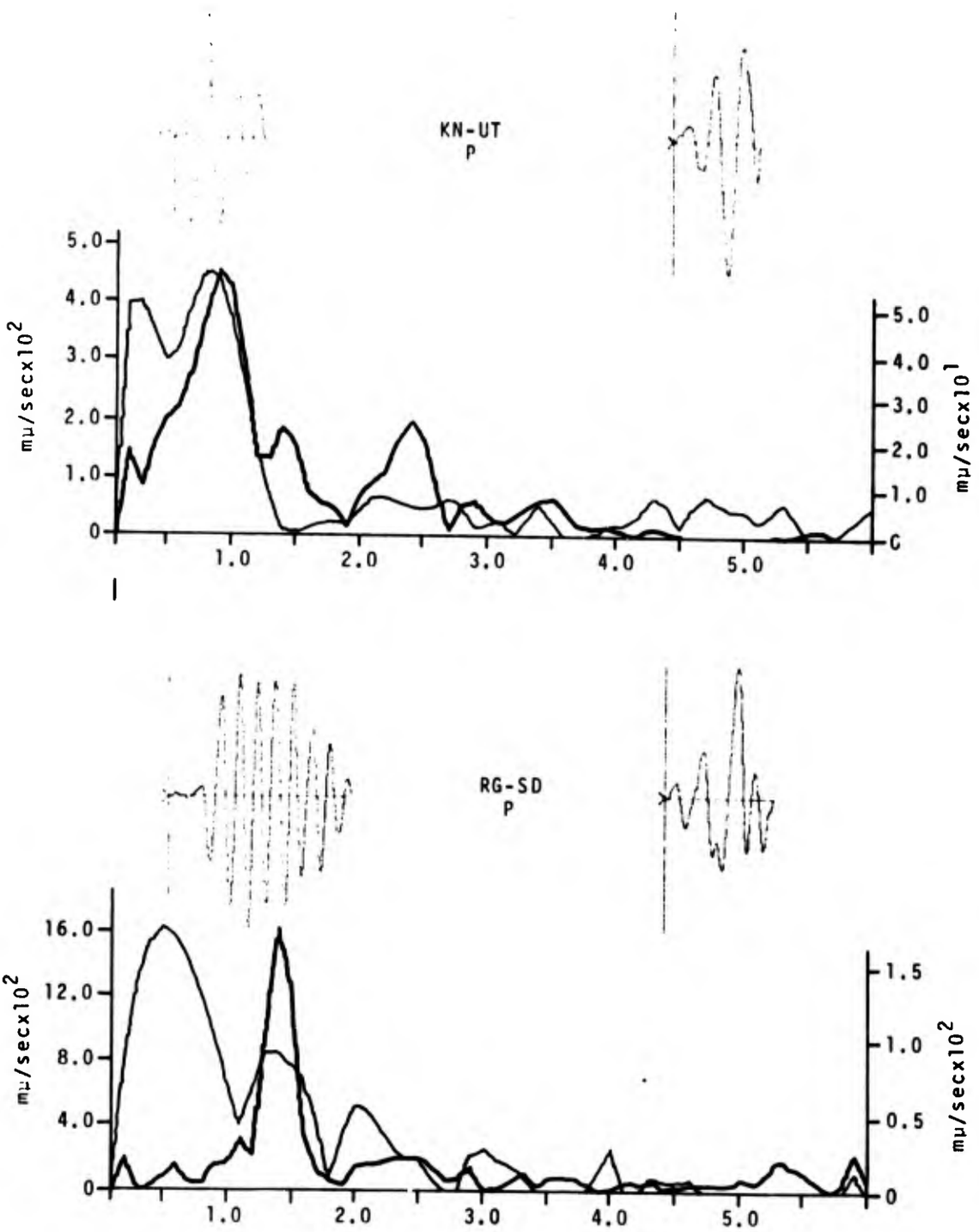

Figure 59. Comparative P time series and amplitude spectra for LONG SHOT and 22 November 1965 earthquake at KN-UT and RG-SD.

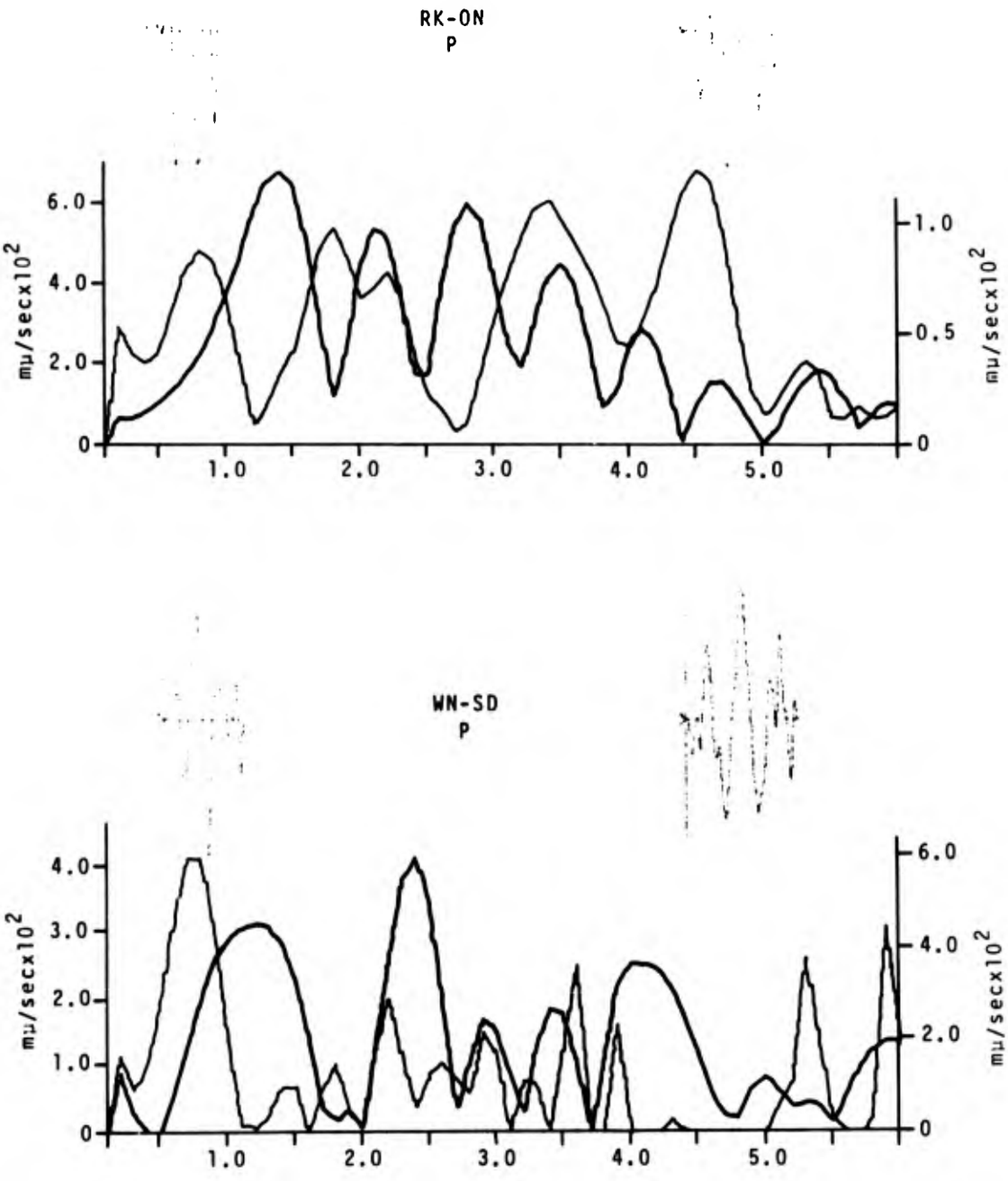

Figure 60. Comparative P time series and amplitude spectra for LONG SHOT and 22 November 1965 earthquake at RK-ON and WN-SD.

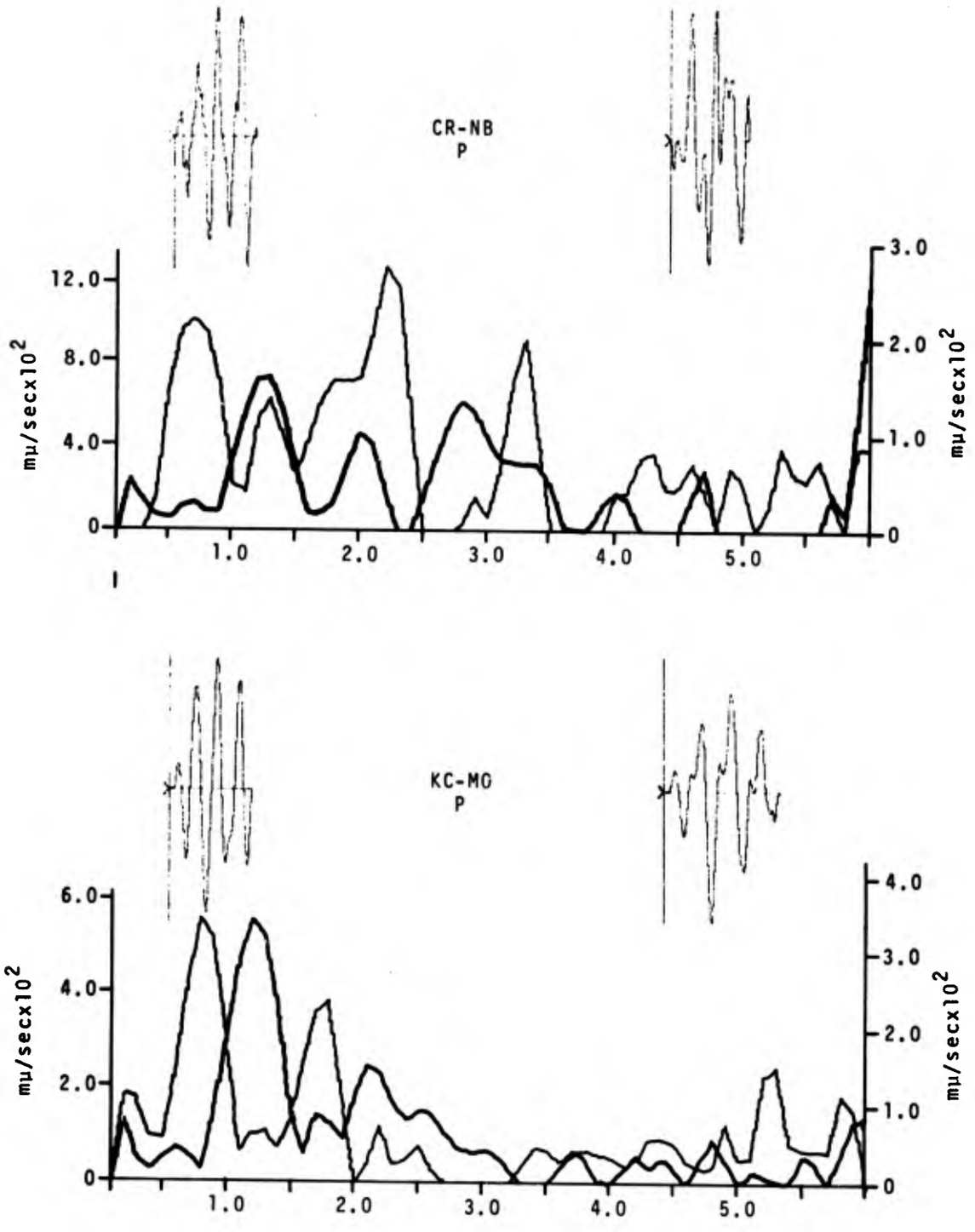

Figure 61. Comparative P time series and amplitude spectra for LONG SHOT and 22 November 1965 earthquake at CR-NB and KC-MO.

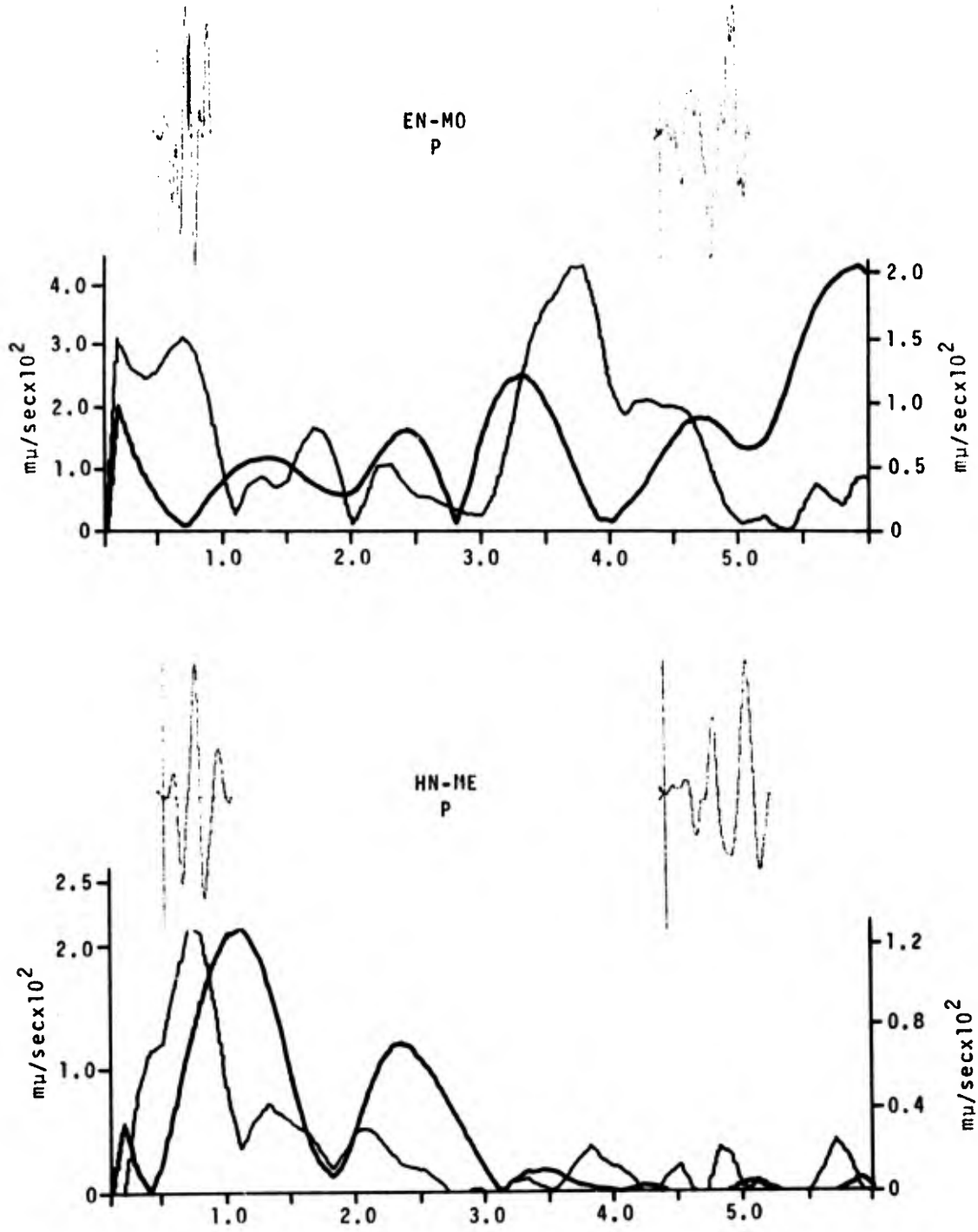

Figure 62. Comparative P time series and amplitude spectra for LONG SHOT and 22 November 1965 earthquake at EN-MO and HN-ME.

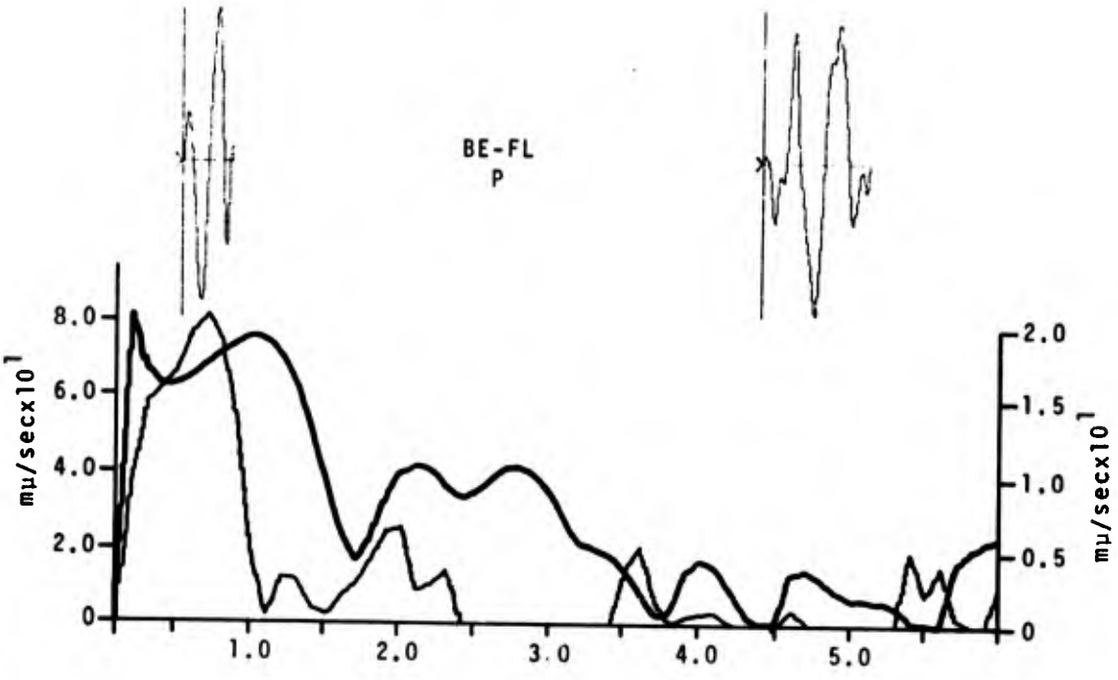

Figure 63. Comparative P time series and amplitude spectra for LONG SHOT and 22 November 1965 earthquake at BE-FL.

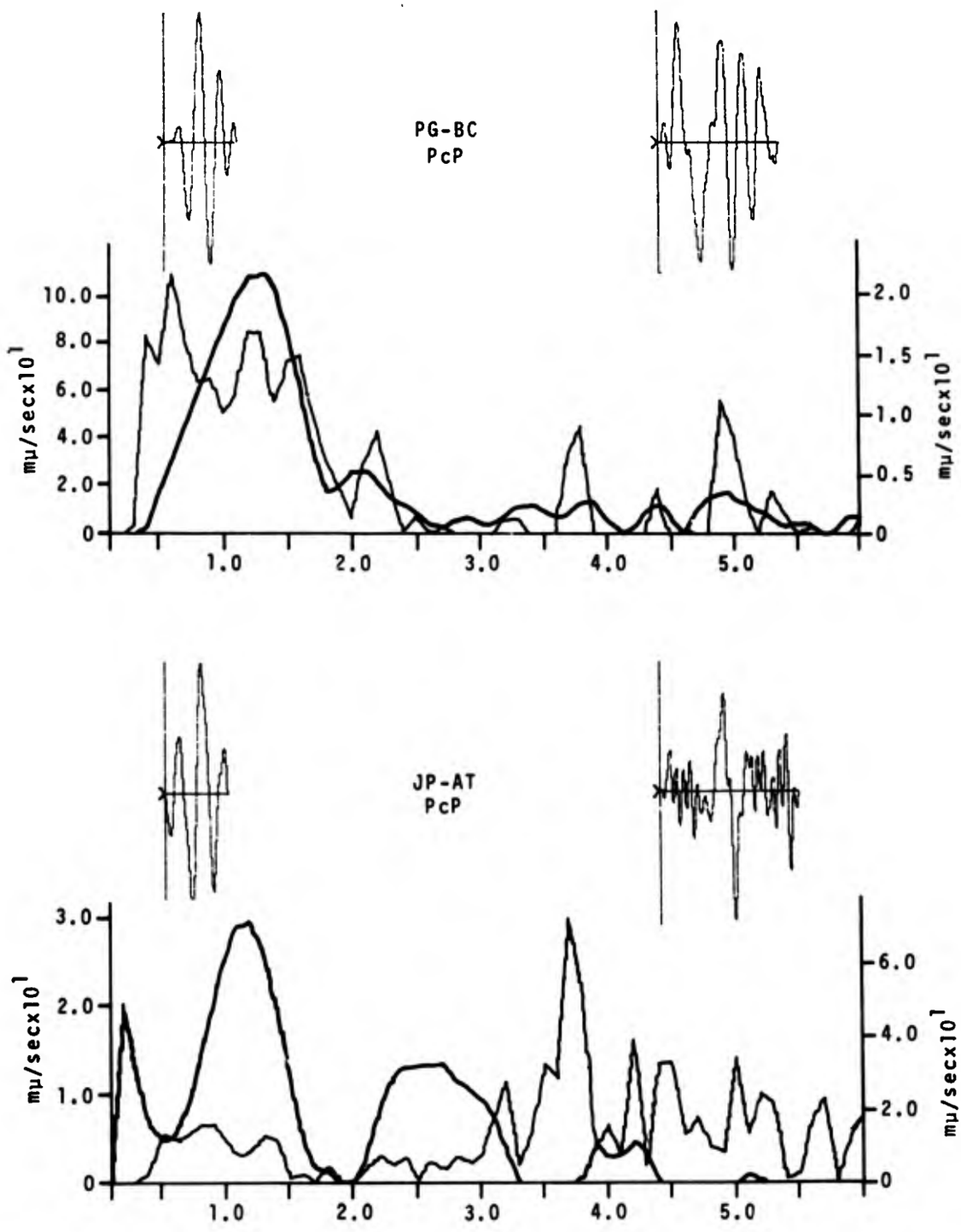

Figure 64. Comparative PcP time series and amplitude spectra for LONG SHOT and 22 November 1965 earthquake at PG-BC and JP-AT.

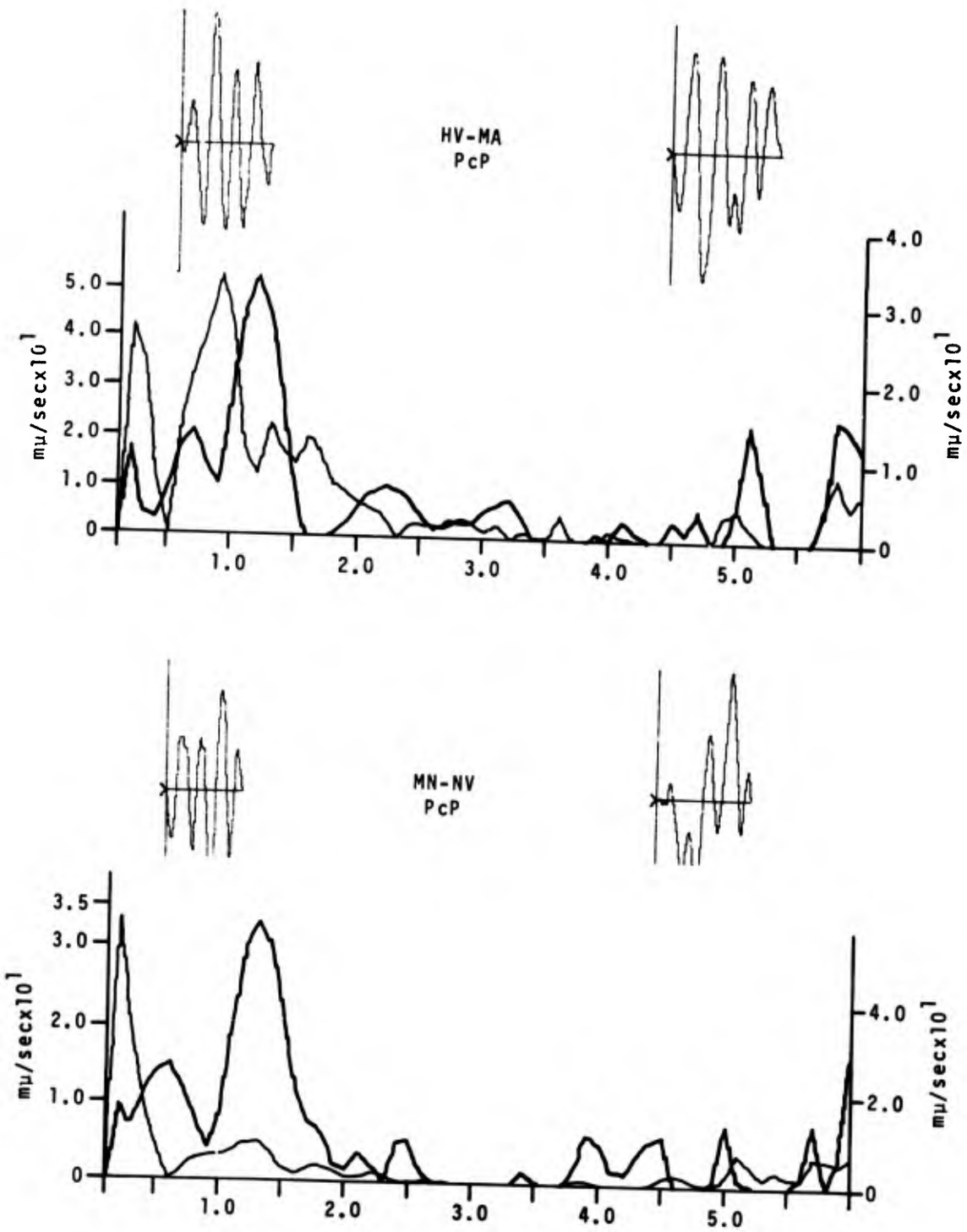

Figure 65. Comparative PcP time series and amplitude spectra for LONG SHOT and 22 November 1965 earthquake at HV-MA and MN-NV.

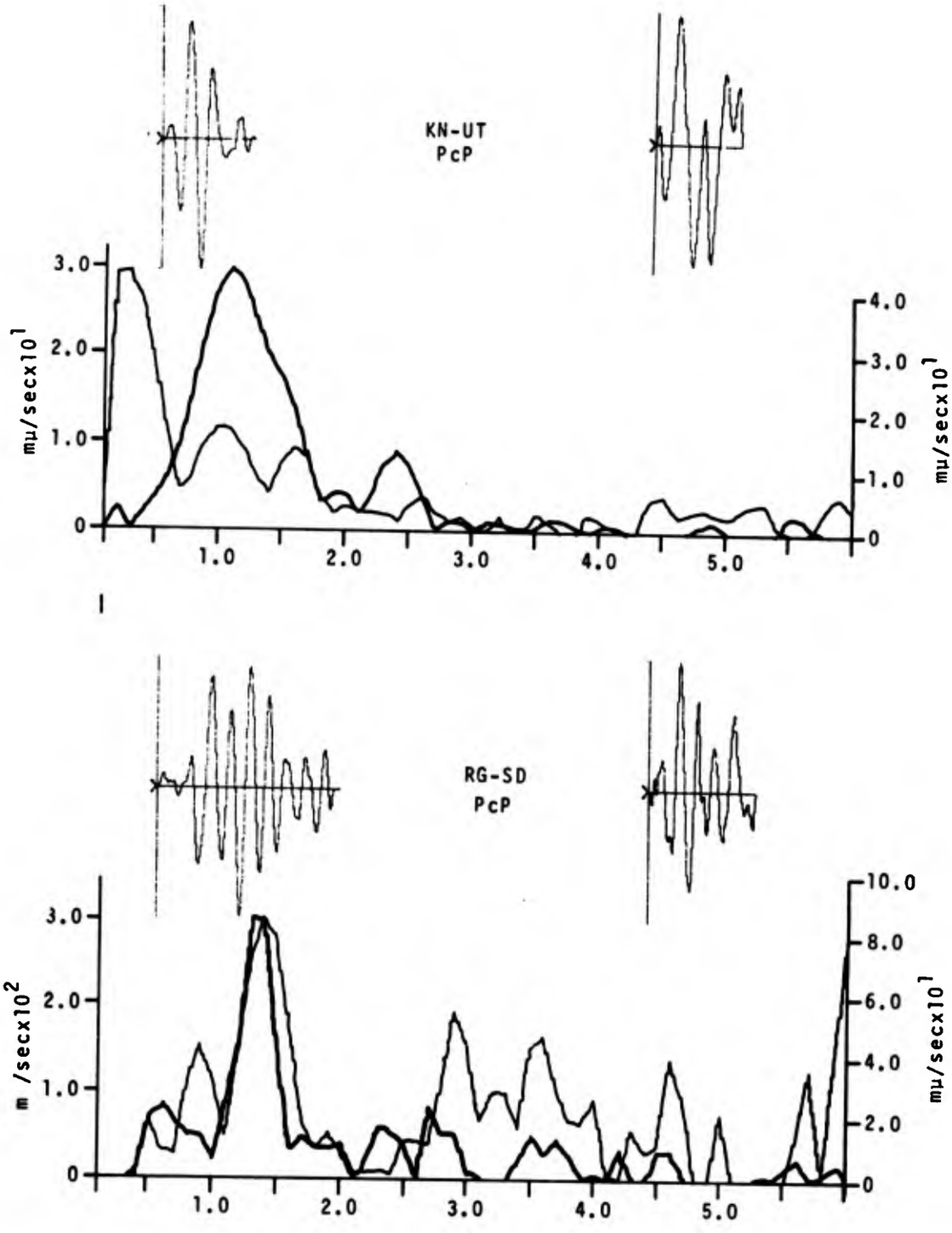

Figure 66. Comparative PcP time series and amplitude spectra for LONG SHOT and 22 November 1965 earthquake at KN-UT and RG-SD.

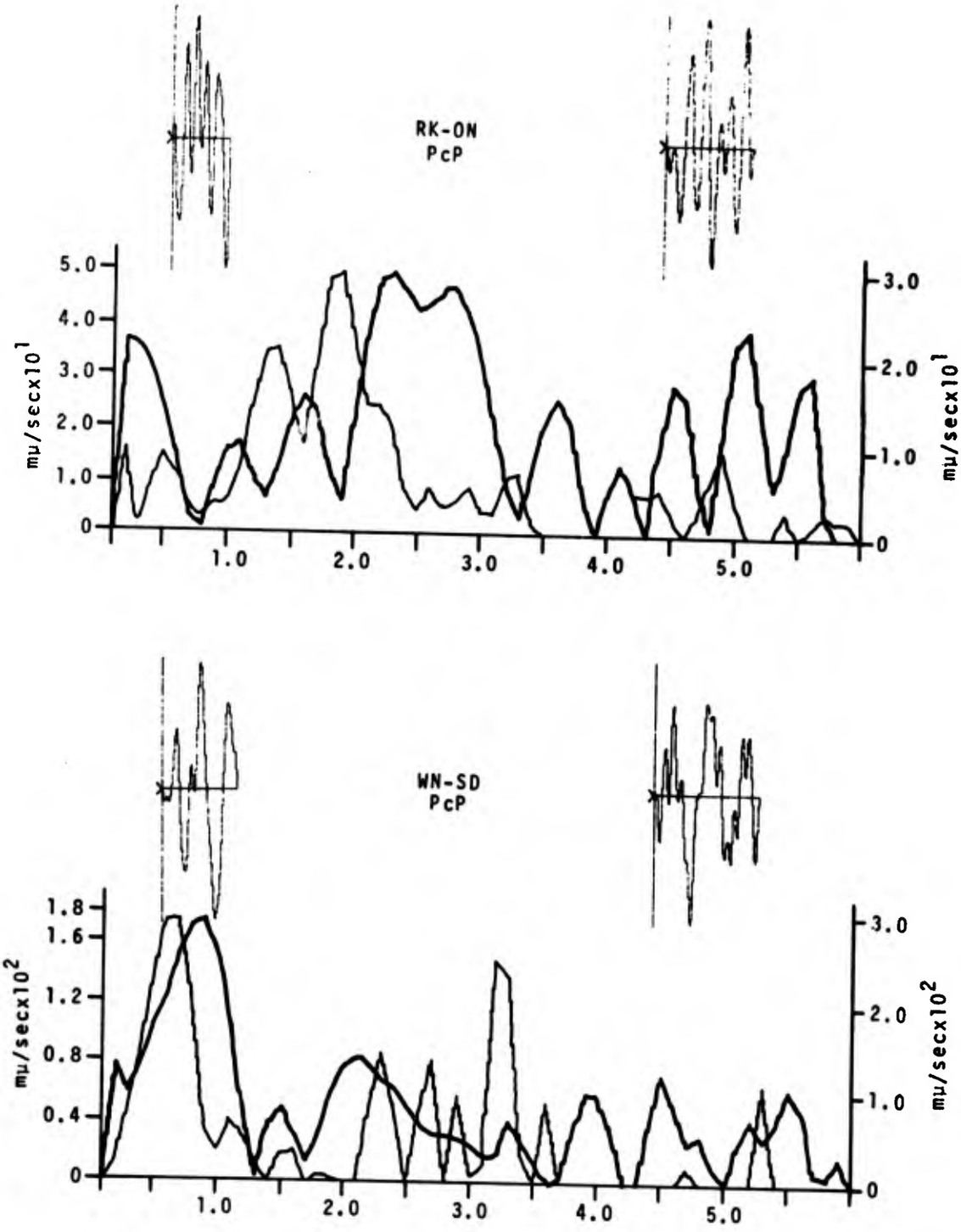

Figure 67. Comparative PcP time series and amplitude spectra for LONG SHOT and 22 November 1965 earthquake at RK-ON and WN-SD.

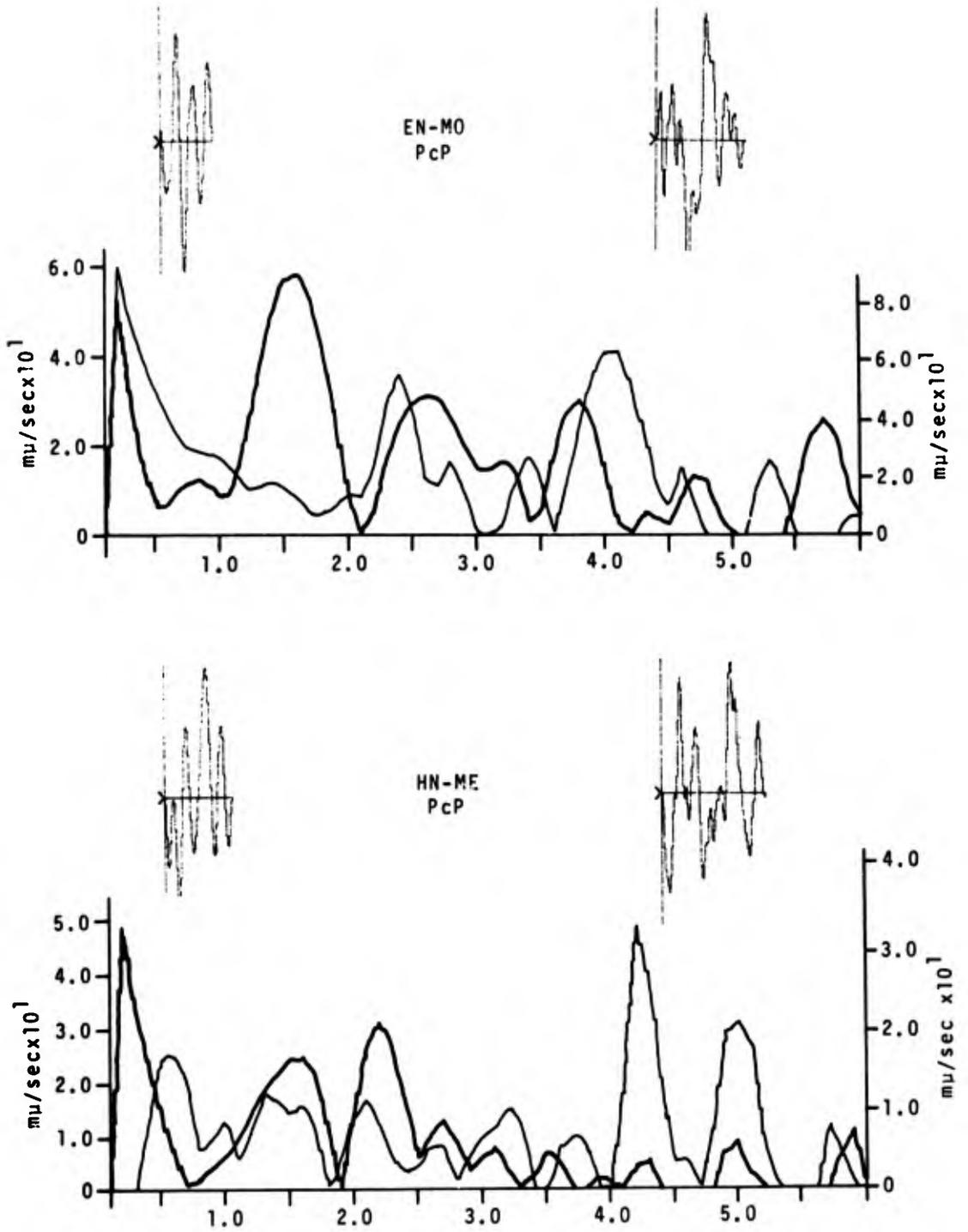

Figure 68. Comparative PcP time series and amplitude spectra for LONG SHOT and 22 November 1965 earthquake at EN-MO and HN-ME.

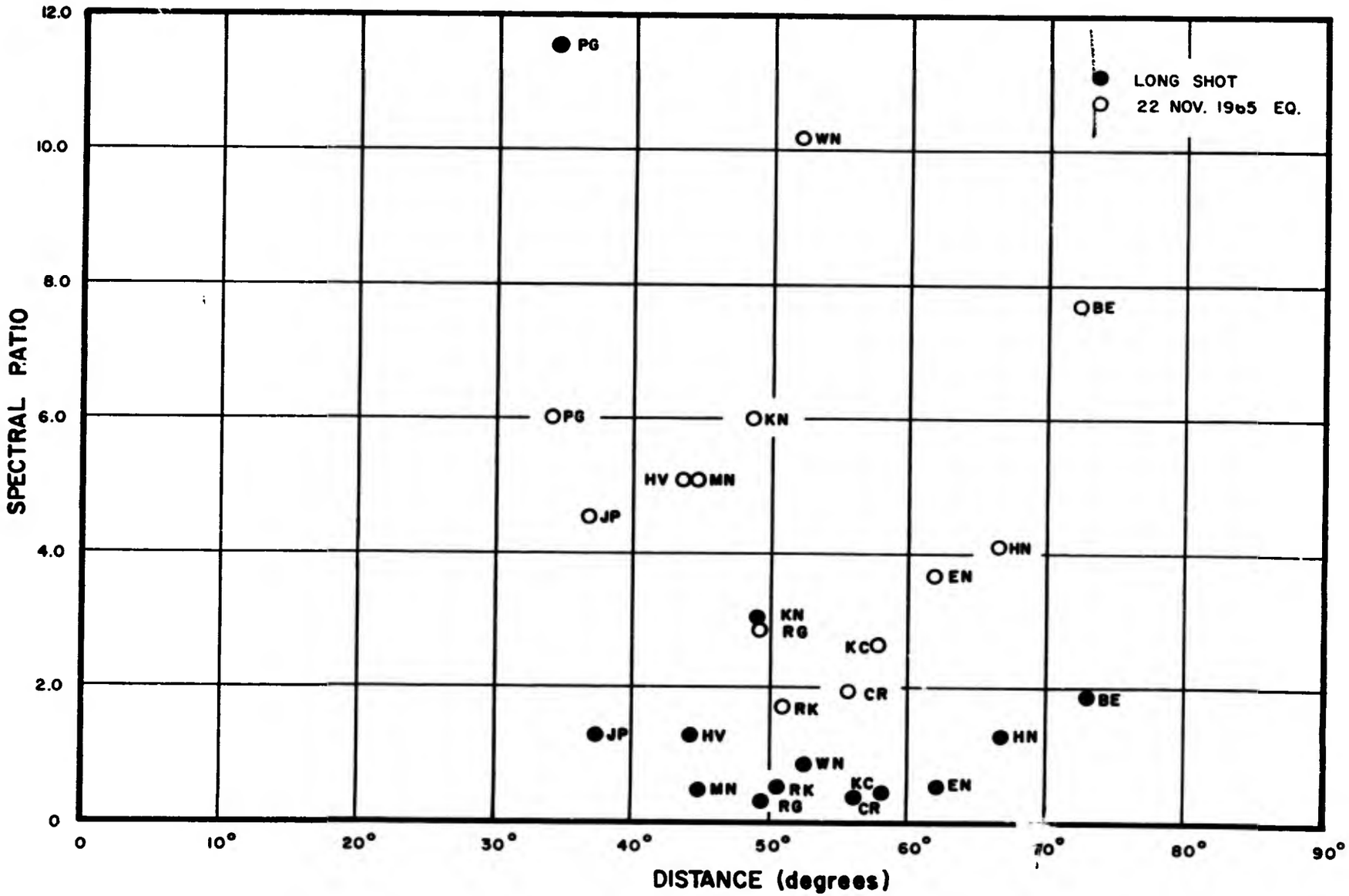

Figure 69. Short-period P-wave spectral ratios for LONG SHOT and the 22 November 1965 earthquake.

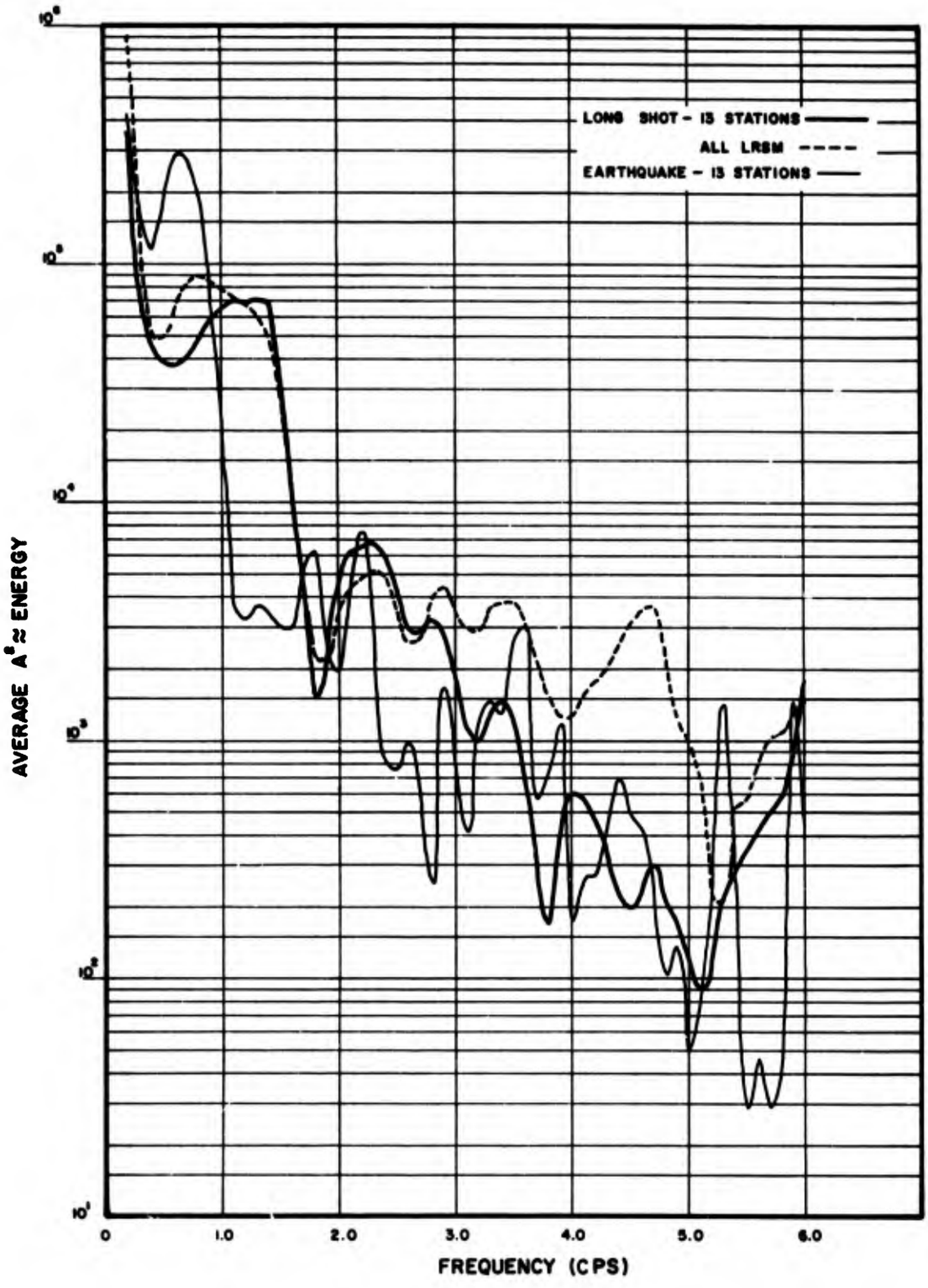

Figure 70. Average P-wave power spectra for LONG SHOT and the 22 November 1965 earthquake.

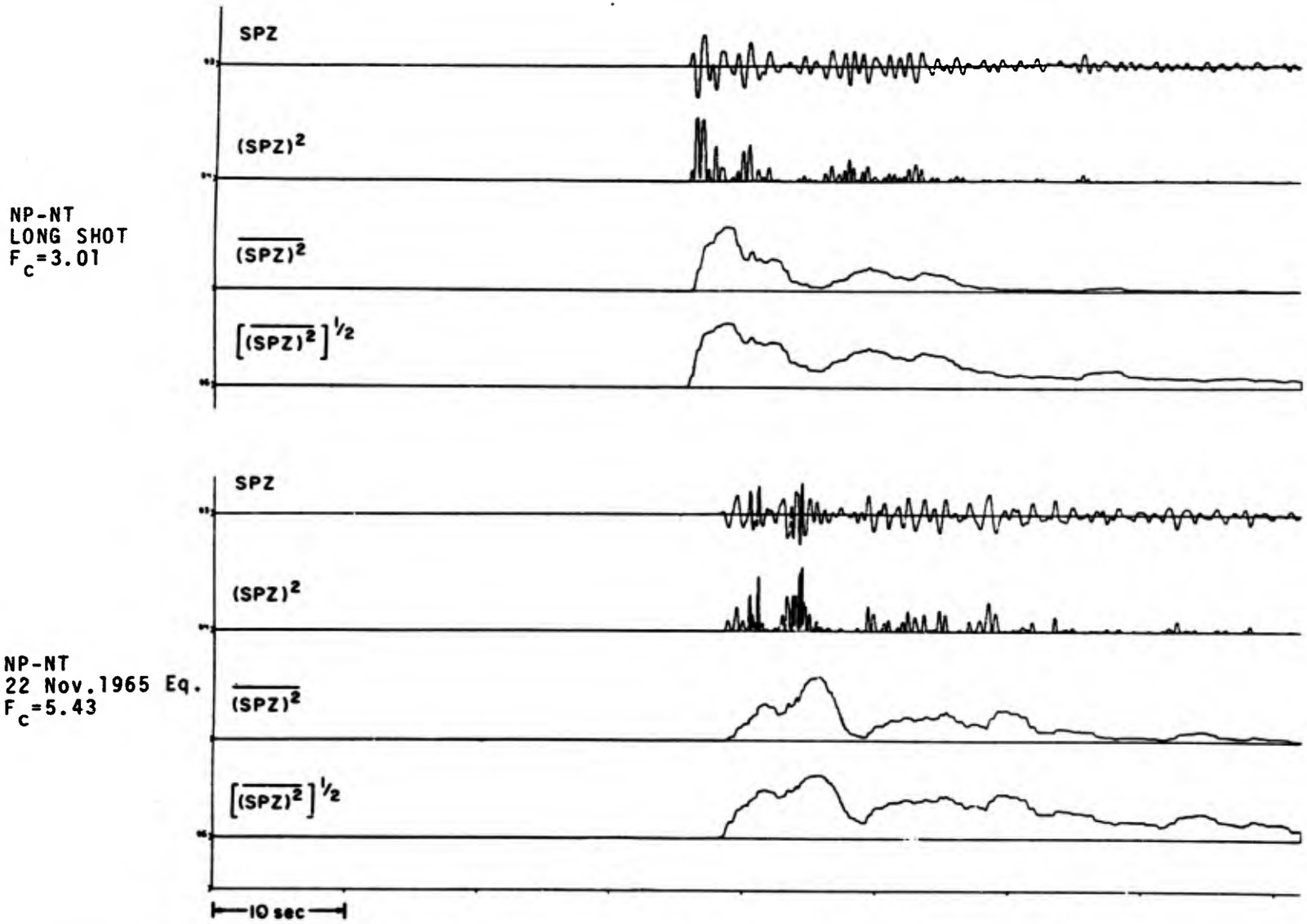

Figure 71. Time series used in calculating complexity factors for LONG SHOT and 22 November 1965 earthquake at NP-NT.

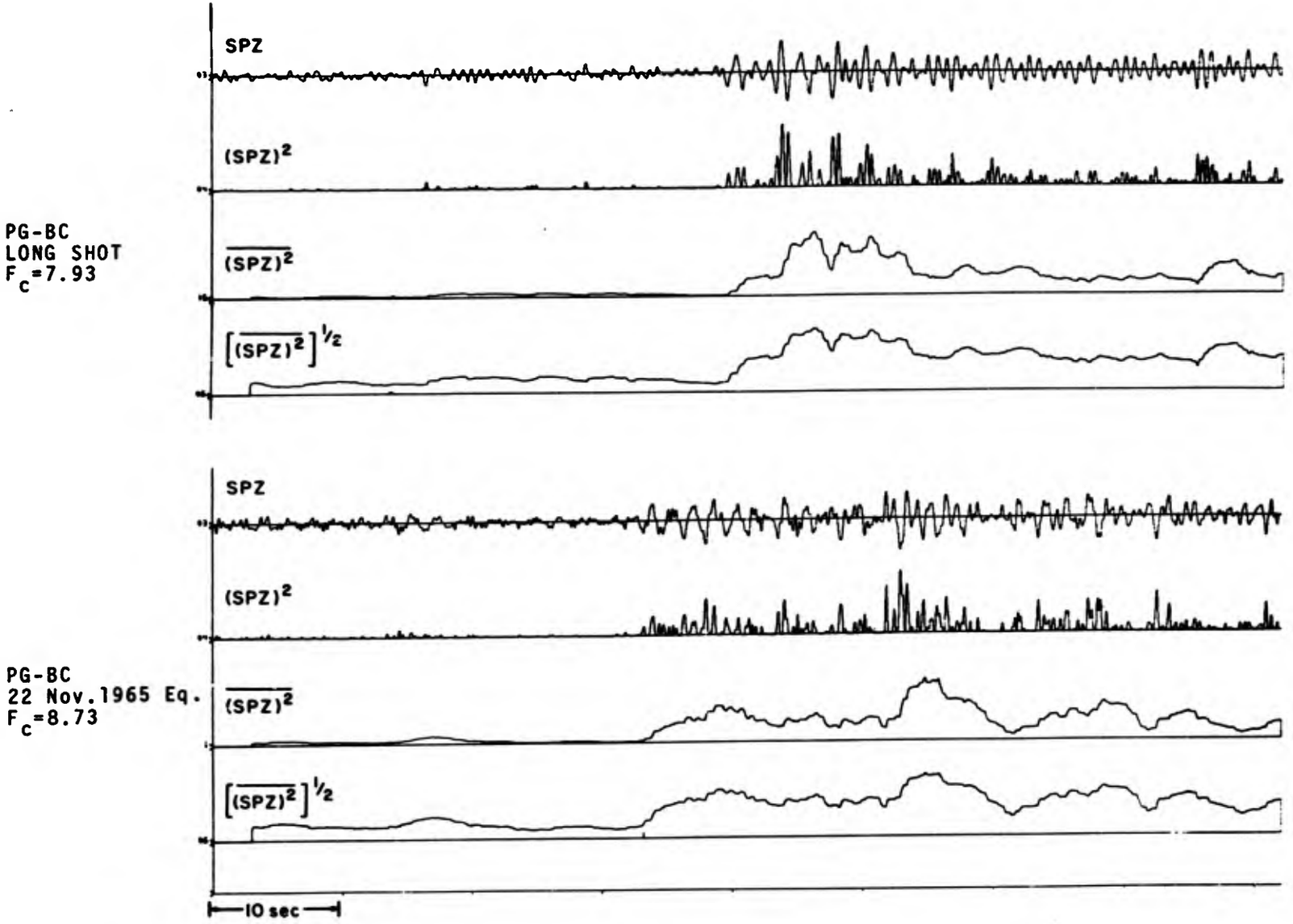

Figure 72. Time series used in calculating complexity factors for LONG SHOT and 22 November 1965 earthquake at PG-BC.

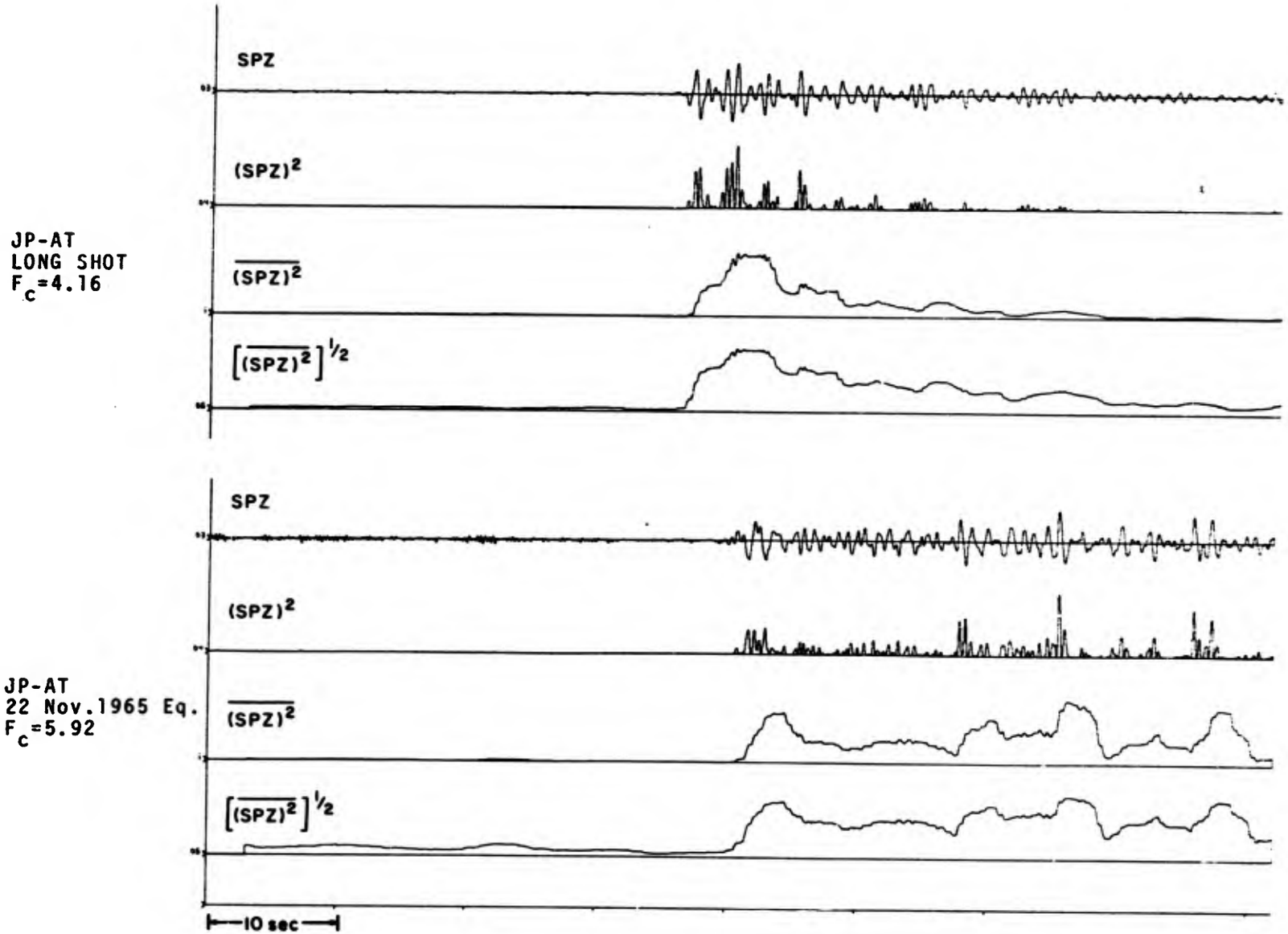

Figure 73. Time series used in calculating complexity factors for LONG SHOT and 22 November 1965 earthquake at JP-AT.

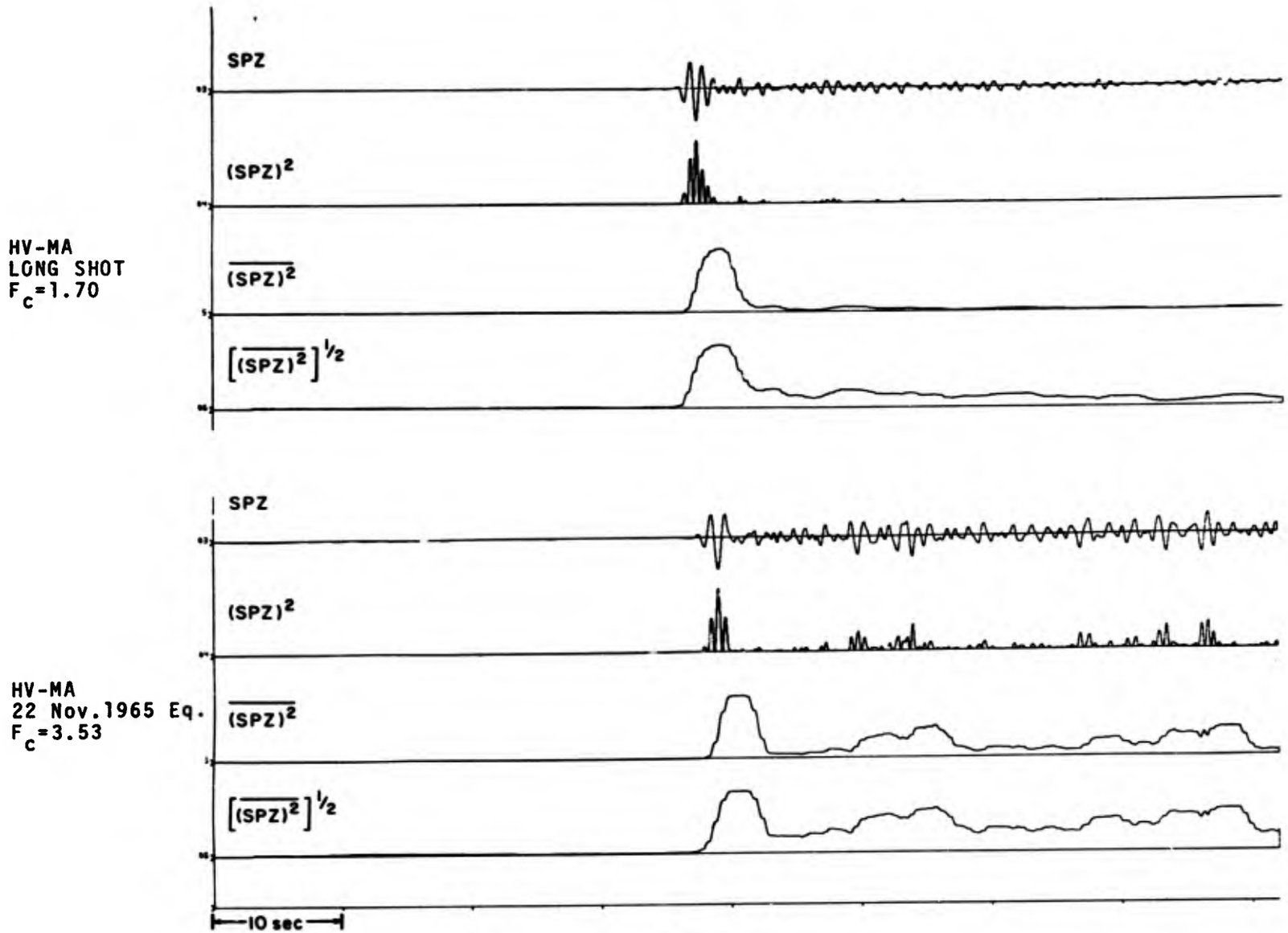

Figure 74. Time series used in calculating complexity factors for LONG SHOT and 22 November 1965 earthquake at HV-MA.

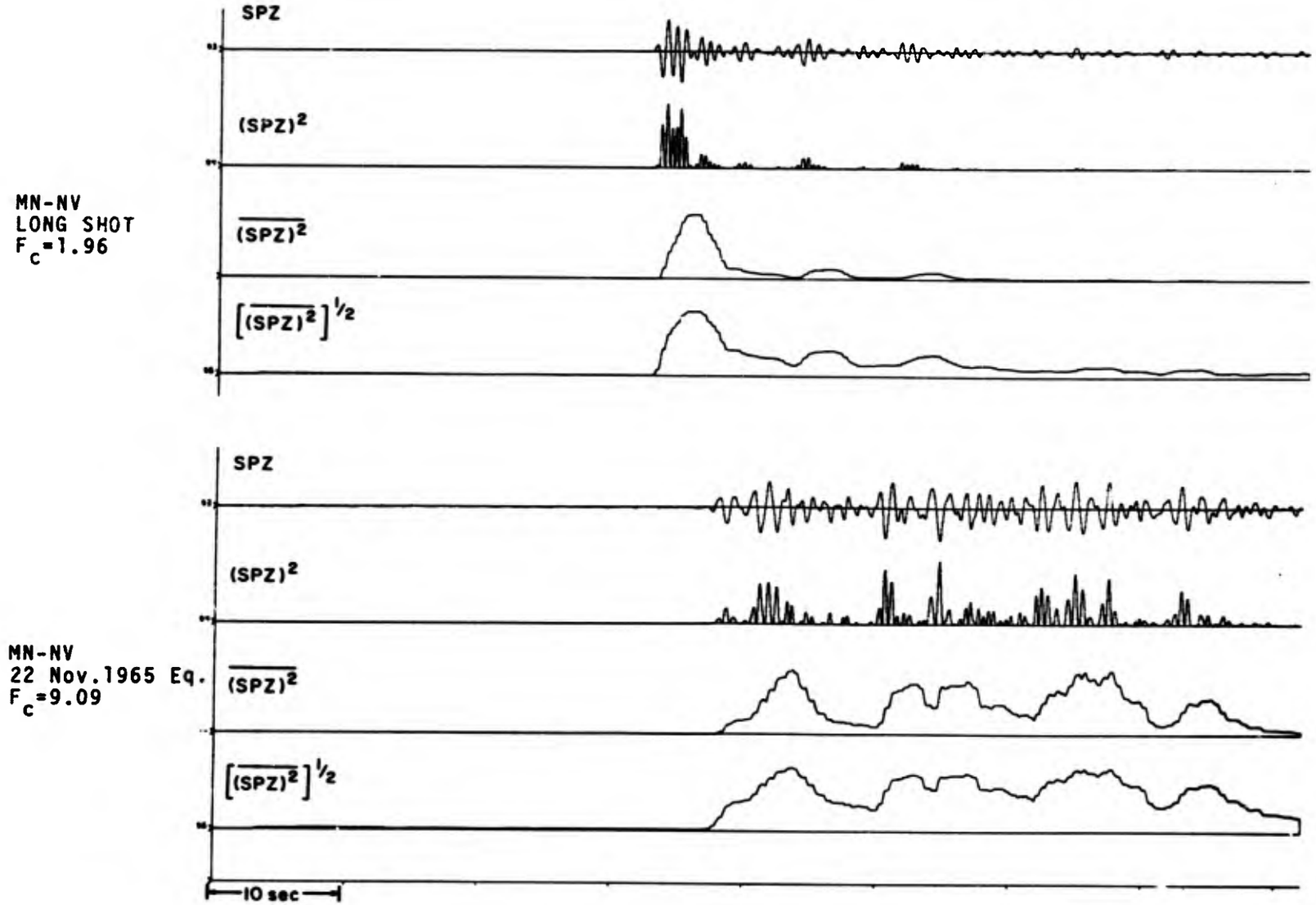

Figure 75. Time series used in calculating complexity factors for LONG SHOT and 22 November 1965 earthquake at MN-NV.

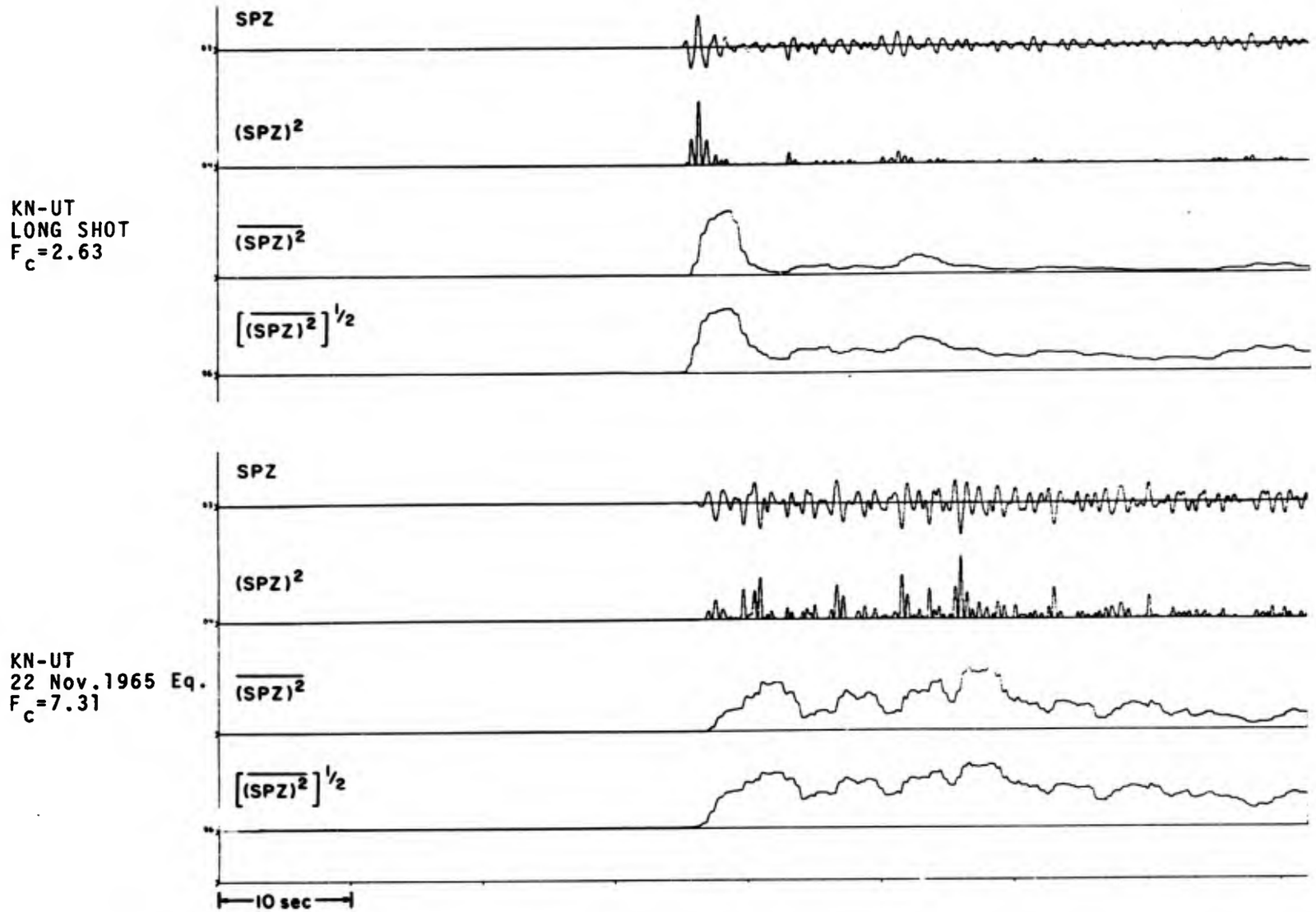

Figure 76. Time series used in calculating complexity factors for LONG SHOT and 22 November 1965 earthquake at KN-UT.

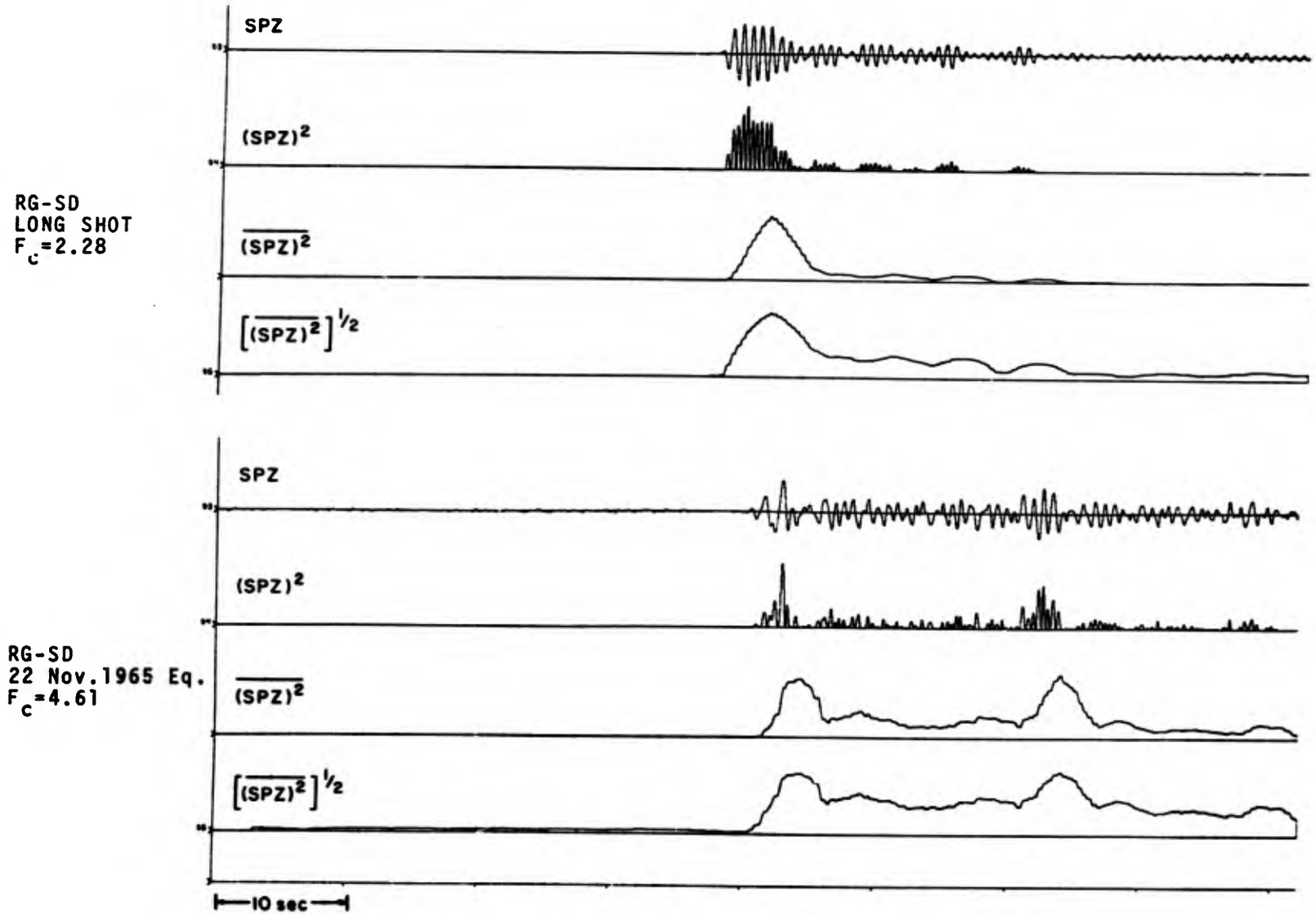

Figure 77. Time series used in calculating complexity factors for LONG SHOT and 22 November 1965 earthquake at RG-SD.

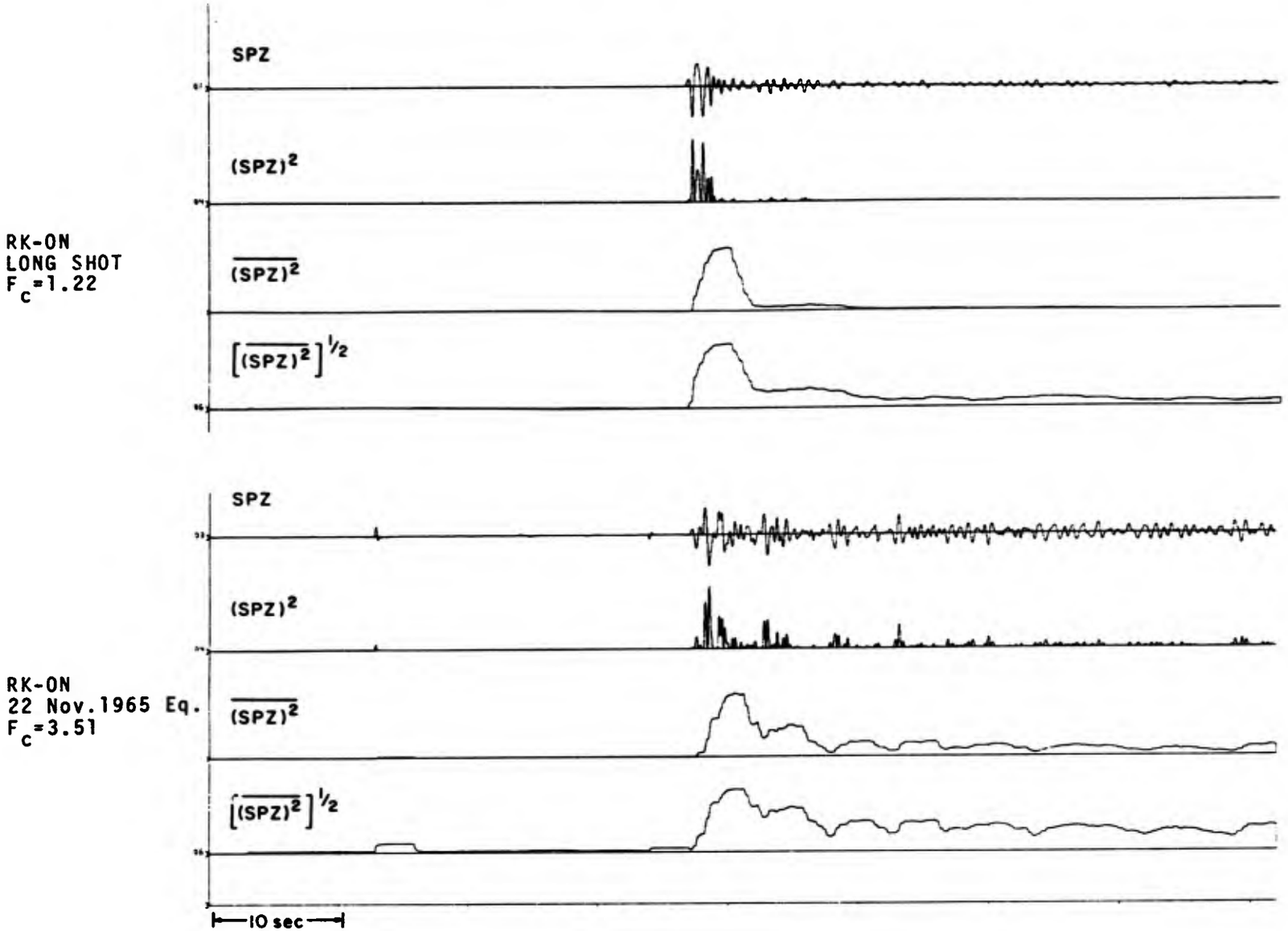

Figure 78. Time series used in calculating complexity factors for LONG SHOT and 22 November 1965 earthquake at RK-ON.

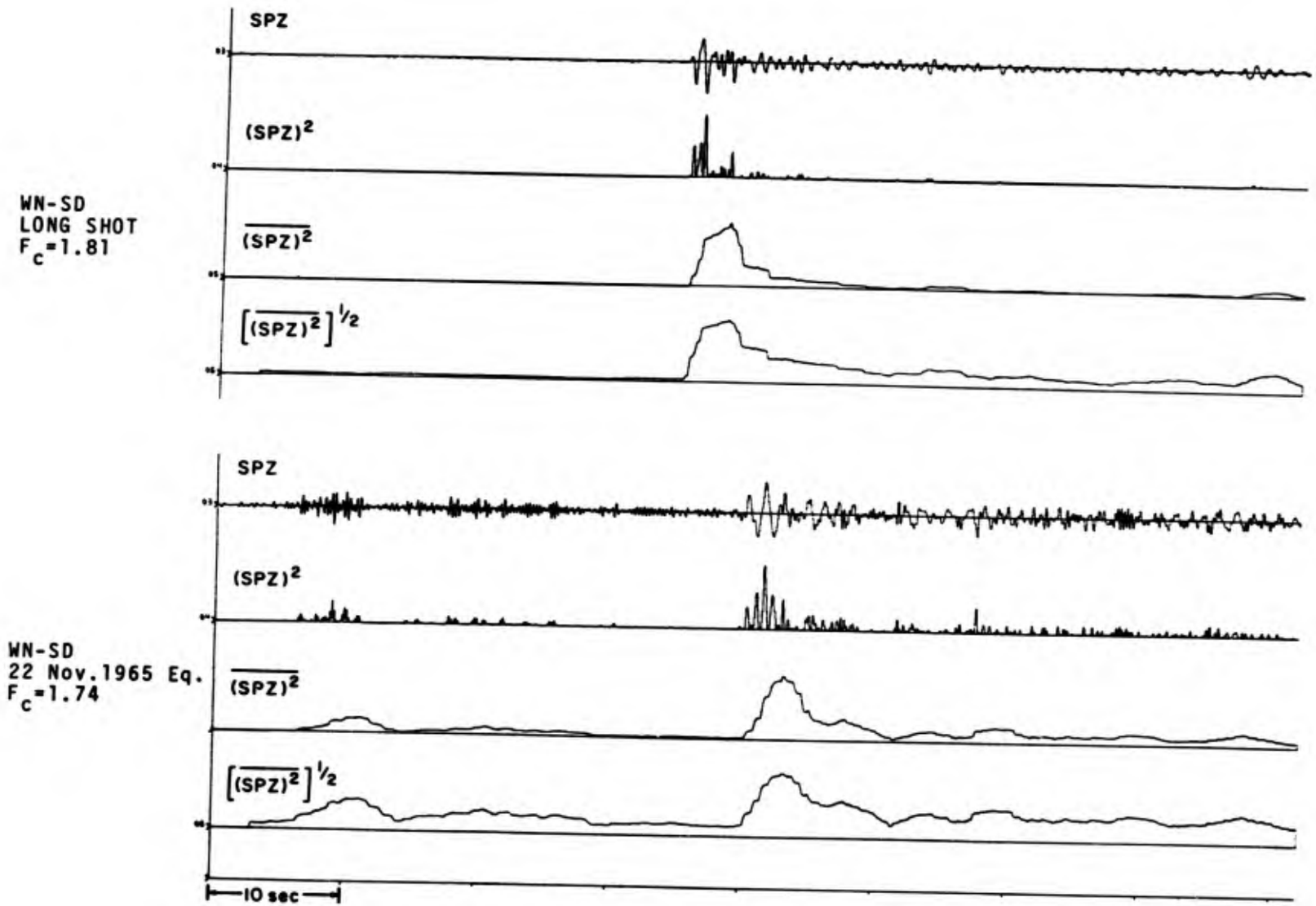

Figure 79. Time series used in calculating complexity factors for LONG SHOT and 22 November 1965 earthquake at WN-SD.

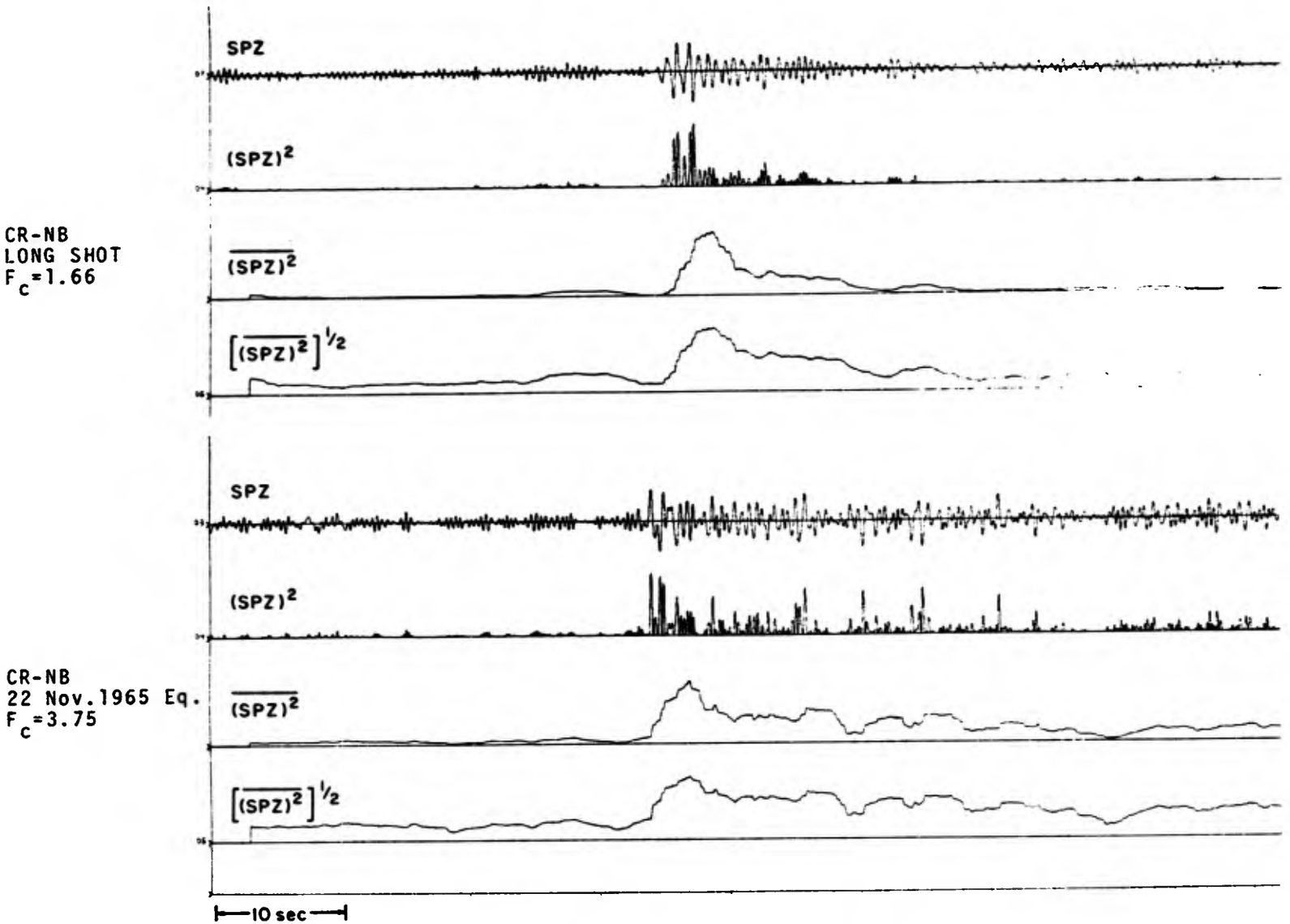

Figure 80. Time series used in calculating complexity factors for LONG SHOT and 22 November 1965 earthquake at CR-NB.

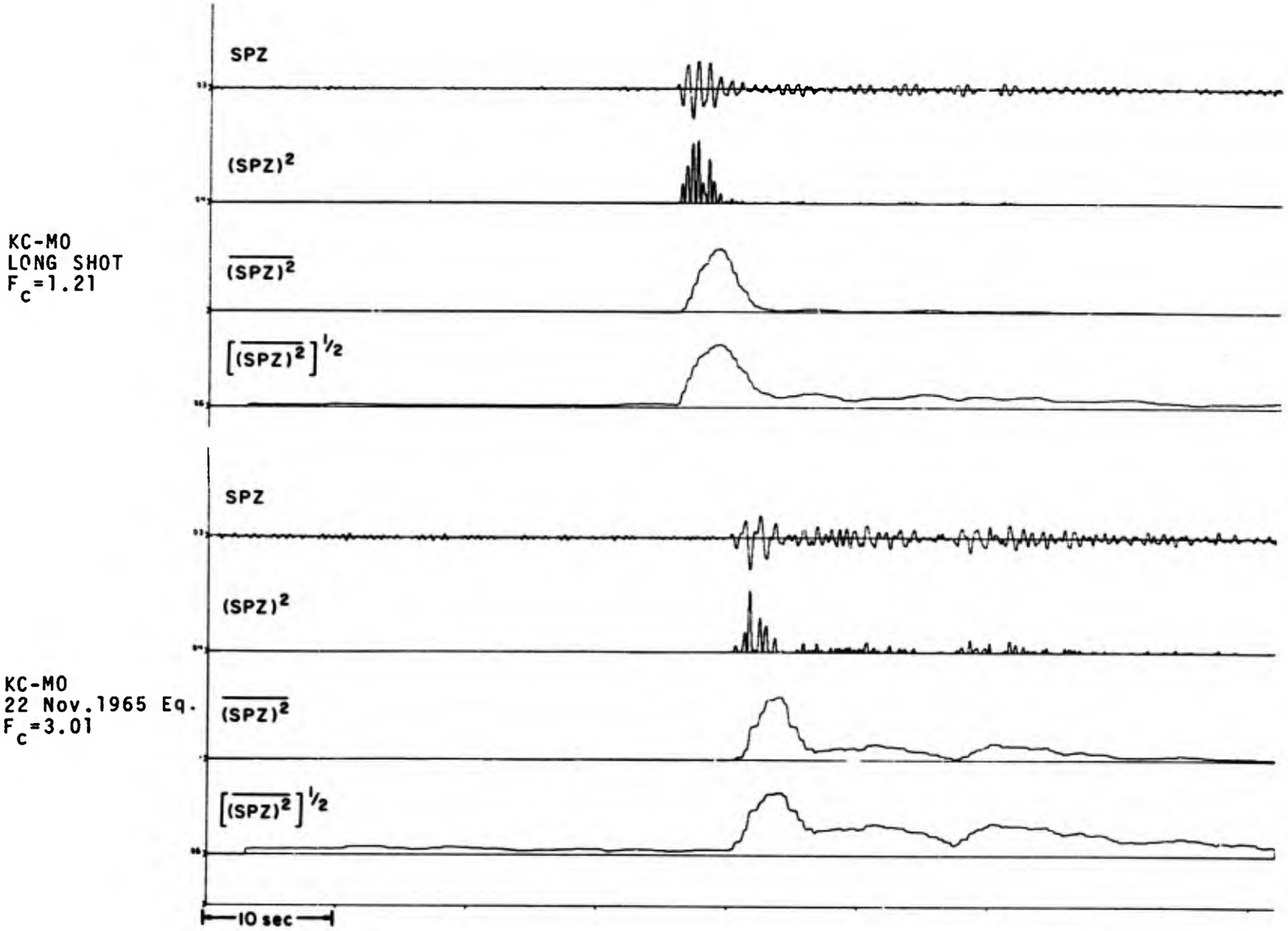

Figure 81. Time series used in calculating complexity factors for LONG SHOT and 22 November 1965 earthquake at KC-MO.

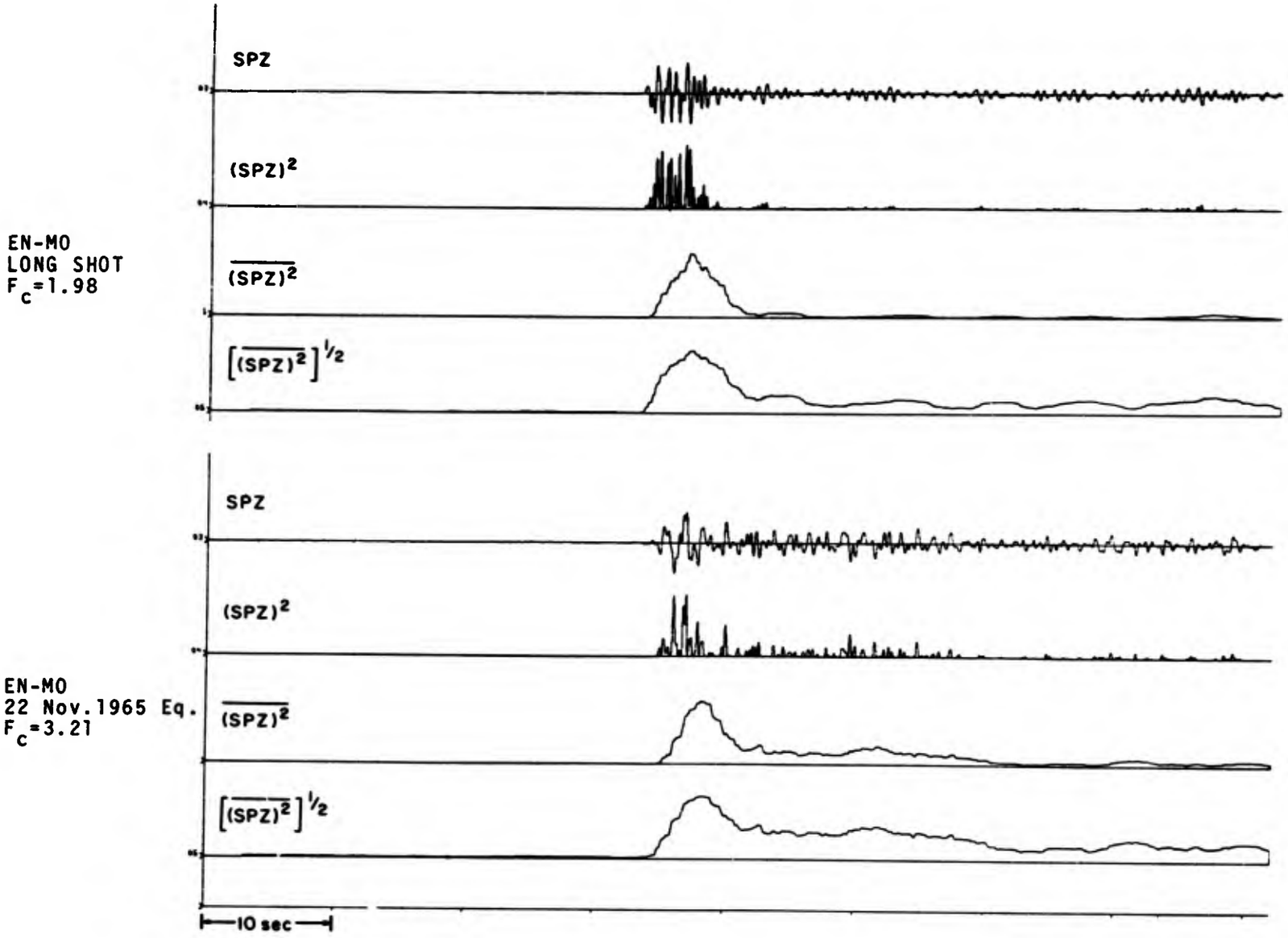

Figure 82. Time series used in calculating complexity factors for LONG SHOT and 22 November 1965 earthquake at EN-MO.

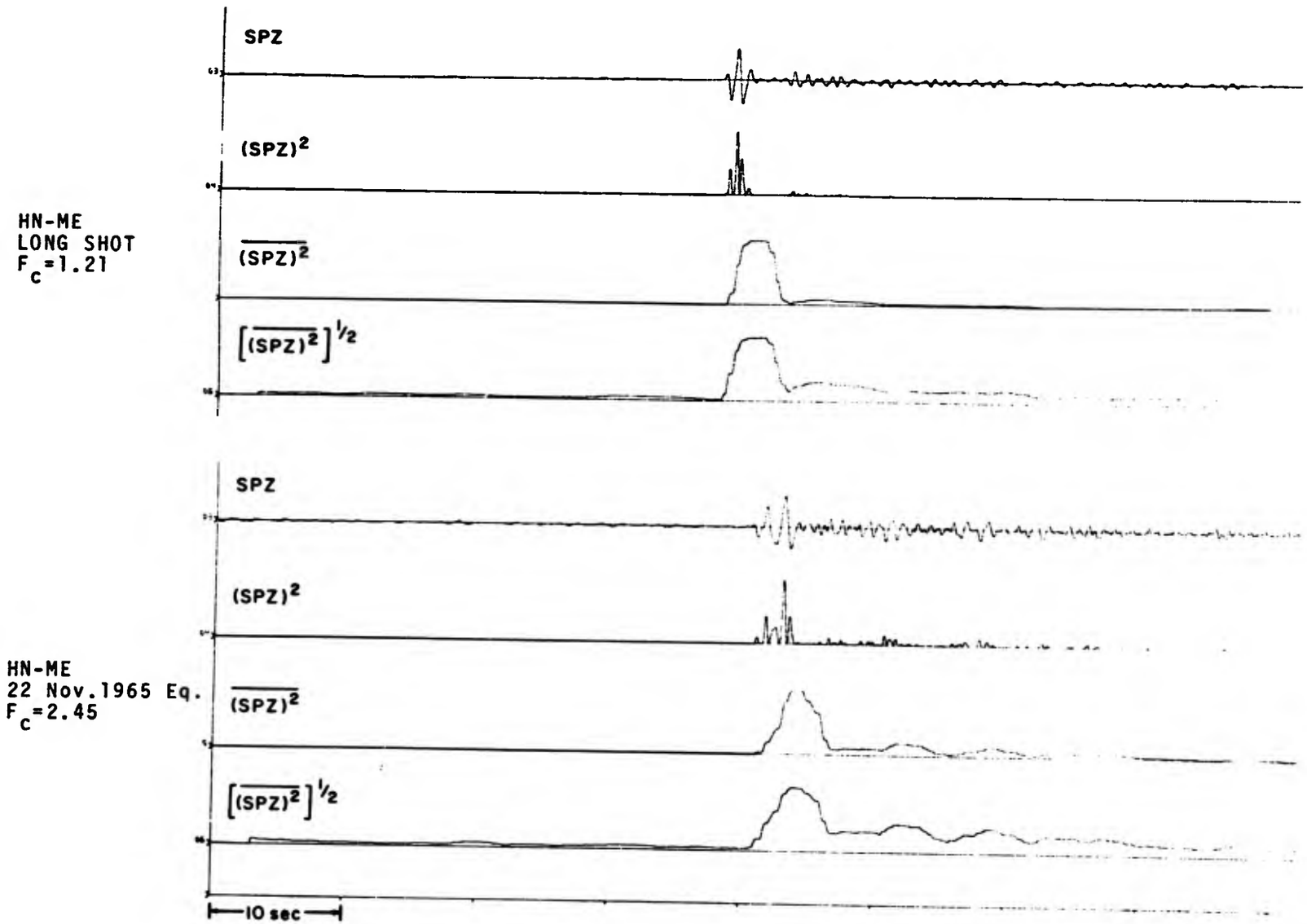

Figure 83. Time series used in calculating complexity factors for LONG SHOT and 22 November 1965 earthquake at HN-ME.

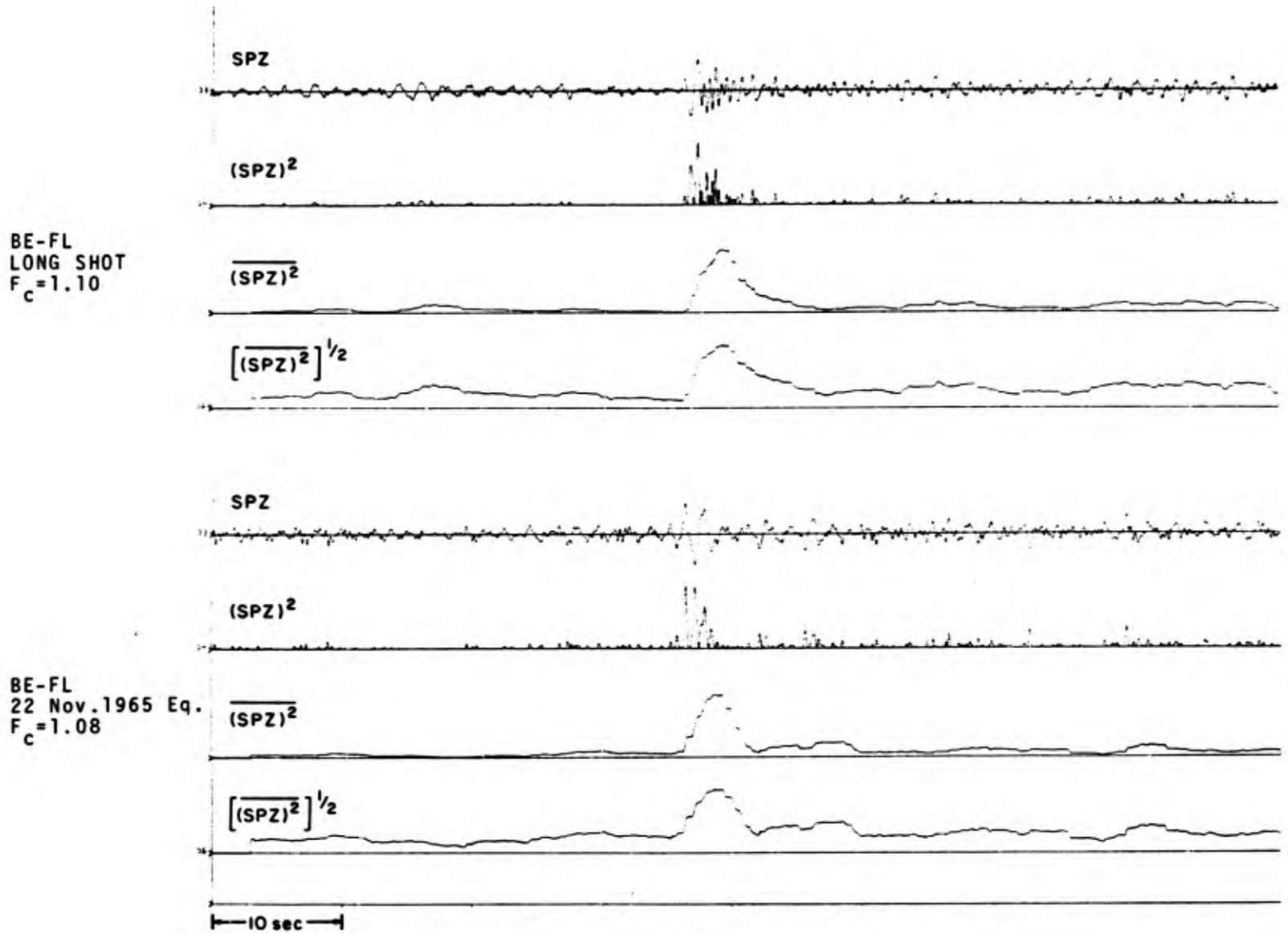

Figure 84. Time series used in calculating complexity factors for LONG SHOT and 22 November 1965 earthquake at BE-FL.

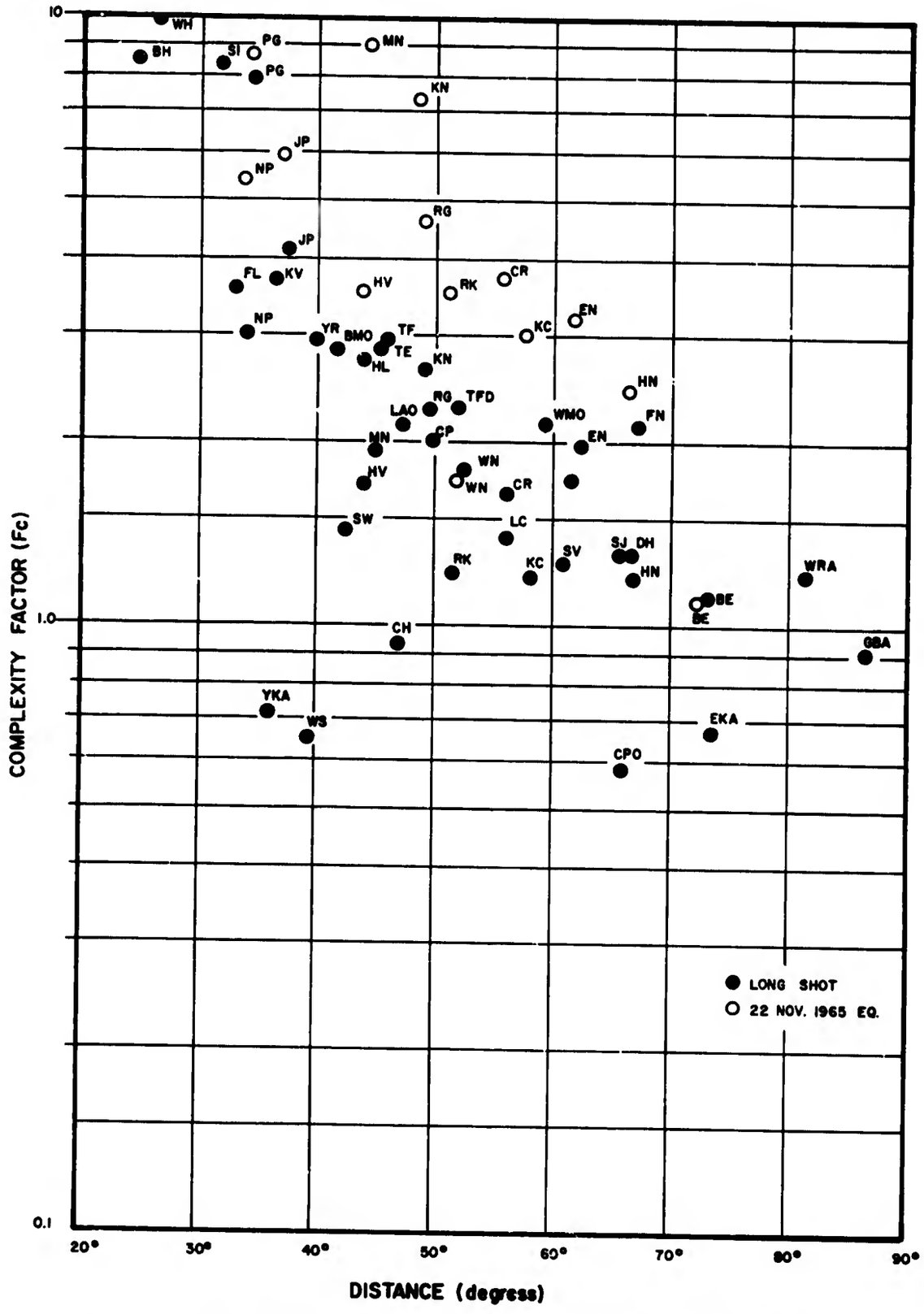

Figure 85. Complexity factors (F_c) versus distance for LONG SHOT and the 22 November 1965 earthquake.

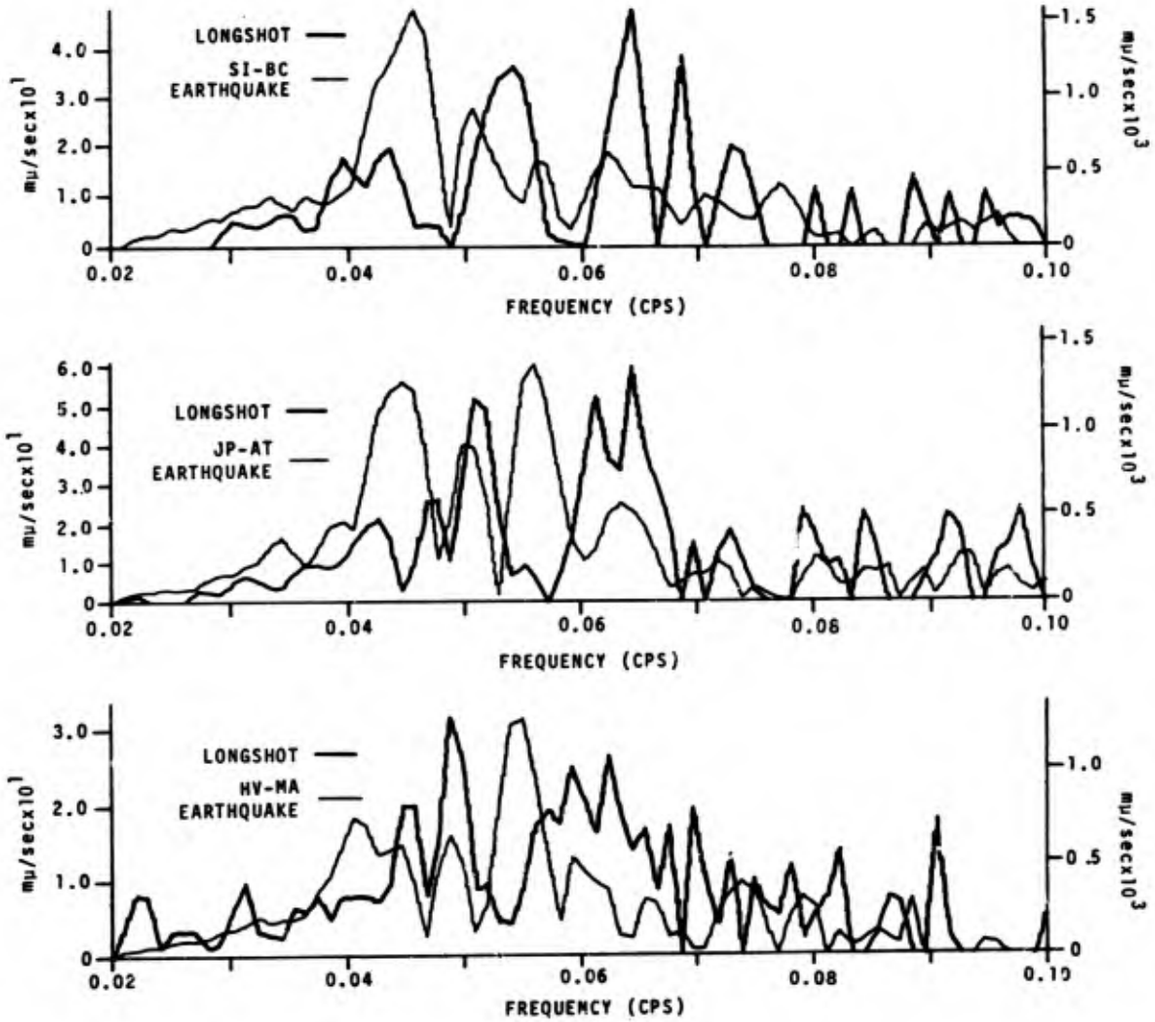

Figure 86. Comparative Rayleigh-wave spectra for LONG SHOT and the 22 November 1965 earthquake at SI-BC, JP-AT, and HV-MA.

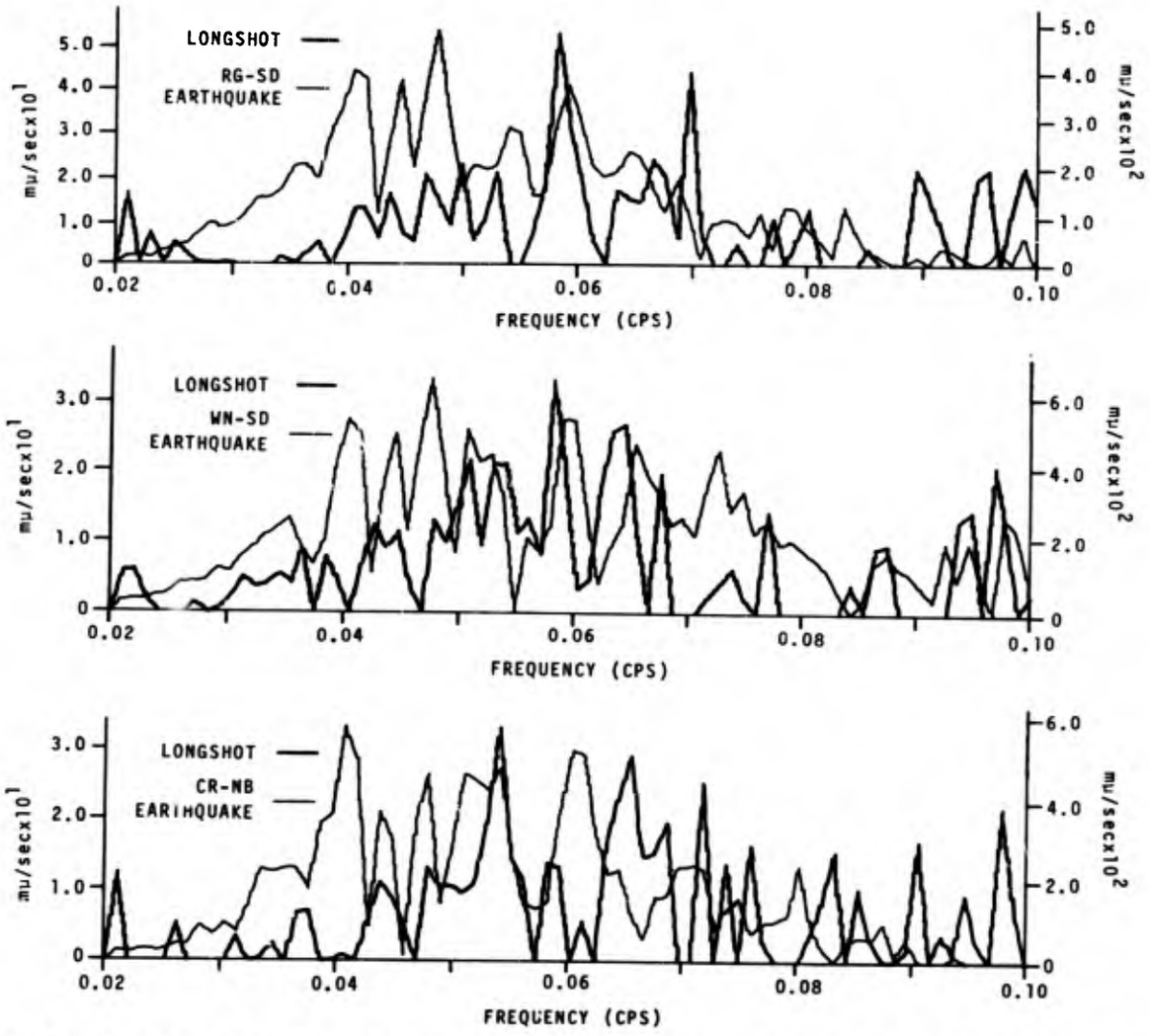

Figure 87. Comparative Rayleigh-wave spectra for LONG SHOT and the 22 November 1965 earthquake at RG-SD, WN-SD, and CR-NB.

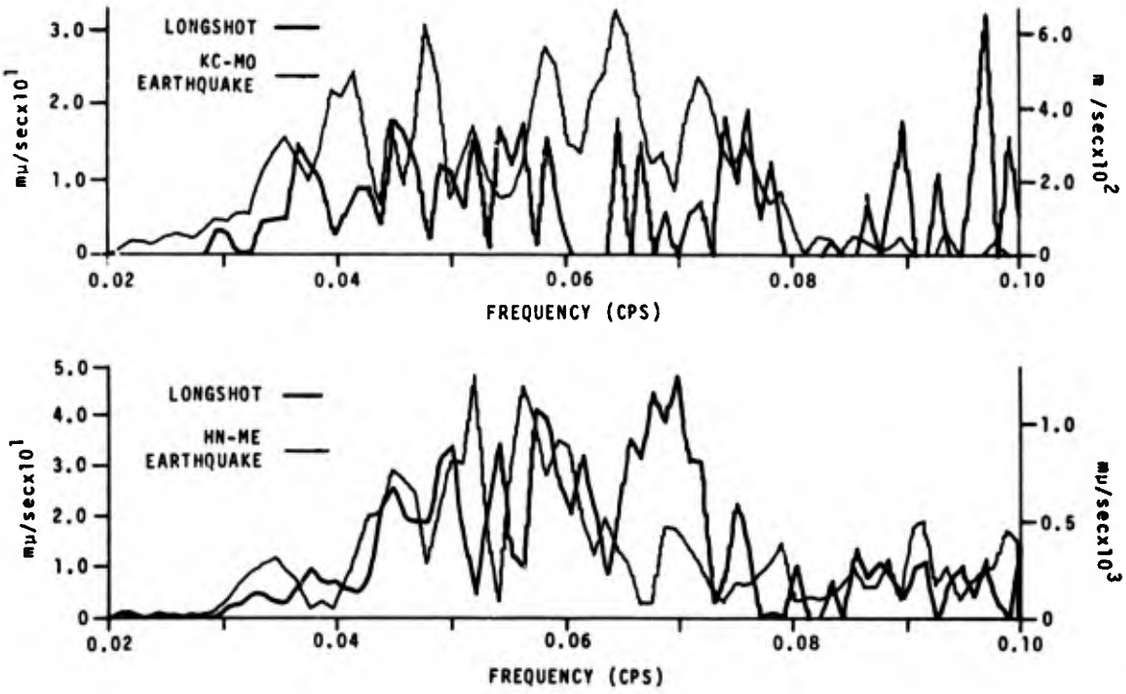

Figure 88. Comparative Rayleigh-wave spectra for LONG SHOT and the 22 November 1965 earthquake at KC-MO and HN-ME.

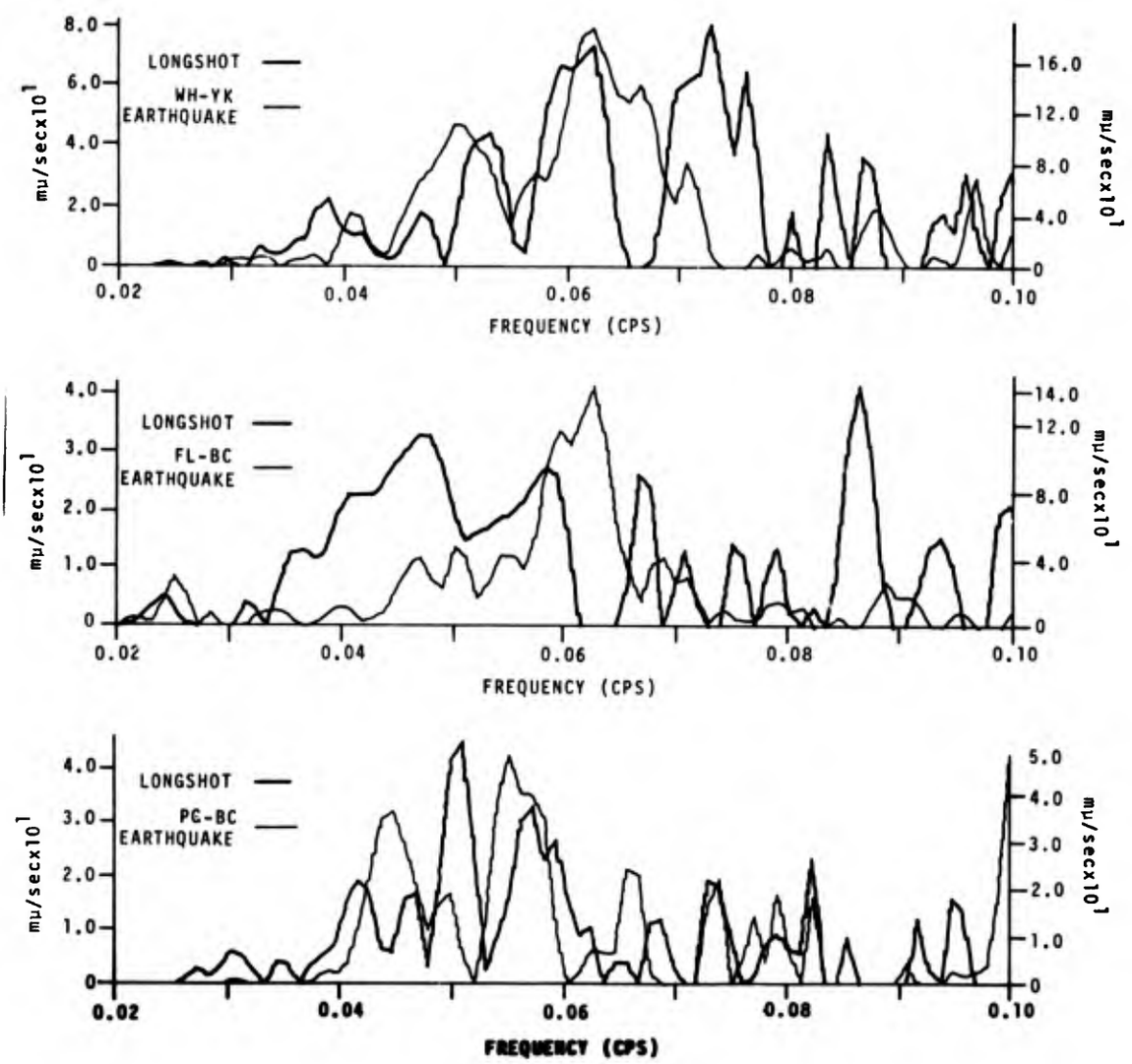

Figure 89. Comparative Rayleigh-wave spectra for LONG SHOT and the 06 November 1965 earthquake at WH-YK, FL-BC, and PG-BC.

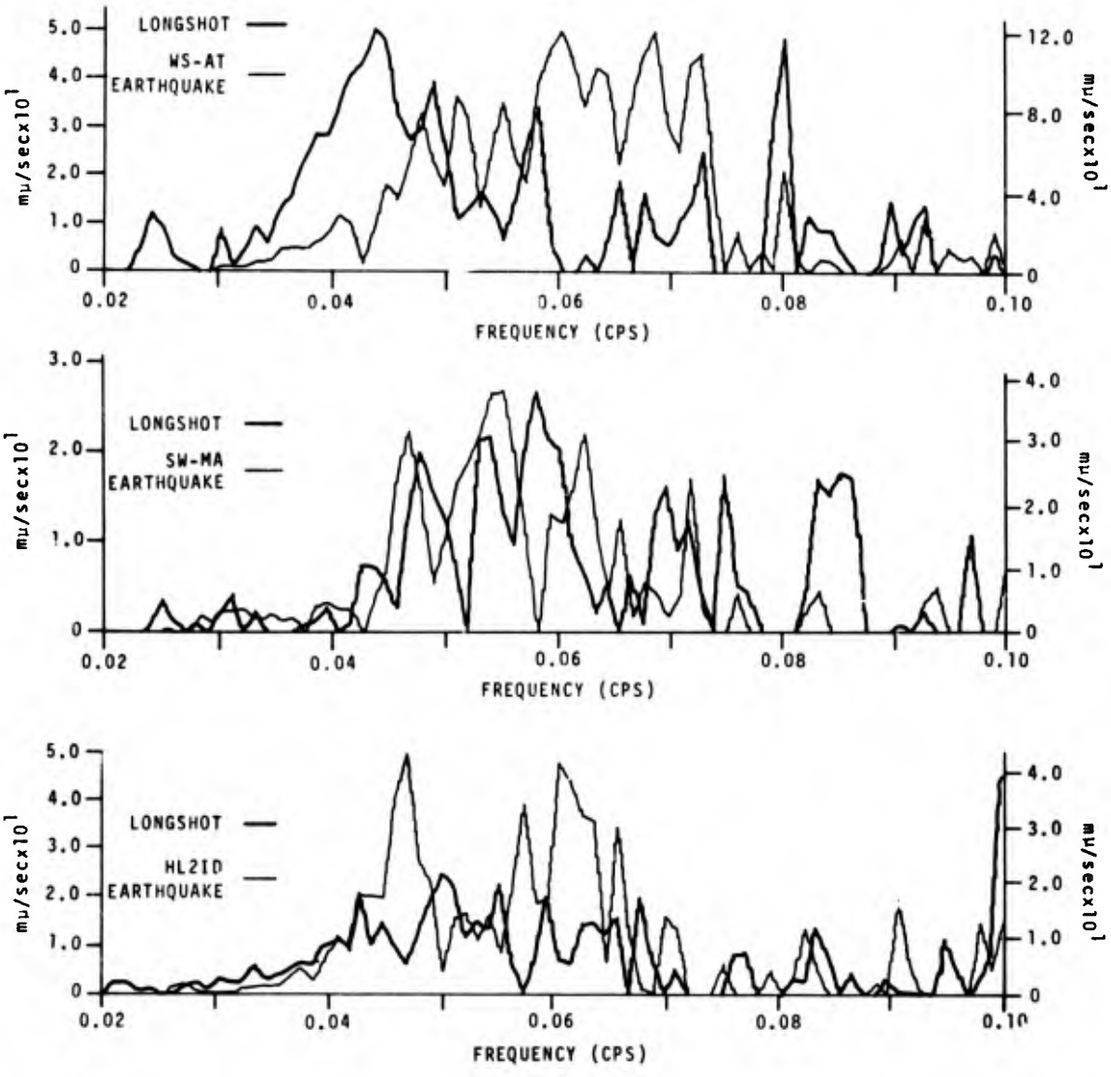

Figure 90. Comparative Rayleigh-wave spectra for LONG SHOT and the 06 November 1965 earthquake at WS-AT, SW-MA, and HL2ID.

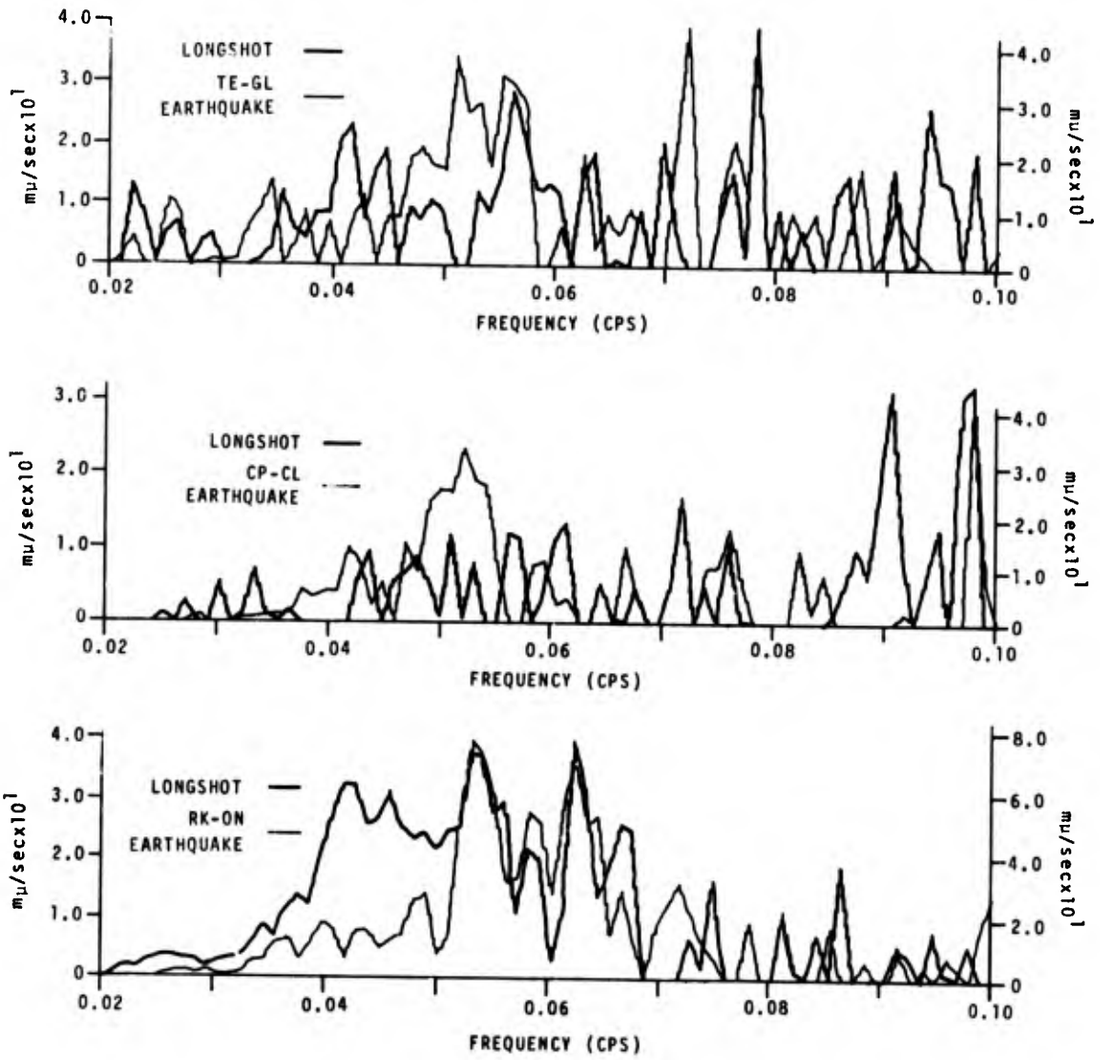

Figure 91. Comparative Rayleigh-wave spectra for LONG SHOT and the 06 November 1965 earthquake at TE-GL, CP-CL, and RK-ON.

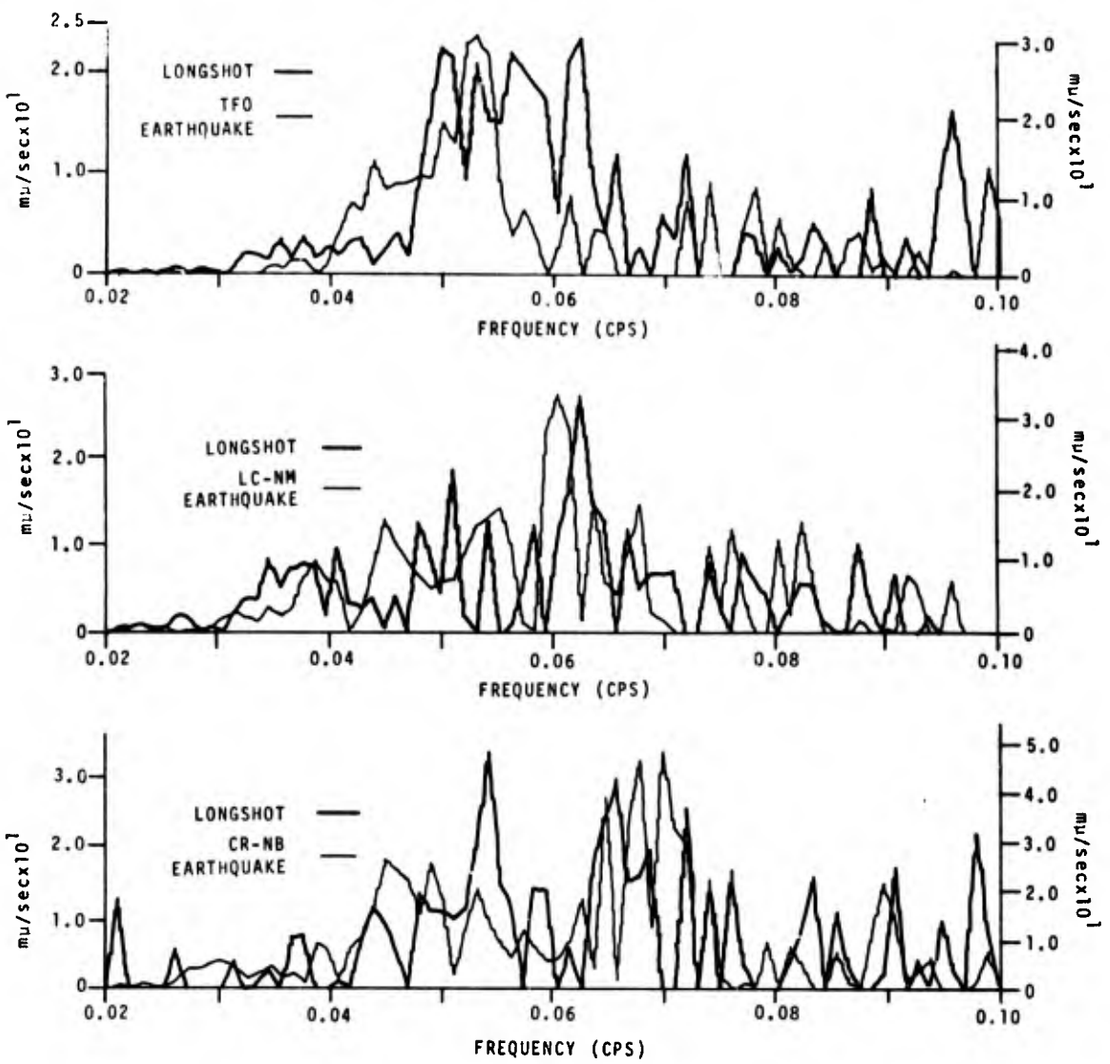

Figure 92. Comparative Rayleigh-wave spectra for LONG SHOT and the 06 November 1965 earthquake at TFO, LC-NM, and CR-NB.

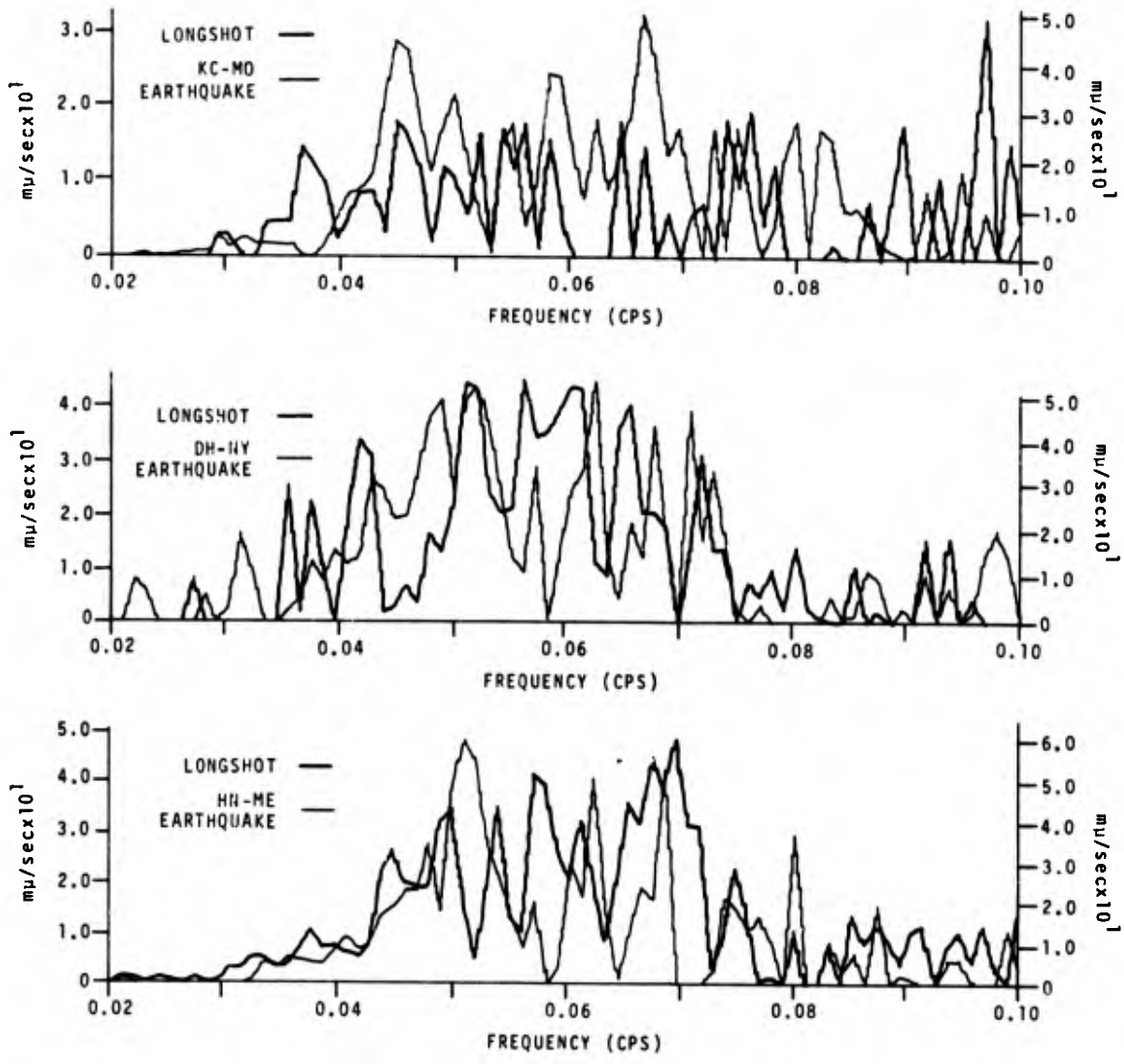

Figure 93. Comparative Rayleigh-wave spectra for LONG SHOT and the 06 November 1965 earthquake at KC-MO, DH-NY, and HN-ME.

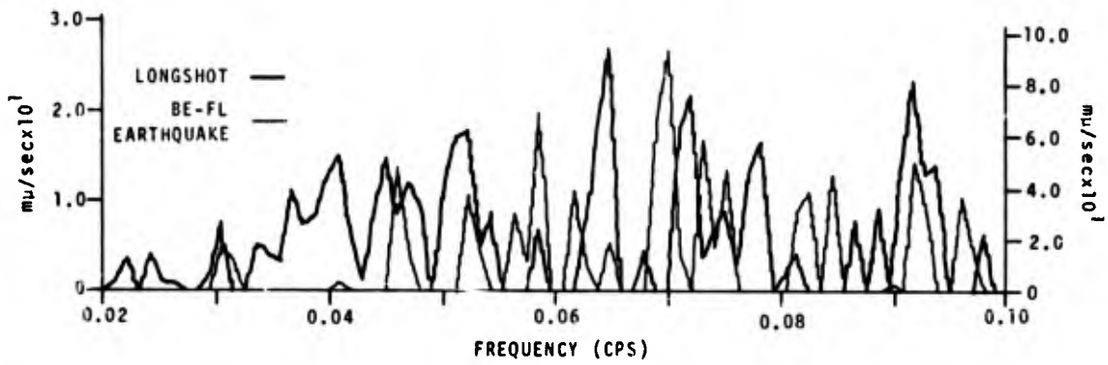

Figure 94. Comparative Rayleigh-wave spectra for LONG SHOT and the 06 November 1965 earthquake at BE-FL.

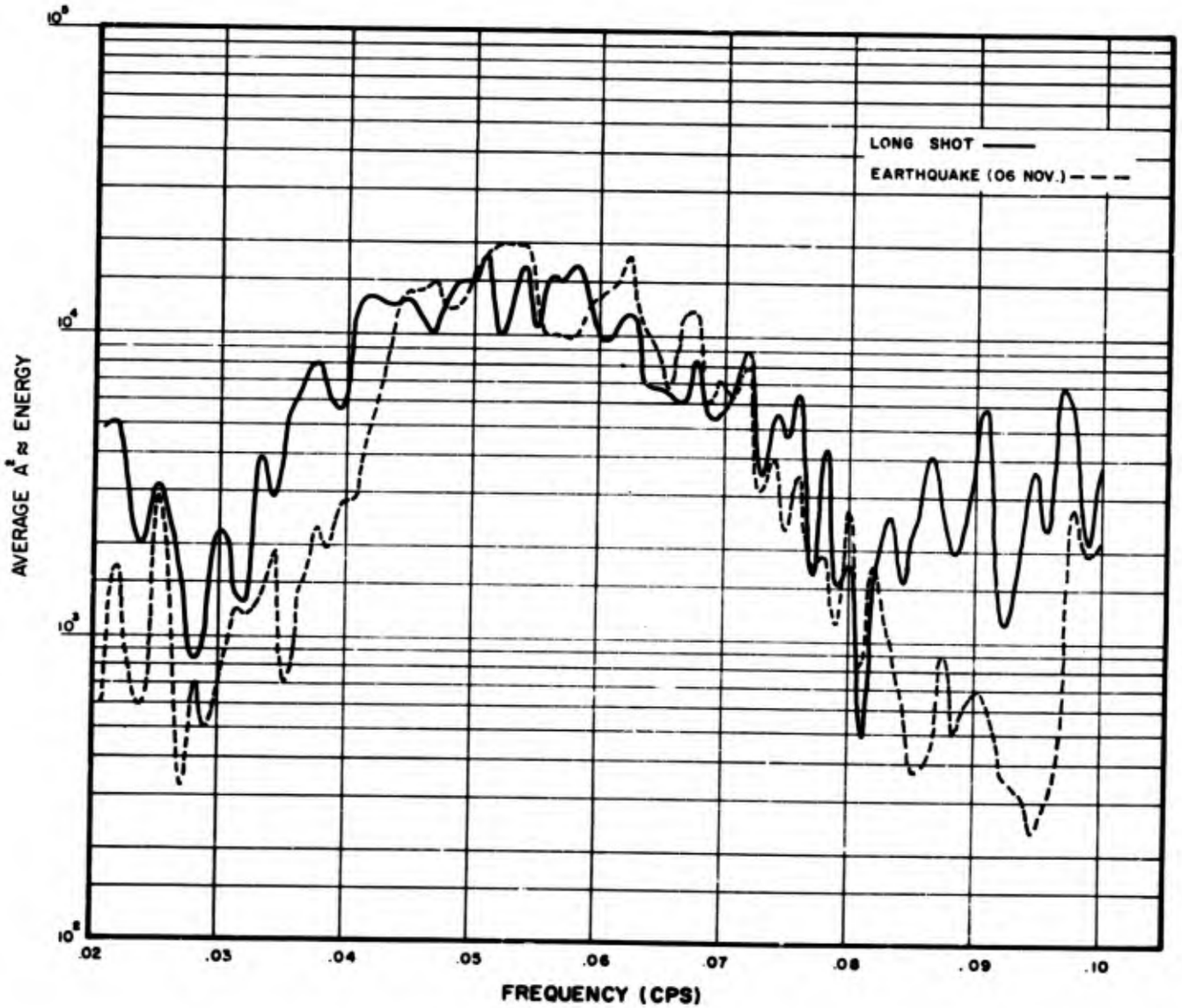

Figure 95. Average Rayleigh-wave power spectra for LONG SHOT and the 06 November 1965 earthquake.

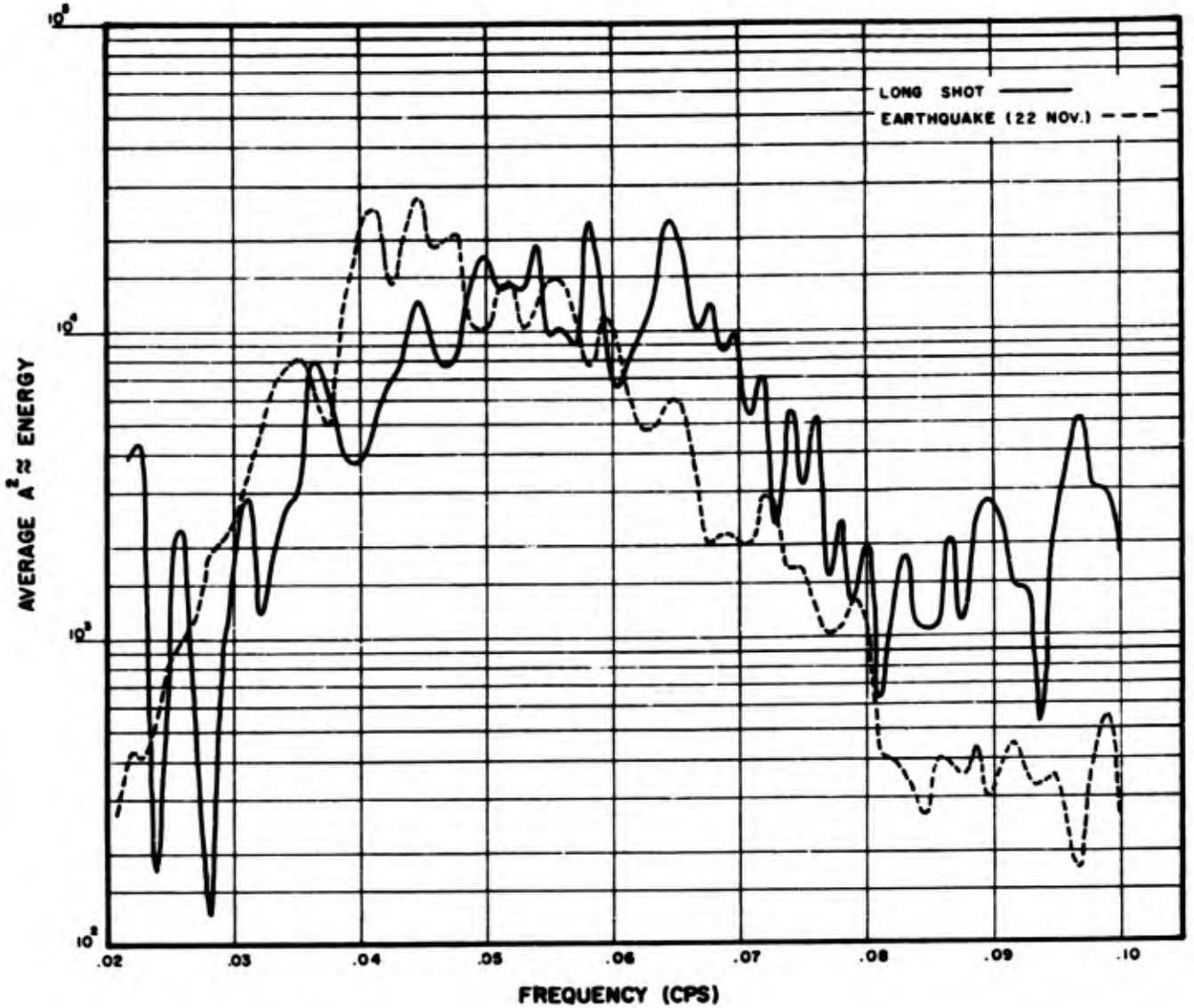

Figure 96. Average Rayleigh-wave power spectra for LONG SHOT and the 22 November 1965 earthquake.

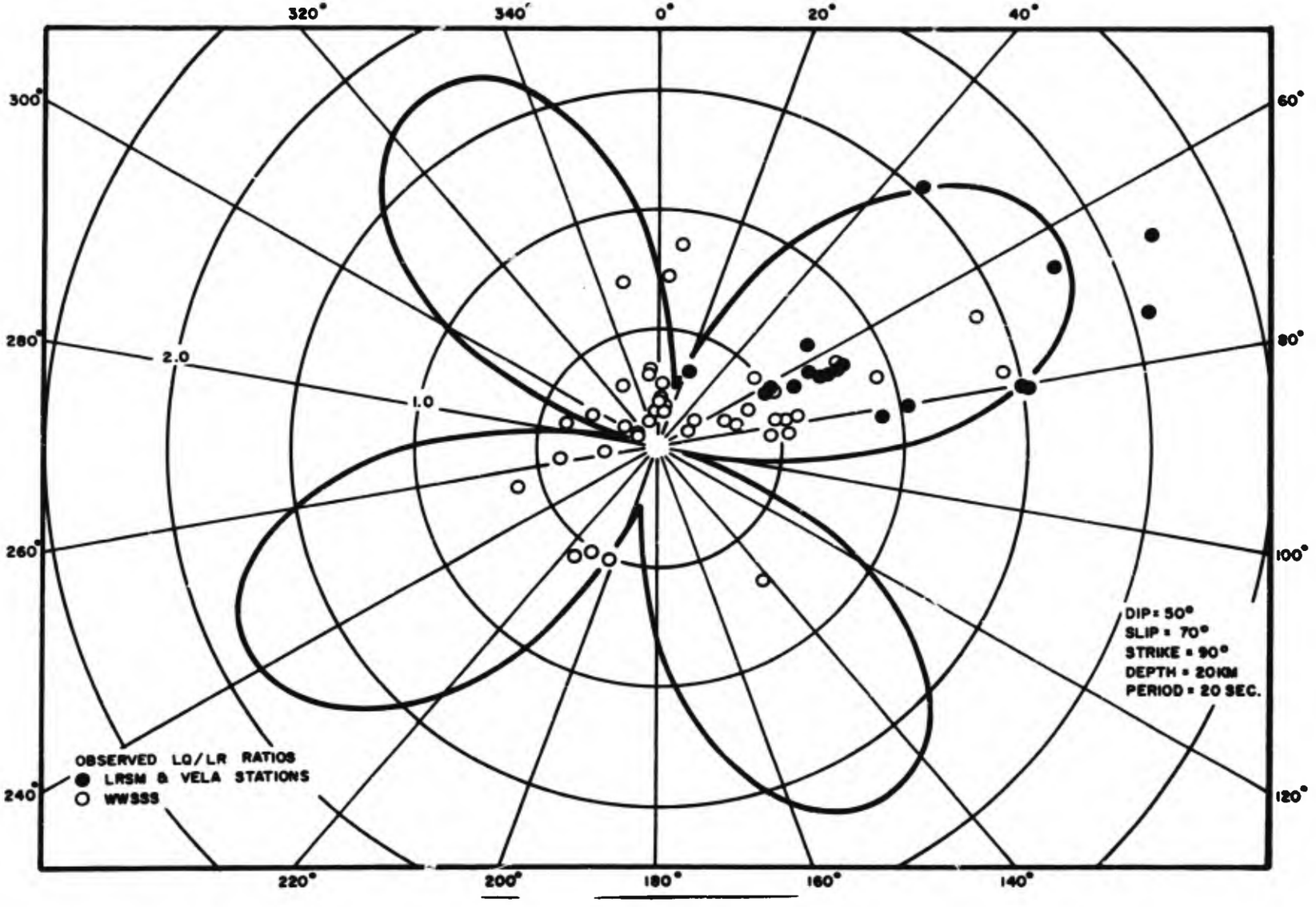

Figure 97. Polar plot of Love-to-Rayleigh amplitude ratios for the 22 November 1965 earthquake.

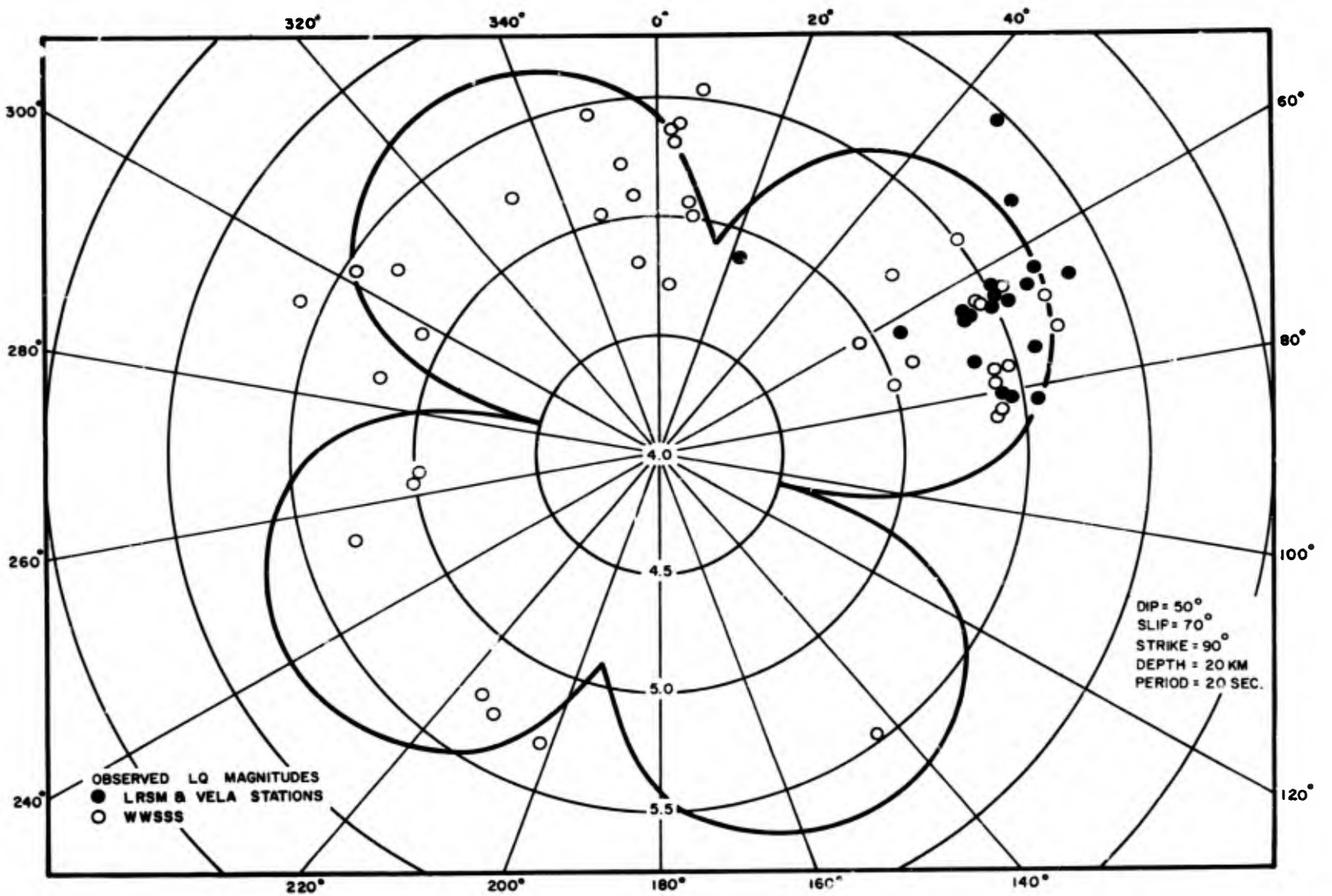

Figure 98. Polar plot of Love-wave (LQ) magnitudes for the 22 November 1965 earthquake.

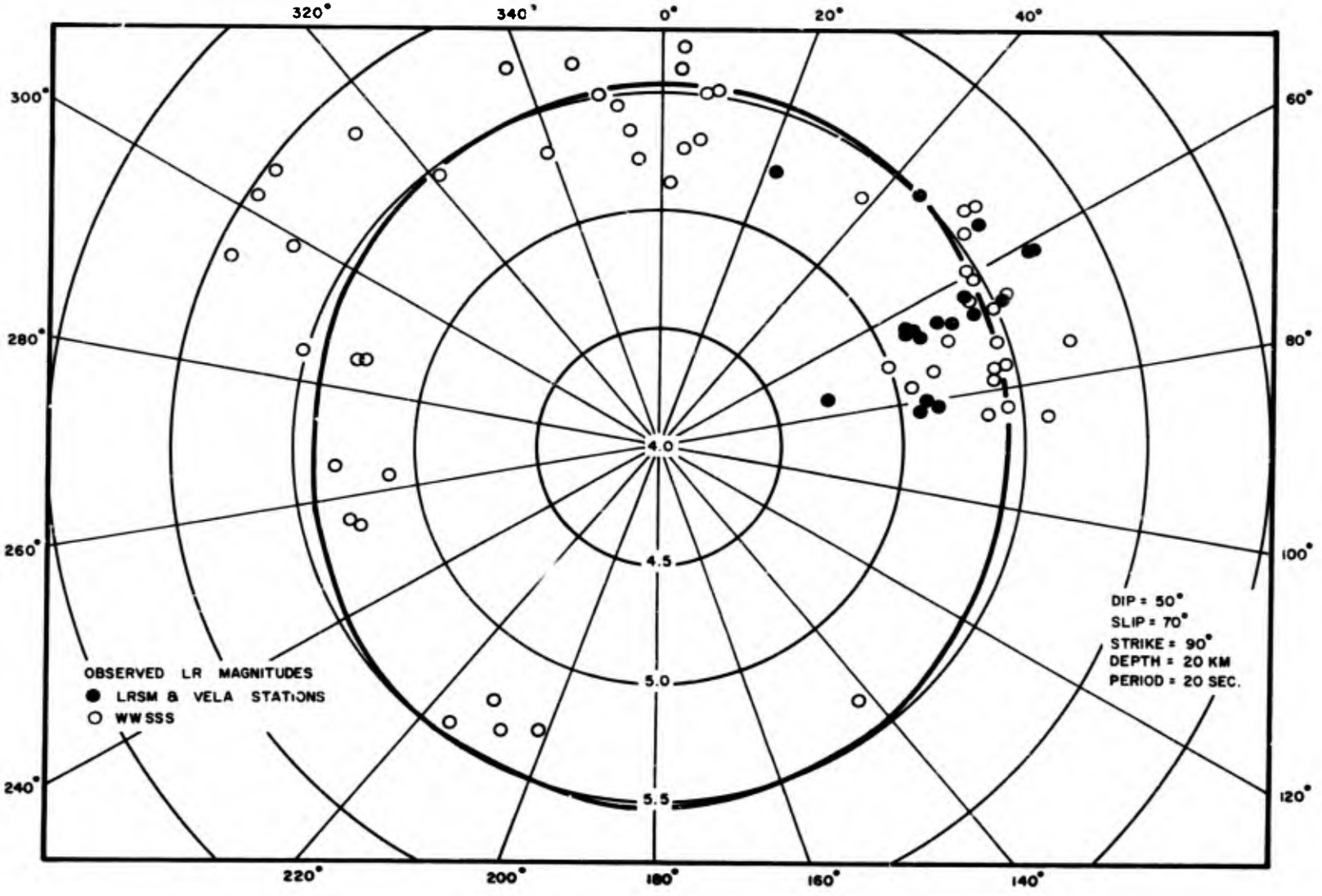

Figure 99. Polar plot of Rayleigh-wave (LR) magnitudes for the 22 November 1965 earthquake.

APPENDIX I

SHORT-PERIOD P AND PCP SPECTRA

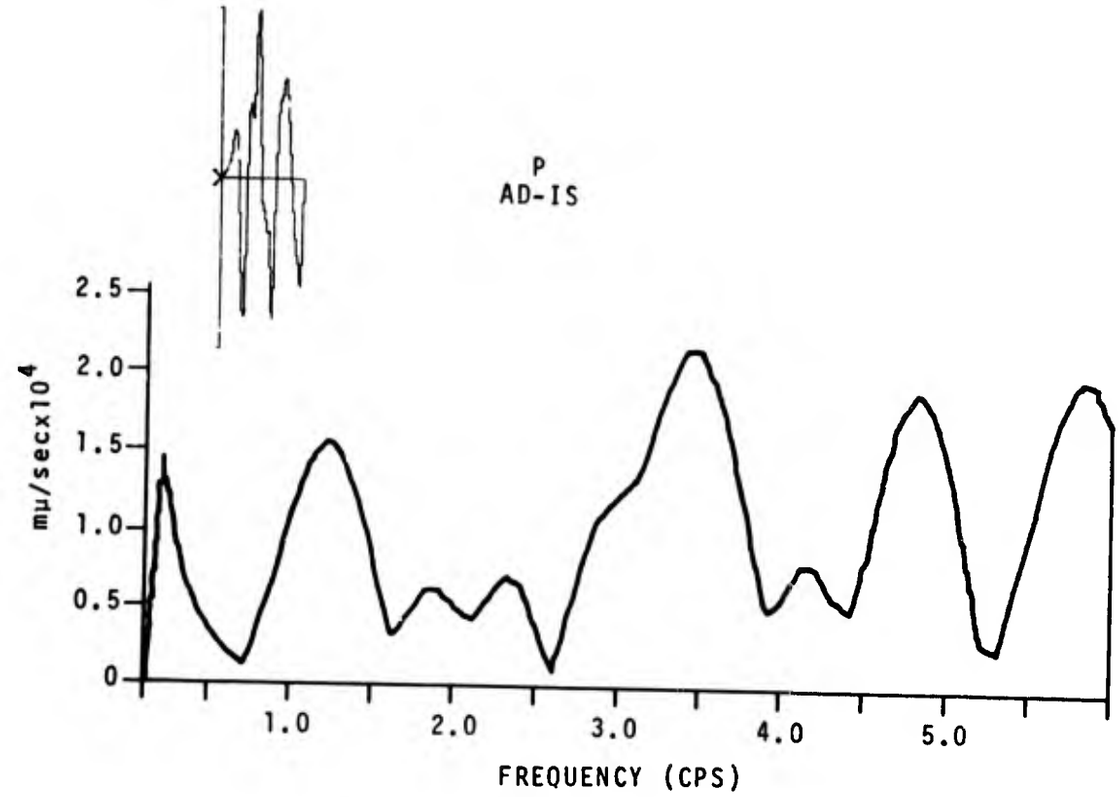
P
AD-IS
2.5
2.0
1.5
1.0
0.5
0
mμ/secx10^4
1.0
2.0
3.0
4.0
5.0
FREQUENCY (CPS)

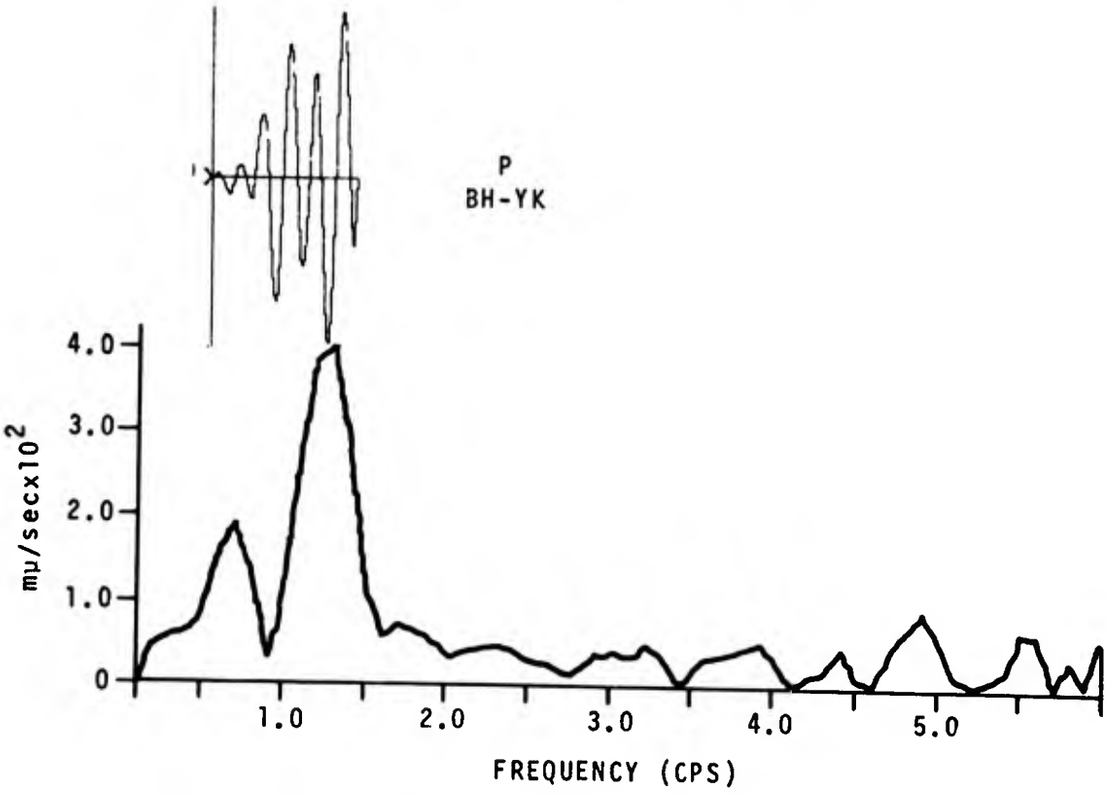
P
BH-YK
4.0
3.0
2.0
1.0
0
mμ/secx10^2
1.0
2.0
3.0
4.0
5.0
FREQUENCY (CPS)

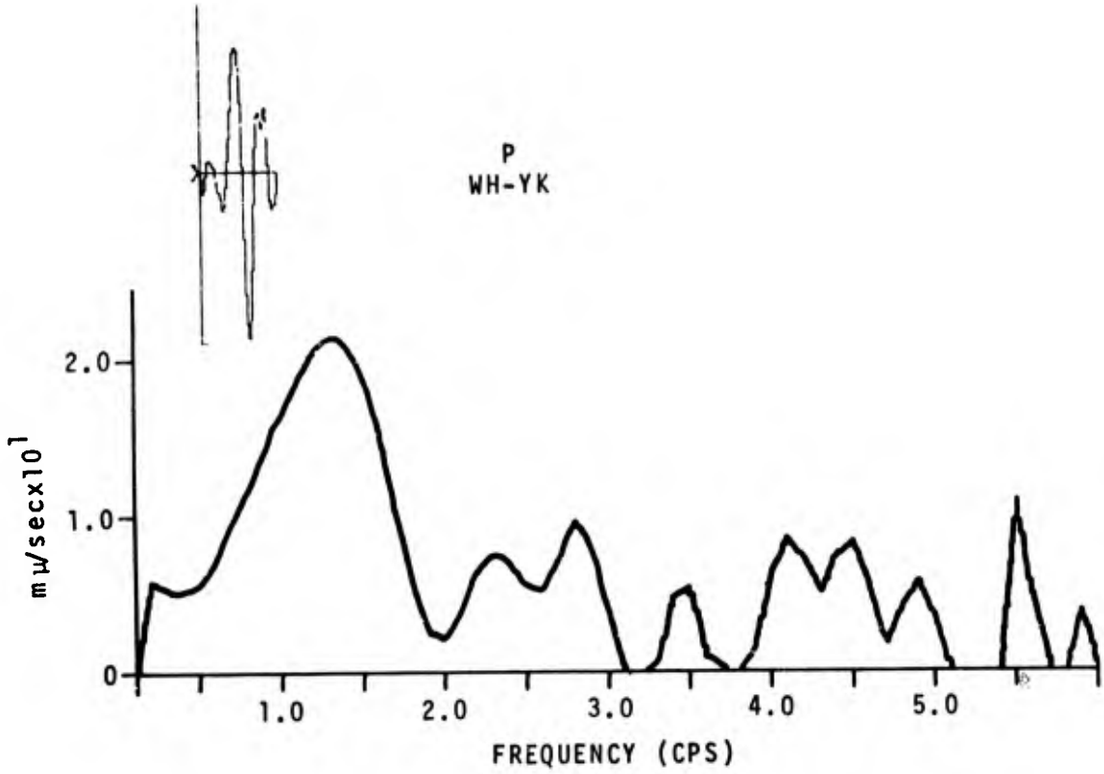
P
WH-YK
2.0
1.0
0
mμ/secx10¹
1.0
2.0
3.0
4.0
5.0
FREQUENCY (CPS)

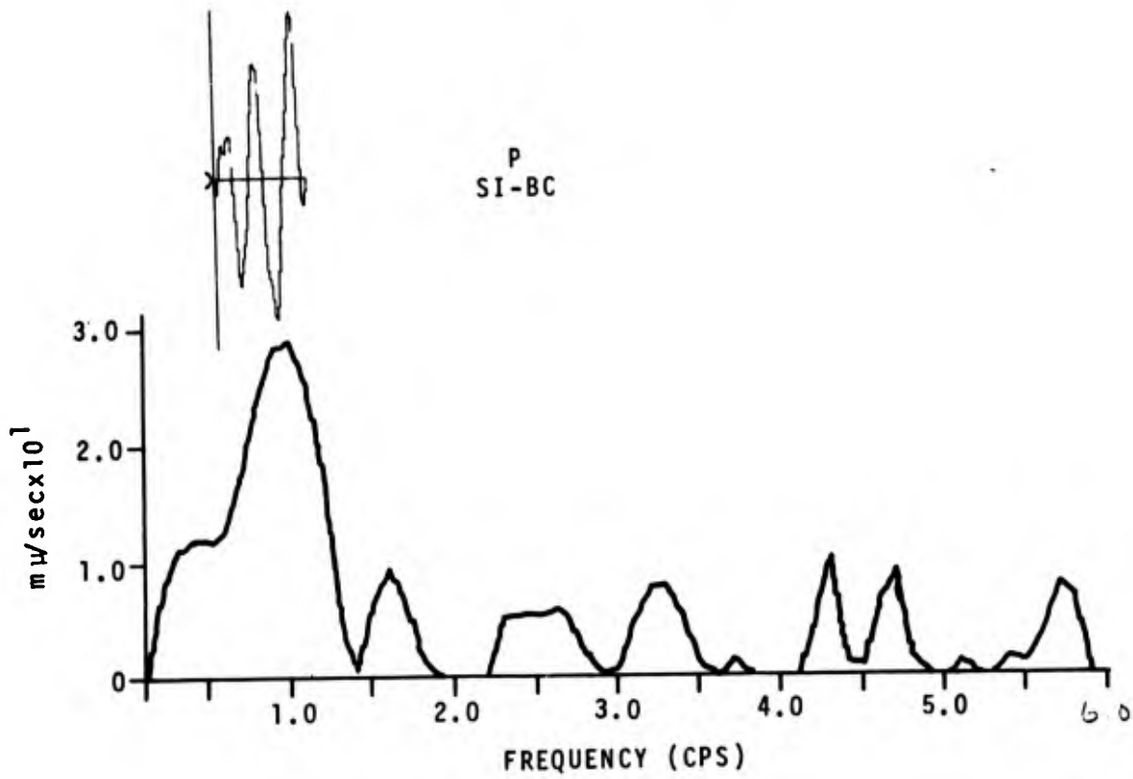
P
SI-BC
3.0
2.0
1.0
0
mμ/secx10¹
1.0
2.0
3.0
4.0
5.0
FREQUENCY (CPS)

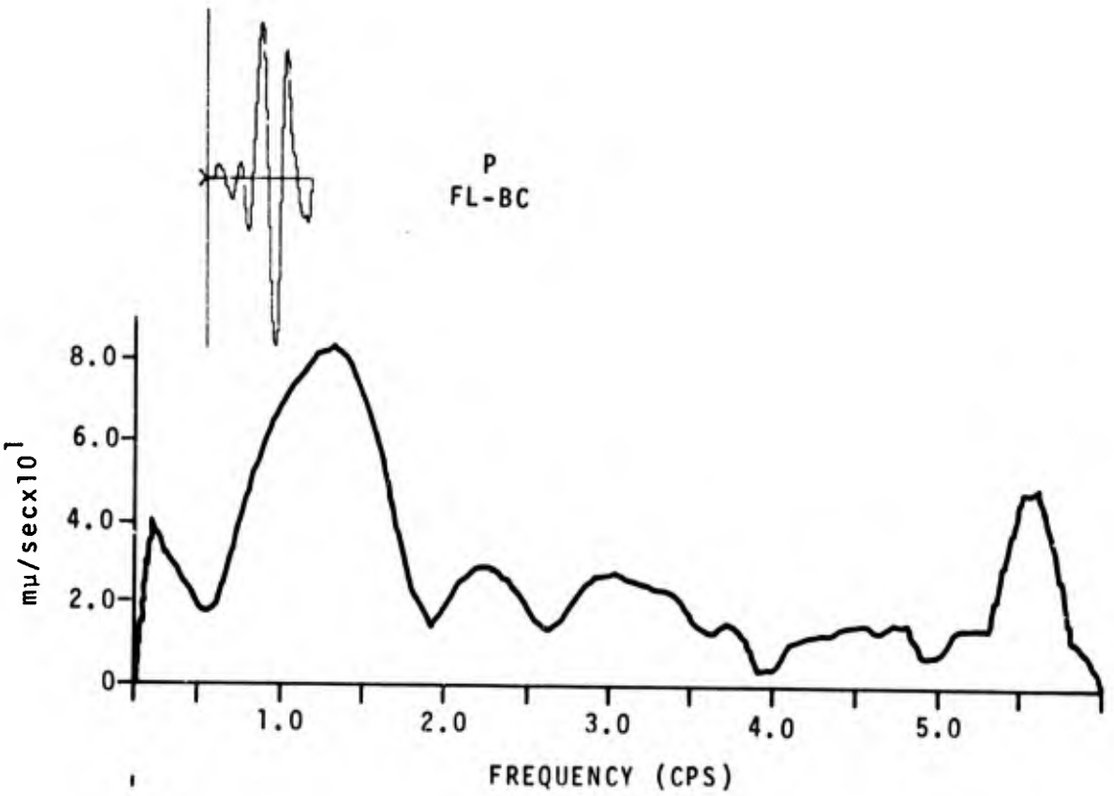
P
FL-BC
8.0
6.0
4.0
2.0
0
mμ/secx10^1
1.0
2.0
3.0
4.0
5.0
FREQUENCY (CPS)

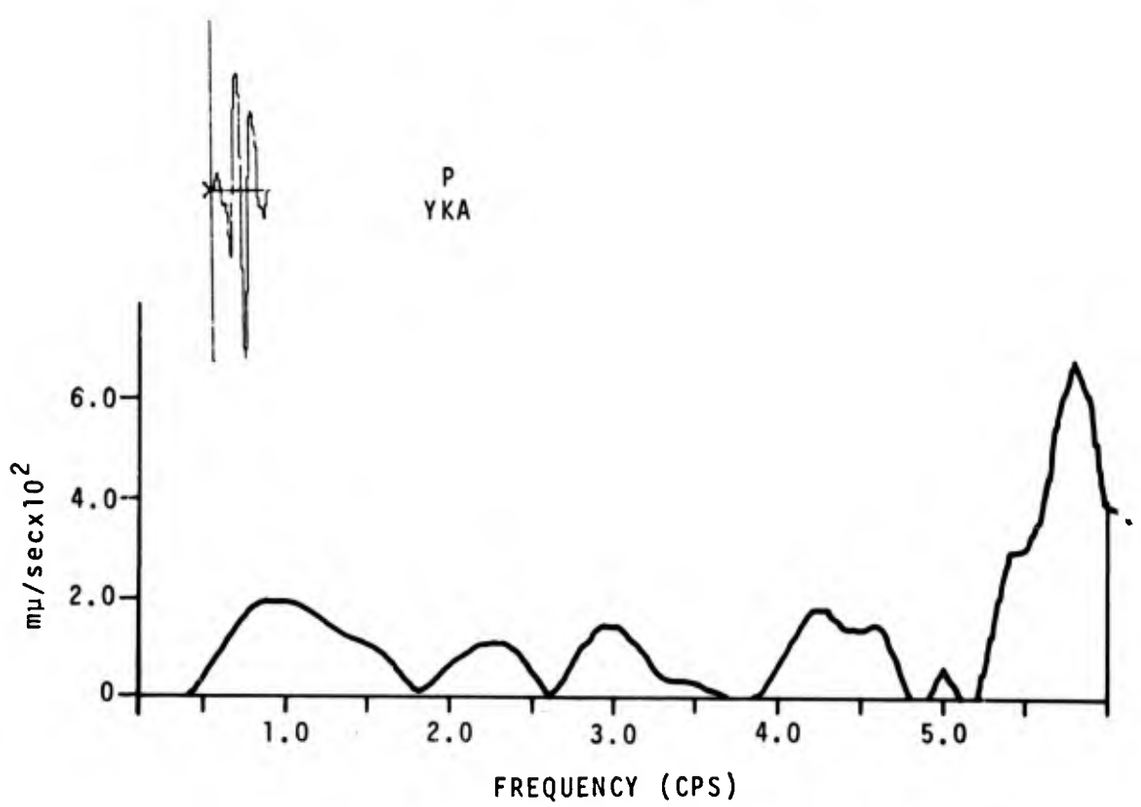
P
YKA
6.0
4.0
2.0
0
mμ/secx10^2
1.0
2.0
3.0
4.0
5.0
FREQUENCY (CPS)

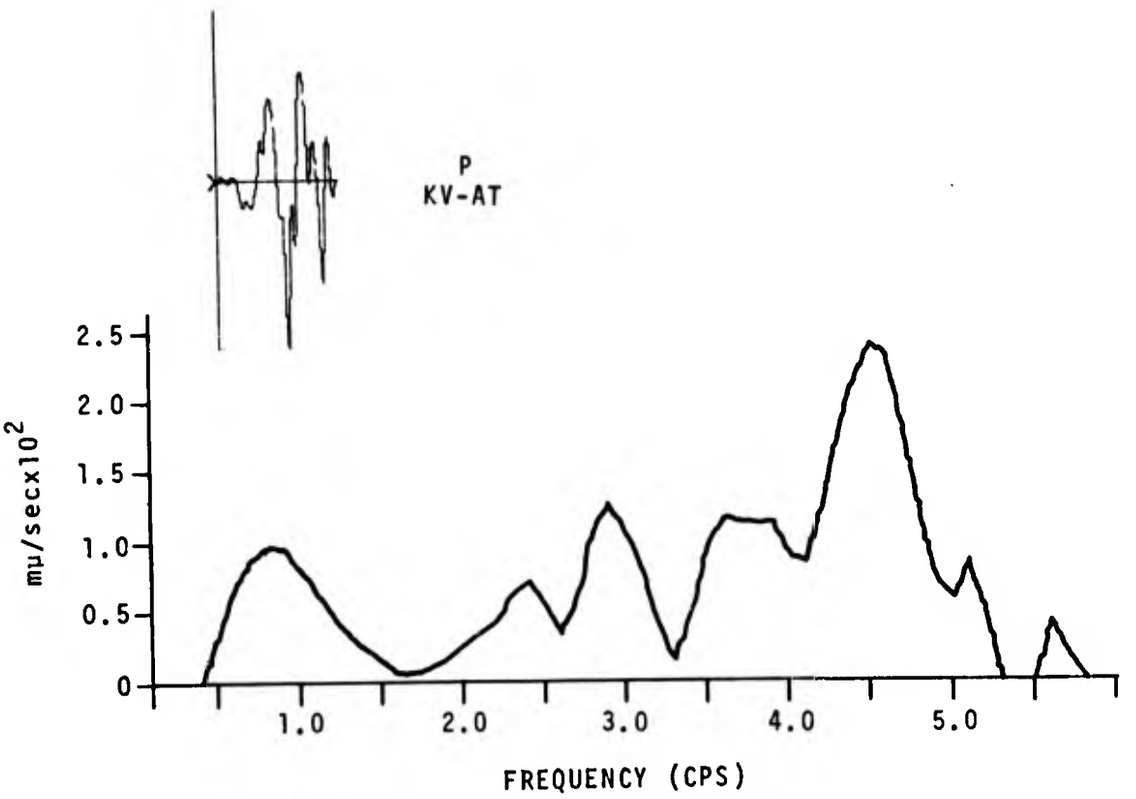
P
KV-AT
2.5
2.0
1.5
1.0
0.5
0
mμ/secx10²
1.0
2.0
3.0
4.0
5.0
FREQUENCY (CPS)

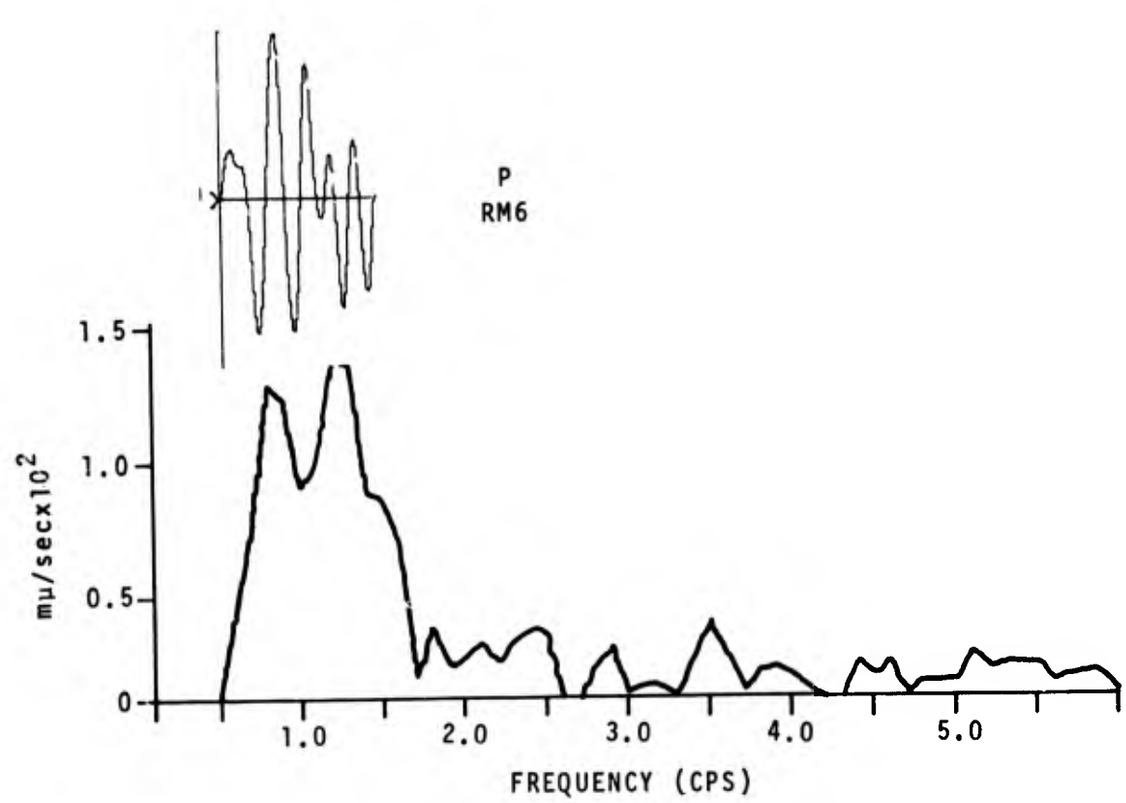
P
RM6
1.5
1.0
0.5
0
mμ/secx10²
1.0
2.0
3.0
4.0
5.0
FREQUENCY (CPS)

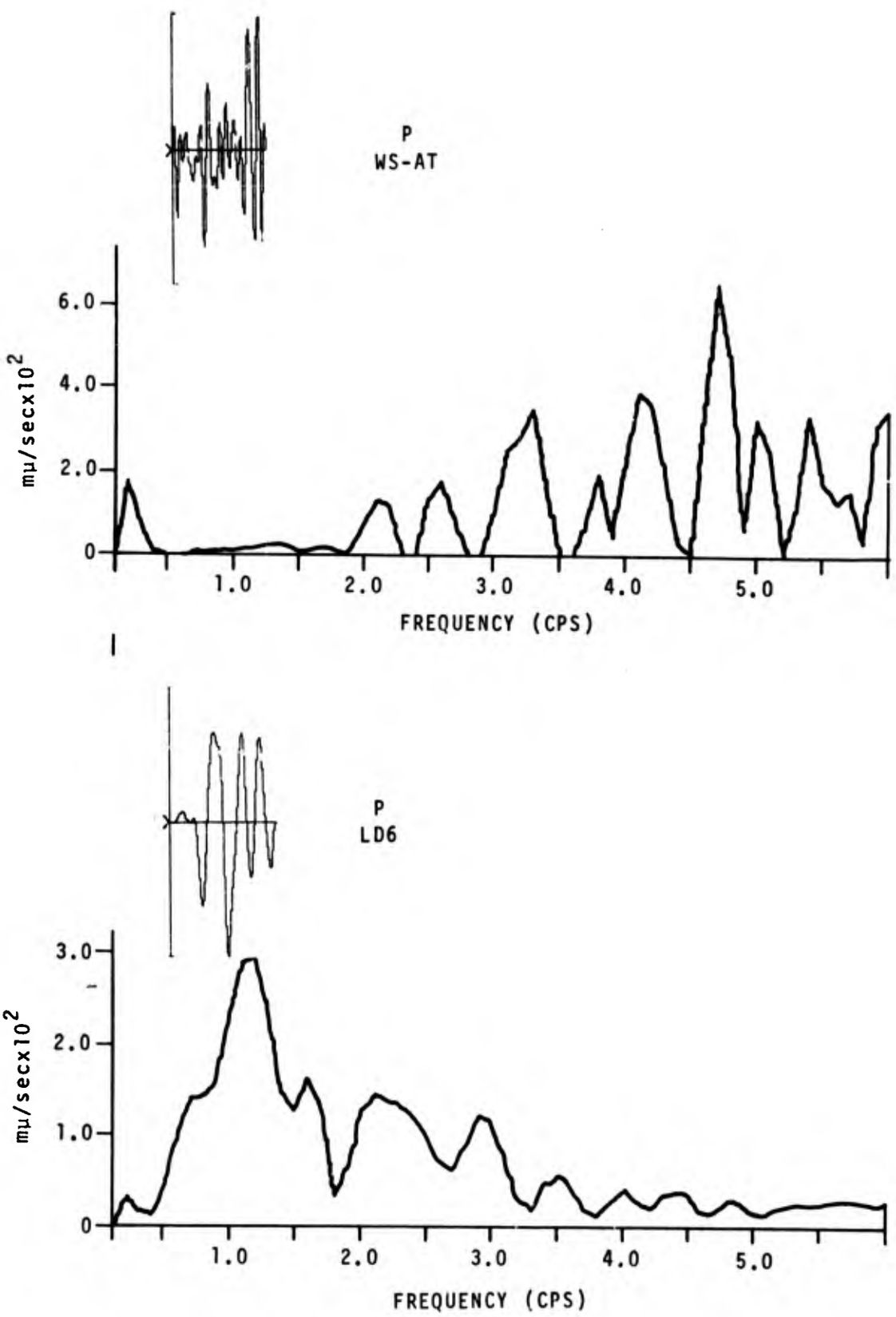
P
WS-AT
6.0
4.0
2.0
0
mμ/secx10²
1.0
2.0
3.0
4.0
5.0
FREQUENCY (CPS)
P
LD6
3.0
2.0
1.0
0
mμ/secx10²
1.0
2.0
3.0
4.0
5.0
FREQUENCY (CPS)

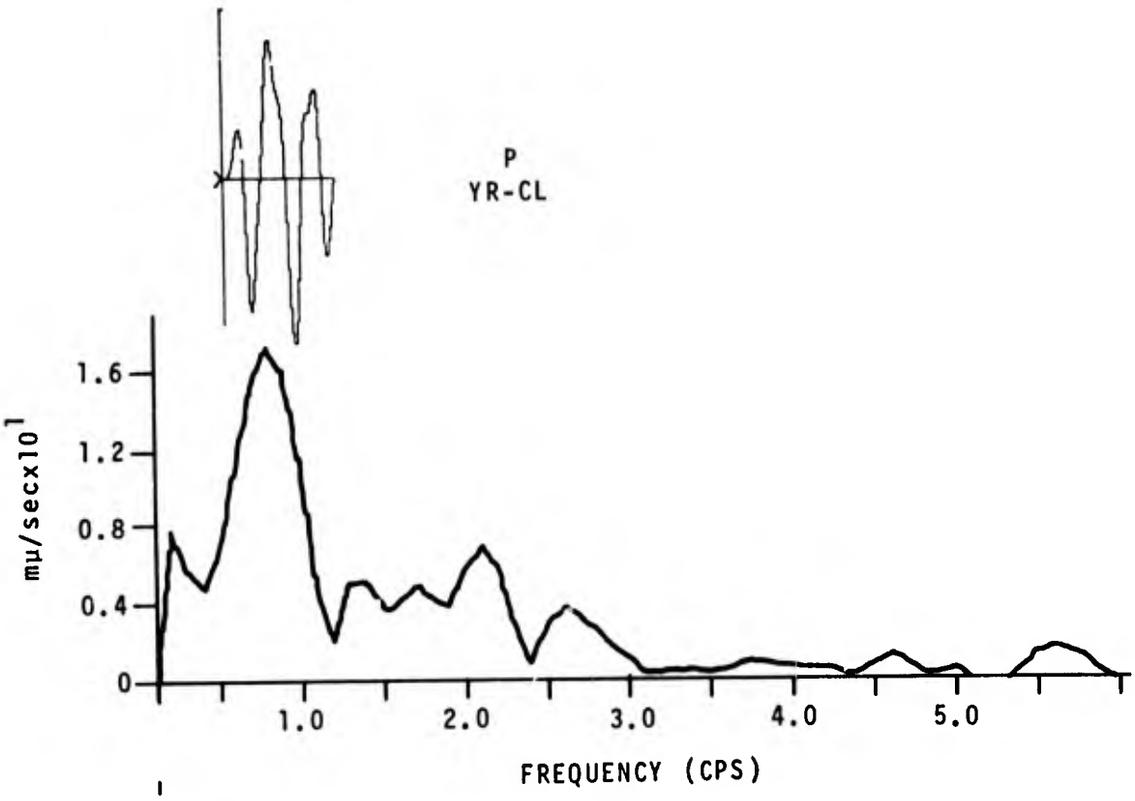
P
YR-CL
1.6
1.2
0.8
0.4
0
mμ/secx10^1
1.0
2.0
3.0
4.0
5.0
FREQUENCY (CPS)

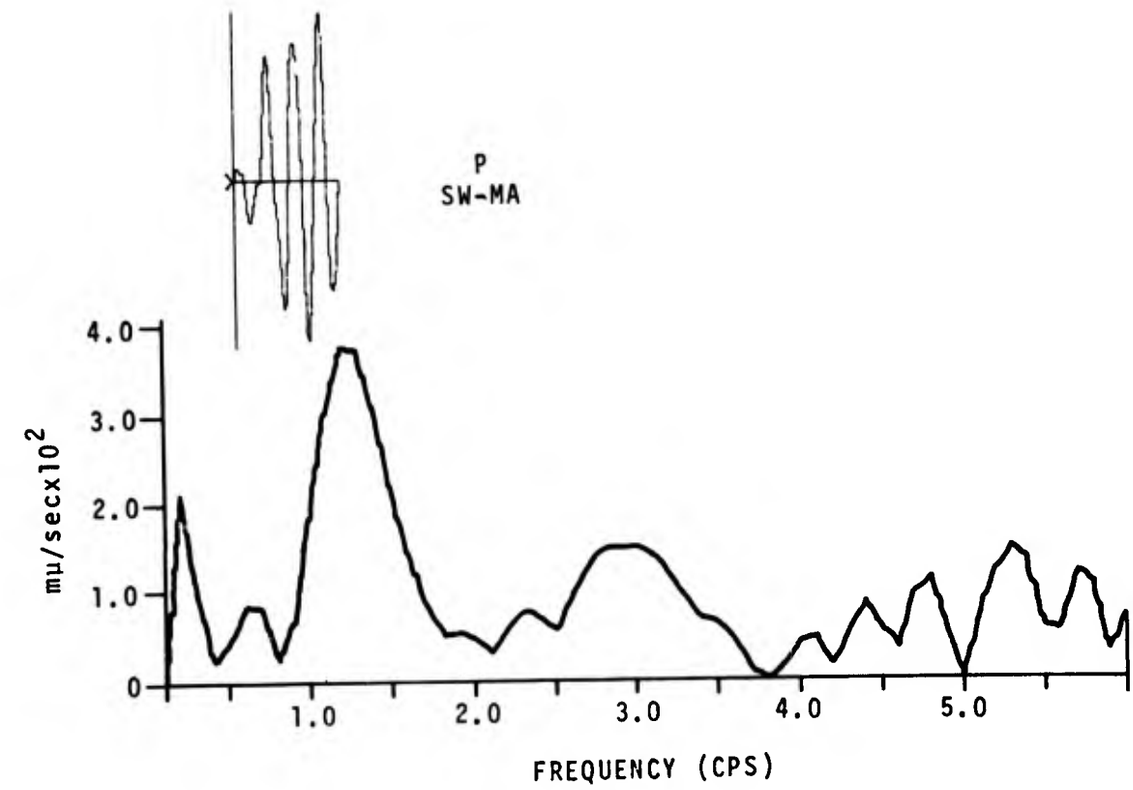
P
SW-MA
4.0
3.0
2.0
1.0
0
mμ/secx10^2
1.0
2.0
3.0
4.0
5.0
FREQUENCY (CPS)

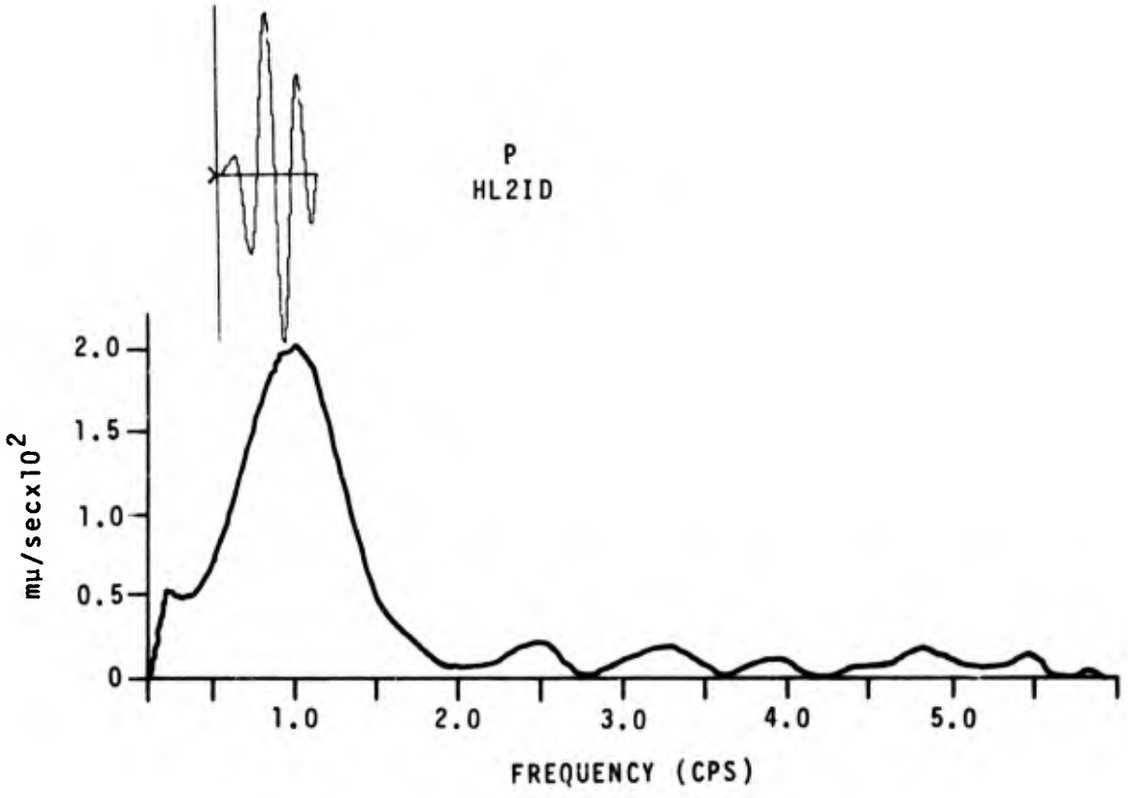
P
HL2ID
2.0
1.5
1.0
0.5
0
mμ/secx10²
1.0
2.0
3.0
4.0
5.0
FREQUENCY (CPS)

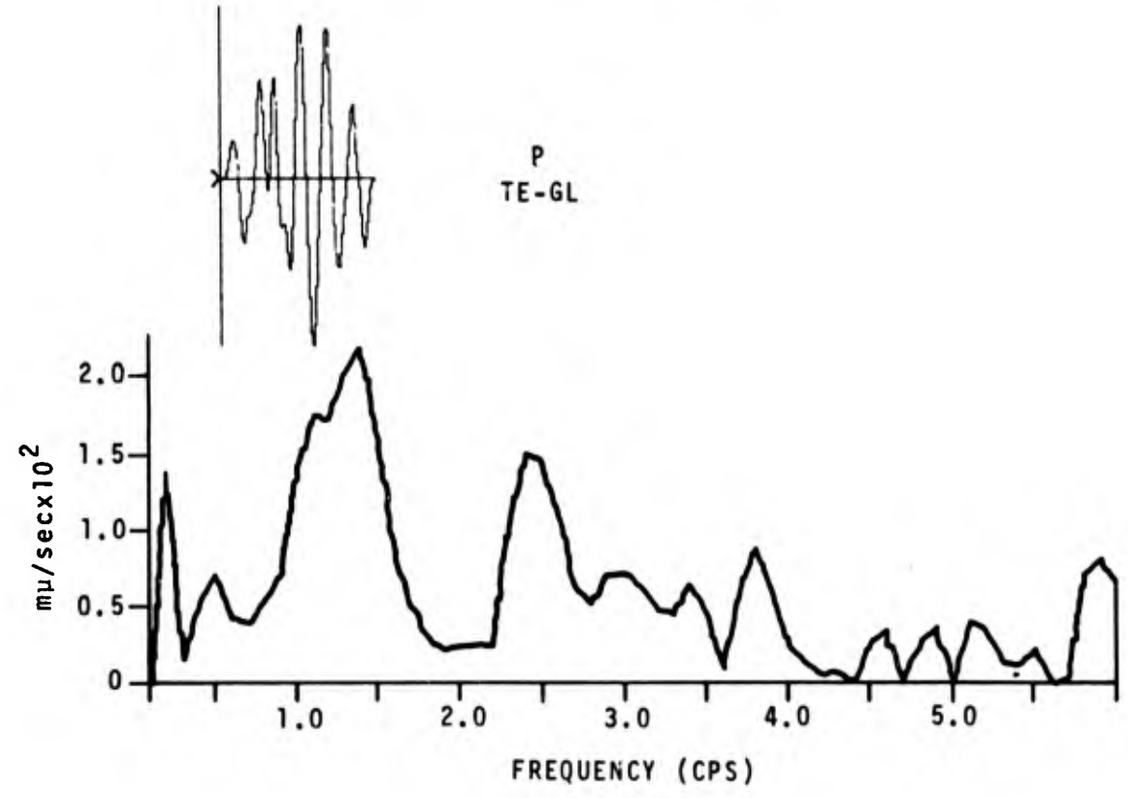
P
TE-GL
2.0
1.5
1.0
0.5
0
mμ/secx10²
1.0
2.0
3.0
4.0
5.0
FREQUENCY (CPS)

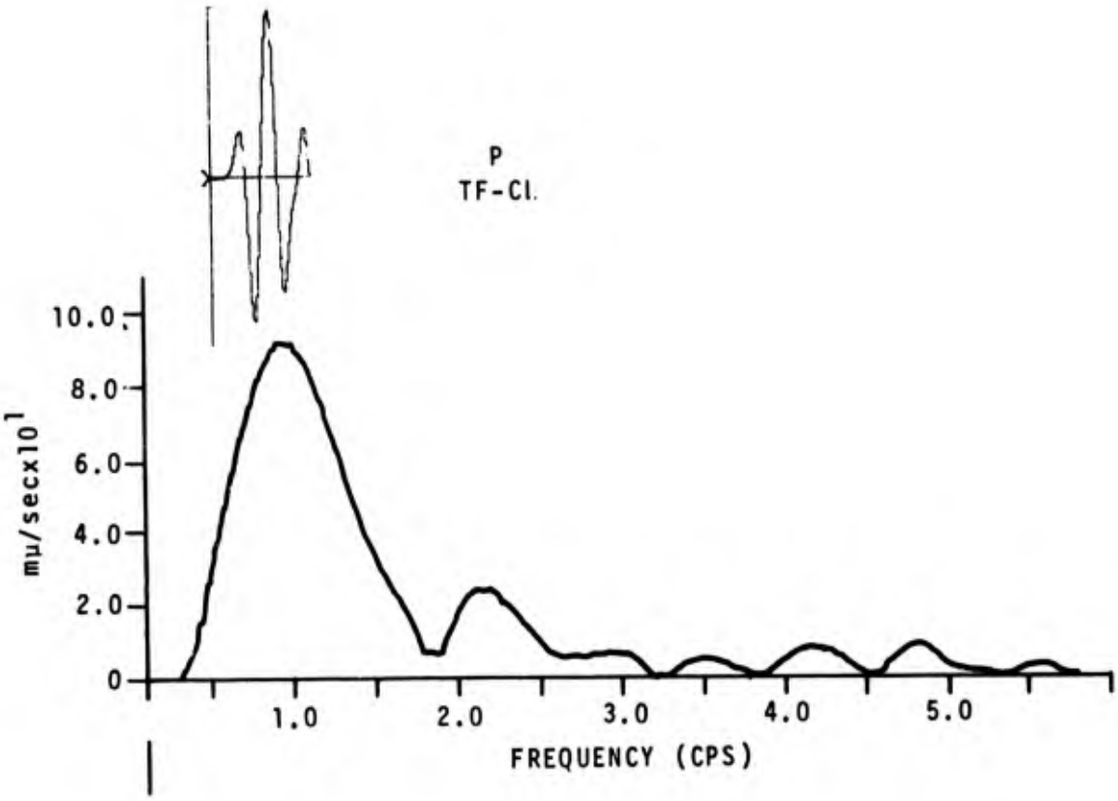
P
TF-CI.
10.0
8.0
6.0
4.0
2.0
0
mμ/secx10¹
1.0
2.0
3.0
4.0
5.0
FREQUENCY (CPS)

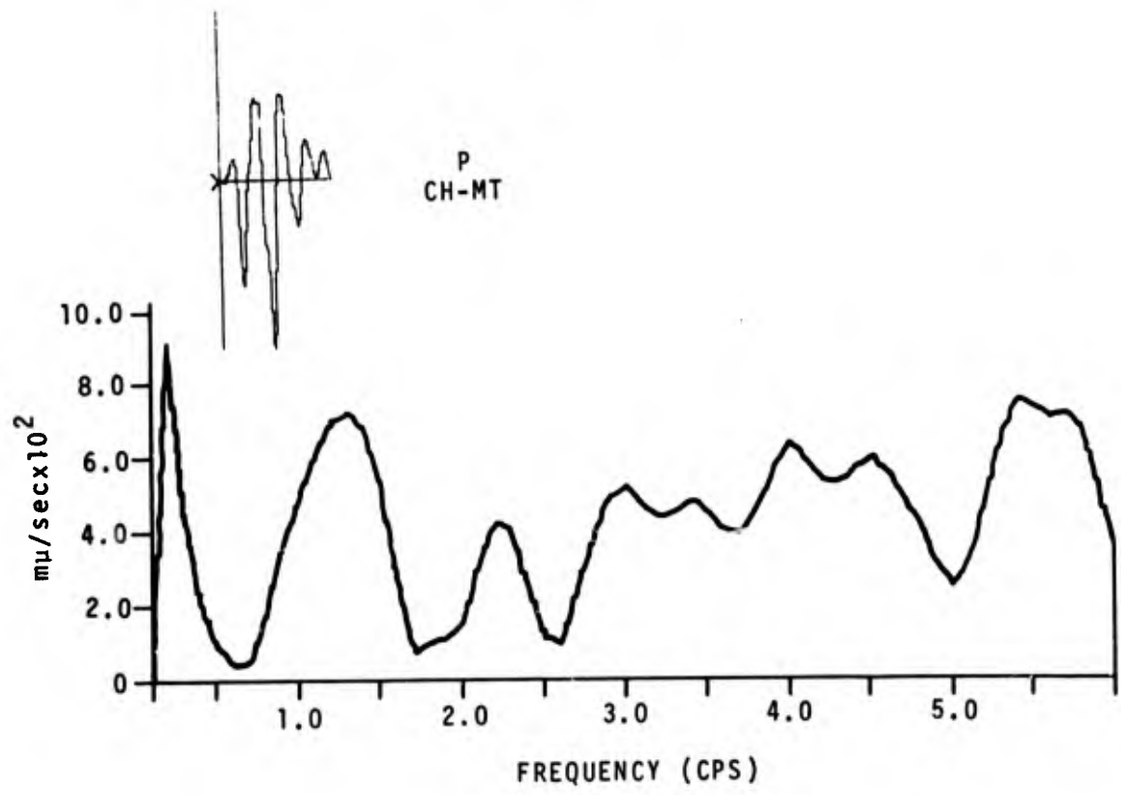
P
CH-MT
10.0
8.0
6.0
4.0
2.0
0
mμ/secx10²
1.0
2.0
3.0
4.0
5.0
FREQUENCY (CPS)

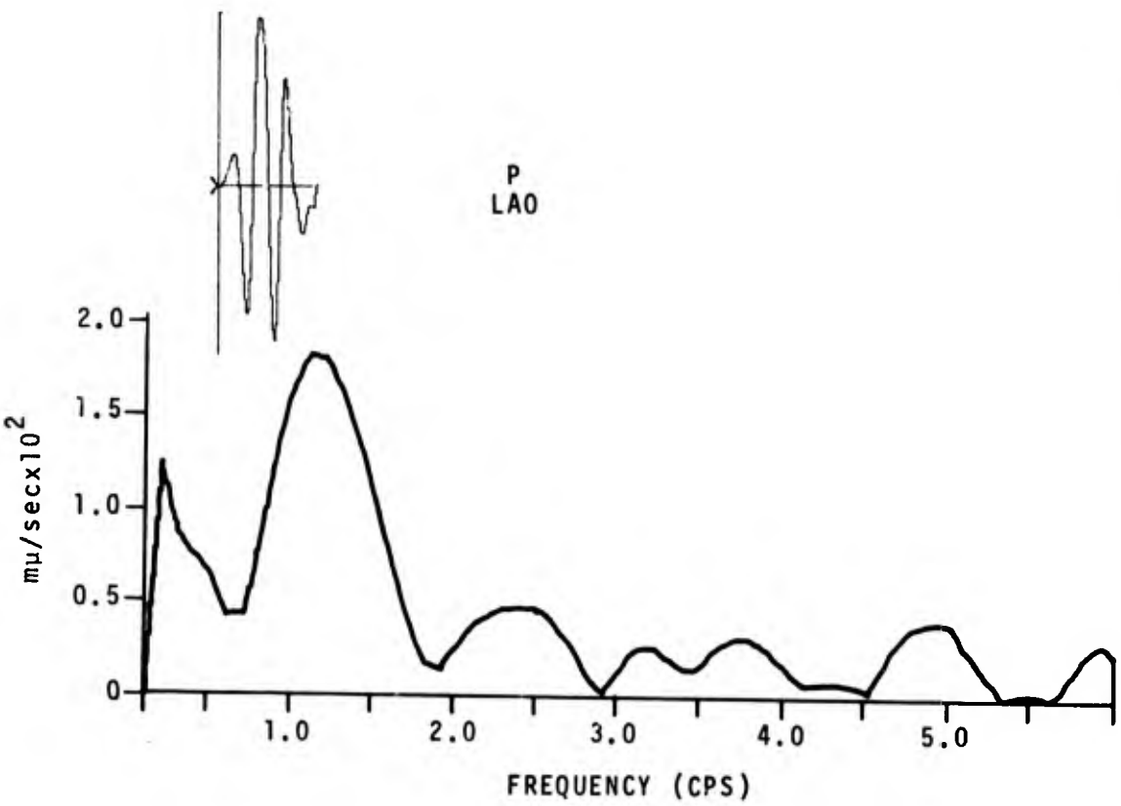
P
LAO
2.0
1.5
1.0
0.5
0
mμ/secx10²
1.0
2.0
3.0
4.0
5.0
FREQUENCY (CPS)

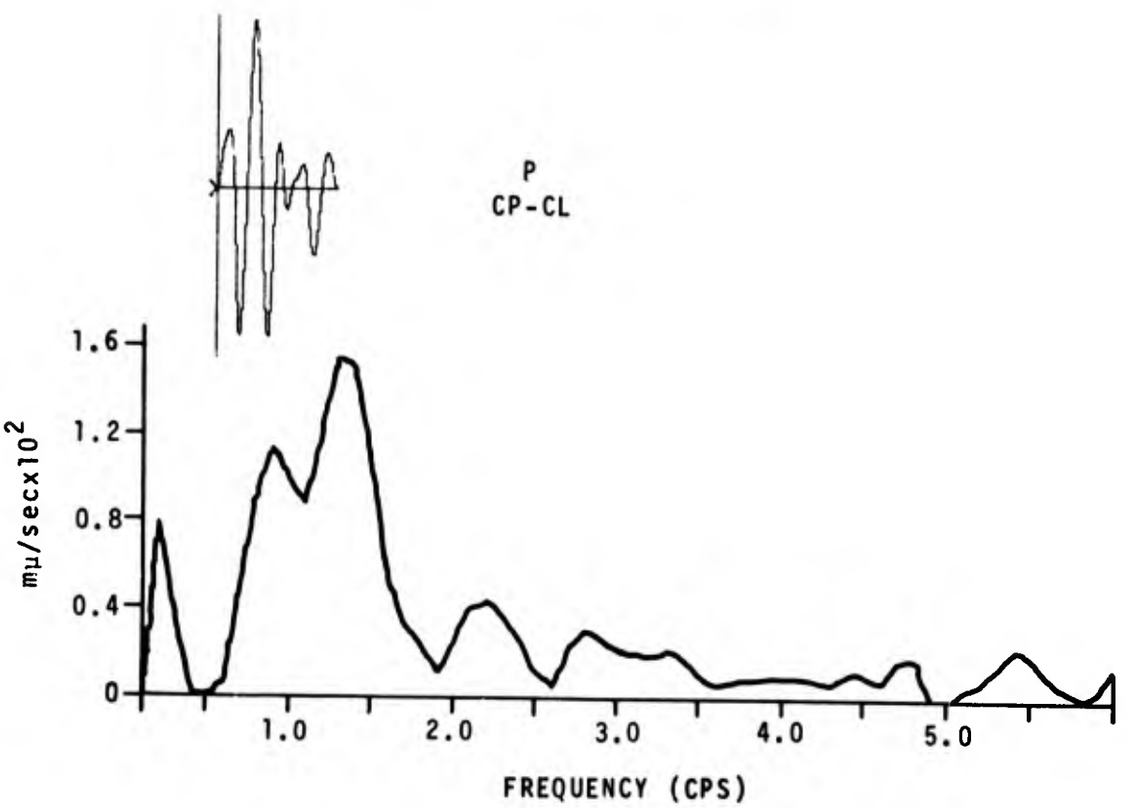
P
CP-CL
1.6
1.2
0.8
0.4
0
mμ/secx10²
1.0
2.0
3.0
4.0
5.0
FREQUENCY (CPS)

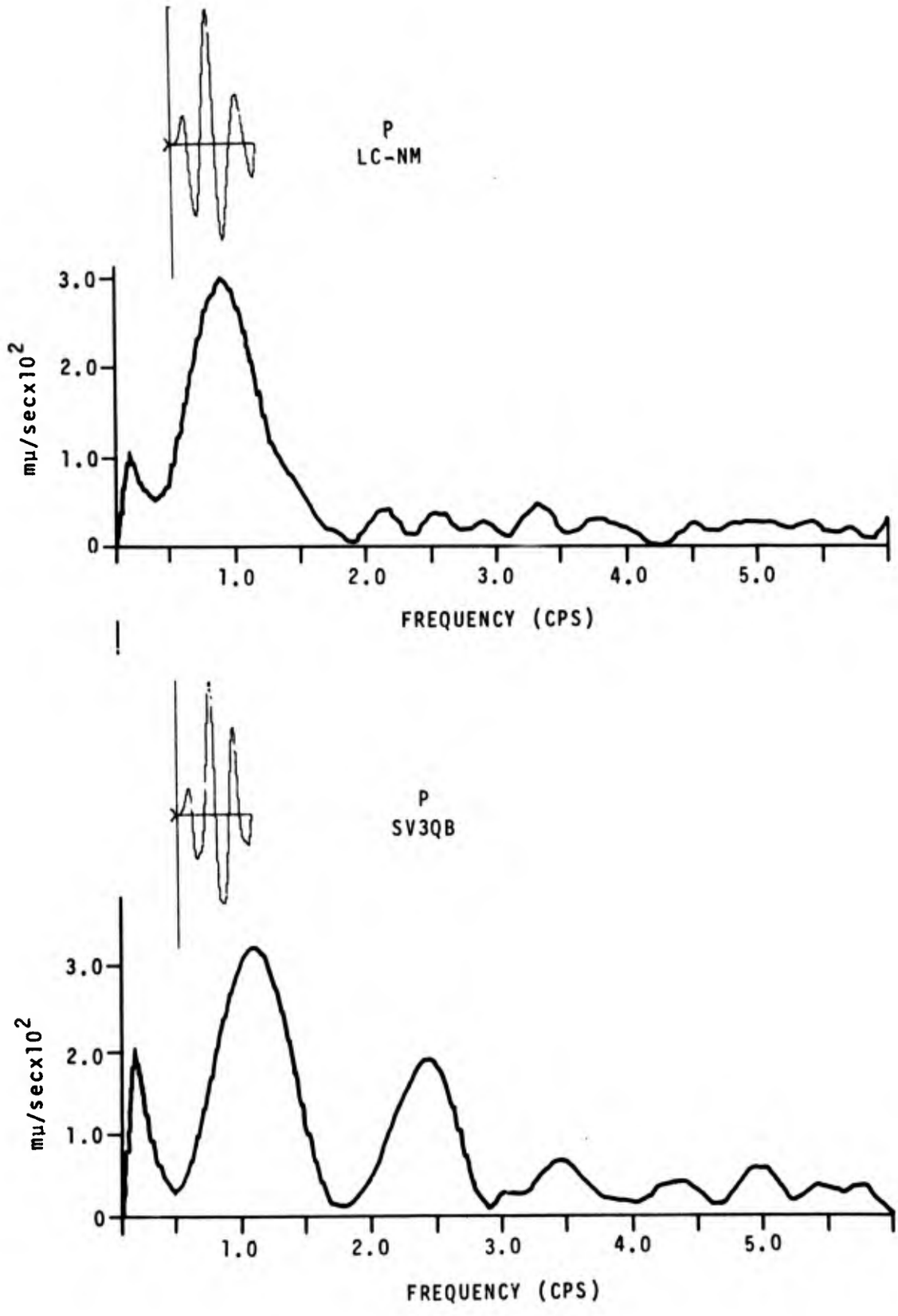
P
LC-NM
3.0
2.0
1.0
0
mμ/secx10²
1.0
2.0
3.0
4.0
5.0
FREQUENCY (CPS)
P
SV3QB
3.0
2.0
1.0
0
mμ/secx10²
1.0
2.0
3.0
4.0
5.0
FREQUENCY (CPS)

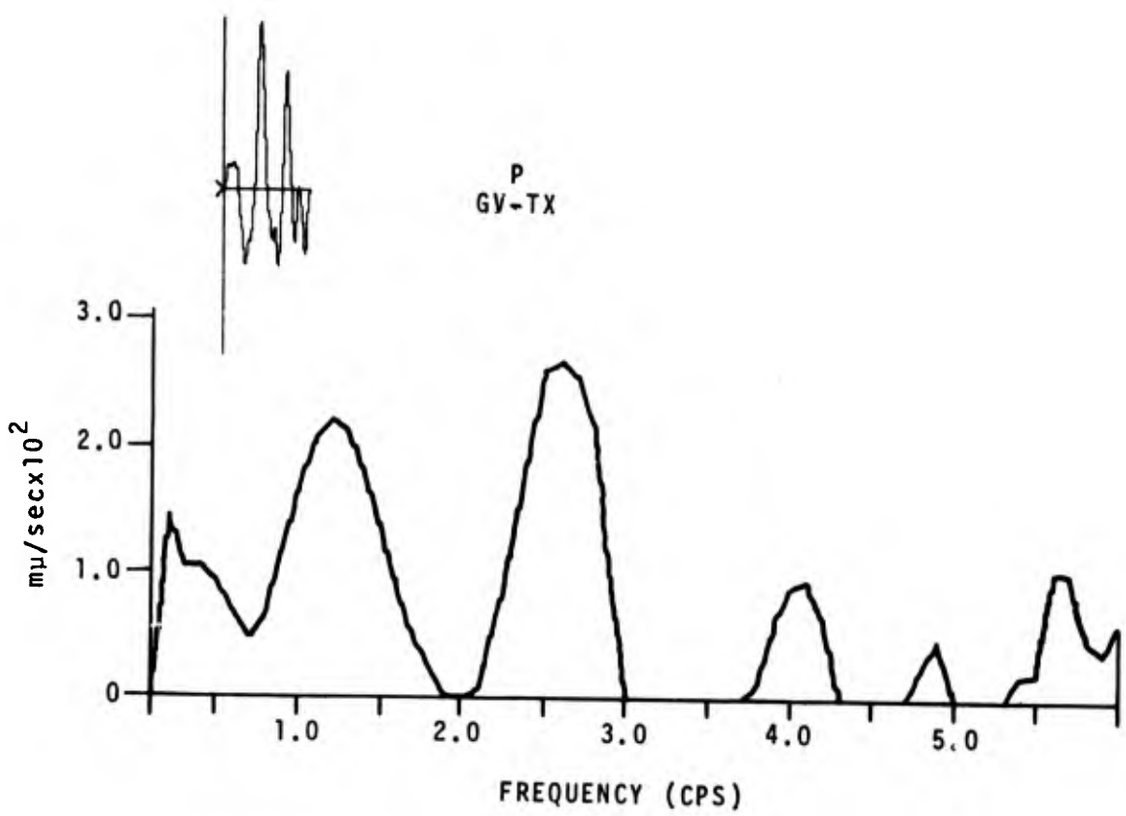
P
GV-TX
3.0
2.0
1.0
0
mμ/secx10²
1.0
2.0
3.0
4.0
5.0
FREQUENCY (CPS)

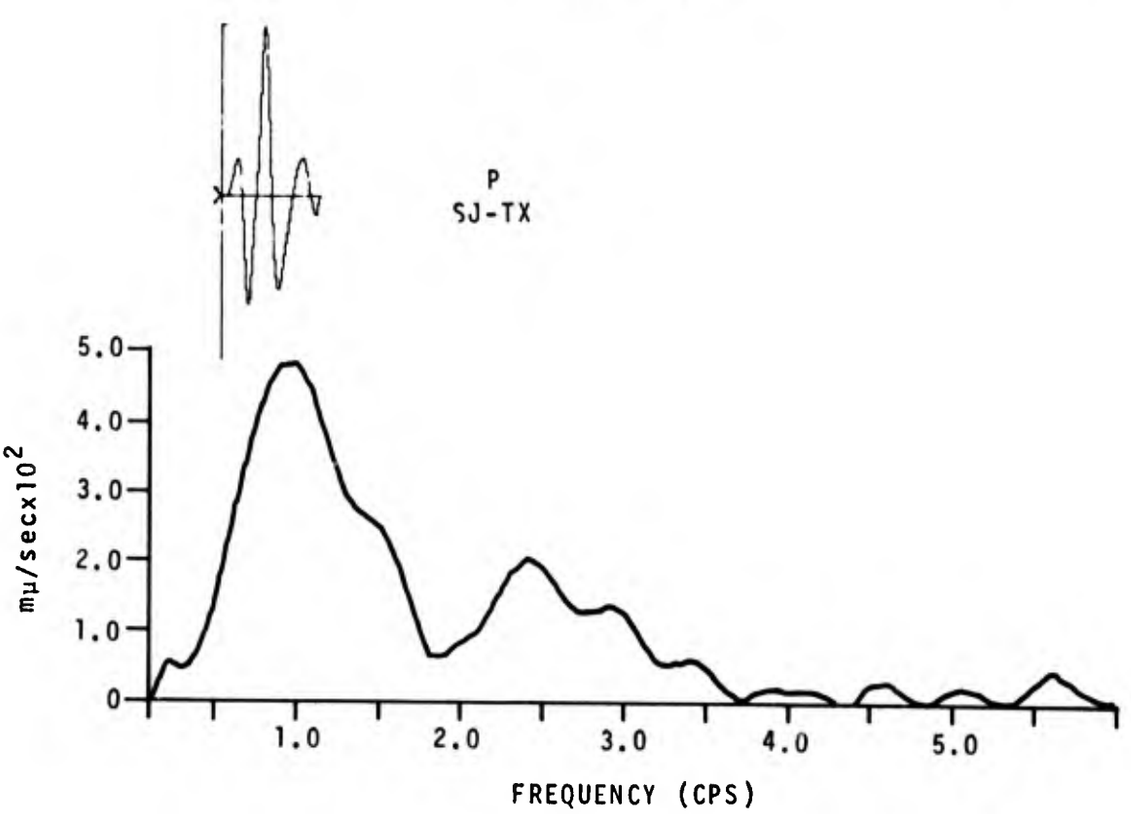
P
SJ-TX
5.0
4.0
3.0
2.0
1.0
0
mμ/secx10²
1.0
2.0
3.0
4.0
5.0
FREQUENCY (CPS)

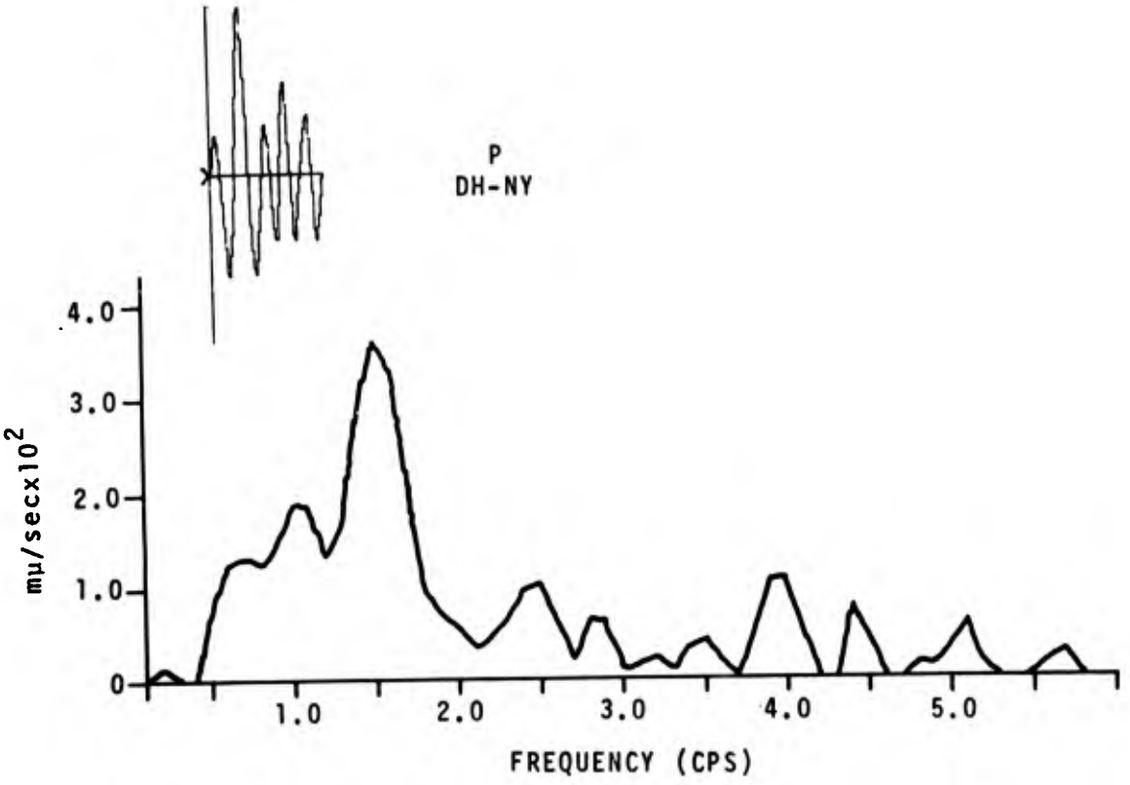
P
DH-NY
4.0
3.0
2.0
1.0
0
mμ/secx10²
1.0
2.0
3.0
4.0
5.0
FREQUENCY (CPS)

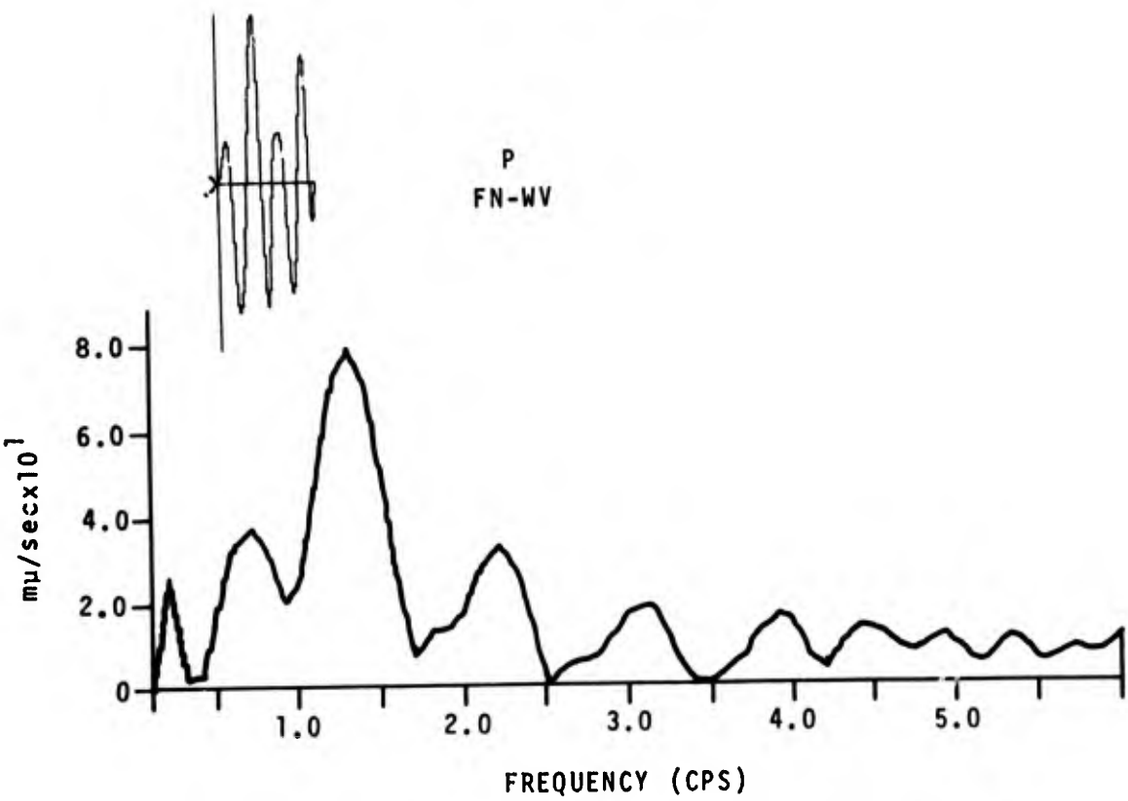
P
FN-WV
8.0
6.0
4.0
2.0
0
mμ/secx10¹
1.0
2.0
3.0
4.0
5.0
FREQUENCY (CPS)

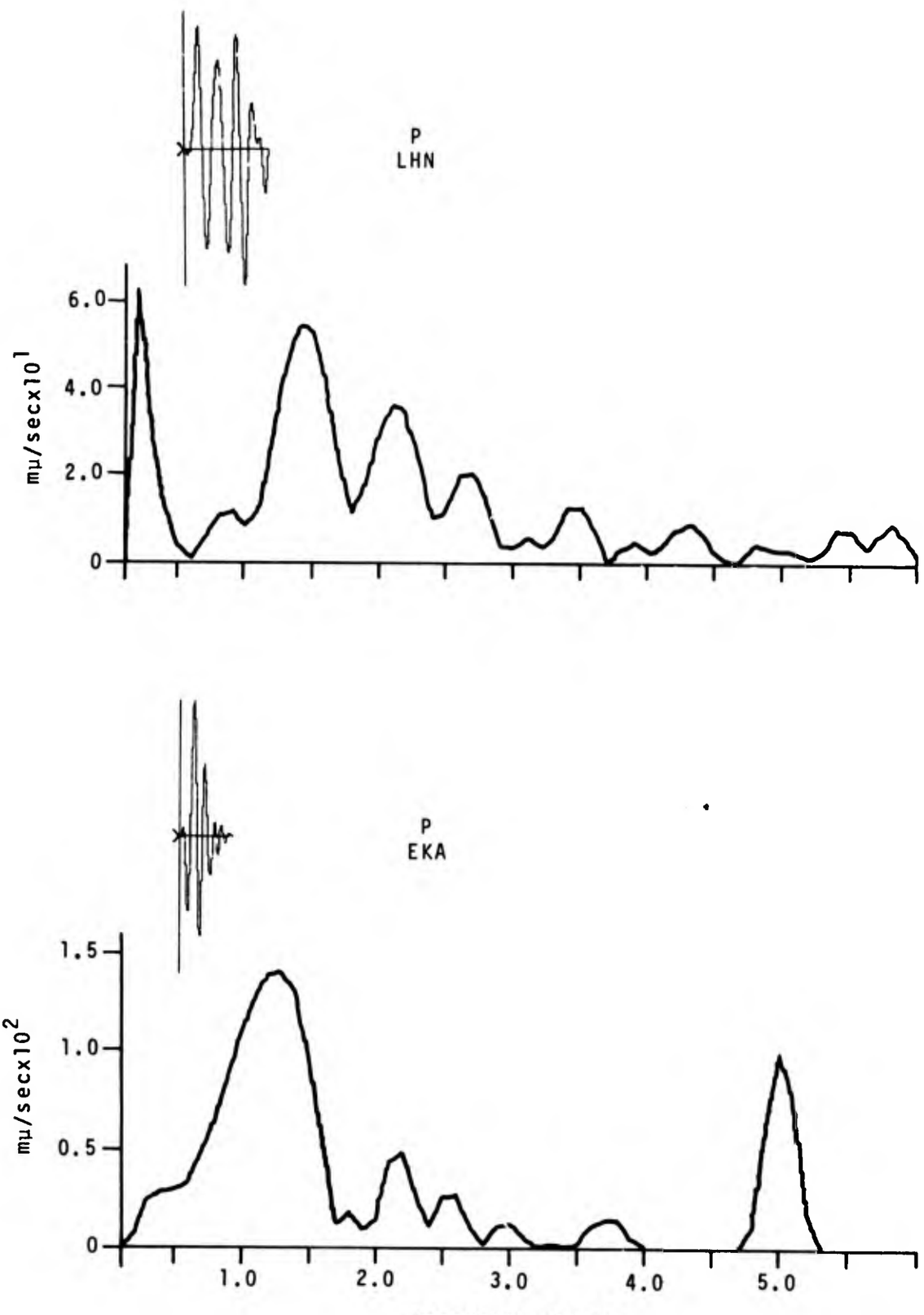
P
LHN
6.0
4.0
2.0
0
mμ/secx10^1
P
EKA
1.5
1.0
0.5
0
mμ/secx10^2
1.0
2.0
3.0
4.0
5.0
FREQUENCY (CPS)

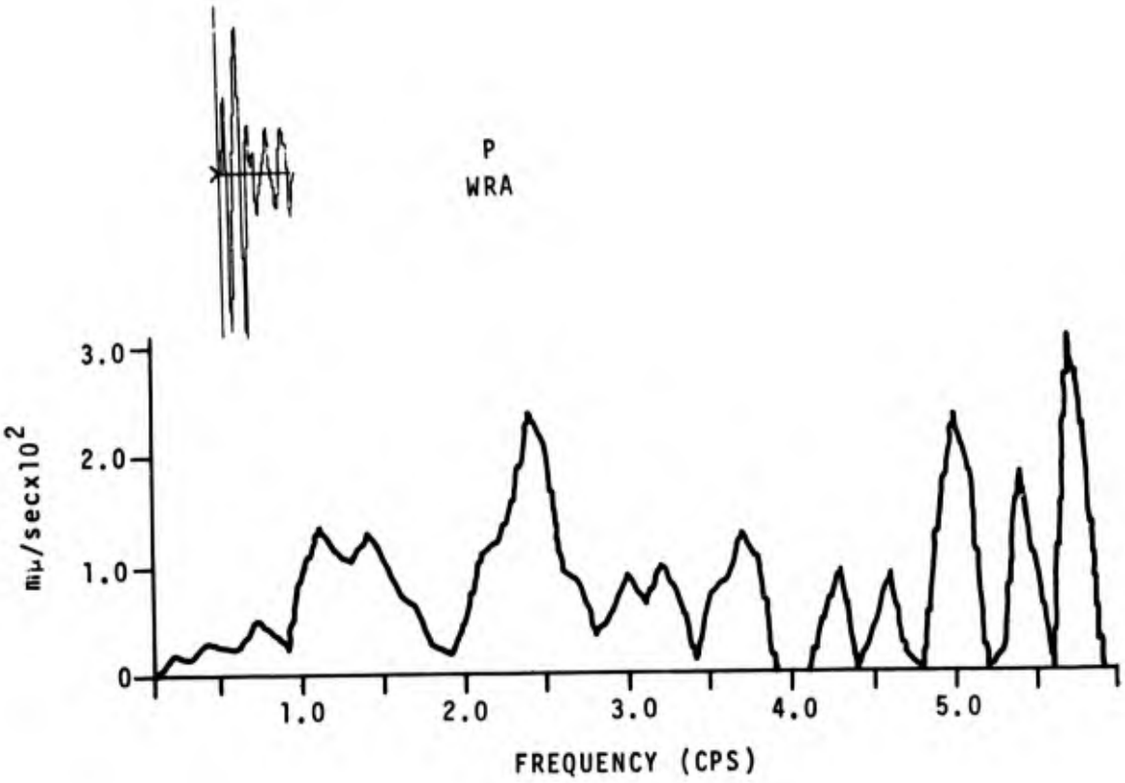
P
WRA
3.0
2.0
1.0
0
mμ/secx10²
1.0
2.0
3.0
4.0
5.0
FREQUENCY (CPS)

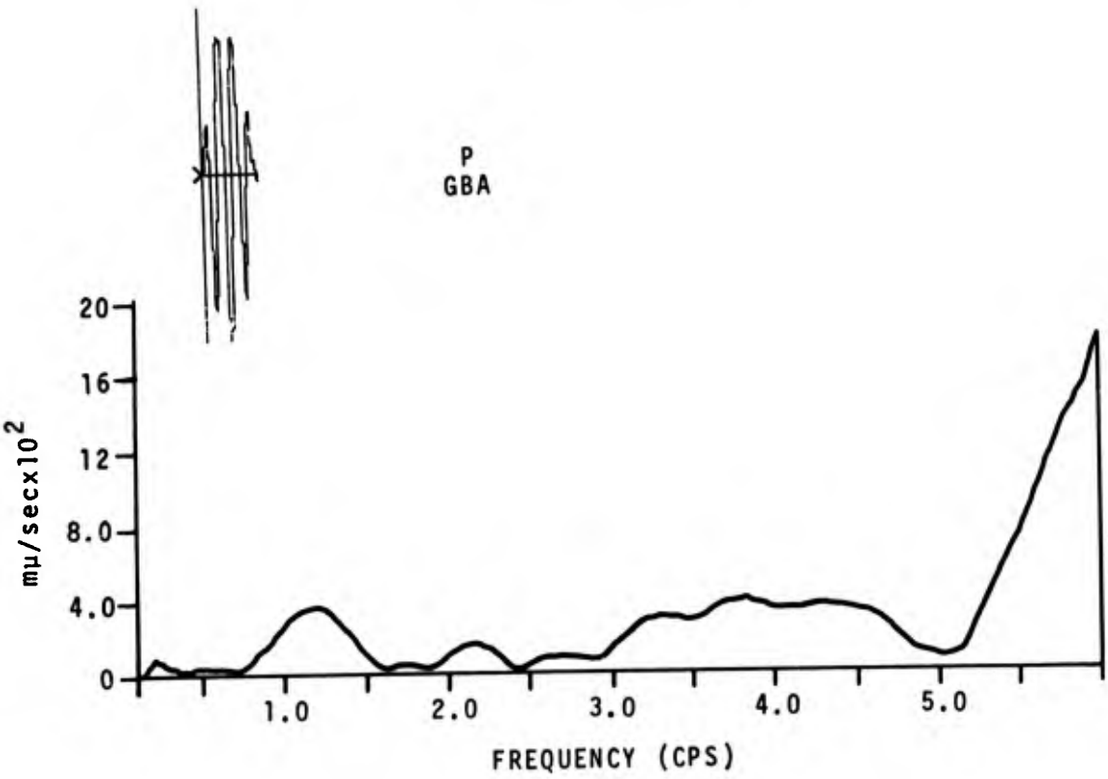
P
GBA
20
16
12
8.0
4.0
0
mμ/secx10²
1.0
2.0
3.0
4.0
5.0
FREQUENCY (CPS)

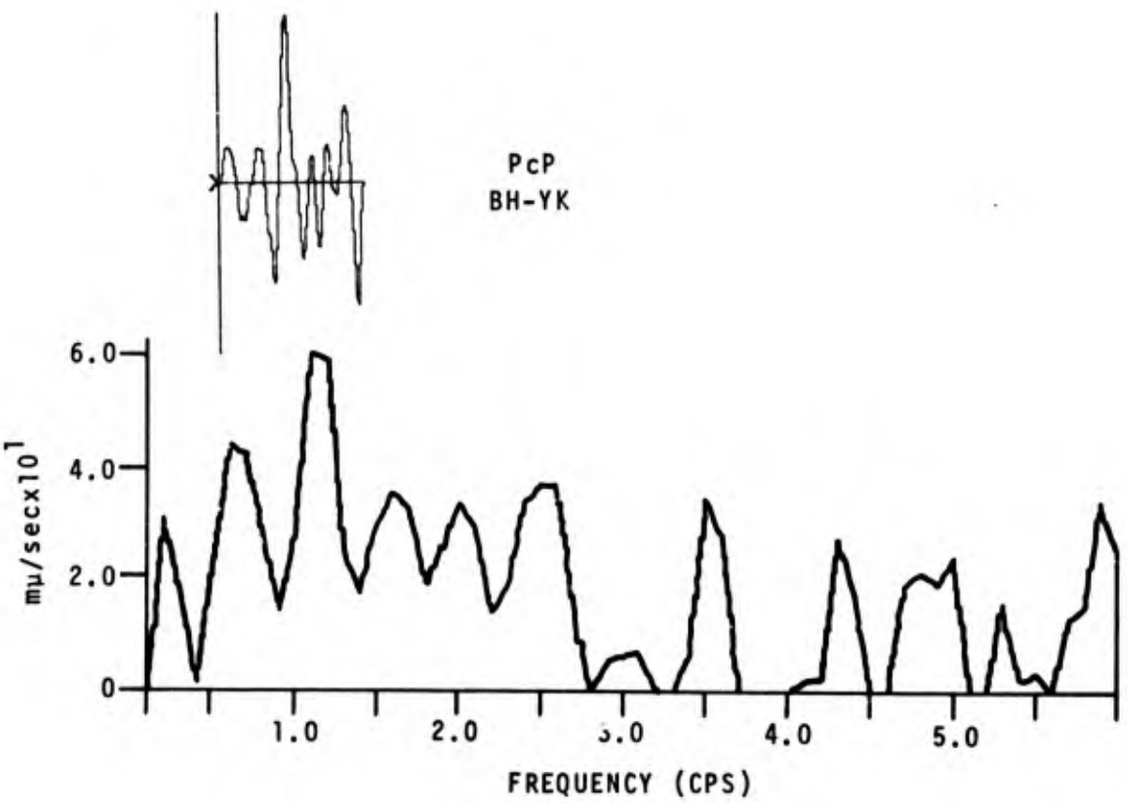
PcP
BH-YK
6.0
4.0
2.0
0
mμ/secx10^1
1.0
2.0
3.0
4.0
5.0
FREQUENCY (CPS)

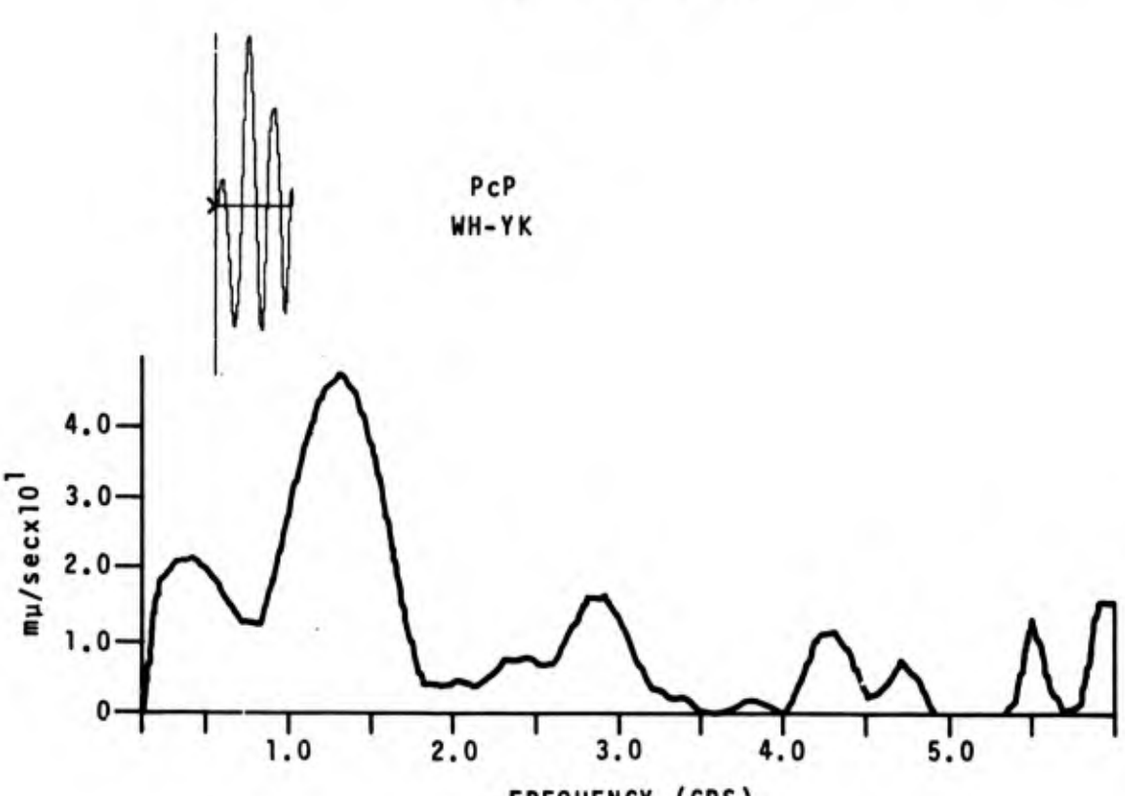
PcP
WH-YK
4.0
3.0
2.0
1.0
0
mμ/secx10^1
1.0
2.0
3.0
4.0
5.0
FREQUENCY (CPS)

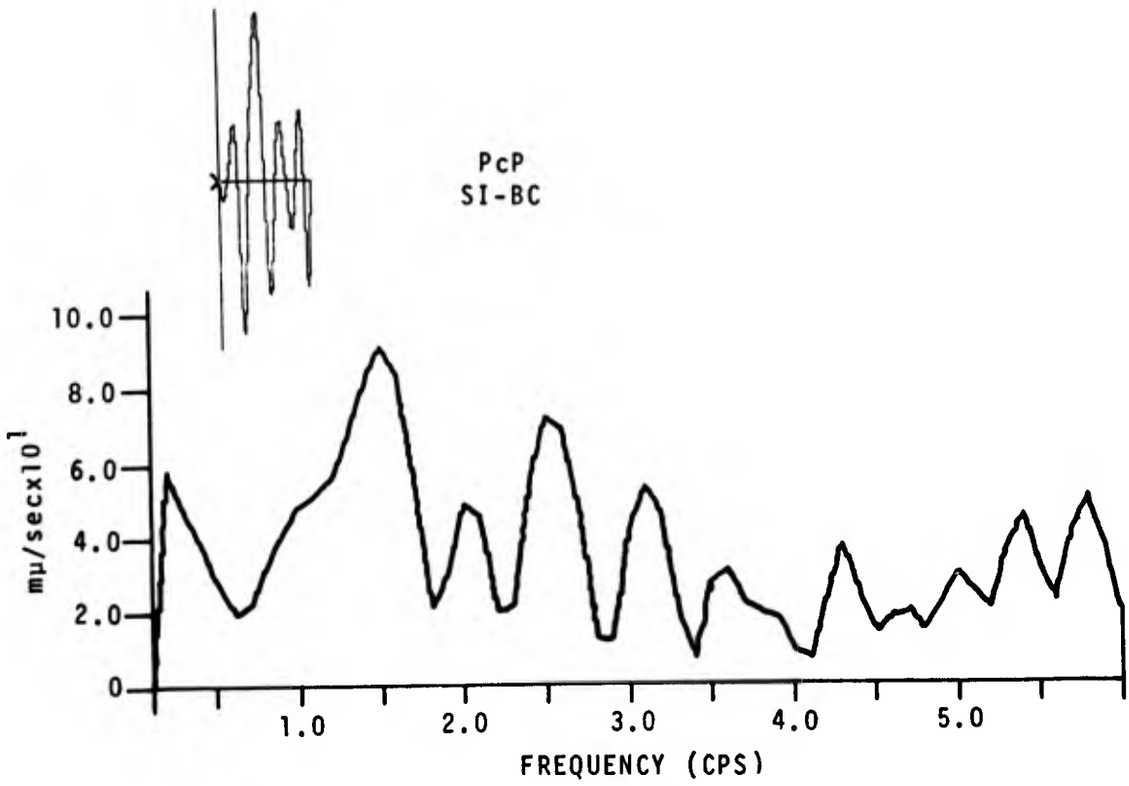
PcP
SI-BC
10.0
8.0
6.0
4.0
2.0
0
mμ/secx10¹
1.0
2.0
3.0
4.0
5.0
FREQUENCY (CPS)

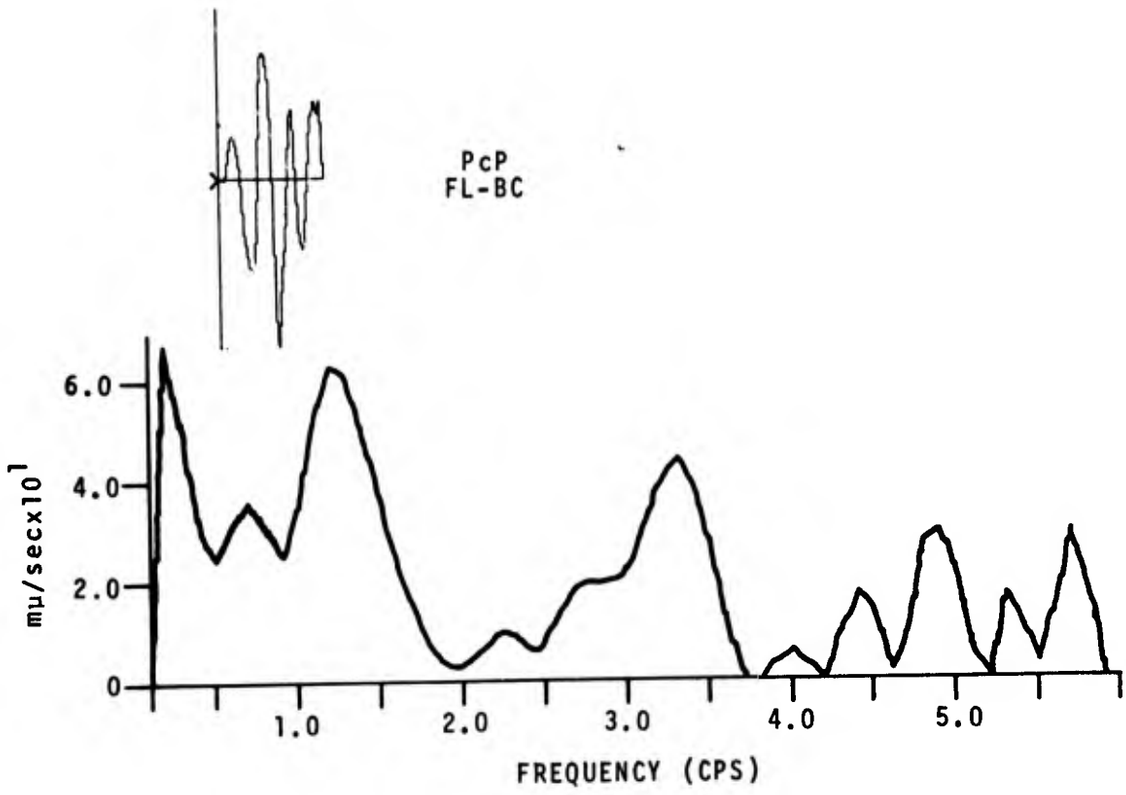
PcP
FL-BC
6.0
4.0
2.0
0
mμ/secx10¹
1.0
2.0
3.0
4.0
5.0
FREQUENCY (CPS)

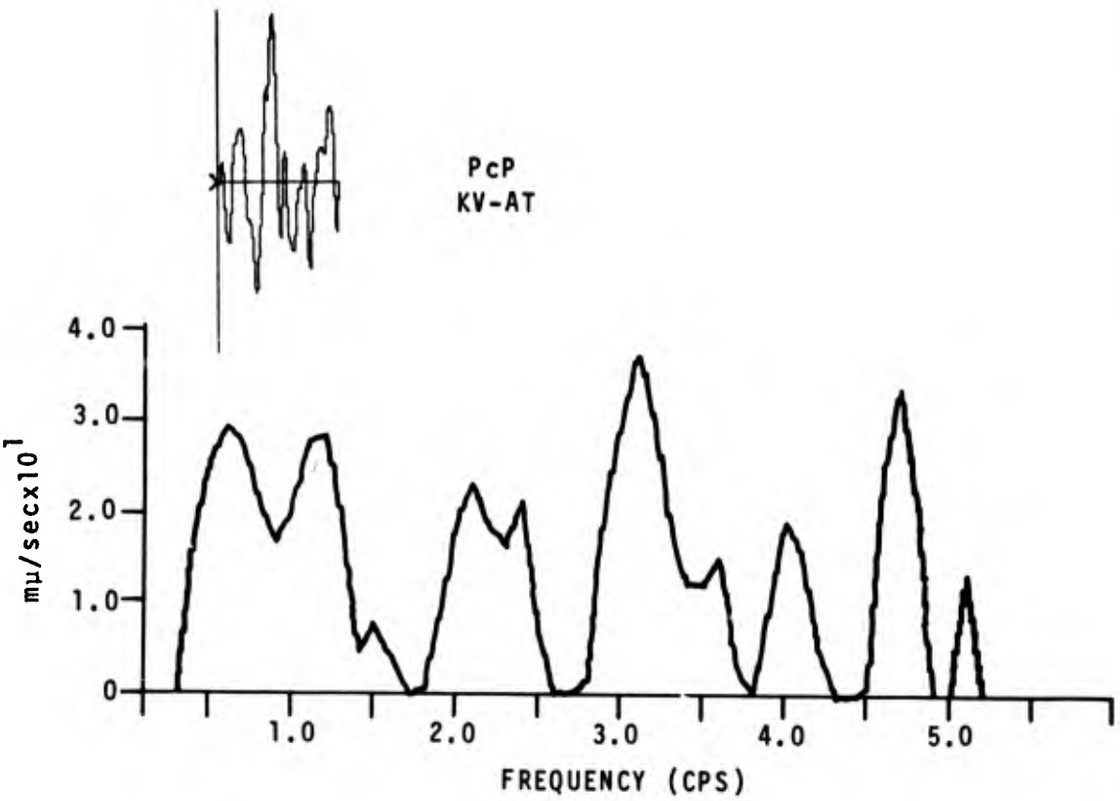
PcP
KV-AT
4.0
3.0
2.0
1.0
0
mμ/secx10^1
1.0
2.0
3.0
4.0
5.0
FREQUENCY (CPS)

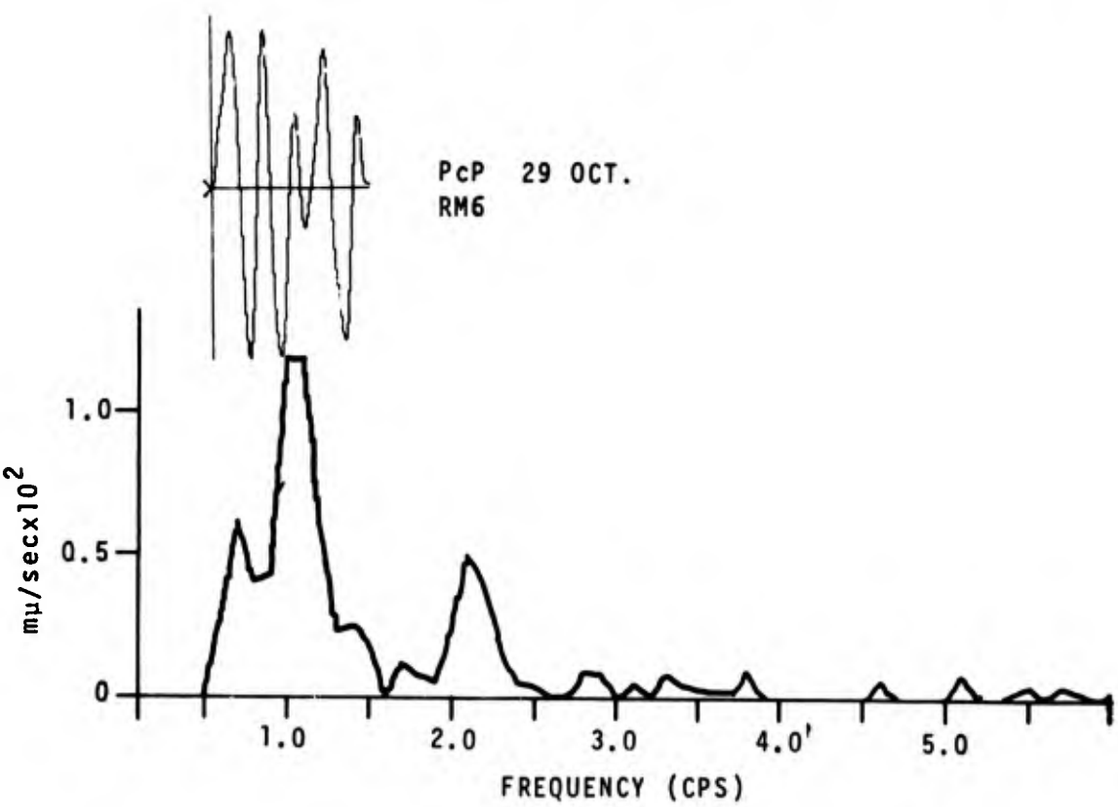
PcP 29 OCT.
RM6
1.0
0.5
0
mμ/secx10^2
1.0
2.0
3.0
4.0'
5.0
FREQUENCY (CPS)

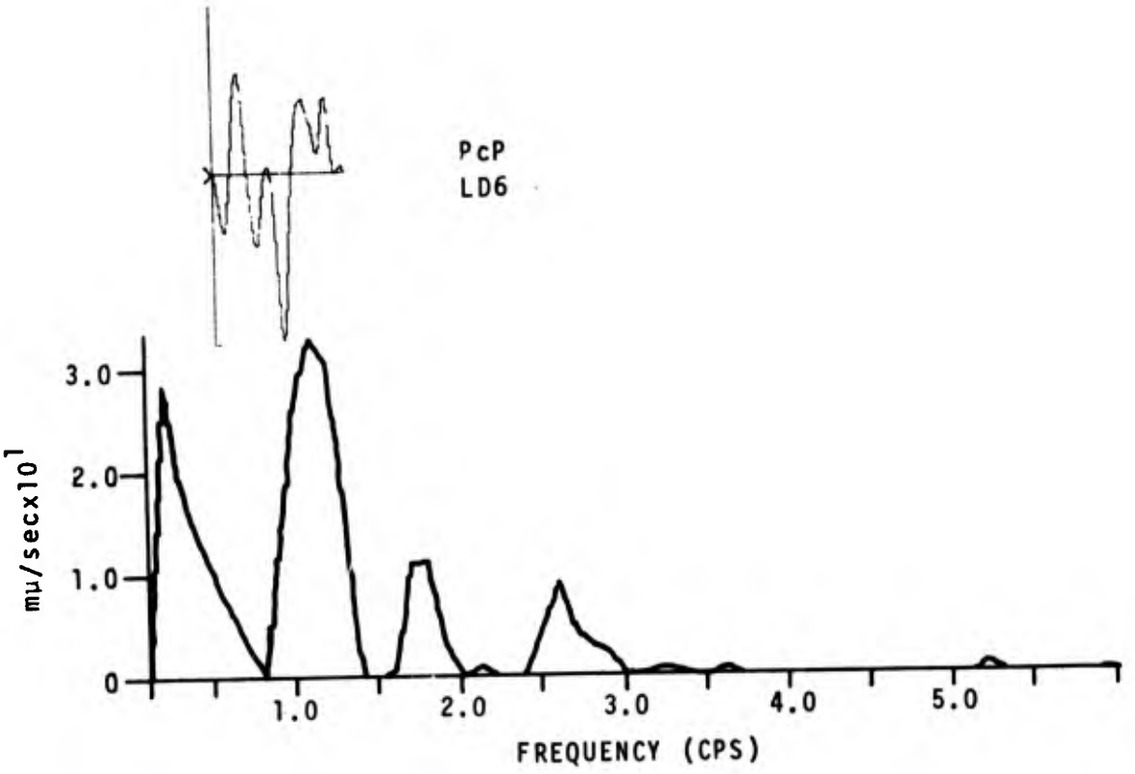
PcP
LD6
3.0
2.0
1.0
0
mμ/secx10¹
1.0
2.0
3.0
4.0
5.0
FREQUENCY (CPS)

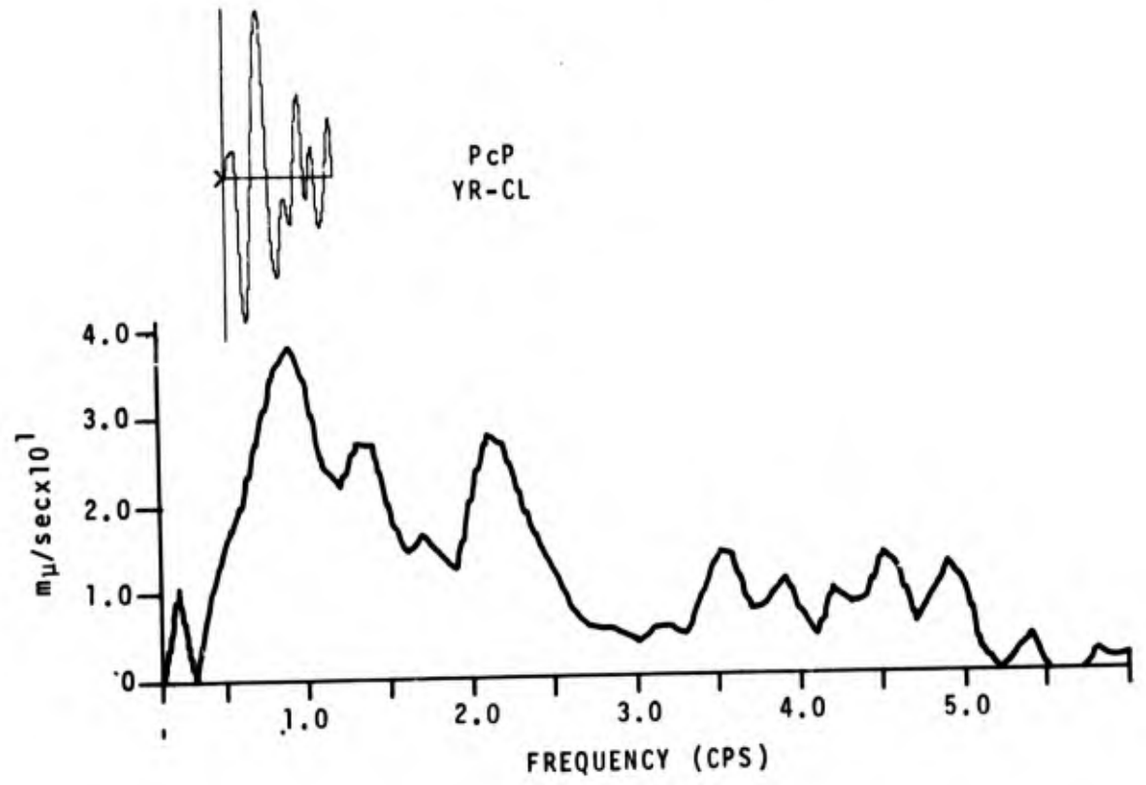
PcP
YR-CL
4.0
3.0
2.0
1.0
0
mμ/secx10¹
1.0
2.0
3.0
4.0
5.0
FREQUENCY (CPS)

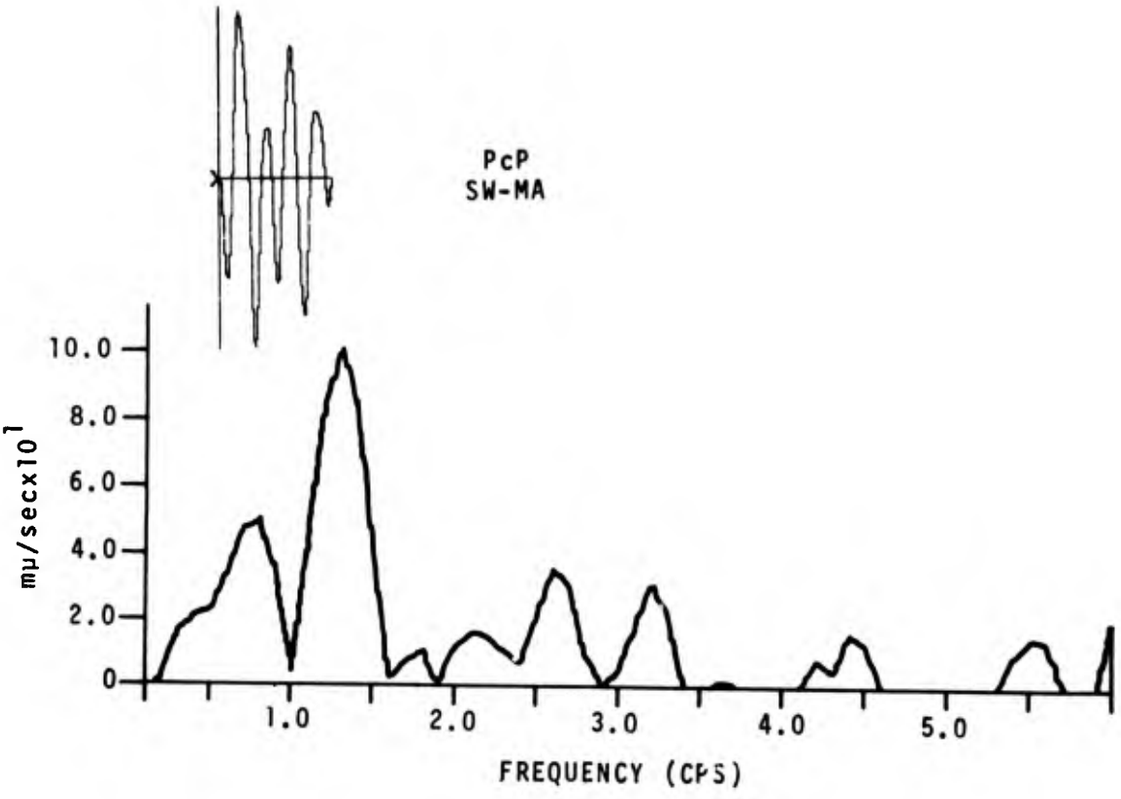
PcP
SW-MA
10.0
8.0
6.0
4.0
2.0
0
mμ/secx10^1
1.0
2.0
3.0
4.0
5.0
FREQUENCY (CPS)

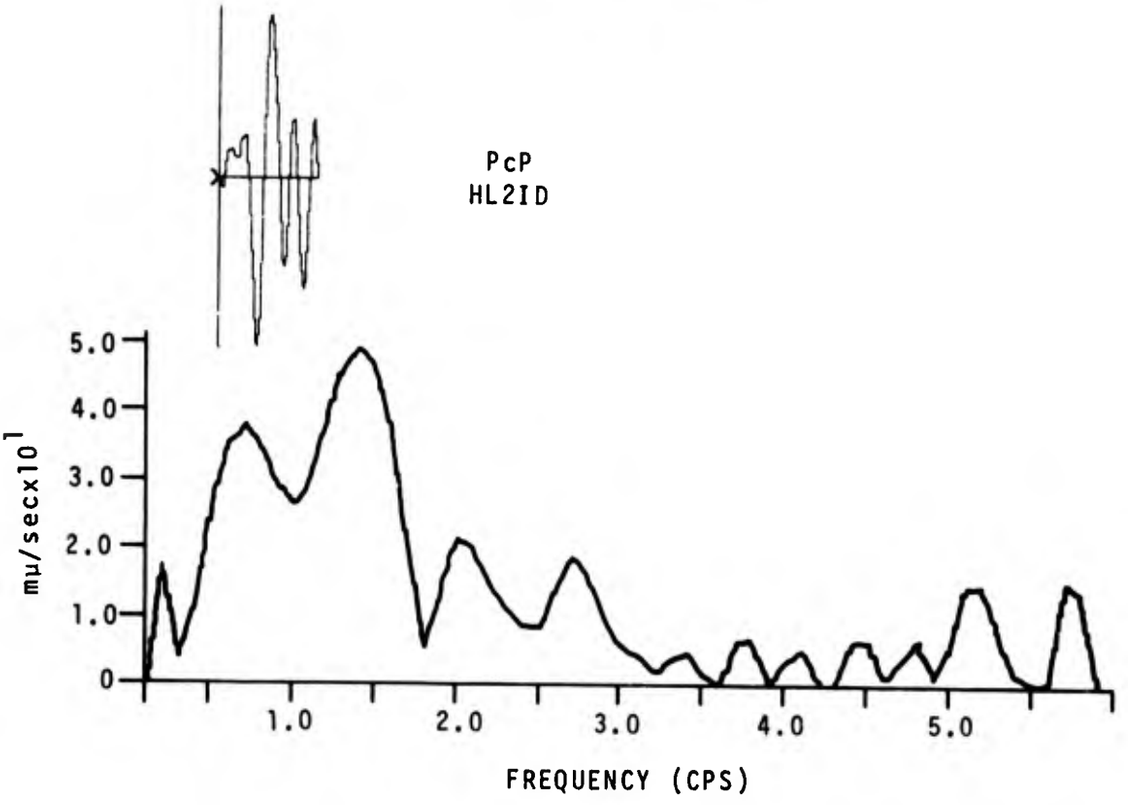
PcP
HL2ID
5.0
4.0
3.0
2.0
1.0
0
mμ/secx10^1
1.0
2.0
3.0
4.0
5.0
FREQUENCY (CPS)

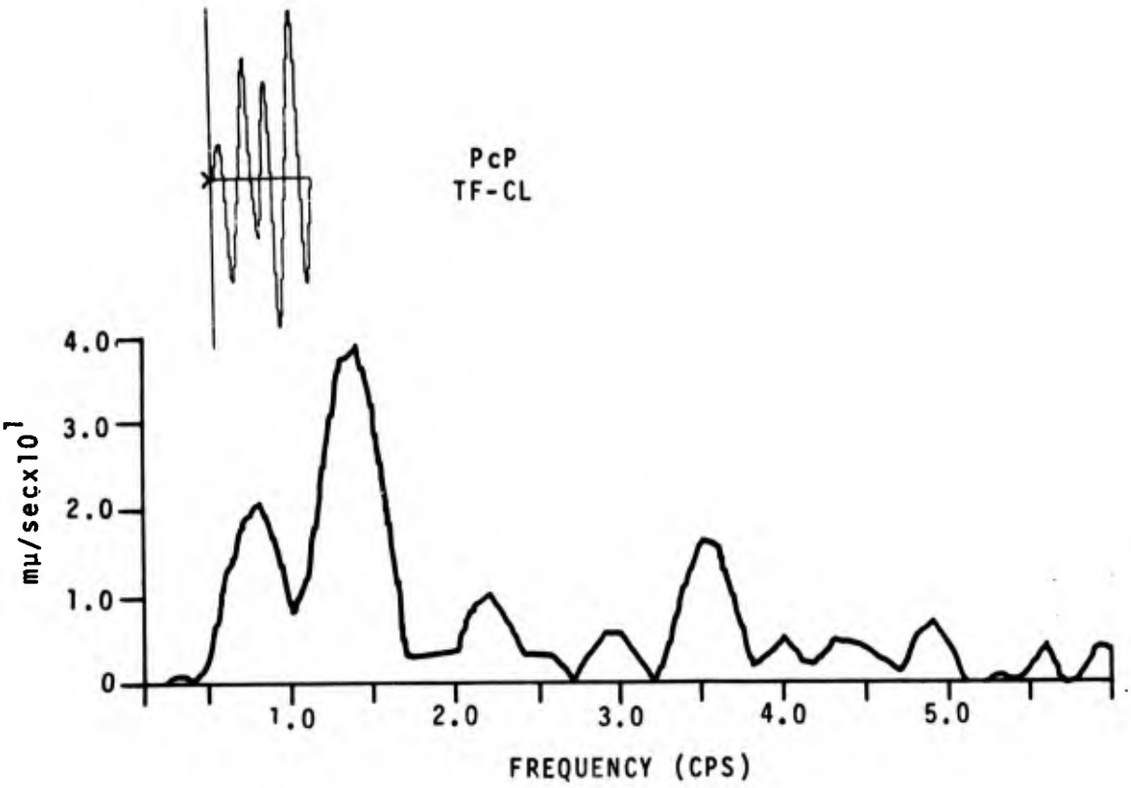
PcP
TF-CL
4.0
3.0
2.0
1.0
0
mμ/secx10^1
1.0
2.0
3.0
4.0
5.0
FREQUENCY (CPS)

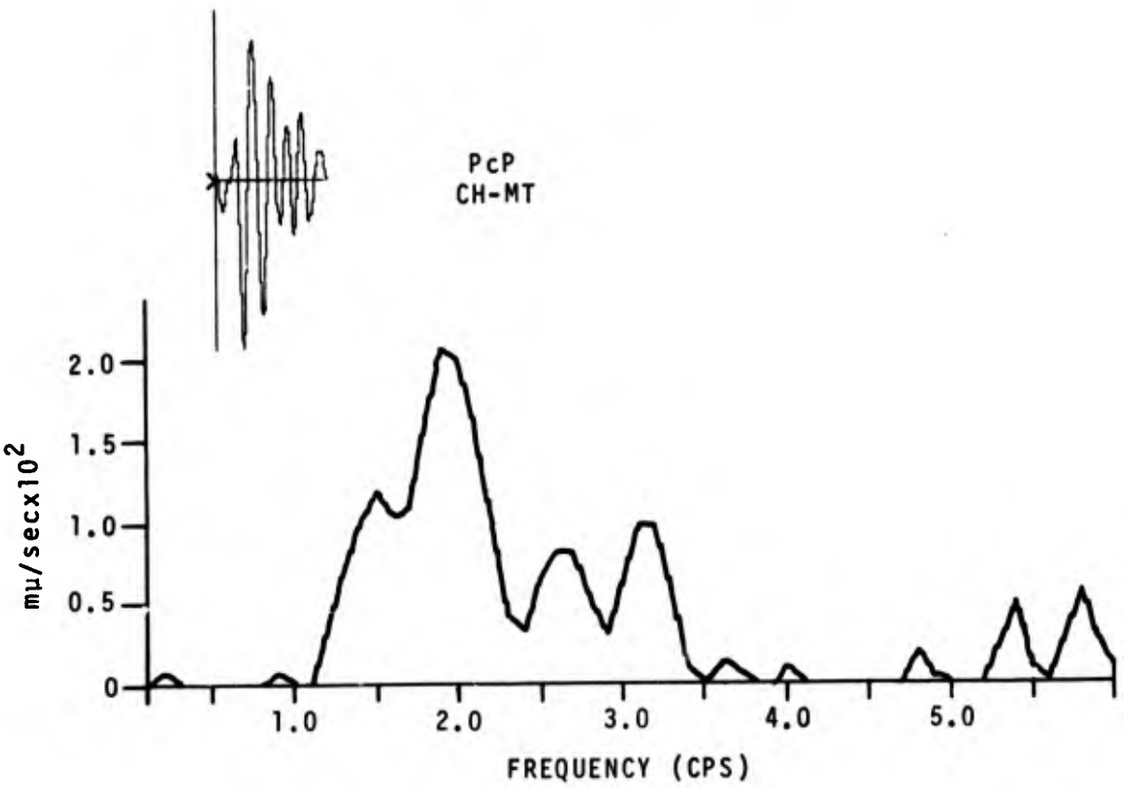
PcP
CH-MT
2.0
1.5
1.0
0.5
0
mμ/secx10^2
1.0
2.0
3.0
4.0
5.0
FREQUENCY (CPS)

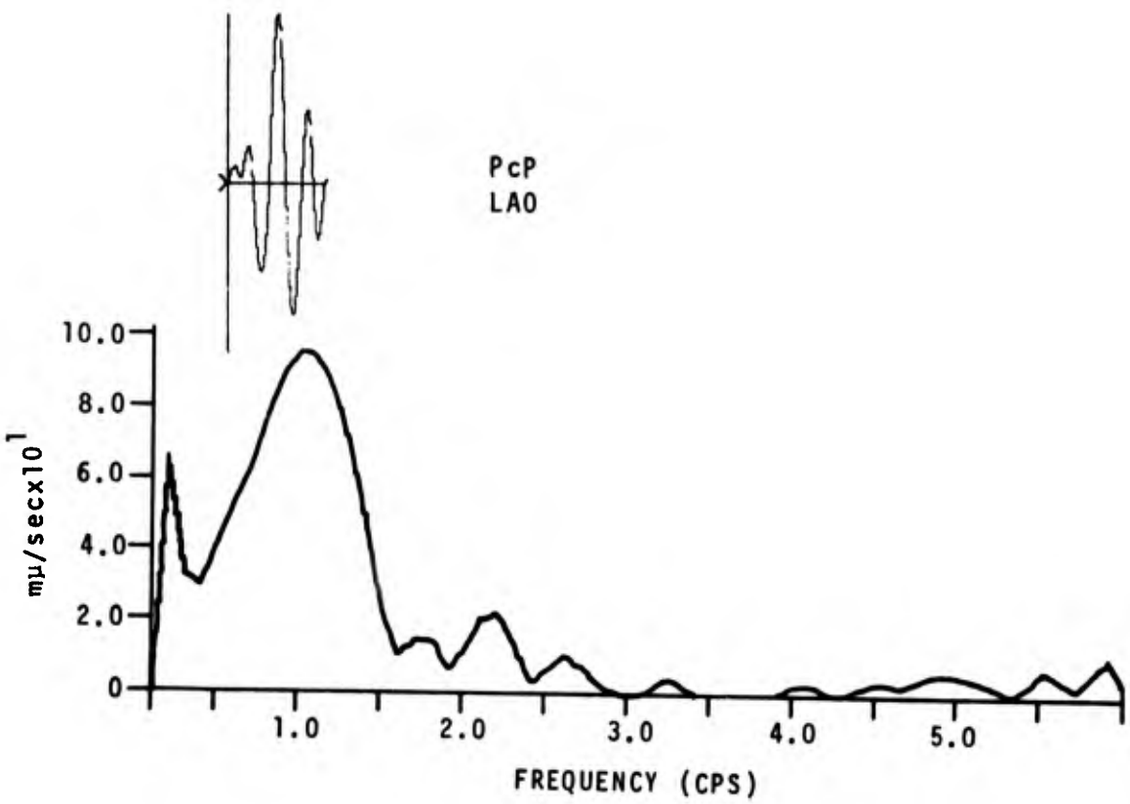
PcP
LAO
10.0
8.0
6.0
4.0
2.0
0
mμ/secx10¹
1.0
2.0
3.0
4.0
5.0
FREQUENCY (CPS)

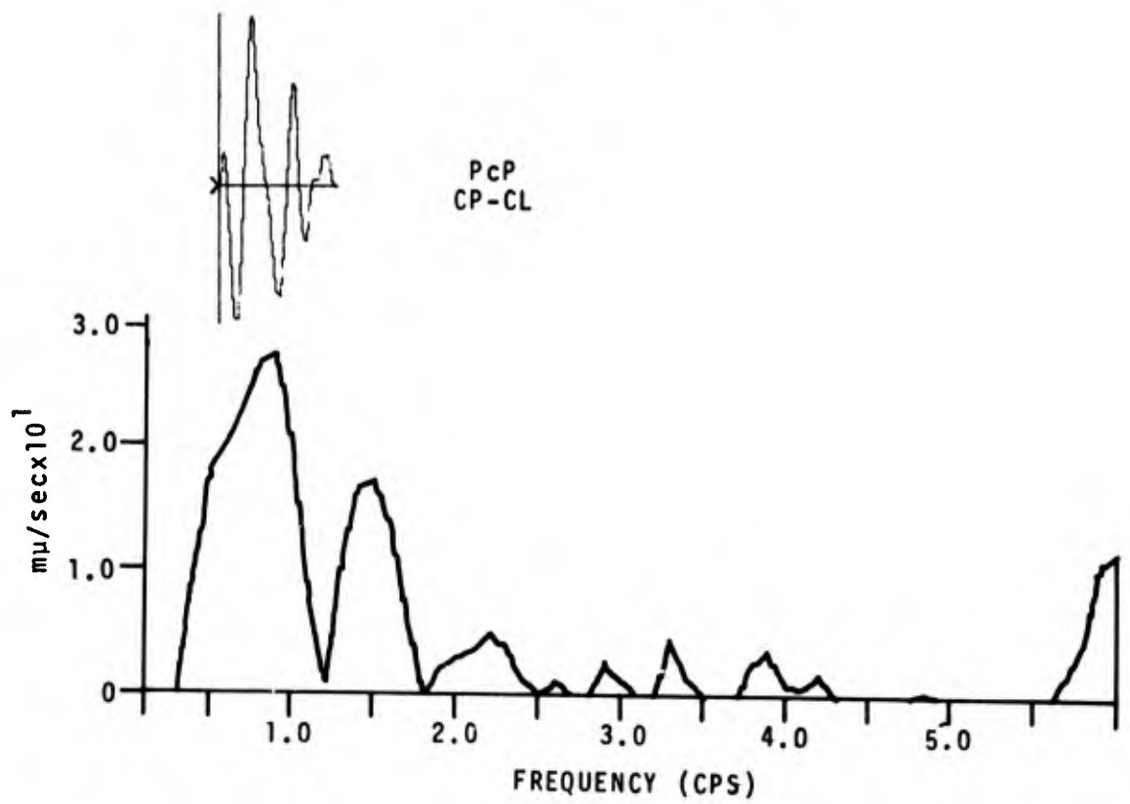
PcP
CP-CL
3.0
2.0
1.0
0
mμ/secx10¹
1.0
2.0
3.0
4.0
5.0
FREQUENCY (CPS)

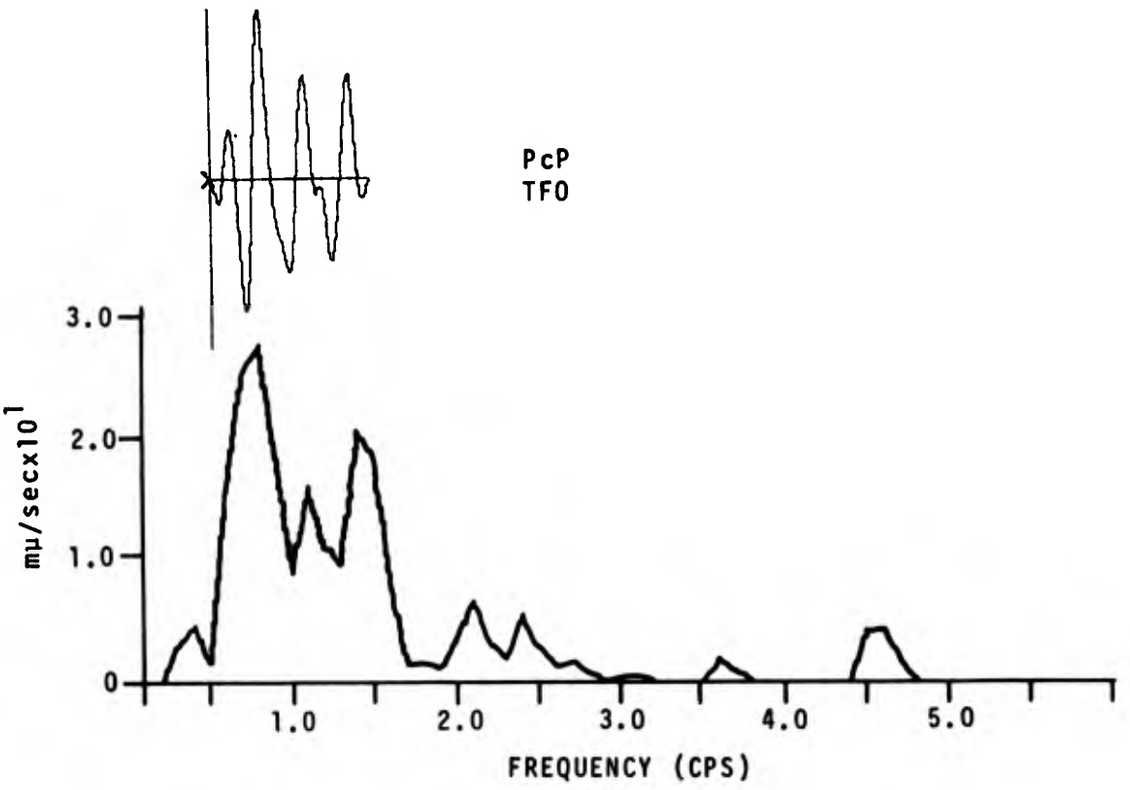
PcP
TFO
3.0
2.0
1.0
0
mμ/secx10^1
1.0
2.0
3.0
4.0
5.0
FREQUENCY (CPS)

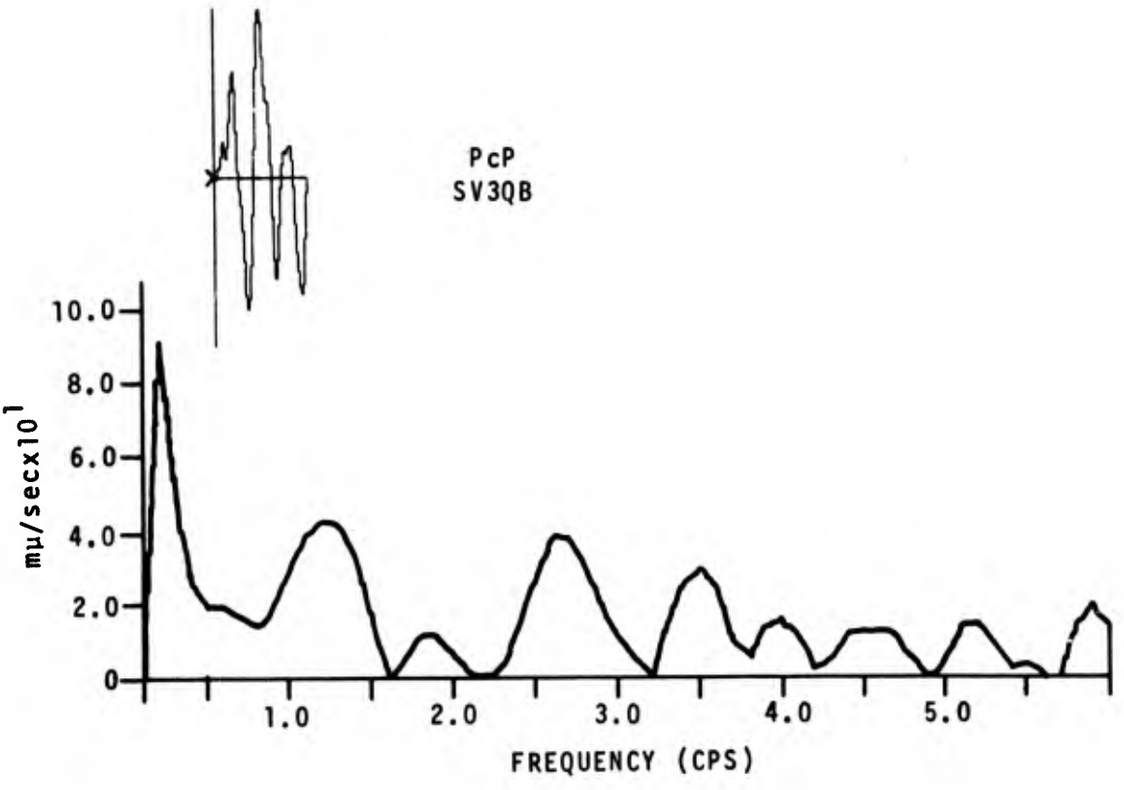
PcP
SV3QB
10.0
8.0
6.0
4.0
2.0
0
mμ/secx10^1
1.0
2.0
3.0
4.0
5.0
FREQUENCY (CPS)

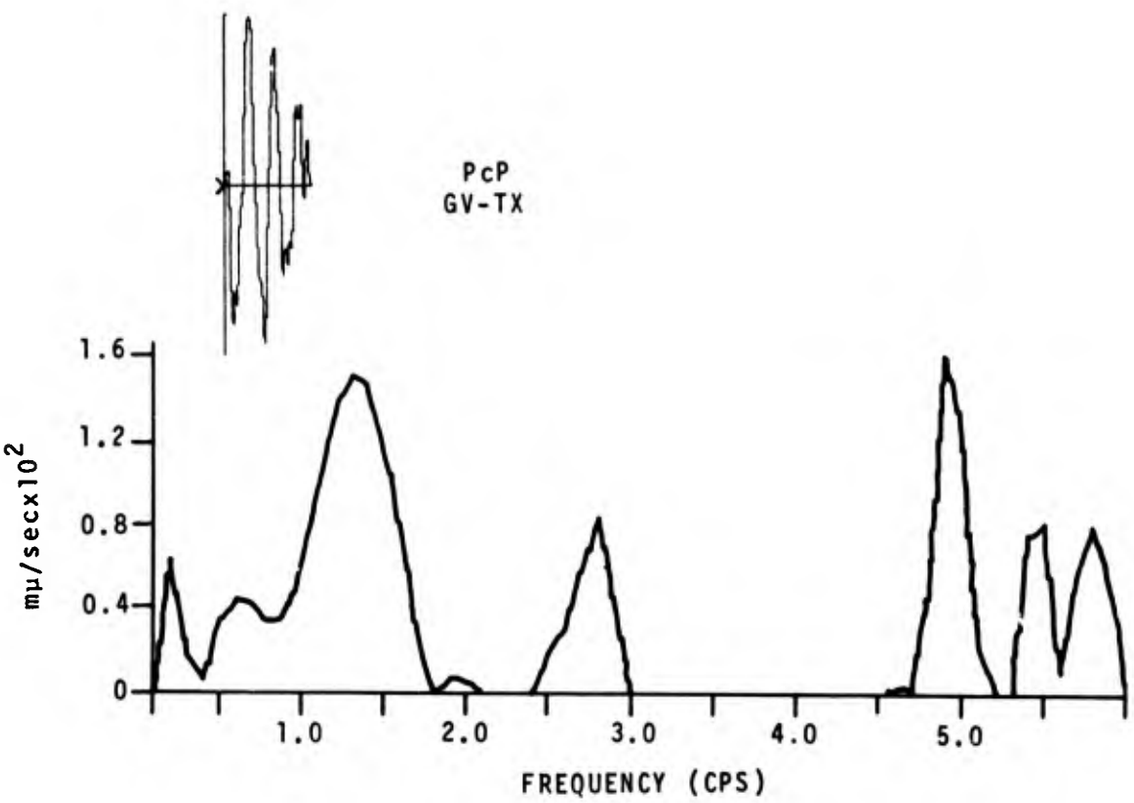
PcP
GV-TX
1.6
1.2
0.8
0.4
0
mμ/secx10²
1.0
2.0
3.0
4.0
5.0
FREQUENCY (CPS)

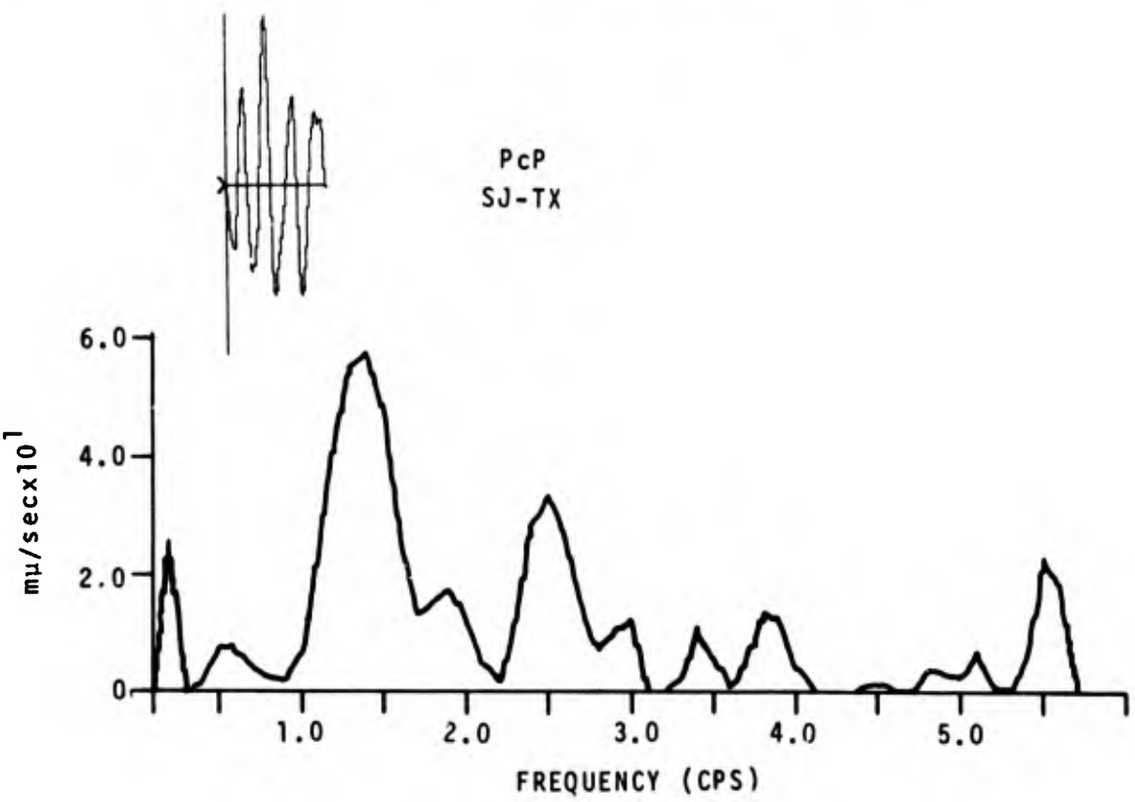
PcP
SJ-TX
6.0
4.0
2.0
0
mμ/secx10¹
1.0
2.0
3.0
4.0
5.0
FREQUENCY (CPS)

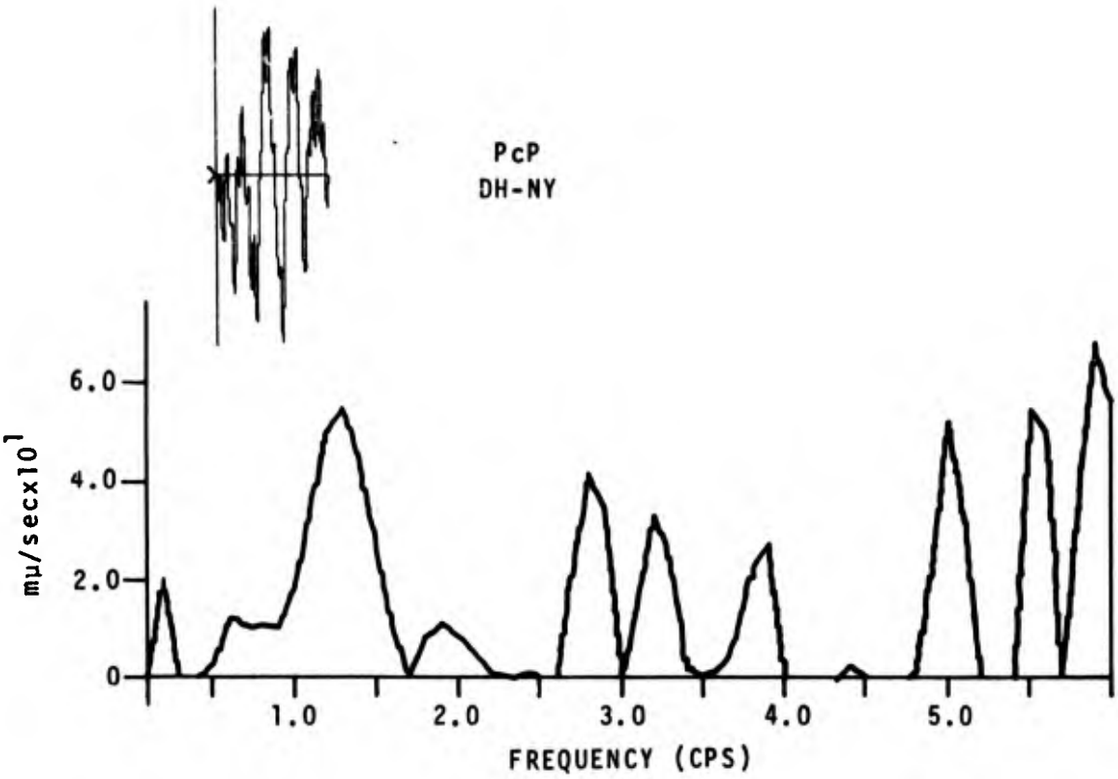
PcP
DH-NY
6.0
4.0
2.0
0
mμ/secx10^1
1.0
2.0
3.0
4.0
5.0
FREQUENCY (CPS)

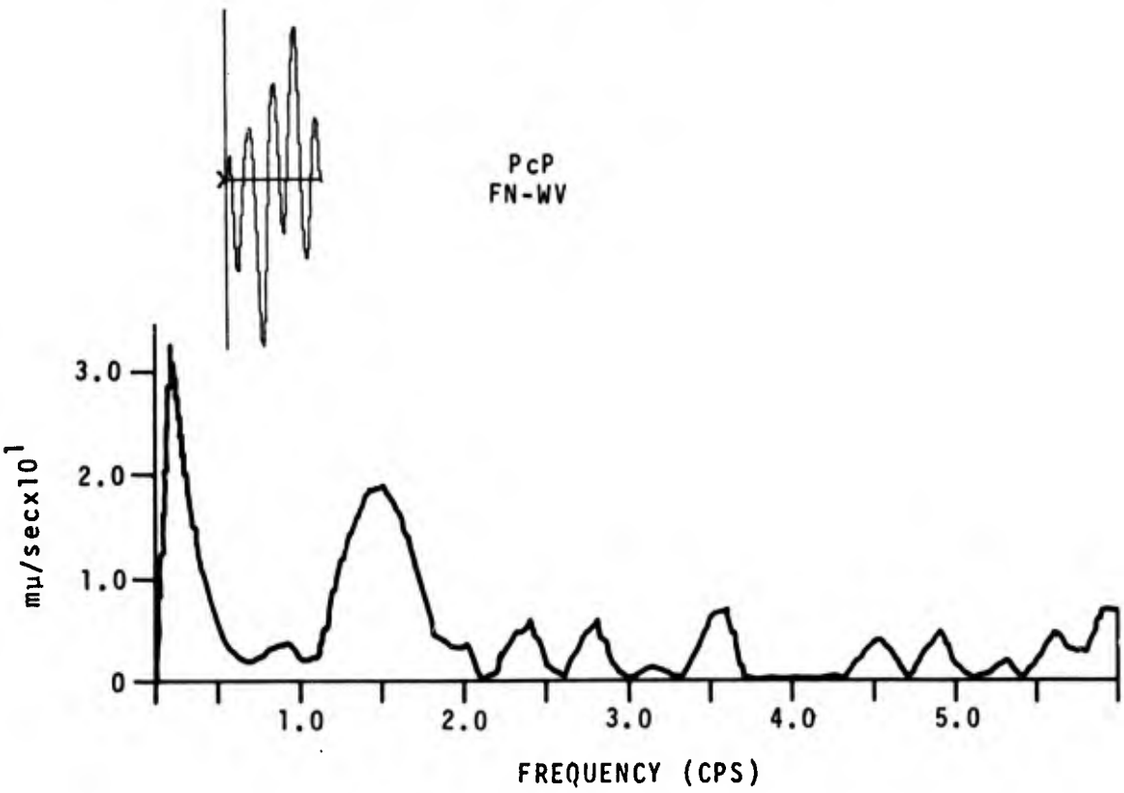
PcP
FN-WV
3.0
2.0
1.0
0
mμ/secx10^1
1.0
2.0
3.0
4.0
5.0
FREQUENCY (CPS)

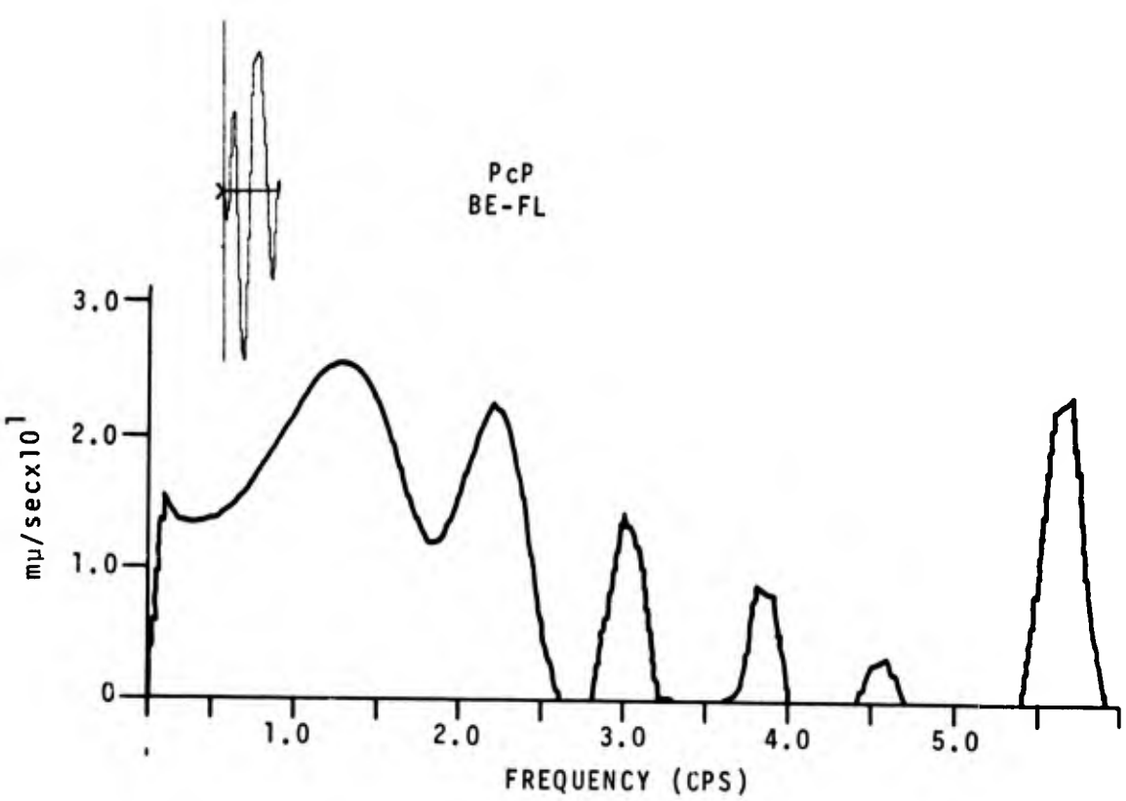
PcP
BE-FL
3.0
2.0
1.0
0
mμ/secx10⁻¹
1.0
2.0
3.0
4.0
5.0
FREQUENCY (CPS)

APPENDIX II

Additional Complexity Factors for LONG SHOT

Station	Distance (km)	Complexity Factor (F_c)
BH-YK	2745	8.52
WH-YK	2958	9.91
SI-BC	3533	8.36
FL-BC	3668	3.61
YKA	4015	0.72
KV-AT	4046	3.69
WS-AT	4399	0.65
YR-CL	4464	2.94
BMO	4636	2.84
SW-MA	4744	1.44
HL2ID	4908	2.74
TE-GL	5042	2.87
TF-CL	5095	2.95
CH-MT	5229	0.94
CP-CL	5523	2.02
TFO	5760	2.28
LC-NM	6221	1.41
WMO	6584	2.15
SV3QB	6758	1.27
GV-TX	6832	1.76
SJ-TX	7162	1.32
CPO	7349	0.58
DH-NY	7422	1.31
FN-WV	7470	2.14
EKA	8182	0.68
WRA	9027	1.22
GBA	9634	0.90

APPENDIX III

LR SPECTRA

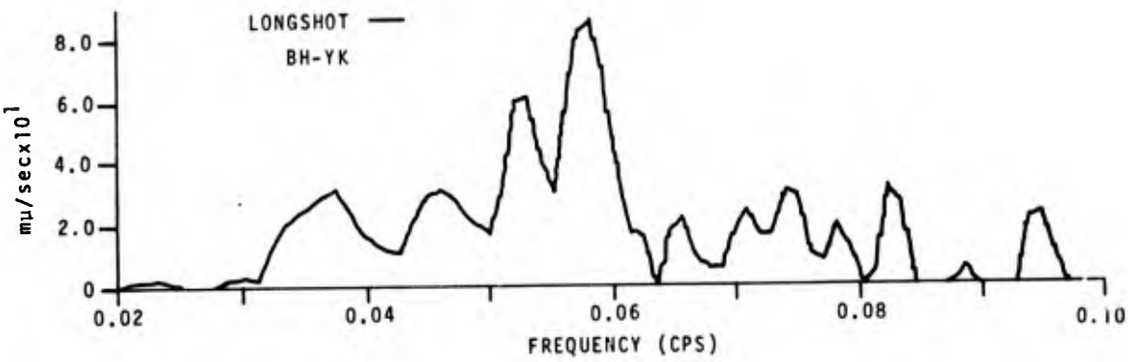
LONGSHOT —
BH-YK
8.0
6.0
4.0
2.0
0
mμ/secx10¹
0.02
0.04
0.06
0.08
0.10
FREQUENCY (CPS)

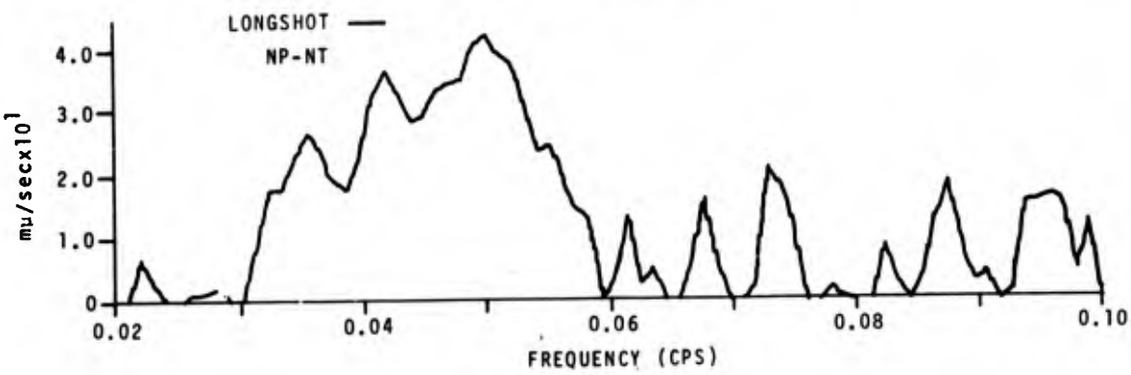
LONGSHOT —
NP-NT
4.0
3.0
2.0
1.0
0
mμ/secx10¹
0.02
0.04
0.06
0.08
0.10
FREQUENCY (CPS)

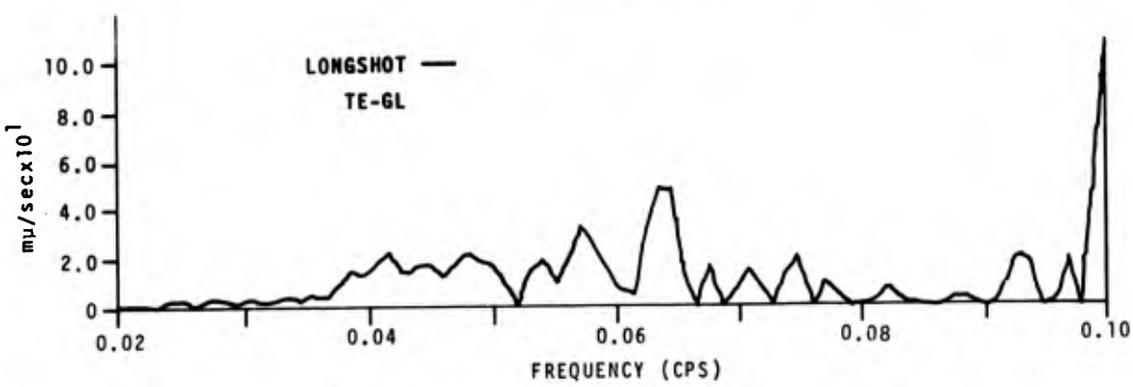
LONGSHOT —
TE-GL
10.0
8.0
6.0
4.0
2.0
0
mμ/secx10¹
0.02
0.04
0.06
0.08
0.10
FREQUENCY (CPS)

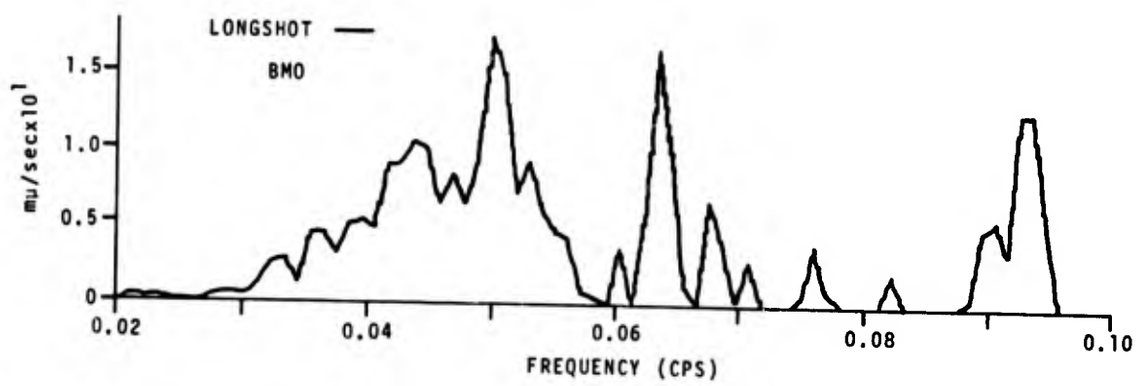
LONGSHOT
BMO
mμ/secx10¹
1.5
1.0
0.5
0
0.02
0.04
0.06
0.08
0.10
FREQUENCY (CPS)

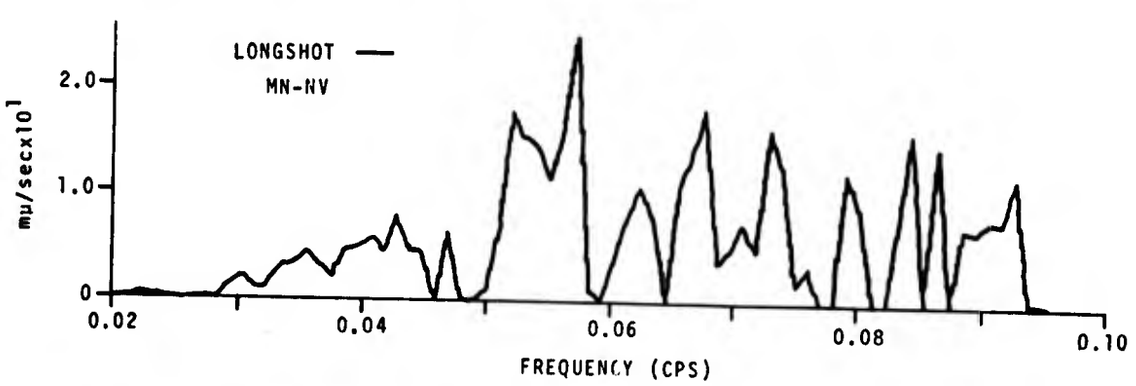
LONGSHOT
MN-NV
mμ/secx10¹
2.0
1.0
0
0.02
0.04
0.06
0.08
0.10
FREQUENCY (CPS)

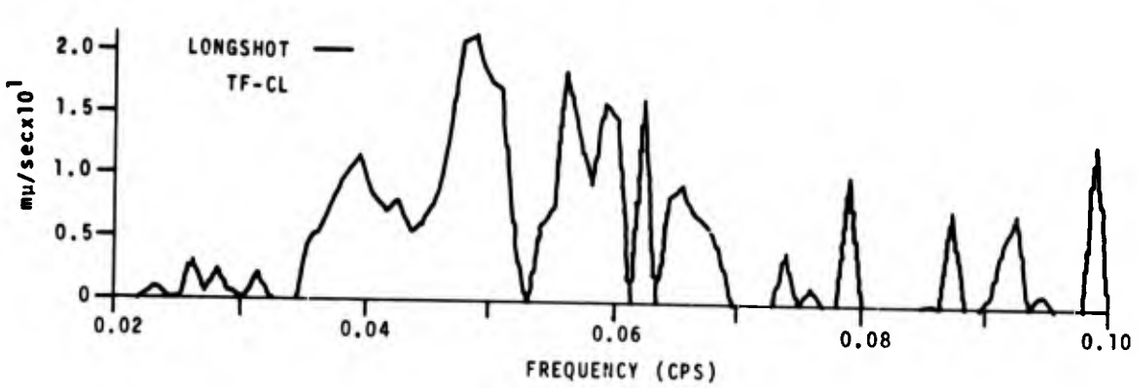
LONGSHOT
TF-CL
mμ/secx10¹
2.0
1.5
1.0
0.5
0
0.02
0.04
0.06
0.08
0.10
FREQUENCY (CPS)

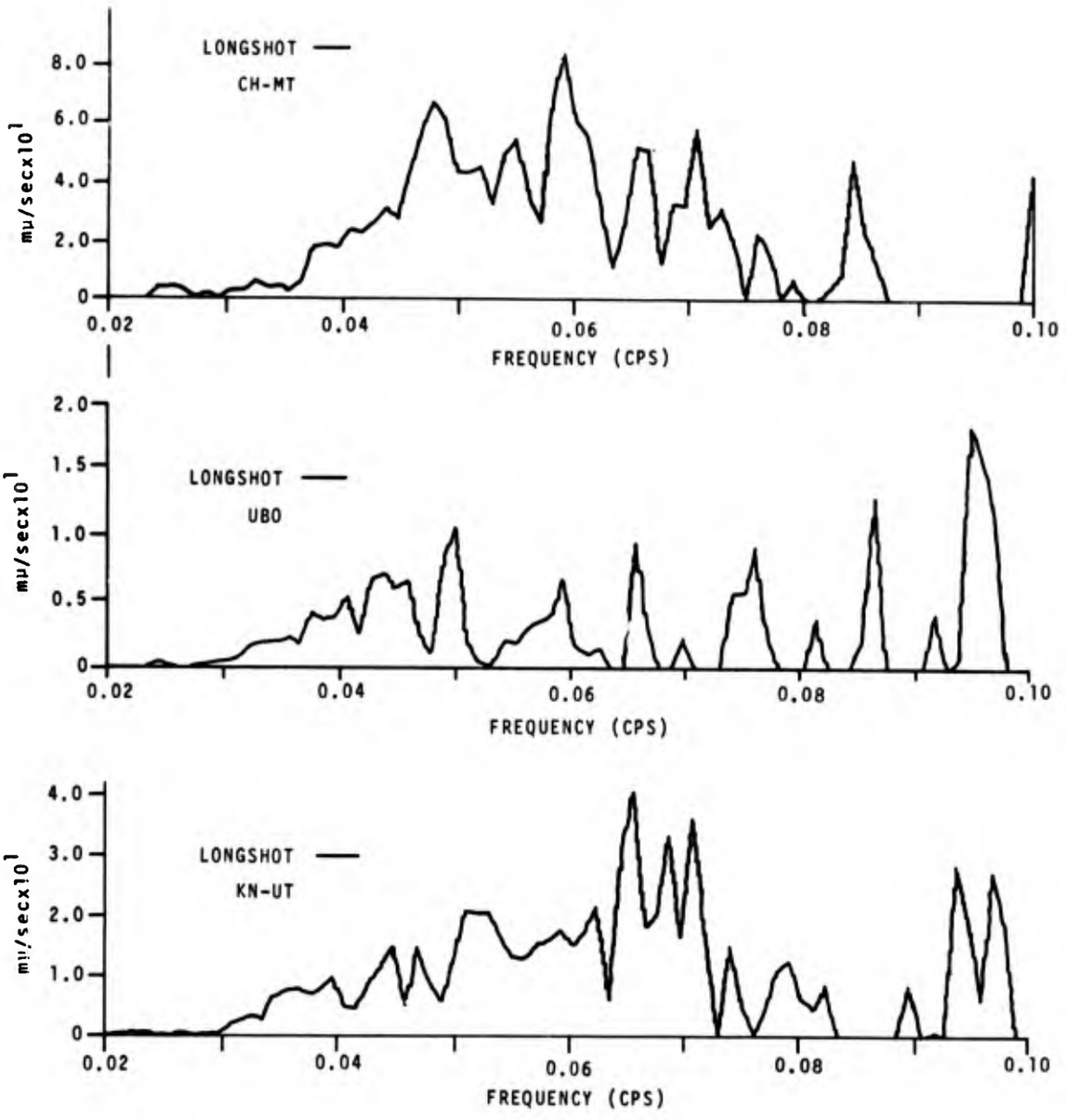
LONGSHOT
CH-MT
8.0
6.0
4.0
2.0
0
mμ/secx10¹
0.02
0.04
0.06
0.08
0.10
FREQUENCY (CPS)
LONGSHOT
UBO
2.0
1.5
1.0
0.5
0
mμ/secx10¹
0.02
0.04
0.06
0.08
0.10
FREQUENCY (CPS)
LONGSHOT
KN-UT
4.0
3.0
2.0
1.0
0
mμ/secx10¹
0.02
0.04
0.06
0.08
0.10
FREQUENCY (CPS)

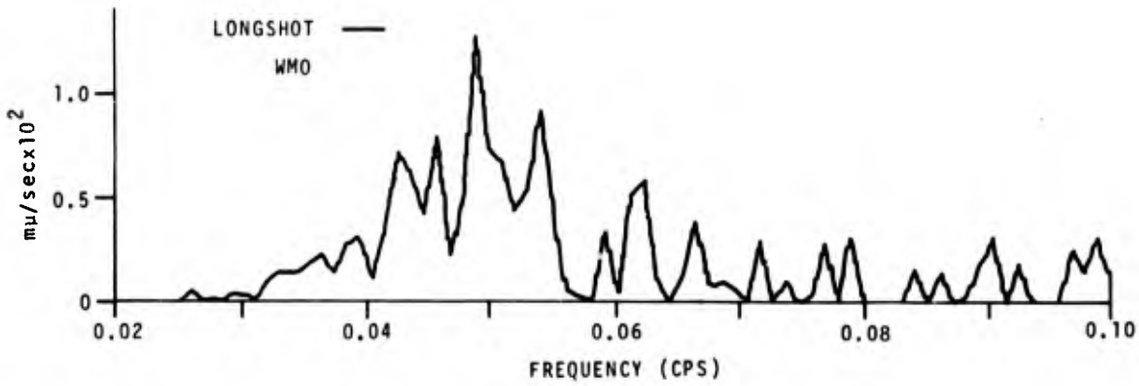
LONGSHOT
WMO
mμ/secx10²
1.0
0.5
0
0.02
0.04
0.06
0.08
0.10
FREQUENCY (CPS)

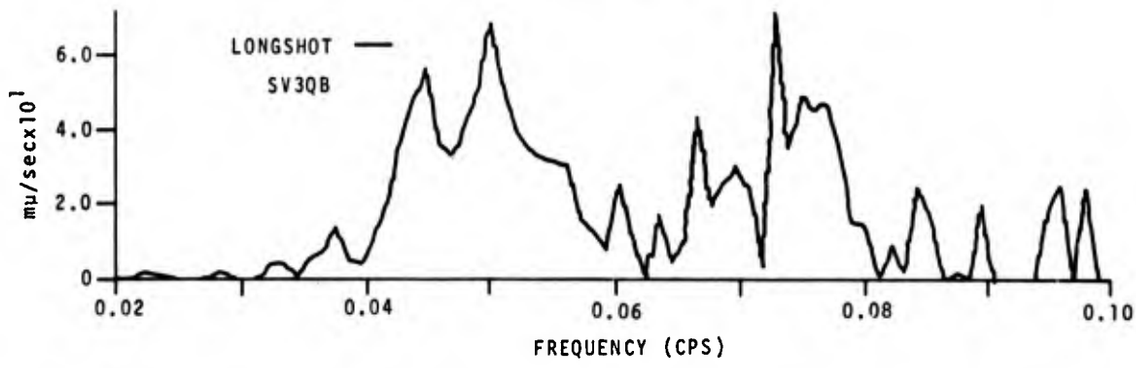
LONGSHOT
SV3QB
mμ/secx10¹
6.0
4.0
2.0
0
0.02
0.04
0.06
0.08
0.10
FREQUENCY (CPS)

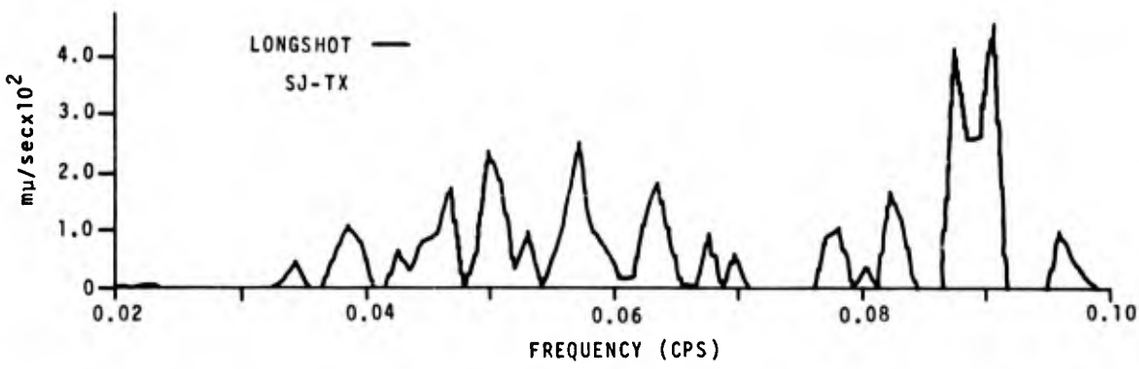
LONGSHOT
SJ-TX
mμ/secx10²
4.0
3.0
2.0
1.0
0
0.02
0.04
0.06
0.08
0.10
FREQUENCY (CPS)

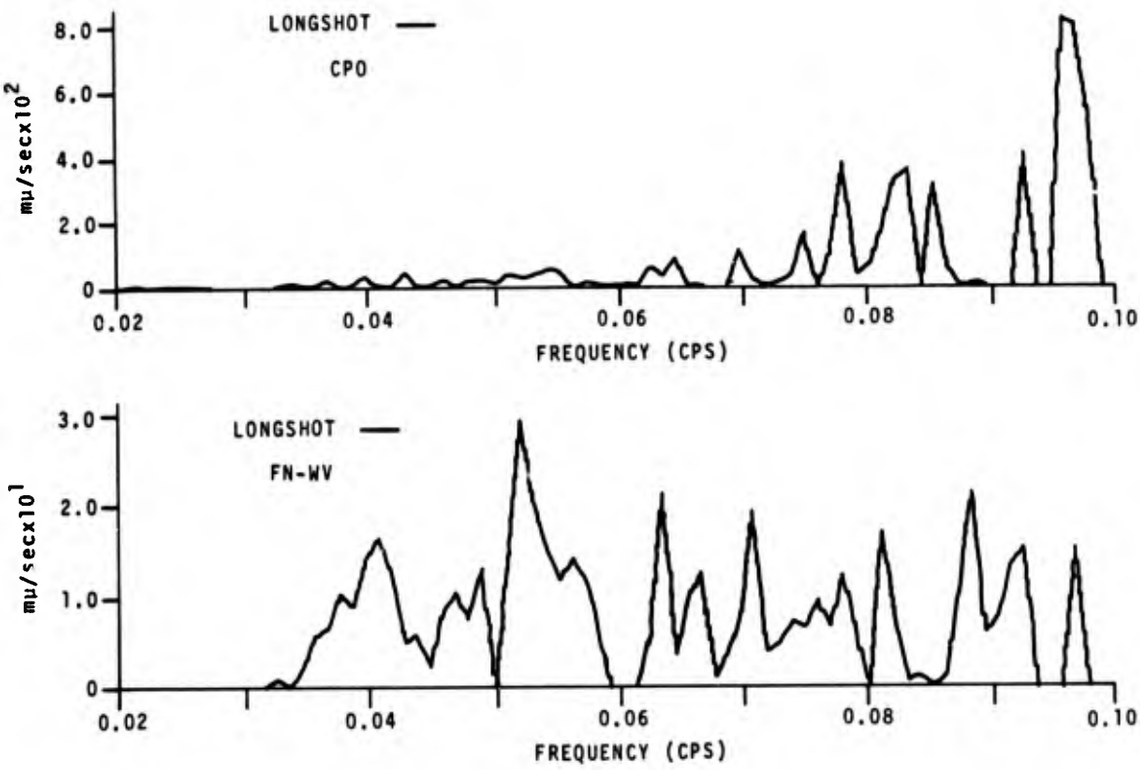
LONGSHOT
CPO
8.0
6.0
4.0
2.0
0
mμ/secx10²
0.02
0.04
0.06
0.08
0.10
FREQUENCY (CPS)
LONGSHOT
FN-WV
3.0
2.0
1.0
0
mμ/secx10¹
0.02
0.04
0.06
0.08
0.10
FREQUENCY (CPS)

Unclassified
Security Classification

DOCUMENT CONTROL DATA - R&D

(Security classification of title, body of abstract and indexing annotation must be entered when the overall report is classified)

1. ORIGINATING ACTIVITY (Corporate author)
TELEDYNE INDUSTRIES, INC.
ALEXANDRIA, VIRGINIA

2a. REPORT SECURITY CLASSIFICATION
Unclassified

2b. GROUP

3. REPORT TITLE
THE LONG SHOT EXPERIMENT - VOLUME II
COMPREHENSIVE ANALYSIS

4. DESCRIPTIVE NOTES (Type of report and inclusive dates)
Scientific

5. AUTHOR(S) (Last name, first name, initial)
Lambert, D.G.
Von Seggern, D.H.
Alexander, S.S. (The Penn. State Univ.)
Galat, G.A.

6. REPORT DATE	7a. TOTAL NO. OF PAGES	7b. NO. OF REFS
25 June 1969	217	64

8a. CONTRACT OR GRANT NO.
F33657-69-C-0913
b. PROJECT NO.
VELA T/9706
ARPA Order No. 624
ARPA Program Code No. 9F10

9a. ORIGINATOR'S REPORT NUMBER(S)
234

9b. OTHER REPORT NO(S) (Any other numbers that may be assigned this report)

10. AVAILABILITY/LIMITATION NOTICES

11. SUPPLEMENTARY NOTES

12. SPONSORING MILITARY ACTIVITY
ADVANCED RESEARCH PROJECTS AGENCY
NUCLEAR MONITORING RESEARCH OFFICE
WASHINGTON, D.C.

13. ABSTRACT

14. KEY WORDS

Unclassified
Security Classification